Synthese und Charakterisierung von Carba-Analoga der K_V7-Kanalöffner Flupirtin und Retigabin

I n a u g u r a l d i s s e r t a t i o n

zur

Erlangung des akademischen Grades eines

Doktors der Naturwissenschaften (Dr. rer. nat.)

der

Mathematisch-Naturwissenschaftlichen Fakultät

der

Universität Greifswald

vorgelegt von
Konrad W. Wurm

Greifswald, 11.10.22

Dekan: Prof. Dr. Gerald Kerth

1. Gutachter: Prof. Dr. Andreas Link

2. Gutachter: Prof. Dr. Bernhard Wünsch

Tag der Promotion: 14.12.22

Inhaltsverzeichnis

Abkürzungsverzeichnis

4-DMAP	4-(Dimethylamino)pyridin
AcOH	Essigsäure
ALS	amyotrophe Lateralsklerose
BTMAC	Benzyltrimethylammoniumchlorid
CDI	1,1'-Carbonyldiimidazol
CFTR	cystic fibrosis transmembrane conductance regulator
DCM	Dichlormethan
DIBAL-H	Diisobutylaluminiumhydrid
DIPEA	*N*,*N*-Diisopropylethylamin
DMF	*N*,*N*-Dimethylformamid
EC_{50}	Konzentration, die einen halbmaximalen Effekt auslöst
E_{max}	maximaler Effekt
E_{pa}	anodisches Peakpotenzial
EtOAc	Ethylacetat
EtOH	Ethanol
FDA	U.S. Food and Drug Administration
Flu	Flupirtin
GABA	γ-Aminobuttersäure
HEK	human embryonic kidney
hERG	human ether-a-go-go related gene
HLA	humanes Leukozytenantigen
HPLC	high performance liquid chromatography
I_{KM}	M-Strom
I_{KS}	langsam aktivierende Komponente des verzögerten Kalium-Gleichrichterstroms
KryoEM	Kryoelektronenmikroskopie
LD_{25}	Konzentration, welche die Zellviabilität auf 75 % senkt
LD_{50}	Konzentration, welche die Zellviabilität auf 50 % senkt
MALDI	matrix assisted laser desorption/ionization
MeOH	Methanol
MQS	molecule quinone formation score

MS	multiple Sklerose
MTT	3-(4,5-Dimethylthiazol-2-yl)-2,5-diphenyltetrazoliumbromid
NaOMe	Natriummethanolat
n-BuOH	*n*-Butanol
NMP	*N*-Methyl-2-pyrrolidon
Pd/C	Palladium auf Aktivkohle
PDB	protein data bank
Ret	Retigabin
TAMH	transforming growth factor-a transgenic mouse hepatocyte
TBAF	Tetrabutylammoniumfluorid
t-BuOK	Kalium-*tert*-butanolat
TEA	Triethylamin
TFA	Trifluoressigsäure
THF	Tetrahydrofuran
TMD	Transmembrandomäne
UAW	unerwünschte Arzneimittelwirkung
VTA	ventrales tegmentales Areal
ZNS	zentrales Nervensystem

1 Einleitung

1.1 Physiologie der K_V7-Kanäle

1.1.1 Tertiär- und Quartärstruktur

Die spannungsabhängigen Kaliumkanäle vom K_V7-Typ werden im menschlichen Genom durch fünf verschiedene KCNQ Gene (KCNQ1-5) codiert, die jeweils die Informationen für ein K_V7-Protein (K_V7.1-5) enthalten.[1] Für die Bildung eines vollständigen Kaliumkanals sind vier dieser K_V7-Untereinheiten notwendig, wobei sowohl homomere als auch heteromere Kombinationen vorkommen. Im Fall von heterotetrameren K_V7-Kanälen findet in der Regel eine Assemblierung von je zwei K_V7-Proteinen eines Subtyps zu einer funktionellen Einheit statt.[2,3] Bei einer strukturell detaillierteren Betrachtung zeigt sich, dass eine K_V7-Untereinheit wiederum aus sechs transmembranären Domänen (S1-S6) besteht. Dabei bilden die Segmente S1 bis S4 den Spannungssensor, wohingegen die Segmente S5 und S6 an der Bildung der kaliumselektiven Ionenpore beteiligt sind. Hinzu kommen ein kurzer N-terminaler Abschnitt und ein längerer C-terminaler Bereich, die beide intrazellulär lokalisiert sind.[4] Dieser für spannungsabhängige Kaliumkanäle typische Aufbau wurde zunächst basierend auf einem Homologiemodelling vorhergesagt und konnte kürzlich durch eine kryoelektronenmikroskopische Aufnahme des K_V7.2-Kanals in grundlegenden Zügen bestätigt werden (Abbildung 1).[5,6]

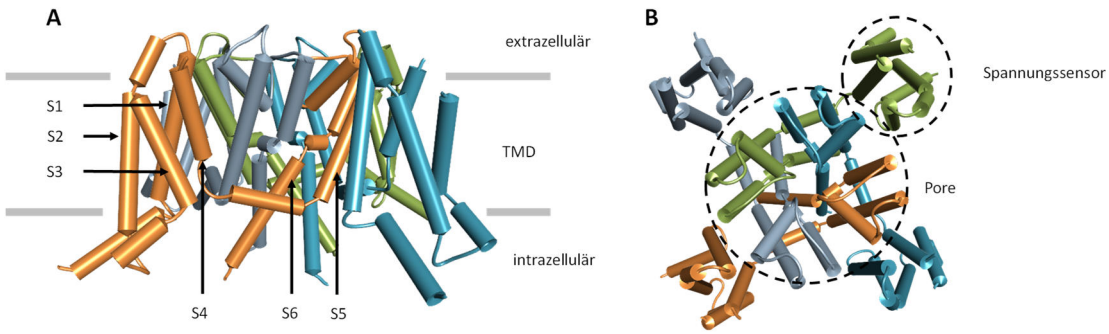

Abbildung 1. Durch Kryoelektronenmikroskopie (KryoEM) erhaltene Struktur des homotetrameren K_V7.2-Kanals im Apo-Zustand (PDB: 7CR0) in Seitenansicht (A) und Aufsicht (B) mit unterschiedlich gefärbten Untereinheiten (TMD = Transmembrandomäne). Die cytosolischen Bereiche des Kanals waren in der KryoEM-Aufnahme schlecht aufgelöst und sind daher nur ansatzweise erkennbar.

Der C-terminale Bereich der K_V7-Kanäle ist in vier Helices (A-D) gegliedert und enthält Regionen, die für die Tetramerisierung verantwortlich sind. Außerdem finden sich in diesem Teil Bindestellen für Signalmoleküle wie z. B. Phosphatidylinositol-4,5-bisphosphat und Interaktionsbereiche für diverse regulatorische Proteine wie beispielsweise Calmodulin.[2,7,8] Neben der Möglichkeit der Beeinflussung durch diese allgemein bekannten, regulatorisch wirksamen Mediatoren, die in zahlreichen Signalkaskaden involviert sind, existiert zudem eine Besonderheit in Hinblick auf die Modulation der K_V7-Öffnungswahrscheinlichkeit. Bestimmte Transmembranproteine, die durch die KCNE1-5 Gene codiert werden, fungieren als Hilfsuntereinheiten und üben einen ausgeprägten Effekt auf viele Eigenschaften der K_V7-Kanäle aus.[9] Dabei kann die K_V7-Öffnungswahrscheinlichkeit sowohl positiv als auch negativ beeinflusst werden in Abhängigkeit davon, welche Kombination aus K_V7-Untereinheit und KCNE-Hilfsuntereinheit im konkreten Fall vorliegt.[10,11]

1.1.2 Subtypen und Gewebeverteilung

K_V7-Kanäle kommen ubiquitär im menschlichen Organismus vor, wobei die Expression der verschiedenen Untereinheiten sowie ihre Kombination stark gewebespezifisch sind. So findet sich etwa der K_V7.1-Subtyp insbesondere in Kardiomyozyten und tritt bevorzugt als Homotetramer in Verbindung mit KCNE1 oder KCNE3 auf. Diese kardialen K_V7-Kanäle spielen eine entscheidende Rolle bei der Repolarisation des Herzpotenzials durch die Erzeugung der langsam aktivierenden Komponente des verzögerten Kalium-Gleichrichterstroms (I_{Ks}-Strom).[12,13] Daneben wird der K_V7.1-Kanal auch in Innenohr, Schilddrüse, Lunge, Niere, Bauchspeicheldrüse, Darm und glatter Gefäßmuskulatur exprimiert.[14–19] Die Expression der K_V7.2- und K_V7.3-Untereinheiten erfolgt hingegen vorwiegend im zentralen und peripheren Nervensystem.[20] Beide Subtypen kommen zwar als Homotetramere vor, aber dominierend ist die heterotetramere K_V7.2/3-Kombination, welche verglichen mit den reinen K_V7.2- oder K_V7.3-Kanälen auch deutlich stärkere Kaliumströme generiert.[21,22] Die K_V7.4-Untereinheit spielt in der homotetrameren Variante eine wichtige Rolle in dopaminergen Neuronen des zentralen Nervensystems (ZNS) sowie im Hör- und Gleichgewichtsorgan.[23,24] Als K_V7.4/5-Heterotetramer findet sie sich zudem in der glatten Muskulatur und wurde in dieser Form in einer Vielzahl von Organen nachgewiesen (z. B. Magen-Darm-Trakt, Blase, Arterien, Atemwege, Gebärmutter, Corpus cavernosum).[25–31] Demgegenüber wird der homotetramere K_V7.5-Kanaltyp wiederum hauptsächlich in Neuronen exprimiert, wo er insbesondere an der verzögerten Nachhyperpolarisation beteiligt ist.[32]

1.1.3 Funktionen von neuronalen K_V7-Kanälen

Das ubiquitäre Vorkommen der K_V7-Kanäle deutet an, dass sie in einer Vielzahl von physiologischen Prozessen involviert sind, deren Diskussion hier nicht umfassend möglich ist. Aus diesem Grund liegt der Fokus im Folgenden ausschließlich auf neuronalen K_V7-Kanälen, die in den meisten Bereichen des zentralen und peripheren Nervensystems, wie bereits erwähnt, vorwiegend aus K_V7.2-, K_V7.3- und K_V7.5-Untereinheiten bestehen.[20] K_V7.4-Kanäle wurden hingegen in peripheren Nervenzellen bisher nicht nachgewiesen und auch im ZNS kommt dieser Subtyp nur in wenigen Regionen vor.[20,33,34] Der durch die Gesamtheit der verschiedenen neuronalen K_V7-Kanäle vermittelte Strom kann durch die Aktivierung von muskarinischen Acetylcholinrezeptoren gehemmt werden und wird daher allgemeinhin auch als M-Strom (I_{KM}) bezeichnet.[35,36] Der M-Strom übt eine Erregbarkeitskontrolle sowohl des zentralen als auch des peripheren Nervensystems einschließlich sympathischer, parasympathischer sowie sensorischer Neuronen aus und beeinflusst in gleicher Weise erregende wie hemmende Nervenbahnen.[37–40]

Eine Besonderheit der K_V7-Kanäle ist die Aktivierung bereits bei unterschwelligen Potenzialen ab etwa −60 mV. Da sie nicht inaktivieren, erzeugen K_V7-Kanäle folglich einen konstanten, spannungsabhängigen Auswärtsstrom, der insbesondere eine Stabilisierung des Ruhepotenzials bewirkt.[41] Des Weiteren leisten K_V7-Kanäle auch einen Beitrag zur Nachhyperpolarisation während der Refraktärphase.[42] Aufgrund der im Vergleich zu anderen spannungsgesteuerten Ionenkanälen relativ langsamen Öffnungskinetik sind K_V7-Kanäle hingegen nicht wesentlich an der Repolarisation individueller Aktionspotenziale beteiligt.[43,44] Im Fall einer hochfrequenten Aktionspotenzialauslösung vergrößert die Aktivierung von K_V7-Kanälen jedoch das sogenannte Spike-Intervall und begrenzt auf diese Weise effektiv die Fähigkeit von Nervenzellen wiederholt und in schneller Abfolge zu feuern.[45,46] Insgesamt üben K_V7-Kanäle also eine tiefgreifende dämpfende Wirkung auf

die allgemeine Erregbarkeit von Neuronen aus, was dazu führt, dass ihre Funktion im Nervensystem gelegentlich mit der einer Bremse verglichen wird.[47,48]

1.2 Pharmakologie der K_V7-Kanäle

1.2.1 Molekulare Pharmakologie: Bindungsstellen und Mechanismen

Die Öffnungswahrscheinlichkeit der K_V7-Kanäle lässt sich durch niedermolekulare Liganden modulieren, wobei sowohl K_V7-Aktivatoren bzw. Öffner als auch K_V7-Inhibitoren bekannt sind.[49] Aufgrund ihres epileptogenen Potenzials sind K_V7-Inhibitoren jedoch im Wesentlichen Modellsubstanzen ohne klinische Anwendung und sollen hier nicht näher diskutiert werden.[50] Für die therapeutisch einsetzbaren K_V7-Öffner werden grundsätzlich zwei unterschiedliche Wirkmechanismen angenommen, die auf verschiedene Bindetaschen am K_V7-Kanal zurückzuführen sind. Diese in Abbildung 2 ersichtlichen Bindungsstellen, die bereits vor längerer Zeit durch Mutationsstudien identifiziert wurden, konnten nun kürzlich durch die oben erwähnten kryoelektronenmikroskopischen Untersuchungen bestätigt werden. Darüber hinaus wurden auf diese Weise auch neue Informationen zum genauen Bindungsmechanismus der Liganden gewonnen.[5,51,52]

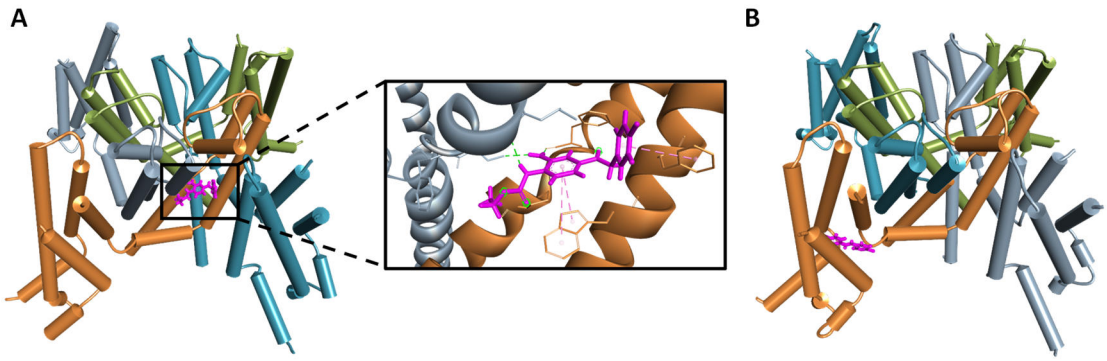

Abbildung 2. Kryoelektronenmikroskopische Struktur des homotetrameren K_V7.2-Kanals im Komplex mit Retigabin (A; PDB: 7CR2) und ztz240 (B; PDB: 7CR1). Die Liganden (in Fuchsia dargestellt) zeigen das Vorhandensein von zwei verschiedenen Bindetaschen in der Porenregion (A) und der Spannungssensordomäne (B). Die Bindetasche von Retigabin ist zusätzlich vergrößert dargestellt.

Der experimentelle K_V7-Öffner ztz240 repräsentiert einen Substanztyp, der in der Region des Spannungssensors zwischen der S3- und S4-Domäne bindet (Abbildung 2B).[5] Im Gegensatz dazu interagiert der klinisch validierte K_V7-Kanalöffner Retigabin mit einer hydrophoben Tasche im intramembranären Bereich der Porenregion, die durch das S5-Segment, die Porenhelix und das S6-Segment der benachbarten Untereinheit gebildet wird (Abbildung 2A).[5] Die Bindung von Retigabin wird dabei über Wasserstoffbrückenbindungen mit der Seitenkette von S303 sowie den Carbonylgruppen von L299 und F305 ermöglicht. Daneben findet die Interaktion hauptsächlich über hydrophobe Wechselwirkungen statt. Hervorzuheben ist weiterhin die Bedeutung des Tryptophanrests 236, dem bei der molekularen Erkennung von Retigabin und anderer potentieller Liganden anscheinend eine Schlüsselrolle zukommt, denn in Mutationsstudien führte ein Austausch gegen Leucin zu einem vollständigen Verlust der Retigabinsensitivität von entsprechenden K_V7-Kanälen.[52] Dieses spezifische Tryptophansegment ist bei den Untereinheiten K_V7.2-5 konserviert, fehlt aber in der Bindetasche von K_V7.1-Kanälen, was erklärt, dass dieser K_V7-Subtyp von Retigabin

und diversen anderen Substanzen, die ebenfalls die Bindungsstelle der Porenregion adressieren, nicht moduliert wird.[53]

Bezogen auf den Wirkungsmechanismus konnte gezeigt werden, dass Liganden des Spannungssensors mit ihrer Bindungsstelle nur im aktivierten Zustand interagieren können, was eine Stabilisierung desselben zur Folge hat und die Sensordeaktivierung drastisch verlangsamt. Retigabin hingegen stabilisiert die offene Konformation der Kaliumpore und bindet unabhängig vom Membranpotenzial. Es kann seine Bindetasche also sowohl im aktivierten Zustand als auch im Ruhezustand erreichen mit der Konsequenz, dass Retigabineffekte sogar bei negativen Spannungen verzeichnet werden, bei welchen die meisten K_V7-Kanäle noch geschlossen sind.[54]

1.2.2 Therapeutisches Potenzial von K_V7-Öffnern

In Anbetracht der Vielzahl an physiologischen Funktionen, die von K_V7-Kanälen erfüllt werden, kommen diverse Indikationen für Substanzen infrage, die in der Lage sind, die Öffnungswahrscheinlichkeit von K_V7-Kanälen zu erhöhen. Auch hier liegt der Fokus dieser Arbeit wieder auf der Modulation von neuronalen K_V7-Kanälen und dem speziell daraus abgeleiteten therapeutischen Potenzial. Als mögliches Einsatzgebiet für K_V7-Öffner ist daher zuerst die Schmerztherapie zu nennen, für welche die umfangreichste Evidenz existiert. K_V7-Kanäle werden in primär afferenten Neuronen ebenso wie in Spinalnerven exprimiert und möglicherweise spielen sie auch in Gehirnbereichen eine Rolle, die an der Schmerzverarbeitung beteiligt sind.[20,55] Somit scheinen K_V7-Kanäle auf allen Ebenen des nozizeptiven Systems involviert zu sein, was sie zu idealen Zielen für die Behandlung von verschiedenen Schmerzzuständen macht.[56] Die Ergebnisse einer in vivo-Studie deuten demgegenüber an, dass der tatsächliche Wirkmechanismus von K_V7-Öffnern etwas eingeschränkter sein könnte. Demnach wird die Analgesie eventuell hauptsächlich über die Wirkung an peripheren sensorischen Nerven erreicht.[57] Gleichwohl ändert diese Einschränkung nichts an dem zweifelsfrei nachgewiesenen analgetischen Effekt von K_V7-Öffnern. So zeigten elektrophysiologische Untersuchungen, dass eine Aktivierung von K_V7-Kanälen die Erregbarkeit von nozizeptiven Neuronen reduziert und über diesen Mechanismus eine Unterdrückung der Schmerzübertragung möglich ist.[58,59] Ferner konnten in präklinischen Schmerzmodellen für K_V7-Aktivatoren eindeutig analgetische, antihyperalgetische und antiallodynische Effekte nachgewiesen werden.[60–62] Nicht zuletzt bestätigt auch die umfangreiche über 30-jährige humanmedizinische Erfahrung mit dem Wirkstoff Flupirtin K_V7-Kanäle als validierte Ziele für die Schmerzbehandlung. Die klinische Evidenz umfasst dabei sowohl die Therapie von akuten Schmerzen, z. B. in der postoperativen Behandlung, als auch die Linderung von subakuten Schmerzzuständen, wie etwa bei Beschwerden im Rückenbereich.[63,64] Weiterhin lassen sich mit vergleichbarer Effektivität chronische Schmerzformen, z. B. bei Osteoporose, durch K_V7-Öffner behandeln.[65] Darüber hinaus deuten präklinische Daten sogar auf eine Wirksamkeit bei neuropathischen Schmerzen hin, welche mit den derzeit verfügbaren Arzneistoffen oft nur unzureichend therapierbar sind.[66]

Neben der Schmerztherapie bietet sich der Einsatz von K_V7-Öffnern vor allem bei einer Reihe von Erkrankungen an, die im Wesentlichen auf einer neuronalen Übererregbarkeit beruhen. Die Fähigkeit von K_V7-Öffnern, eine überschießende Auslösung von Aktionspotenzialen zu unterbinden, prädestiniert sie insbesondere für die Anwendung als Antiepileptika. Verschiedene K_V7-Öffner

haben folglich ihre Wirksamkeit in einer ganzen Reihe von präklinischen Epilepsiemodellen gezeigt. Das experimentelle Set-up umfasste dabei sowohl chemisch als auch elektrisch induzierte Modelle für tonisch-klonische, komplex-partielle und sekundär-generalisierte Anfälle.[67–69] Einzig in einem Tiermodell, welches entwickelt wurde, um Absenceepilepsie zu simulieren, konnte für den K_V7-Öffner Retigabin kein Effekt nachgewiesen werden,[70] dennoch ist seine Wirksamkeit, insbesondere bei fokalen Anfällen, durch klinische Studien eindeutig belegt.[71]

Über die bereits etablierte Anwendung als Analgetika und Antiepileptika hinaus befinden sich K_V7-Öffner derzeit auch für weitere Indikationen in unterschiedlichen Phasen der präklinischen und klinischen Erprobung. Es konnte beispielsweise gezeigt werden, dass K_V7-Öffner die Dopaminfreisetzung von bestimmten Neuronen modulieren, die im ventralen tegmentalen Areal (VTA) an neuronalen Belohnungsmechanismen beteiligt sind. Damit kommen K_V7-Öffner prinzipiell für die Behandlung von Schizophrenie, Angstzuständen oder Depressionen sowie zur Suchttherapie in Betracht.[20] Als vielversprechend ist hier insbesondere das Potenzial von K_V7-Öffnern bei Depressionen einzustufen. Im Tiermodell konnte eine Hyperaktivierung von dopaminergen VTA-Neuronen, die mit schweren depressiven Störungen assoziiert ist, durch Anwendung des K_V7-Öffners Retigabin signifikant reduziert werden.[72] Eine offene klinische Pilotstudie zeigte zudem eine deutliche Verringerung von depressiven und anhedonischen Symptomen bei betroffenen Patienten nach Retigabinbehandlung.[73]

Abseits von diesen psychiatrischen Erkrankungen deuten in vivo-Daten aus Tiermodellen darauf hin, dass der frühzeitige Einsatz von K_V7-Öffnern außerdem die Folgen verschiedener Formen von Hirnschädigungen effektiv abmildern könnte. Dies umfasst sowohl Schädel-Hirn-Traumata als auch chronisch-stressinduzierte oder durch ischämische Ereignisse hervorgerufene Hirnverletzungen.[74–77] Diese initialen Schädigungen führen häufig zu Entzündungsreaktionen und einer neuronalen Übererregbarkeit, die im Verlauf weitere Folgeschäden verursachen können. K_V7-Öffner vermitteln ihren neuroprotektiven Effekt hier vermutlich durch Reduktion der pathologischen Übererregbarkeit. Nicht zuletzt wurde die Anwendung von K_V7-Öffnern auch bei neurodegenerativen Erkrankungen wie amyotropher Lateralsklerose (ALS) oder multipler Sklerose (MS) in klinischen Studien untersucht. Die Ergebnisse waren dabei jedoch sehr heterogen. Während der Einsatz eines K_V7-Öffners die bei ALS auftretende Übererregbarkeit von Motoneuronen erfolgreich reduzieren konnte, wurde bei MS kein neuroprotektiver oder den Krankheitsverlauf beeinflussender Effekt gefunden.[78,79]

1.2.3 Klinisch validierte K_V7-Öffner vom problematischen Triaminoaryltyp

Flupirtin

Das bereits erwähnte Analgetikum Flupirtin (**1**, Abbildung 3) war der erste zugelassene Arzneistoff, der hauptsächlich als Öffner von K_V7-Kanälen fungierte. Der genaue Wirkmechanismus war jedoch zunächst ungewiss und wurde erst einige Jahre nach seiner Markteinführung aufgeklärt.[80] Anfänglich war lediglich bekannt, dass die Analgesie weder über Opioidrezeptoren noch über eine Hemmung der Prostaglandinsynthese erreicht wird.[62,81] Diverse klinische Studien haben die Wirksamkeit und Verträglichkeit von Flupirtin im Vergleich zu anderen gängigen Analgetika wie Ibuprofen, Diclofenac oder Tramadol untersucht und kamen zu dem Schluss, dass Flupirtin vergleichbare schmerzlindernde Effekte erzielt und gleichzeitig besser verträglich ist als z. B.

Diclofenac oder Tramadol.[63,82] Neben einer schmerzlindernden Wirkung weist Flupirtin auch eine muskelrelaxierende Wirkkomponente auf,[83] welche wahrscheinlich zum Teil aus einem zusätzlichen Agonismus am $GABA_A$ Rezeptor resultiert.[84] Die simultanen muskelrelaxierenden und analgetischen Eigenschaften prädestinieren Flupirtin insbesondere für die Behandlung von schmerzhaften Muskelverspannungen und machen es zu einem einzigartigen Analgetikum.

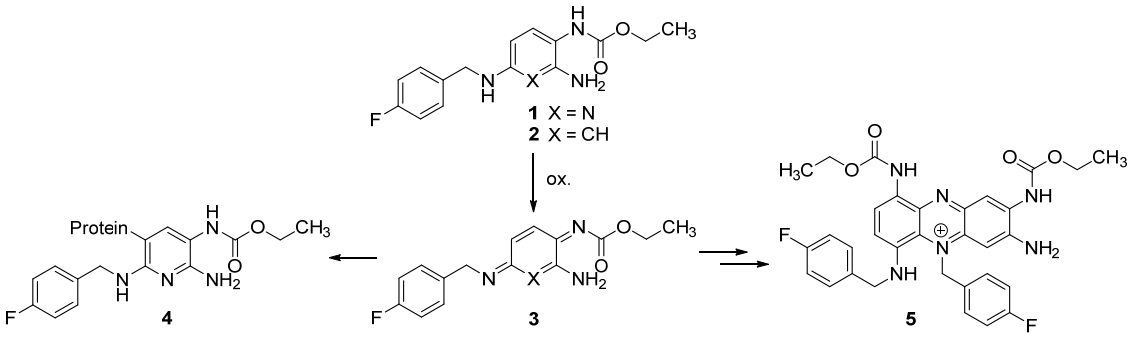

Abbildung 3. Strukturen von Flupirtin (**1**) bzw. Retigabin (**2**) und entsprechende *para*-Azachinondiimin- oder *para*-Chinondiimin-Metabolite (**3**). *Ortho*-Azachinondiimin- bzw. *ortho*-Chinondiimin-Oxidationsprodukte sind ebenfalls möglich aber hier nicht gezeigt. Die Toxifizierung erfolgt bei Flupirtin vermutlich über einen Haptenmechanismus unter Bildung von Flupirtin-Protein-Addukten (**4**). Retigabin bildet hingegen nach Oxidation, Dimerisierung und erneuter Oxidation wahrscheinlich Phenaziniumstrukturen (**5**), die für blaue Gewebepigmentierungen verantwortlich sind.

Insgesamt war Flupirtin in Deutschland mehr als 30 Jahre erfolgreich in der klinischen Anwendung und galt allgemeinhin als gut verträglicher Arzneistoff mit relativ milden Nebenwirkungen.[85] In den Jahren 2011 und 2012 wurden dann jedoch erste Berichte über Leberschäden unter Flupirtinbehandlung veröffentlicht.[86,87] Die schweren hepatotoxischen Ereignisse waren mit einer Melderate von 1,68 Fällen pro 100.000 Patientenjahren sehr selten, aber zwangen die zuständigen Behörden aufgrund der teilweise tödlichen Verläufe Anwendungsbeschränkungen für die Behandlung mit flupirtinhaltigen Arzneimitteln zu erlassen. Nachdem sich diese Maßnahmen als unzureichend erwiesen hatten, um die durch Flupirtin verursachten Leberschäden zu vermeiden, wurde in letzter Konsequenz Medikamenten mit dem Wirkstoff Flupirtin die Zulassung entzogen.[88] In der Schmerztherapie hinterließ Flupirtin seitdem eine bislang nicht geschlossene Behandlungslücke, denn es war eine wertvolle Alternative zu nichtsteroidalen Antirheumatika (NSAR) und schwachen Opioiden, da es weder wie NSARs Magen-Darm-Blutungen hervorgerufen hat, noch Nebenwirkungen wie Abhängigkeit, Obstipation oder Atemdepression verursachte, die bekanntermaßen mit Opioidanalgetika in Verbindung gebracht werden.[89]

Retigabin

Bei Retigabin (**2**, Abbildung 3) handelt es sich um ein strukturelles Analogon von Flupirtin, welches seine Wirkung ebenfalls über die Öffnung von K_V7-Kanälen vermittelt. Die Zulassung erfolgte 2011 zur Zusatzbehandlung von fokalen Anfällen bei erwachsenen Patienten mit Epilepsie und unzureichender Wirksamkeit anderer geeigneter Arzneimittel.[90] Retigabin ist ein pan-$K_V7.2$-5-Öffner, d. h., es verfügt lediglich über eine begrenzte K_V7-Subtypselektivität. So besteht zwar keine nennenswerte Affinität zu $K_V7.1$-Kanälen, was ein sicherheitsrelevantes Merkmal ist, da somit eine proarrhythmogene Wirkung ausgeschlossen werden kann, aber zwischen den übrigen Untereinheiten ($K_V7.2$-5) existieren hinsichtlich der Potenz nur marginale Unterschiede.[53,91,92]

Ähnlich wie Flupirtin agiert auch Retigabin zusätzlich als Agonist an $GABA_A$-Rezeptoren, was ebenfalls zur antikonvulsiven Wirkung beitragen könnte.[93]

Aufgrund des innovativen Wirkmechanismus sowie des im Vergleich zu anderen Antiepileptika geringen Interaktionspotenzials galt Retigabin bei seiner Markteinführung als sehr vielversprechender Wirkstoff.[94] Bereits kurze Zeit später wurde jedoch in Post-Marketing-Studien eine ungewöhnliche Nebenwirkung registriert. Die Langzeitbehandlung mit Retigabin führte bei einigen Patienten zu Blauverfärbungen der Haut und bestimmter Augengewebe.[95] Da die Folgen und die Reversibilität dieser Verfärbungen zunächst unklar waren und befürchtet werden musste, dass die Veränderungen am Auge die Sehfähigkeit beeinflussen, veröffentlichte die FDA einen Warnhinweis. Obwohl zusätzlich durchgeführte Studien nicht darauf hindeuteten, dass das Sehvermögen durch die Gewebeverfärbungen beeinträchtigt wird, wurde die Vermarktung von Retigabin durch den Hersteller wegen stark rückläufiger Anwendung 2017 eingestellt.[96]

Weitere Nachteile von Retigabin trugen wahrscheinlich ebenfalls zu seiner abnehmenden Bedeutung bei. Allem voran kann hier die mangelnde K_V7-Subtypselektivität genannt werden. Die daraus resultierende Aktivierung von K_V7.4/5-Kanälen in urogenitalen glatten Muskelzellen kann unter Umständen zu Harnverhalt führen, was für die betroffenen Patienten eine sehr unangenehme Nebenwirkung darstellt.[97,98] Weiterhin besitzt Retigabin im Vergleich zu anderen Antiepileptika nur eine relativ kurze Halbwertszeit von 6–8 h und erfordert daher eine dreimal tägliche Dosierung.[99] Zudem ist die Blut-Hirn-Schranken-Gängigkeit mit einem Gehirn-zu-Plasma-Konzentrationsverhältnis von 0,16 nicht optimal, was vergleichsweise hohe Dosen von bis zu 1200 mg pro Tag notwendig machte.[99,100] Alles in allem bot Retigabin jedoch trotz dieser Schwächen einen einzigartigen Wirkmechanismus für die Epilepsiebehandlung, der aktuell mangels alternativer Arzneistoffe nicht genutzt werden kann. Insbesondere bei der Pharmakotherapie von genetisch bedingten Epilepsieformen, die auf Mutationen in den KCNQ-Genen beruhen, kann Retigabin nicht adäquat durch andere Antiepileptika ersetzt werden. Folglich wurden bereits Stimmen laut, die eine Wiedereinführung von Retigabin zumindest für die personalisierte Therapie fordern.[101]

Ursachenanalyse der unerwünschten Arzneimittelwirkungen von Flupirtin und Retigabin

Die für die Marktrücknahme verantwortlichen unerwünschten Arzneimittelwirkungen (UAWs) von Flupirtin und Retigabin wurden in beiden Fällen näher untersucht. Für Flupirtin konnten zunächst in einem in vitro-Assay nach Oxidation durch Peroxidasen und Inkubation mit Glutathion entsprechende Flupirtin-Glutathion-Konjugate nachgewiesen werden.[102] Diese stabilen und isolierbaren Metabolite, bei denen Glutathion als Thioether kovalent an den zentralen Pyridinring von Flupirtin gebunden ist, gelten wiederum als indirekter Beweis für das Auftreten von Azachinondiimin-Intermediaten wie Verbindung **3** (Abbildung 3), die selbst zu reaktiv sind, um sie direkt zu detektieren. Eine Bestätigung dieser initialen in vitro-Ergebnisse erfolgte wenig später durch eine klinische Studie, welcher es gelang nach Verabreichung von Flupirtin an gesunde Probanden, den Nachweis von entsprechenden Mercaptursäurederivaten im Urin zu erbringen.[103,104] Da ein Zusammenhang zwischen der Bildung von reaktiven, chinoiden Metaboliten und Hepatotoxizität für eine ganze Reihe von Arzneistoffen bekannt ist,[105] kann mit hoher

Wahrscheinlichkeit davon ausgegangen werden, dass die Azachinondiimin-Metabolite in die Pathogenese der durch Flupirtin induzierten Leberschäden entscheidend involviert sind.

Darüber hinaus deuten jedoch die geringe Prävalenz der hepatotoxischen Reaktionen und das Fehlen einer klaren Dosisabhängigkeit darauf hin, dass eine zusätzliche Komponente am Pathomechanismus beteiligt ist.[88] Hier wurden zunächst genetische Polymorphismen metabolisierender Enzyme als Ursache in Betracht gezogen. Nachdem diese Vermutung jedoch weitestgehend ausgeschlossen werden konnte,[104] rückt die Theorie einer möglichen Beteiligung des adaptiven Immunsystems in den Fokus, welche im Wesentlichen durch zwei Fallstudien gestützt wird. So kam etwa eine Untersuchung von Lebergewebe betroffener Patienten zu dem Schluss, dass basierend auf klinischen und histologischen Merkmalen die Möglichkeit einer immunvermittelten Toxizität gegeben ist. Darüber hinaus konnte eine genetische Analyse ein bestimmtes Allel eines humanen Leukozytenantigens (HLA) als Risikofaktor für die Flupirtin-induzierte Hepatotoxizität identifizieren.[86,106] Ähnliche Zusammenhänge zwischen bestimmten HLA-Genvarianten und einer Arzneistoffhypersensitivität wurden auch für andere Substanzen wie z. B. Abacavir, Carbamazepin oder Flucloxacillin beschrieben.[107] Im Fall von Flucloxacillin wurden zudem Wirkstoff-Peptid-Konjugate als HLA-Liganden identifiziert, welche auf der Oberfläche von Antigen-präsentierenden Zellen vermutlich die arzneistoffspezifische Aktivierung der T-Zell-Antwort auslösen.[108] Dieser Nachweis wurde für Flupirtin noch nicht erbracht, aber die Vermutung liegt dennoch nahe, dass Flupirtin ebenso als Hapten fungieren könnte, welches nach Konjugation seiner reaktiven Azachinondiimin-Metabolite mit endogenen Trägerproteinen Addukte wie Verbindung **4** bildet, die dann eine toxische Autoimmunreaktionen hervorrufen. Die über einen solchen immunvermittelten Mechanismus ausgelöste idiosynkratische Form der Hepatotoxizität ist typischerweise sehr selten, nicht dosisabhängig und tritt oft mit zeitlicher Verzögerung auf,[109] wie es auch im Fall der Flupirtin-assoziierten Leberschäden beschrieben wurde.[88] Sie ist damit eindeutig von der intrinsischen Hepatotoxizität abzugrenzen, wie sie z. B. bei Paracetamol beobachtet wird, wo ein chinoider Metabolit direkt eine dosisbezogene, zellschädigende Wirkung vermittelt.[110]

Im Gegensatz zu Flupirtin ist der hepatische Metabolismus von Retigabin nicht durch Oxidation, sondern durch Phase-II-Reaktionen wie insbesondere N-Glucuronidierungen geprägt. Dementsprechend gibt es auch keine Hinweise auf eine Metabolisierung zu reaktiven Chinondiimin-Metaboliten oder mögliche hepatotoxische Wirkungen von Retigabin bei therapeutischer Dosierung.[90,111] Unter anderen Bedingungen abseits der Leber scheint Retigabin jedoch ebenfalls zu einem Chinondiimin-Intermediat wie Verbindung **3** oxidiert zu werden. Darauf deutet das Auftreten der Phenaziniumverbindung **5** hin, die in Rattenaugen nach Retigabinbehandlung mit Hilfe von MALDI-Imaging-Massenspektrometrie nachgewiesen wurde. Diese Substanz, welche im Verdacht steht, für die blaue Gewebeverfärbung verantwortlich zu sein, entsteht vermutlich aus Chinondiimin-Metaboliten von Retigabin durch Dimerisierung und erneute Oxidation. Interessanterweise wurden die Phenaziniumverbindungen bei Albinoratten, die kein Melanin bilden, nicht nachgewiesen, was darauf hindeutet, dass die Oxidation und/oder die Dimerisierung von Retigabin in Assoziation mit Melanin ablaufen oder zumindest eine lokale Anreicherung begünstigt wird.[112,113]

Zusammenfassend existieren derzeit also keine Hinweise, dass der Wirkmechanismus, d. h. die Öffnung von K_V7-Kanälen, bei den Pathomechanismen der Gewebeverfärbung bzw. Hepatotoxizität

eine Rolle spielt. Sowohl im Fall von Flupirtin als auch bei Retigabin sind die für das Scheitern verantwortlichen UAWs wahrscheinlich auf den substanzspezifischen Metabolismus zurückzuführen, der insbesondere das labile und oxidationsempfindliche Triaminoarylgrundgerüst betrifft, das die strukturell eng verwandten Arzneistoffe gemeinsam haben.

1.3 Entwicklung alternativer K_V7-Öffner

Bereits vor Bekanntwerden der oben beschriebenen kritischen UAWs von Flupirtin und Retigabin wurde aufgrund minderschwerer Unzulänglichkeiten, wie z. B. mangelnder K_V7-Subtypselektivität, kurzer Halbwertszeit und mäßiger Blut-Hirn-Schranken-Gängigkeit, an der Entwicklung von alternativen Wirkstoffen gearbeitet. Spätestens aber seit der Marktrücknahme der beiden K_V7-Öffner wurden diese Anstrengungen weiter intensiviert. Über die Jahre wurde so eine Vielzahl von experimentellen K_V7-Öffnern entwickelt, die unterschiedliche Stufen der präklinischen und klinischen Entwicklung erreichten, wobei keiner dieser Wirkstoffkandidaten bisher die Marktreife erlangt hat. Im Folgenden werden ohne Anspruch auf Vollständigkeit einige alternative K_V7-Öffner vorgestellt und Herausforderungen bei der Entwicklung aufgezeigt.

Prinzipiell lässt sich das Hauptproblem von Flupirtin und Retigabin, die oxidationsempfindliche Triaminoarylstruktur und die damit verbundene Bildung von chinoiden Oxidationsprodukten, bei der Entwicklung von neuen Wirkstoffen durch verschiedene Vorgehensweisen vermeiden. Eine Möglichkeit ist das Screening von Substanzbibliotheken, um K_V7-Öffner mit gänzlich neuartigen Chemotypen zu identifizieren. Ein solches Vorgehen führte z. B. zur Entdeckung des 4-Aminotetrahydrochinolin-Derivats ZK21 (**6**, Abbildung 4).[114] Auch der neuartige K_V7-Öffner GRT-X (**7**), der zudem einen innovativen dualen Wirkmechanismus besitzt und neben einer Modulation der K_V7-Aktivität ebenso eine Erhöhung der Synthese von protektiven Neurosteroiden bewirkt, hat keine nennenswerte strukturelle Ähnlichkeit mehr zu Flupirtin und Retigabin.[115] Sowohl ZK21 als auch GRT-X könnten somit verglichen mit den problematischen K_V7-Öffnern vom Triaminoaryltyp über verbesserte Sicherheitseigenschaften verfügen. Diese Annahme bedarf jedoch noch einer Bestätigung, denn beide Substanzen befinden sich erst am Anfang der präklinischen Entwicklung, und die Vergangenheit zeigt, dass vollständig neue Chemotypen auch das Risiko von unerwarteten Toxizitätsproblemen bergen. Dies war z. B. bei dem K_V7-Öffner PF-04895162 (**8**) der Fall, welcher zwar in verschiedenen Tiermodellen ein breites Spektrum an antiepileptischer Wirkung demonstrierte, aber auf der anderen Seite im menschlichen Organismus unerwartet die Gallensäurehomöostase störte und aus diesem Grund in einer Phase-I-Studie scheiterte.[116] Auch der vielversprechende, selektive $K_V7.2/3$-Öffner ICA-27243 (**9**), ein Vertreter der am Spannungssensor angreifenden Substanzen, offenbarte unvorhergesehene toxikologische Probleme. Die Verbindung führte im Tierversuch zu nicht-hämolytischen Anämien und wurde daher ebenfalls von der weiteren Entwicklung ausgeschlossen.[117]

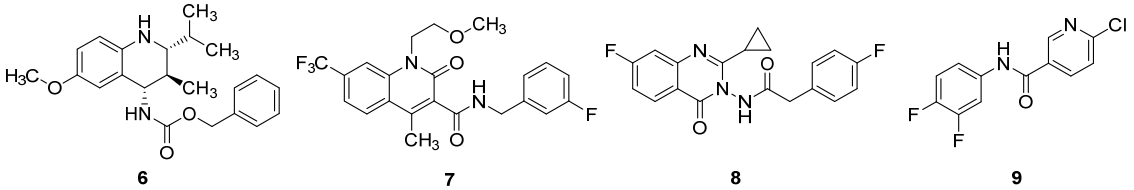

Abbildung 4. Auswahl von literaturbekannten K_V7-Öffnern mit neuartigen Chemotypen.

Ein alternativer Ansatz, um zu neuartigen K_V7-Öffnern zu gelangen, ist ein ligandenbasiertes Design unter Verwendung von Flupirtin und Retigabin als Leitstrukturen. Auf diese Weise können K_V7-Öffner mit verbesserten Eigenschaften durch kleinere strukturelle Änderungen erhalten werden. In der Literatur finden sich zahlreiche Beispiele für ligandenbasierte Ansätze, wobei, wie in Abbildung 5 ersichtlich ist, in vielen Fällen die Problematik der Bildung von chinoiden Metaboliten beim Design nicht ausreichend berücksichtigt wurde. So wird für den K_V7-Öffner HN37 (**10**) zwar eine verbesserte chemische Stabilität im Vergleich zu Retigabin angegeben, aber es besteht theoretisch noch immer die Möglichkeit der Entstehung von *para*-Chinondiimin-Oxidationsprodukten. Ungeachtet dieser Problematik ist HN37 derzeit Gegenstand einer Phase-I-Studie in China.[118] Auch der K_V7-Öffner Lu AA41178 (**11**), der sich in präklinischen Modellen für Epilepsie, Schizophrenie und Depression als effektiv erwies, besitzt trotz deutlicher struktureller Modifikationen noch immer ein Risiko für die Bildung von chinoiden Metaboliten.[119] Das Gleiche gilt für das erst kürzlich veröffentlichte Retigabinanalogon **12**.[120] Auf der einen Seite erwies sich dieses Derivat der Muttersubstanz in vielerlei Hinsicht überlegen. So wurden etwa ein besseres Gehirn-zu-Plasma-Konzentrationsverhältnis, eine längere Plasmahalbwertszeit und eine potentere Öffnung von K_V7-Kanälen beschrieben. Auf der anderen Seite ist jedoch das problematische Triaminobenzen-Grundgerüst nach wie vor enthalten und stellt ein erhebliches Sicherheitsrisiko dar. Bei XEN1101, einer Verbindung aus einer Reihe von Anilidderivaten mit Tetrahydroisochinolin-Substituenten (**13**),[121] wurde zwar im Vergleich zu Retigabin eine Aminogruppe entfernt, aber die Grundstruktur enthält gleichwohl ein *para*-Diaminobenzen-Strukturmotiv. Da die Substanz bereits Phase-II-Studien abgeschlossen hat, kann davon ausgegangen werden, dass keine akuten toxikologischen Probleme bestehen. Wie sich jedoch insbesondere bei Flupirtin gezeigt hat, werden sehr seltene Nebenwirkungen in kleineren Patientenkollektiven nicht zuverlässig erfasst. Es stellt sich also dennoch die Frage, ob nicht aus Sicherheitsgründen ein Verzicht auf das riskante *para*-Diaminobenzen-Strukturelement ratsamer gewesen wäre.

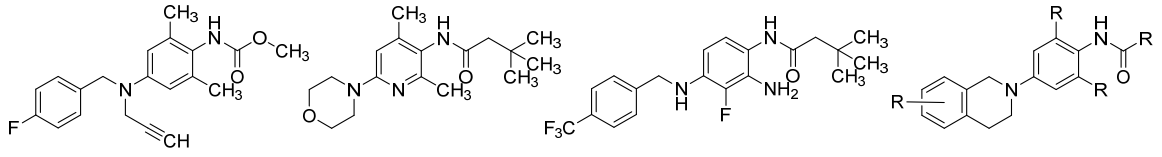

Abbildung 5. Auswahl von literaturbekannten K_V7-Öffnern, welche strukturell mit Flupirtin und Retigabin verwandt sind.

2 Zielstellung

K_V7-Öffner stellen in vielerlei Hinsicht vorteilhafte Behandlungsalternativen bei verschiedenen Erkrankungen dar, die eine Verminderung der neuronalen Erregbarkeit erfordern. Leider kann das vielversprechende Potenzial aktuell nicht genutzt werden, weil kein sicherer Arzneistoff mit diesem spezifischen Wirkmechanismus zur Verfügung steht. Das ist insofern bedauerlich, als dass die beiden klinisch validierten K_V7-Öffner vom Triaminoaryltyp nicht wegen ihres Wirkmechanismus, sondern wahrscheinlich hauptsächlich aufgrund ihrer oxidationsempfindlichen Struktur gescheitert sind. Aus diesem Grund war das Ziel dieser Arbeit, in einem retro-metabolischen Designansatz ausgehend von Flupirtin und Retigabin, oxidationsresistente Grundstrukturen zu entwickeln. Im Unterschied zu den ligandenbasierten Strategien, welche in Kapitel 1.2.4 erwähnt wurden, galt es dabei bedenkliche Strukturmotive wie ortho- oder para-ständige Aminogruppen gänzlich zu vermeiden, um die Bildung von Chinondiimin- oder Azachinondiimin-Oxidationsprodukten bereits durch das Design auszuschließen.

Um dieses Ziel zu erreichen, sollten im Wesentlichen zwei Strategien parallel verfolgt werden. Der erste Ansatz, welcher auf die in Abbildung 6 dargestellten Carba-Analoga mit der Grundstruktur **14** abzielte, basiert auf einer Invertierung der Aminomethylenfunktion der ursprünglichen Triaminoarylgrundstruktur kombiniert mit dem Austausch der primären Aminofunktion gegen eine Methylgruppe. Dies führt zusammengenommen zu einem aromatischen Kern, der nur noch einen stickstoffhaltigen Substituenten trägt. Die zweite Vorgehensweise sah eine Modifikation der Carbamatstruktur von Flupirtin und Retigabin zu Nicotinamid- bzw. Benzamidfunktionen vor, um Analoga mit der Grundstruktur **15** zu erhalten. Diese Carba-Derivate besitzen lediglich meta-ständige Aminogruppen, die in Bezug auf die Bildung von chinoiden Metaboliten unproblematisch sind.

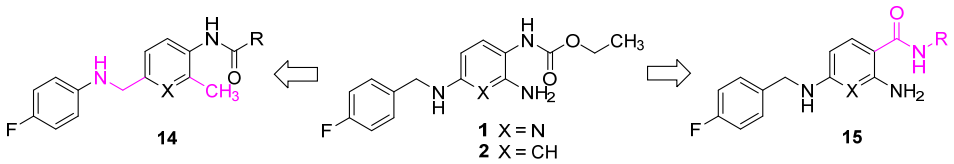

Abbildung 6. Strukturen von Flupirtin (**1**) und Retigabin (**2**) sowie Modifikationen (**14**/**15**), die ausgehend von der Triaminoaryl-Grundstruktur vorgenommen werden sollten, um die Bildung von Chinondiimin- bzw. Azachinondiimin-Oxidationsprodukten zu verhindern (X = N oder CH und R = Alkyl oder Benzyl).

Einem iterativen Zyklus aus Design, Synthese und biologischer Testung folgend, sollten beide Grundstrukturen im Anschluss weiter optimiert werden. Über eine Verbesserung von Substanzeigenschaften hinaus sollten in diesem Zusammenhang auch Erkenntnisse zu grundlegenden Struktur-Wirkungs-Beziehungen gewonnen werden. Ergänzt durch Dockingstudien können dadurch Hypothesen zu den Bindungsmechanismen der neuen Carba-Analoga erarbeitet werden, die perspektivisch eine Basis für die rationale Weiterentwicklung der Grundstrukturen bieten. Es stand jedoch nicht nur die biologische Aktivität im Fokus, sondern es galt auch potenzielle toxikologische Risiken der neuen Carba-Derivate auszuschließen, daher wurden alle Verbindungen zusätzlich in einem Zellviabilitätsassay charakterisiert. Basierend auf den kombinierten Aktivitäts- und Toxizitätsdaten sollten schließlich im Idealfall geeignete Analoga identifiziert werden, die für eine weitergehende Charakterisierung infrage kommen.

3 Methoden und Ergebnisse

3.1 Synthese ausgewählter Analoga von Flupirtin und Retigabin

Im Rahmen dieser Arbeit wurden insgesamt ca. 170 Substanzen erfolgreich synthetisiert. Daraus ergaben sich 48 Endverbindungen mit einer großen strukturellen Diversität, die für die biologische Testung bereitgestellt werden konnten. Die Synthesen der Carba-Analoga mit invertierter Aminomethylenfunktion (Grundstruktur **14**) sind in Publikation I enthalten, wohingegen die Publikationen II und III die Nicotinamid- und Benzamidanaloga (Grundstruktur **15**) sowie verwandte Verbindungen behandeln. Im Folgenden werden exemplarisch einige ausgewählte Synthesen aus verschiedenen Substanzklassen erläutert.

3.1.1 Carba-Analoga mit invertierter Aminomethylenfunktion

Die Synthese des ersten Carba-Analogons **21** wurde ausgehend vom kommerziell erhältlichen Pyridinderivat **16** in fünf Stufen realisiert (siehe Schema 1). Im initialen Schritt erfolgte die Einführung einer Nitrilfunktion über eine modifizierte Version der typischerweise kupferkatalysierten Rosenmund-von-Braun-Reaktion. Anstelle von CuCN wurde in diesem Fall jedoch eine Kombination aus Palladiumkatalysator und $Zn(CN)_2$ verwendet, was eine nahezu quantitative Ausbeute ermöglichte. Die Nitrogruppe der resultierenden Verbindung **17** wurde anschließend mit Eisen in Essigsäure reduziert, um das Aminopyridin **18** zu erhalten, das wiederum mit Isobutylchlorformiat zum Carbamat **19** umgesetzt wurde. Im nächsten Reaktionsschritt erfolgte die Reduktion der Cyanogruppe von Verbindung **19** mit Diisobutylaluminiumhydrid (DIBAL-H), die zunächst zu einem Iminintermediat (nicht gezeigt) führte und nach saurer wässriger Aufarbeitung den entsprechenden Aldehyd **20** in schlechter, aber dennoch ausreichender Ausbeute ergab. Abschließend wurde eine reduktive Aminierung mit 4-Fluoranilin und $NaBH_4$ durchgeführt, um die invertierte Aminomethylenfunktion der Zielverbindung **21** zu bilden.[122]

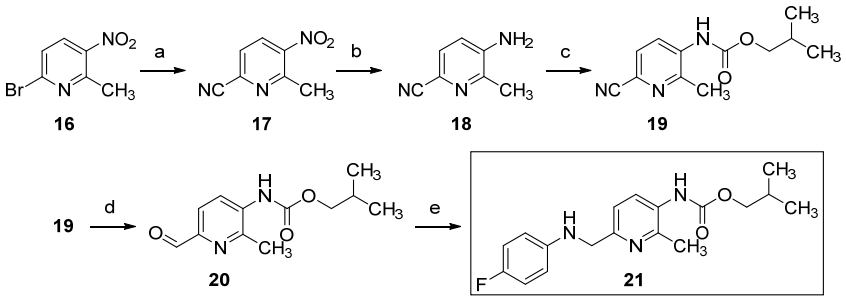

Schema 1. Synthese von Analogon **21**: a) $Zn(CN)_2$, $Pd(PPh_3)_4$, DMF, 70 °C, 24 h, 96 %; b) Fe, AcOH, $CaCl_2$, EtOH, 22 °C, 2 h, 71 %; c) Isobutylchlorformiat, TEA, 4-DMAP, DCM, 22 °C, 4 d, 34 %; d) DIBAL-H, DCM, −85 °C, 4 h, 23 %; e) 1. 4-Fluoranilin, DCM, 22 °C, 5 h, 2. $NaBH_4$, MeOH, 22 °C, 1 h, 82 %.

In vorangegangenen Arbeiten stellte sich heraus, dass mehrere Amidderivate von Flupirtin und Retigabin im Vergleich zu Carbamatanaloga eine überlegene K_V7-Öffnungsaktivität besaßen.[123,124] Außerdem deutet eine Metabolismusstudie darauf hin, dass die Carbamatfunktion von Flupirtin anfällig für die Spaltung durch Esterasen ist,[102,125] was wiederum die Vermutung zulässt, dass Amidderivate möglicherweise eine verbesserte metabolische Stabilität aufweisen. Aus diesem Grund wurden im nächsten Schritt Amidderivate mit der Grundstruktur **14** synthetisiert. Parallel

zur Einführung einer Amidgruppe wurde hier jedoch eine weitere Strukturänderung vorgenommen, die den zentralen aromatischen Ring betraf. Da Retigabin im Vergleich zu seinem Pyridinanalogon Flupirtin bei der $K_V7.2/3$-Öffnung ca. um den Faktor sieben potenter ist, besitzen die folgenden Derivate in Analogie zu Retigabin einen zentralen Phenylring (siehe Schema 2). Verwandte Verbindungen der in diesem Abschnitt behandelten Analoga **29a**-**d** sind auch in Patenten der Firma Lundbeck beschrieben, wobei allerdings nur begrenzte Informationen veröffentlicht wurden, sodass die Berücksichtigung des Substanztyps in dieser Arbeit gleichwohl neue Erkenntnisse zu Synthese, Struktur-Wirkungs-Beziehungen, in vitro-Toxizität und Oxidationsverhalten ermöglichte.[126,127]

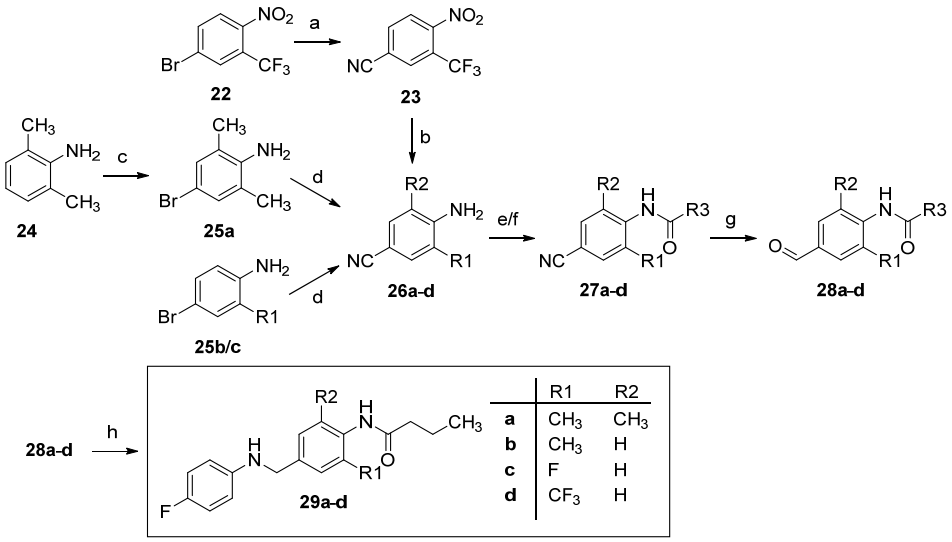

Schema 2. Synthese der Analoga **29a**-**d:** a) $Zn(CN)_2$, $Pd(OAc)_2$, PPh_3, DMF, 100 °C, 1,5 h, 83 %; b) $SnCl_2$, EtOAc, 70 °C, 0,5 h, 99 %; c) Br_2, DCM, −78–22°C, 1 h, 96 %; d) CuCN, NMP, 170 °C, 7–8 h, 42–47 %; e) 1. Butyrylchlorid, TEA, 4-DMAP, THF, 0 °C, 0,5 h, 2. 22/70 °C, 16 h–7 d, 56–74 % (**27a**,**d**); f) 1. Butyrylchlorid, TEA, DCM, 22 °C, 1 h, 2. 22 /40 °C, 3–89 h, 67–88 % (**27b**,**c**); g) Ni, HCOOH, 80 °C, 6–8 h, 37–88 %; h) 1. 4-Fluoranilin, Molekularsieb, Toluen, 120 °C, 4–8 h, 2. $NaBH_4$, MeOH, 1,4-Dioxan, 0–22 °C, 17 h, 42–73 %.

Die Synthesen der entsprechenden Analoga **29a**-**d** erfolgten, wie in Schema 2 ersichtlich, ausgehend von kommerziell erhältlichen 4-Bromanilinverbindungen. Für die Synthese eines 2,6-dimethylierten Derivats wurde das notwendige 4-Bromanilin **25a** zuvor durch Bromierung des Anilins **24** dargestellt. Nachfolgend wurden die 4-Bromaniline **25a**-**c** in einer Rosenmund-von-Braun-Reaktion unter Verwendung von CuCN, das eine Doppelfunktion als Katalysator und Cyanidquelle erfüllte, in die Nitrile **26a**-**c** überführt. Im Fall eines trifluormethylierten Analogons erfolgte die Synthese über einen abweichenden Weg. Ausgehend vom Nitrobenzenderivat **22**, wurde zuerst das Nitril **23** dargestellt, welches dann mit $SnCl_2$ zum Anilin **26d** reduziert wurde. Erneut ermöglichte eine palladiumkatalysierte Version der Rosenmund-von-Braun-Reaktion eine bessere Ausbeute (83 %) im Vergleich zum zuvor verwendeten kupferkatalysierten Verfahren (43–47 %). Im nächsten Schritt verliefen die Synthesewege wieder gleich, und es folgte für alle Derivate eine Amidkupplung. Da sich die als Edukte eingesetzten 4-Aminobenzonitrile **26a**-**d** aufgrund der elektronenziehenden Eigenschaften der Cyanogruppe und der sterischen Hinderung durch ortho-Substituenten als unreaktive Aminkomponenten erwiesen, waren erhöhte Temperaturen, lange Reaktionszeiten oder der zusätzliche Einsatz eines Katalysators (4-DMAP) notwendig, um ausreichende Umsetzungen zu erzielen. Die Nitrilfunktion der so erhaltenen Amide **27a**-**d** wurde anschließend mit Nickel in Ameisensäure reduziert, was die entsprechenden Aldehyde **28a**-**d** ergab.

Im letzten Reaktionsschritt wurde auch hier eine reduktive Aminierung mit Natriumborhydrid und 4-Fluoranilin durchgeführt, um die gewünschten Analoga **29a**-**d** zu erhalten.[122]

Ein Austausch des zentralen Pyridinrings gegen einen Phenylring, wie bei den Analoga **29a**-**d** realisiert, war naheliegend in Hinblick auf die K_V7-Öffnungsaktivität. Der Pyridinring hat allerdings wiederum attraktive physikochemische Eigenschaften. Aus diesem Grund wurde untersucht, ob ein invertierter Pyridinring, der gegenüber dem Substitutionsmuster von Flupirtin um 180° rotiert inkorporiert ist, besser toleriert wird und eventuell nicht zu einer Beeinträchtigung der K_V7.2/3-Öffnung führt. Die Synthese dieser neuartigen Analoga mit invertiertem Pyridinring wurde in sieben Stufen durchgeführt. Da der Methylsubstituent hier erst im letzten Reaktionsschritt eingeführt wurde, bot der in Schema 3 dargestellte Syntheseweg zudem auch die Möglichkeit, die Methylgruppe durch alternative Kohlenwasserstoffreste zu ersetzen.

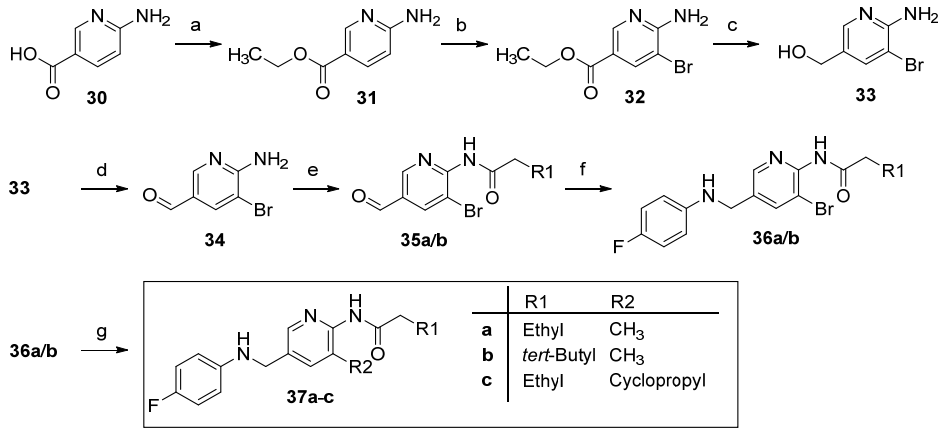

Schema 3. Synthese der Analoga **37a**-**c**: a) EtOH, $SOCl_2$, 90 °C, 18 h, 88 %; b) NBS, THF, 0–22 °C, 17 h, 77 %; c) $LiAlH_4$, THF, 22 °C, 5 h, 54 %; d) MnO_2, Toluen, 80 °C, 2 h, 41 %; e) Säurechlorid, DIPEA, DCM, 0–22 °C, 16,5–24,5 h 48–50 %; f) 1. 4-Fluoranilin, Toluen, Molekularsieb, 120 °C, 5 h, 2. $NaBH_4$, MeOH, 1,4-Dioxan, 0 °C, 17 h, 57–74 %; g) Trimethylboroxin oder Cyclopropylboronsäure, $Pd(PPh_3)_4$, Na_2CO_3, 1,4-Dioxan, H_2O, 140 °C, 75 min im Mikrowellenreaktor, 15–43 %.

Ausgangspunkt der Synthesen war 6-Aminonicotinsäure (**30**), welche in einer ersten Reaktion mit Ethanol und Thionylchlorid zum Ethylester **31** verestert wurde (siehe Schema 3). Die anschließende Bromierung, um Verbindung **32** zu erhalten, geschah durch eine Umsetzung mit *N*-Bromsuccinimid (NBS). Die Konvertierung des Ethylnicotinats **32** zum Aldehyd **34** erfolgte in diesem Fall nicht direkt, sondern wurde durch ein zweistufiges Verfahren realisiert. Im ersten Schritt wurde $LiAlH_4$ verwendet, um den Ethylester **32** zum entsprechenden Alkohol **33** zu reduzieren, der dann in der Folgereaktion unter Verwendung von aktiviertem Mangandioxid reoxidiert wurde, was schließlich den gewünschten Aldehyd **34** ergab. Diesem Reduktions-Oxidations-Verfahren folgte die Synthese der Amide **35a**/**b** unter Einsatz der erforderlichen Säurechloride. Anschließend wurde die Aldehydgruppe der resultierenden Amide in einem reduktiven Aminierungsverfahren mit 4-Fluoranilin gekuppelt, um die sekundären Amine **36a**/**b** darzustellen. Im letzten Schritt erfolgte die Einführung der Methylgruppe über eine Suzuki-Reaktion mit Trimethylboroxin als Methylquelle, wodurch die Endverbindungen **37a**/**b** erhalten wurden. Im Fall von Verbindung **37b** wurde zudem ein 3,3-Dimethylbutanamidsubstituent als eine sterisch anspruchsvollere Amidseitenkette gewählt, was in dieser Form beispielsweise auch von Lu AA41178 (**11**) bekannt ist.[119] Des Weiteren wurde das Analogon **37c** mit einem Cyclopropylrest anstelle der bei den Derivaten **37a**/**b** verwendeten Methylgruppe synthetisiert, um in diesem Bereich der Grundstruktur ebenfalls möglichen Platz für

einen raumfordernderen Substituenten zu eruieren. Die Synthese von Verbindung **37c** erfolgte dabei analog zu den Methylverbindungen unter Verwendung von Cyclopropylboronsäure anstelle von Trimethylboroxin.[122]

3.1.2 Carba-Analoga mit Nicotinamid- oder Benzamidstruktur

Das strukturell eng an Flupirtin angelehnte Nicotinamidanalogon **45b** wurde in einer dreistufigen Synthese ausgehend von 2,6-Dichlornicotinsäure (**42b**) erhalten (siehe Schema 4). Im ersten Schritt erfolgte die Darstellung von Verbindung **43b** durch die Einführung der primären Aminogruppe an Position 2 des Pyridinrings, was durch eine kupferkatalysierte Ullmann-artige Reaktion mit Natriumazid als Stickstoffquelle gelang. Diese Methode von Zhao et al. ermöglichte im Gegensatz zu einer zuvor durchgeführten Umsetzung mit Ammoniak die selektive Aminierung an Position 2 ohne Bildung des an Position 6 substituierten Regioisomers.[128] Nachfolgend wurde eine Amidkupplung mit Carbonyldiimidazol (CDI) als Kupplungsreagenz und *n*-Butylamin als Aminkomponente durchgeführt, um das Nicotinamid **44b** zu erhalten. Die anschließende nukleophile Substitution des verbleibenden Chloratoms mit 4-Fluorbenzylamin lieferte schlussendlich die Zielverbindung **45b**.

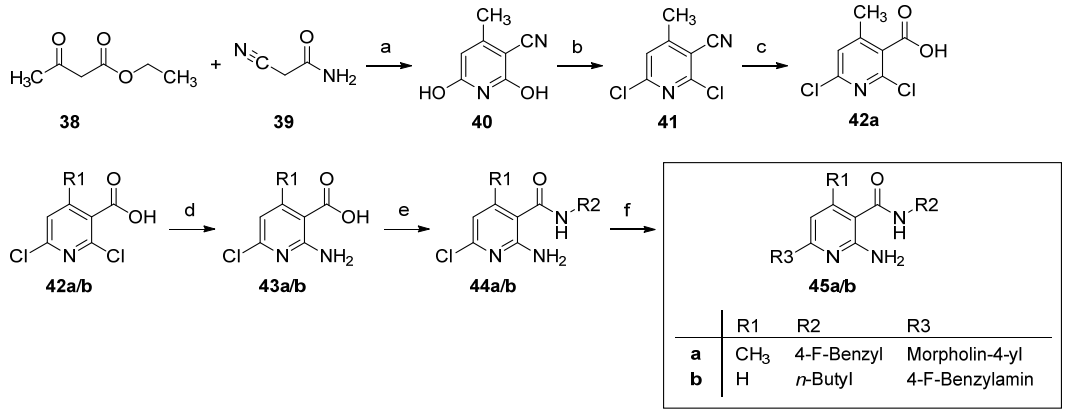

Schema 4. Synthese der Analoga **45a/b**: a) KOH, MeOH, 65 °C, 2 h, 75 %; b) BTMAC, $POCl_3$, 90 °C, 16 h, 55 %; c) H_2SO_4, HNO_3, 105 °C, 2 h, 77 %; d) NaN_3, K_2CO_3, CuI, Ethylendiamin, EtOH, Ar, Reflux, 11,5–28 h, 54–87 %; e) 1. CDI, THF, 50 °C, 1 h, 2. Amin, THF, 22 °C, 12 h, 35–55 %; f) Morpholin, NMP, 165 °C, 1–3 h im Mikrowellenreaktor, 16–73 %.

Bei der Synthese des alternativen Nicotinamidanalogons **45a** (Schema 4) wurde die von Flupirtin bekannte Grundstruktur deutlicher verändert, indem weitere Strukturelemente eingeführt wurden, die sich bei literaturbekannten K_V7-Öffnern mit anderer Grundstruktur als erfolgreich erwiesen hatten. Hierbei fiel die Wahl auf einen Morpholinring anstelle des 4-Fluorbenzylaminsubstituenten, wie er z. B. auch in Lu AA41178 (**11**) enthalten ist. Zudem wurde eine benzylische Amidseitenkette gewählt, die sich in einer Arbeit von Surur et al. als günstig erwiesen hat.[124] Auch eine Methylgruppe in ortho-Position zur Amidfunktion, wie sie sich beispielsweise in HN37 (**10**) findet, wurde der Grundstruktur hinzugefügt. Dieser zusätzliche Methylsubstituent ließ sich, wie in Schema 4 gezeigt, synthetisch durch eine Guareschi-Reaktion einführen, bei der Acetessigester und Cyanacetamid zu einem Pyridinderivat kondensierten.[129] Das resultierende Dihydroxypyridin **40** wurde anschließend durch Umsetzung mit Phosphorylchlorid zweifach chloriert, was das Dichlorpyridin **41** ergab. Danach erfolgte eine saure Hydrolyse der Cyanogruppe, um das Nicotinsäurederivat **42a** zu erhalten. Hier wurden verschiedene Hydrolyseverfahren evaluiert. Das beste Ergebnis lieferte die als Nitriersäure bekannte Mischung

aus konzentrierter Schwefelsäure und konzentrierter Salpetersäure, wobei eine Nitrierung des elektronenarmen Pyridinrings nicht zu befürchten war. Die weiteren Reaktionsschritte bis zum finalen Analogon **45a** erfolgten in analoger Weise, wie es bereits für die vorherige Nicotinamidverbindung **45b** beschrieben wurde.[130]

In den vorangegangenen Arbeiten von Surur et al. erwies sich zudem ein Austausch der primären Aminogruppe von Flupirtin bzw. Retigabin gegen einen Alkoxyrest als vorteilhaft für die K_V7.2/3-Öffnung,[124] daher wurde diese Strukturänderung im Folgenden auch auf ein Benzamidderivat angewendet. Die Synthese eines entsprechenden methoxysubstituierten Analogons erfolgte ausgehend von 4-Nitrotoluen (**46**), wie in Schema 5 dargestellt. Nach anfänglicher regioselektiver Bromierung des Edukts **46** wurde die Methylgruppe der resultierenden Verbindung **47** mit $KMnO_4$ zur Carboxyfunktion oxidiert, um das Benzoesäurederivat **48** zu erhalten. Es folgte eine Amidkupplung, bei der zunächst durch Umsetzung mit Thionylchlorid das Säurechlorid vom Intermediat **48** gebildet wurde, welches anschließend durch Reaktion mit 4-Fluorbenzylamin das Amid **49** ergab. Die Methoxyfunktion ließ sich im nächsten Schritt in einer kupferkatalysierten C-O-Kreuzkupplungsreaktion mit Methanol einführen. Nachfolgend wurde die aromatische Nitroverbindung **50** zum Anilinderivat **51** reduziert, welches wiederum nach einer reduktiven Aminierung die Zielverbindung **52** ergab.[130]

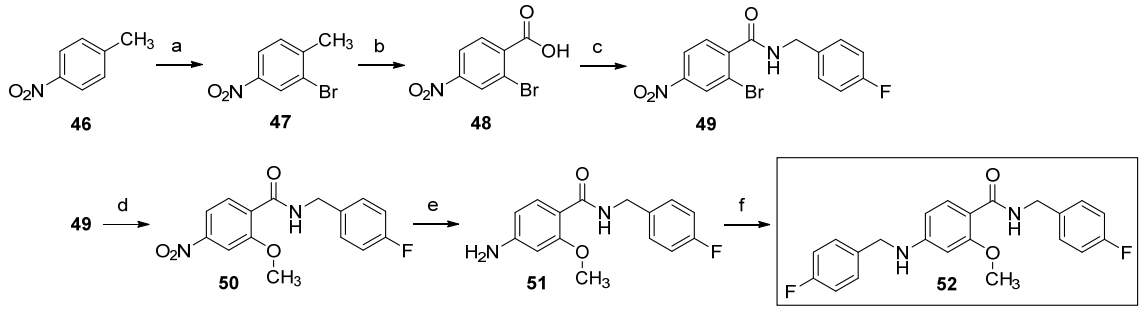

Schema 5. Synthese des Analogons **52**: a) Br_2, Fe, 80 °C, 1,5 h, 55 %; b) $KMnO_4$, H_2O, Pyridin, 100 °C, 17 h, 18 %; c) 1. $SOCl_2$, Toluen, 120 °C, 2,5 h, 2. 4-Fluorbenzylamin, TEA, DCM, 0–22 °C, 2,5 h, 42 %; d) MeOH, K_2CO_3, CuI, Ethylenediamin, N_2, 95 °C, 15 h, 51 %; e) $SnCl_2$, EtOAc, 80 °C, 30 min, 100 %; f) 1. 4-Fluorbenzaldehyd, Molekularsieb, Toluen, 120 °C, 5 h, 2. $NaBH_4$, 1,4-Dioxan, MeOH, 22 °C, 17 h, 69 %.

Die Neukombination von Partialstrukturen aus den Derivaten **45a**/**b** bzw. **52** und das Einführen von weiteren ausgewählten Strukturelementen ergab im Folgenden die Nicotinamidanaloga **55a**-**f** (siehe Schema 6). Anstelle eines Methoxysubstituenten wurden auch alternative Alkoxyreste ausgewählt, deren Einführung ausgehend von Verbindung **42a** über eine nukleophile Substitutionsreaktion erfolgte. Das als Nukleophil fungierende Alkoholat wurde in situ durch Umsetzung des entsprechenden Alkohols mit Natriumhydrid erzeugt. Die Substitutionsreaktion verlief aufgrund des dirigierenden Effekts der benachbarten Carboxygruppe mit ausgeprägter Regioselektivität an Position 2 des Pyridinrings.[131] Im nächsten Schritt erfolgte eine Amidkupplung, wobei die Aktivierung der Nicotinsäurederivate **53a**-**c** in diesem Fall über die Bildung von Säurechloriden in einer DMF-katalysierten Reaktion mit Oxalylchlorid erreicht wurde. Die Säurechloride wurden dann direkt mit den entsprechenden Aminen umgesetzt, um die gewünschten Amide **54a**-**d** zu erhalten. Die Einführung des Aminosubstituenten an Position 6 des Pyridinrings erfolgte im letzten Reaktionsschritt über eine erneute nukleophile Substitutionsreaktion, welche jedoch drastischere Reaktionsbedingungen als die vorangegangene erforderte

und daher durch mikrowellengestütztes Erhitzen auf 165 °C erfolgte.[130] 6-Morpholinonicotinamide wie die Verbindungen **55a**-**d** wurden zuvor bereits auch in einem Patent der Firma Grünenthal als K_V7-Öffner beschrieben. Es fehlte bisher allerdings eine umfassende Diskussion der zugrunde liegenden Struktur-Wirkungs-Beziehungen, welche in diesem Projekt im Kontext zu den weiteren Carba-Analoga ermöglicht werden konnte. Darüber hinaus wurde die bestehende Arbeit von Grünenthal um zuvor noch nicht berücksichtigte Strukturelemente erweitert, von denen einige vorbehaltlich einer eingehenderen Prüfung nicht mehr durch das entsprechende Patent beansprucht sein dürften.[132]

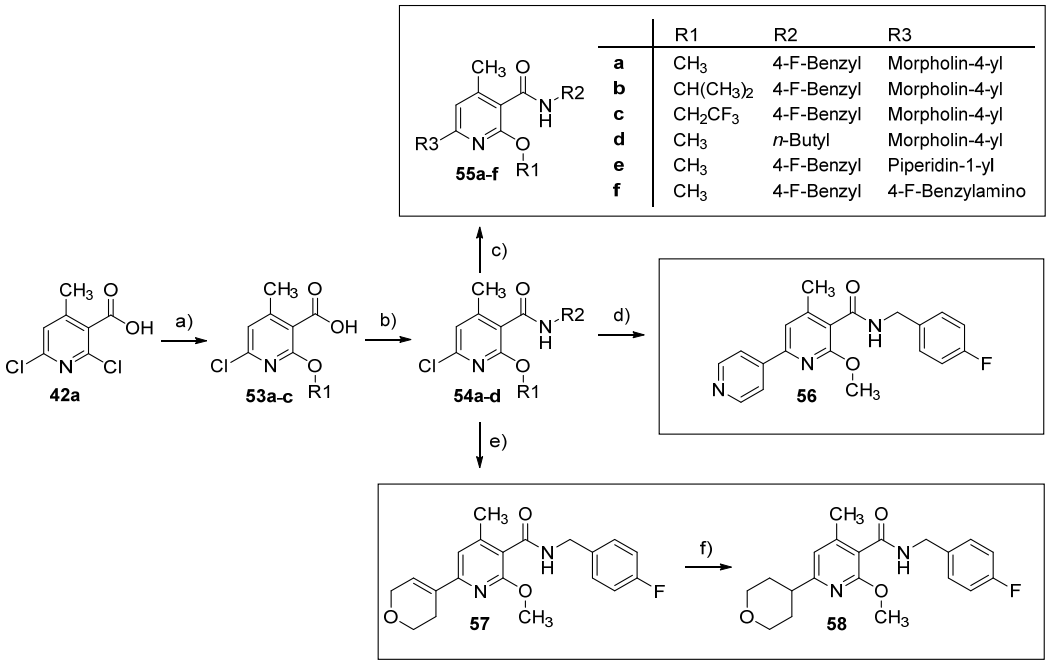

Schema 6. Synthese der Analoga **55**-**58**: a) Alkohol, NaH, THF, 0 °C–70 °C, 7–23 h, 96–99 %; b) 1. $(COCl)_2$, DMF, DCM, 0–22 °C, 3 h, 2. Amin, TEA, DCM, 0–22 °C, 16 h, 49–61 %; c) Amin, NMP, 165 °C, 0,5–1 h, 23–53 %; d) Pyridin-4-ylboronsäure, $Pd(PPh_3)_4$, Na_2CO_3, 1,4-Dioxan, H_2O, Ar, 140 °C, 30 min im Mikrowellenreaktor, 59 %; e) 1-Cyclohexenylboronsäure Pinacolester, $Pd(PPh_3)_4$, Na_2CO_3, 1,4-Dioxan, H_2O, Ar, 140 °C, 15 min, Mikrowellenreaktor, 86 %; f) H_2, Pd/C, MeOH, 22 °C, 5 h, 74 %.

Um die Rolle des Morpholinrings, der in diversen literaturbekannten K_V7-Öffnern mit unterschiedlicher Grundstruktur enthalten ist, näher zu untersuchen, wurde er in den Derivaten **56**, **57** und **58** durch verschiedene Carba-Analoga ersetzt (siehe Schema 6). Rückschlüsse über die Bedeutung des Morpholinstickstoffatoms sollten ein Tetrahydro-2*H*-pyran-Ring und ein 3,6-Dihydro-2*H*-pyran-Substituent liefern. Zudem wurde mit einem Pyridin-4-yl-Rest auch ein aromatischer und somit planarer Substituent ausgewählt, um die Struktur-Wirkungs-Beziehungen zu vervollständigen. Ein Piperidin-1-yl-Ring, der bereits bei Verbindung **55e** eingeführt wurde, sollte des Weiteren Erkenntnisse zur Relevanz des Morpholinsauerstoffatoms für die molekulare Erkennung durch die $K_V7.2/3$-Bindetasche generieren. Die für die Carba-Analoga **56**, **57** und **58** notwendige Knüpfung von C-C-Bindungen wurde, wie in Schema 6 dargestellt, über Suzuki-Reaktionen unter Verwendung der entsprechenden Boronsäure oder des Boronsäurepinacolesters realisiert. Der Tetrahydropyransubstituent im Fall von Analogon **58** wurde durch katalytische Hydrierung des Dihydropyranvorgängers **57** erhalten.

3.1.3 Carba-Analoga mit Nicotinamid-ähnlichen Strukturen

Wie in Kapitel 1.2.1 erwähnt, ist die Carbamatteilstruktur von Retigabin an der Ausbildung von Wasserstoffbrückenbindungen zur $K_V7.2$-Bindetasche beteiligt (Abbildung 2). Dementsprechend wurde eine analoge Funktion für die Amidgruppe der Benzamid- und Nicotinamidderivate vermutet. Durch strukturelle Variation der Amidpartialstruktur sollte ihre Bedeutung für die Interaktion mit der Bindungsstelle verifiziert werden. Zu diesem Zweck wurde die ursprüngliche Amidfunktion beispielsweise durch eine amidähnliche Struktur ersetzt, die zudem in ein anelliertes Ringsystem integriert ist. Das aus diesem Ansatz hervorgegangene Isoxazolo[5,4-*b*]pyridin-3-amin **65** ist in Schema 8 abgebildet und stellt im Prinzip ein konformationell eingeschränktes Amidmimetikum dar. Ein zweiter Modifikationsansatz zielte darauf ab, die Amidgruppe durch zyklische Amidbioisostere wie einen 1,2,4-Oxadiazol- oder einen 1,2,4-Triazolring zu ersetzen, was zu den Analoga **62** respektive **68** führte (siehe Schemata 7 und 8).

Die Synthese des Triazolanalogons **62** konnte, wie in Schema 7 dargestellt, in vier Schritten realisiert werden. Als Ausgangspunkt wurde das oben erwähnte Nicotinsäurederivat **53a** verwendet, welches im ersten Schritt durch Alkylierung mit Iodmethan in den entsprechenden Methylester **59** überführt wurde. Anschließend erfolgte die Substitution des Chloratoms von Verbindung **59** durch Morpholin. Die Methylesterfunktion des resultierenden Morpholinderivats **60** wurde darauffolgend einer Hydrazinolyse unterzogen, um das Hydrazid **61** zu erhalten. Im finalen Schritt wurde dann die Triazolsynthese nach einer Methode von Yeung et al. durchgeführt,[133] die eine einstufige, basenkatalysierte Kondensation eines Hydrazids, wie Verbindung **61**, mit einem Nitril vorsieht, wobei in diesem Fall 4-Fluorbenzonitril eingesetzt wurde, um das finale Analogon **62** zu erhalten.

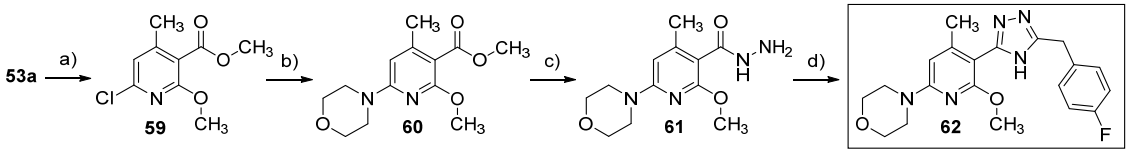

Schema 7. Synthese des Analogons **62**: a) CH_3I, K_2CO_3, DMF, 22 °C, 8 h, 98 %; b) Morpholin, TEA, NMP, 90 °C, 2 d, 39 %; c) N_2H_4*H_2O, MeOH, Reflux, 24 h, 67 %; d) 4-Fluorbenzonitril, K_2CO_3, *n*-BuOH, 150 °C, 4 h, Mikrowellenreaktor, 47 %.

Die Darstellung des Isoxazolo[5,4-*b*]pyridin-3-amin-Analogons **65** erfolgte, wie in Schema 8 dargestellt, in drei Stufen. Ausgangspunkt war in diesem Fall 2,6-Dichlor-4-methylnicotinonitril (**41**), dessen Chlorsubstituent in Position 6 durch Morpholin substituiert wurde. Die Umsetzung verlief regioselektiv mit einer Präferenz für Position 6, wie von Antczak et al. beschrieben.[134] Trotzdem wurde eine kleine Menge des an Position 2 substituierten Regioisomers gebildet. Das Produktgemisch wurde chromatographisch getrennt, und das gewünschte Regioisomer **63** wurde anschließend durch Reaktion mit Acetohydroxamsäure zyklisiert, um das entsprechende Isoxazolo[5,4-*b*]pyridin-3-amin **64** zu erhalten.[135] Im letzten Reaktionsschritt wurde dann durch Umsetzung der Aminogruppe von Verbindung **64** mit 4-Fluorbenzaldehyd ein Imin (nicht gezeigt) gebildet, das durch Hydrosilylierung mit Triethylsilan und Trifluoressigsäure ohne vorherige Isolierung zum sekundären Amin **65** reduziert wurde.

Die Synthese des Oxadiazolderivats **68** begann mit dem oben erwähnten Intermediat **63** (siehe Schema 8). Im ersten Schritt erfolgte die Einführung der Methoxygruppe durch Substitution des verbliebenen Chloratoms mit Natriummethoxid. Die Nitrilfunktion der auf diese Weise erhaltenen

Verbindung **66** wurde dann unter Verwendung einer wässrigen Hydroxylaminlösung in eine Amidoximgruppe überführt, was die Substanz **67** in nahezu quantitativer Ausbeute ergab. Diese Reaktion benötigte eine ungewöhnlich lange Zeit (4 Tage) bis zur vollständigen Konversion. Der Grund dafür war wahrscheinlich die ortho-Disubstitution relativ zur Nitrilgruppe und die daraus resultierende sterische Hinderung derselben. Ferner verringern die elektronenschiebenden Eigenschaften der Morpholin- und Methoxysubstituenten die Reaktivität der Nitrilfunktion für einen nukleophilen Angriff durch Hydroxylamin. Das Amidoxim **67** wurde anschließend durch Umsetzung mit Phenylessigsäurechlorid acyliert. Eine Isolierung des entsprechenden *O*-Acylamidoxim-Zwischenprodukts (nicht gezeigt) erfolgte nicht, sondern es wurde durch Zugabe von Tetrabutylammoniumfluorid (TBAF), das als Katalysator fungierte, direkt der Ringschluss zum Oxadiazolanalogon **68** induziert.[136]

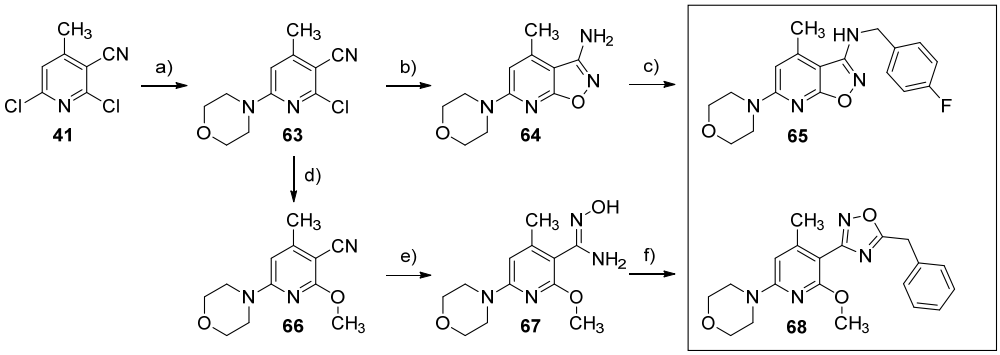

Schema 8. Synthese der Analoga **65**-**68**: a) Morpholin, MeOH, 0–22 °C, 16 h, 70 %; b) Acetohydroxamsäure, *t*-BuOK, Ar, DMF, 22–50 °C, 5,5 h, 43 %; c) 4-Fluorbenzaldehyd, $(C_2H_5)_3SiH$, TFA, DCM, 22–60 °C, 25 h, 80 %; d) NaOMe, MeOH, Reflux, 24 h, 90 %; e) Hydroxylamin, EtOH, H_2O, Reflux, 4 d, 99 %; f) 1. Phenylacetylchlorid, TEA, DCM, 0 °C, 1 h, 2. TBAF, THF, 22 °C, 2 h, 36 %; g) Ni, H_2, NH_3, MeOH, 50 °C, 5 h, 71 %; h) 4-Fluorbenzoylchlorid, TEA, DCM, 22 °C, 16 h, 64 %.

3.2 Bestimmung der K_V7.2/3-Öffnungsaktivität

Die K_V7-Kanalöffnungsaktivität der synthetisierten Analoga wurde mit HEK293-Zellen bestimmt, die den heterotetrameren K_V7.2/3-Kanal überexprimieren. Für diesen Zweck wurde ein kommerziell erhältlicher Assay verwendet, der auf einem thalliumsensitiven Fluoreszenzfarbstoff beruht und die Durchlässigkeit von K_V7-Kanälen für Thalliumionen nutzt. Die genaue Struktur des Fluoreszenzfarbstoffs wurde nicht offengelegt, aber es handelt sich dabei um einen Ester, der intrazellulär durch Esterasen gespalten wird, um so die thalliumkomplexierende Carboxyform freizusetzen. Diese aktivierte Verbindung generiert bei einem Thalliumeinstrom ein entsprechendes Fluoreszenzsignal, dessen Intensität proportional zur Anzahl der offenen K_V7-Kanäle ist und somit Aufschluss über ihre funktionelle Aktivität gibt. Die korrigierte Fluoreszenzintensität als Funktion der Substanzkonzentration wurde verwendet, um EC_{50}-Werte zu berechnen, welche die Konzentration ausdrücken, die erforderlich ist, um das halbmaximale Fluoreszenzsignal zu erreichen. Außerdem wurde die intrinsische Aktivität als Maß für die maximale Wirkstärke bestimmt. Sie beschreibt das prozentuale Verhältnis des maximalen durch eine Testsubstanz induzierten Fluoreszenzsignals zu dem maximalen Fluoreszenzsignal, das durch Flupirtin hervorgerufen wird. Eine Zusammenfassung der Aktivitätsdaten befindet sich in Tabelle 1.

Tabelle 1. K_V7.2/3-Öffnung, in vitro-Toxizität und log$D_{7,4}$-Werte der Analoga im Vergleich zu Flupirtin und Retigabin.[a]

		HEK293	HEK293	TAMH	TAMH	HEP-G2	HEP-G2	
Nr.	log$D_{7,4}$[b]	EC_{50}[c] [µM]	E_{max}[d] [%]	LD_{50}[e] [µM]	LD_{25}[f] [µM]	LD_{50}[e] [µM]	LD_{25}[f] [µM]	LD_{25}/ EC_{50}[g]
Flu	2,1	1,837 ± 0,844	100	487 ± 51	103 ± 47	547 ± 111	74 ± 40	40
Ret	2,1	0,249 ± 0,052	119 ± 7	>400	>400	>400	269 ± 166	1080
21	3,4	4,123 ± 3,945	94 ± 15	>250	76 ± 15	>250	136 ± 38	18
29a	3,0	0,143 ± 0,020	143 ± 7	>125	>125	>125	>125	875
29b	2,9	0,675 ± 0,276	176 ± 14	>125	>125	>125	88 ± 9	88
29c	3,0	1,505 ± 0,364	167 ± 16	>63	>63	>63	>63	42
29d	3,0	0,362 ± 0,093	156 ± 14	>125	>125	>125	75 ± 17	207
37a	2,3	4,840 ± 2,907	89 ± 32	>125	110 ± 54	>125	46 ± 24	10
37b	3,0	0,677 ± 0,419	153 ± 12	>125	>125	>125	66 ± 27	97
37c	2,8	2,015 ± 1,195	138 ± 20	>125	76 ± 52	>125	55 ± 17	27
45a	2,2	6,858 ± 1,319	113 ± 28	>500	349 ± 36	>500	123 ± 73	18
45b	2,7	-[h]	-[h]	>125	>125	>125	56 ± 40	-
52	4,3	-[h]	-[h]	>8	>8	>8	>8	-
55a	3,0	0,117 ± 0,029	144 ± 11	>63	>63	>63	>63	539
55b	3,8	0,017 ± 0,009	132 ± 16	>31	>31	>31	15 ± 1	882
55c	3,3	0,012 ± 0,004	117 ± 19	>15	>15	>15	>15	1250
55d	2,6	3,799 ± 1,730	170 ± 4	>250	>250	>250	>250	66
55e	4,7	0,040 ± 0,007	127 ± 1	>31	>31	>31	32 ± 10	775
55f	4,1	0,310 ± 0,119	105 ± 12	>63	>63	>16	>16	52
56	2,7	0,500 ± 0,105	112 ± 11	>63	>63	>63	26 ± 20	52
57	3,1	0,143 ± 0,003	111 ± 11	>125	>125	>63	>63	440
58	3,1	2,402 ± 0,759	129 ± 16	>125	>125	>125	>125	52
62	3,3	2,245 ± 0,338	149 ± 25	>30	>30	>30	>30	13
65	3,2	-[h]	-[h]	>125	>125	>125	>125	-
68	4,7	1,179 ± 0,193	45 ± 4	>30	>30	>30	>30	25

[a] Alle Werte sind Mittelwerte von mindestens drei unabhängigen Bestimmungen. [b] log$D_{7,4}$-Werte wurden mit einer HPLC-basierten Methode bestimmt. [c] Notwendige Konzentration, um die halbmaximale K_V7.2/3-Öffnung zu erhalten. [d] Maximale K_V7.2/3-Öffnung relativ zur maximalen K_V7.2/3-Öffnung von Flupirtin. [e] Konzentration, die notwendig war, um die Zellviabilität verglichen mit unbehandelten Kontrollen auf 50 % zu reduzieren. [f] Konzentration, die notwendig war, um die Zellviabilität verglichen mit unbehandelten Kontrollen auf 75 % zu reduzieren. [g] Für die Berechnung des LD_{25}/EC_{50} Verhältnisses wurde der geringere der beiden LD_{25} Werte verwendet. [h] Keine K_V7.2/3-Öffnung bis zu einer Konzentration von 20 µM.

3.3 Bestimmung von in vitro-Toxizität und Oxidierbarkeit

Um die strukturell teilweise deutlich von Flupirtin und Retigabin abgewandelten Analoga auf mögliche toxikologische Risiken hin zu untersuchen, wurden alle Verbindungen in einem Zellviabilitätsassay analysiert. Die für den Assay eingesetzten humanen Hep-G2 bzw. murinen TAMH Zellen sind hepatischen Ursprungs und für in vitro-Toxizitätstests etabliert.[137,138] Der Nachweis der Zellviabilität mit dem verwendeten MTT-Assay basiert auf der in lebenden Zellen stattfindenden mitochondrialen Reduktion des gelben, wasserlöslichen 3-(4,5-Dimethylthiazol-2-yl)-2,5-diphenyltetrazoliumbromids (MTT) zu einem blauvioletten, wasserunlöslichen Formazan, das durch kolorimetrische Messung quantifiziert werden kann.[139] Ein limitierender Faktor bei der

durchgeführten Toxizitätsprüfung war für viele Analoga die Wasserlöslichkeit. Die meisten Verbindungen erwiesen sich zudem als eher untoxisch, sodass LD_{50}-Werte nur selten ermittelt werden konnten, da die erforderlichen hohen Konzentrationen nicht erreicht wurden, ohne dass die Substanzen im Assaysystem präzipitierten. Aus diesem Grund wurden alternativ die weniger gebräuchlichen LD_{25}-Werte berechnet, welche die Konzentration angeben, bei der die Zellviabilität auf 75 % reduziert wurde. Die Ergebnisse des MTT-Assays sind ebenfalls in Tabelle 1 zusammengefasst.

Oxidationsstabilität ist ein Schlüsselmerkmal für neue Derivate von Flupirtin und Retigabin, da das oxidationsempfindliche Triaminoarylgrundgerüst der Hauptschwachpunkt beider Wirkstoffe zu sein scheint. Aus diesem Grund wurden einige Analoga hinsichtlich ihrer Oxidierbarkeit untersucht. Da für Flupirtin und Retigabin zwei unterschiedliche Oxidationsmechanismen berücksichtigt werden müssen, erschien die elektrochemische Oxidation mit Hilfe von Cyclovoltammetrie als ein praktikables Verfahren, um einen ersten Eindruck von der allgemeinen Oxidationsempfindlichkeit der Analoga zu gewinnen. Diese Methode wurde bereits verwendet, um das elektrochemische Oxidationsverhalten anderer oxidativ toxifizierbarer Wirkstoffe, wie z. B. Paracetamol oder Diclofenac, zu untersuchen.[140] Darüber hinaus konnte gezeigt werden, dass bei einer elektrochemischen Oxidation prinzipiell ein vergleichbares Produktspektrum wie bei einer Inkubation mit Lebermikrosomen erhalten wird.[141] Die mit der Cyclovoltammetrie bestimmten anodischen Peakpotenzialwerte der Carba-Derivate mit invertierter Aminomethylenfunktion finden sich in Tabelle 2. Um neben der allgemeinen Oxidationsempfindlichkeit zusätzlich das Risiko der Analoga für die Bildung von chinoiden Metaboliten einschätzen zu können, wurde XenoSite genutzt. Dabei handelt es sich um eine in silico-Methode, die auf einem Deep-Learning-Ansatz basierend die Vorhersage der metabolischen Entstehung verschiedener Chinonspezies ermöglicht.[142] Die vorhergesagten Molekülchinonbildungsscores (MQS) sind ebenfalls in Tabelle 2 enthalten, wobei ein Wert von 0,52 als Grenzwert gilt, oberhalb dessen eine Verbindung mit großer Wahrscheinlichkeit chinoide Metaboliten bildet.

Tabelle 2. Untersuchungen zur Oxidierbarkeit von Flupirtin, Retigabin und der Analoga **21**-**37c**, einschließlich durch Cyclovoltammetrie bestimmte anodische Peakpotenzialwerte ($E_{p.a.}$) und in silico-Molekülchinonbildungsscores (MQS).

Nr.	E_{pa} [mV]	MQS	Nr.	E_{pa} [mV]	MQS
Flu	306	0,91	**29c**	643	0,73
Ret	260	0,94	**29d**	663	0,56
21	648	0,87	**37a**	678	0,42
29a	633	0,50	**37b**	663	0,45
29b	618	0,57	**37c**	678	0,34

4 Diskussion

4.1 K_V7.2/3-Öffnungsaktivität

Die K_V7.2/3-Aktivitätsdaten der im Rahmen dieser Arbeit entstandenen Analoga zeigen ein bemerkenswert heterogenes Bild, denn es wurden sowohl inaktive als auch im nanomolaren Bereich aktive Substanzen erhalten. Diese deutlich abgestuften Ergebnisse ermöglichten es, valide Struktur-Wirkungs-Beziehungen abzuleiten, die in Kapitel 4.2 in Auszügen diskutiert werden. Interessanterweise waren nicht nur bei den Analoga mit invertierter Aminomethylenfunktion, sondern auch bei den Nicotinamidderivaten die anfänglich synthetisierten Verbindungen **21** bzw. **45b** lediglich schwach aktiv oder gänzlich inaktiv, obwohl sie unter allen Substanzen die geringsten strukturellen Änderungen im Vergleich zu Flupirtin aufweisen. Diese Aktivitätseinbußen deuten an, dass die Veränderungen der Grundstruktur, die auf eine Verbesserung der Oxidationsstabilität ausgelegt waren, zunächst nachteilige Auswirkungen auf die K_V7.2/3-Öffnung hatten. Im Fall beider Grundstrukturen gelang es aber nachfolgend, durch weitere Modifikationen die initialen Aktivitätsverluste zu kompensieren. Schließlich wurden sogar Analoga erhalten, welche die Leitstrukturen Flupirtin und Retigabin hinsichtlich der K_V7.2/3-Öffnung deutlich übertrafen. Das gilt sowohl in Hinblick auf die Potenz, bei der ein EC_{50}-Wert von 0,012 µM erreicht wurde, als auch für die intrinsische Aktivität, die auf bis zu 176 % gesteigert werden konnte.

Aktuell liegen zur Beurteilung der biologischen Aktivität der Analoga nur die Daten des K_V7.2/3-Kanals vor. Perspektivisch ist jedoch ebenfalls eine Testung an den anderen K_V7-Subtypen angedacht, die zum Teil auch bereits begonnen hat. Kenntnisse über das Selektivitätsprofil der Substanzen sind für eine Weiterentwicklung notwendig, denn eine Erhöhung der Öffnungswahrscheinlichkeit von kardialen K_V7.1-Kanälen muss bei therapeutischer Dosierung unbedingt ausgeschlossen werden, da andernfalls gefährliche proarrhythmogene Effekte zu befürchten wären.[143] Wünschenswert ist auch eine möglichst geringe Affinität der Analoga zu den K_V7.4/5-Untereinheiten, da vermutlich hauptsächlich über diese Subtypen der für Retigabin als Nebenwirkung beschriebene Harnverhalt vermittelt wird.[97,98] Neben einer Ausweitung der Testung auf die anderen K_V7-Kanaltypen ist auch eine Verifizierung von ausgewählten Ergebnissen des in dieser Arbeit verwendeten fluoreszenzbasierten Aktivitätsassays durch Patch-Clamp-Messungen ratsam, denn die Methode gilt für die Beurteilung der funktionellen Aktivität von Ionenkanälen nach wie vor als Goldstandard.[144] Im Unterschied zum fluoreszenzbasierten Verfahren erlaubt es diese Technik, die Interaktion von Ligand und Ionenkanal bei variablen Potenzialen und somit unterschiedlichen konformationellen Zuständen des Kanals zu studieren, was zusätzliche Rückschlüsse über den Mechanismus eines Kanalmodulators zulässt.

4.2 Struktur-Wirkungs-Beziehungen

4.2.1 Relevanz der Amidpartialstruktur für die K_V7.2/3-Öffnung

Mehrere literaturbekannte K_V7-Öffner, wie beispielsweise die Verbindungen **10** oder **11**, besitzen zwei zur Amidfunktion ortho-ständige Methylgruppen und auch in dieser Arbeit konnte der günstige Einfluss einer ortho-Disubstitution relativ zur Amidstruktur auf die K_V7.2/3-Öffnung bestätigt werden. Bei den Carba-Analoga mit invertierter Aminomethylenfunktion führte der Einbau einer

zweiten Methylgruppe im Fall von Derivat **29a** zu einer Reduktion des EC_{50}-Wertes um den Faktor 4,7 verglichen mit dem direkten Monomethylanalogon **29b**. Bemerkenswerterweise schien dieser Effekt bei den Nicotinamid- und Benzamidanaloga sogar noch erheblich ausgeprägter zu sein. Hier machte die zusätzliche ortho-Methylgruppe den Unterschied zwischen kompletter Inaktivität und submikromolarem EC_{50}-Wert aus, wie der Vergleich der Verbindungen **52** und **55f** verdeutlicht.

In Publikation II konnte mithilfe von Dockingstudien gezeigt werden, dass die Amidfunktion der Derivate **52** und **55f** im gebundenen Zustand in der K_V7.2/3-Bindetasche wahrscheinlich um ca. 90° aus der Ebene des benachbarten aromatischen Rings gedreht ist. Nur in dieser Konformation kann die Amidstruktur mit dem Carbonylsauerstoffatom von L338 und der Indol-NH-Gruppe von W236 zwei Wasserstoffbrückenbindungen eingehen, die in analoger Weise auch für die anderen Nicotinamidderivate sowie für die Carba-Analoga mit invertierter Aminomethylenfunktion vorhergesagt wurden (siehe Abbildung 7A). Die Bedeutung dieser konservierten Wasserstoffbrückenbindungen, die ebenfalls durch die Carbamatgruppen von Flupirtin und Retigabin ermöglicht werden, offenbart insbesondere ein Vergleich der Analoga **62** und **68**. Das Triazolderivat **62** ist in der Lage, in Analogie zu den Amidverbindungen beide Wasserstoffbrückenbindungen auszubilden, wohingegen das Oxadiazolanalogon **68** nur eine der beiden Interaktionen eingehen kann (siehe Publikation III). Vermutlich aus diesem Grund befand es sich mit einer intrinsischen Aktivität von lediglich 45 % an der Grenze zur Inaktivität, während die Triazolverbindung **62** sogar einen deutlich verbesserten E_{max}-Wert von 149 % erreichte.

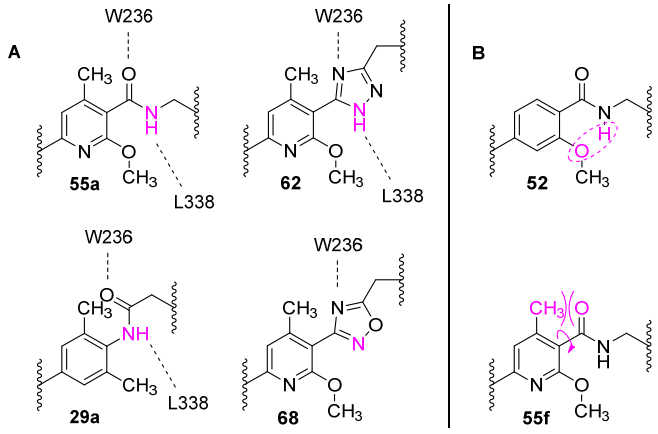

Abbildung 7. A: Durch Docking vorhergesagte Wasserstoffbrückenbindungen (gestrichelte Linien) der Amidfunktion des Nicotinamidanalogons **55a** und des Anilidderivats **29a** zur K_V7.2/3-Bindetasche im Vergleich zum Triazol- und Oxadiazolderivat (**62**/**68**). B: Stabilisierung einer koplanaren Ausrichtung der Amidfunktion durch eine intramolekulare Wasserstoffbrückenbindung bei Analogon **52** und Einfluss der zusätzlichen ortho-Methylgruppe auf den Torsionswinkel der Amidfunktion bei Verbindung **55f**.

Wieder Bezug nehmend auf das inaktive Benzamidanalogon **52**, konnte in Publikation II durch Moleküldynamiksimulationen gezeigt werden, dass die gedrehte Konformation der Amidgruppe, welche die gleichzeitige Ausbildung von beiden potenziell wichtigen Wasserstoffbrückenbindungen erst ermöglicht, in diesem Fall energetisch sehr ungünstig ist. Eine intramolekulare Wasserstoffbrückenbindung zwischen der Methoxygruppe und der Amidfunktion stabilisiert im Gegenteil eine unvorteilhafte koplanare Ausrichtung der Amidstruktur zum benachbarten Aromaten (Abbildung 7B). Die zusätzliche Methylgruppe des submikromolar aktiven Nicotinamidanalogons **55f** hingegen erzwingt durch sterische Wechselwirkungen mit dem Carbonylsauerstoffatom einen Torsionswinkel der Amidgruppe, der in guter Übereinstimmung mit dem für den gebundenen

Zustand vorhergesagten 90°-Winkel ist. Die Bindung von Analogon **55f** in die K_V7.2/3-Bindetasche wird in diesem Fall also durch eine Präorganisation der erforderlichen Molekülgeometrie begünstigt, welche den Entropieverlust bei der Ligandenbindung reduziert. Das Gleiche gilt wahrscheinlich auch für das erwähnte Anilidderivat **29a** sowie für alle weiteren K_V7-Öffner mit einer ortho-disubstituierten Amidgruppe. Zusätzliche Evidenz für den vermuteten Bindungsmodus, der eine Rotation der Amidfunktion vorsieht, lieferte zudem auch das konformationell eingeschränkte Amidmimetikum **65**. Die Integration einer amidähnlichen Struktur in ein anelliertes Ringsystem erzwingt in diesem Fall die als ungünstig angenommene koplanare Anordnung, was mit der fehlenden K_V7.2/3-Öffnungsaktivität von Verbindung **65** korreliert.

4.2.2 Bedeutung der Molekülgeometrie bei der Variation des 4-Fluorbenzylaminbereichs

Die bevorzugte Orientierung des 4-Fluorphenylrings von entsprechenden Analoga in Relation zum zentralen aromatischen Ring beeinflusst maßgeblich die K_V7.2/3-Öffnung. Dies wird insbesondere bei Betrachtung des in Abbildung 8 dargestellten Analogons **69** deutlich, dessen Synthese in Publikation I beschrieben ist und hier nicht näher erläutert wurde. Verbindung **69** war eine Vorstufe auf dem Weg zur Entwicklung der Carba-Analoga mit der Grundstruktur **14**. Es besitzt als strukturelle Besonderheit einen Ethylenlinker und wies mit einem EC_{50}-Wert von >10 µM lediglich eine schwache K_V7.2/3-Öffnung auf. Diese deutlichen Aktivitätseinbußen, verglichen mit Flupirtin und Retigabin, waren unerwartet, denn in der KryoEM-Struktur von Retigabin im Komplex mit dem K_V7.2-Kanal deutete nichts auf eine direkte Interaktion der sekundären Aminofunktion mit der Bindetasche hin, sodass ihr Austausch gegen eine Methylengruppe theoretisch möglich sein sollte. In der Konsequenz musste der Aktivitätsverlust von Analogon **69** also auf Ursachen in der Molekülgeometrie zurückzuführen sein. Anhand der Modellsubstanz 1,2-Diphenylethan konnte schließlich mit Moleküldynamiksimulationen gezeigt werden, dass Verbindung **69** durch den Ethylenlinker wahrscheinlich eine antiperiplanare Konformation bevorzugt, d. h., der 4-Fluorphenylring und der zentrale Pyridinring sind ungefähr in einer Linie ausgerichtet. Der Aminomethylenlinker von Retigabin hingegen begünstigt eine gewinkelte Konformation, die in etwa auch der Molekülgeometrie im gebundenen Zustand an den K_V7.2-Kanal entspricht. Darauf deutet die Analyse des Konformationsraums von *N*-Benzylanilin als Modellsubstanz hin, die in Abbildung 8 dargestellt ist. Für die Entwicklung der Carba-Analoga musste also ein alternatives Strukturelement gefunden werden, da sich ein Ethylenlinker wie bei Verbindung **69** als ungeeignet erwiesen hat. Durch die Invertierung des Linkerelements von Retigabin gelang es schließlich, trotz Entfernung der sekundären Aminofunktion vom zentralen aromatischen Ring, einen Amino-methylenlinker zu erhalten, der die als vorteilhaft angenommene, gewinkelte Geometrie sicherstellt. Die aus diesem Vorgehen entstandenen Carba-Analoga mit der Grundstruktur **14** erwiesen sich verglichen mit Verbindung **69** als deutlich potenter und übertrafen teilweise auch Flupirtin und Retigabin in Hinblick auf die K_V7.2/3-Öffnung.

In der KryoEM-Struktur von Retigabin im Komplex mit dem K_V7.2-Kanal finden sich Hinweise darauf, warum die Lokalisierung des 4-Fluorphenylrings in der Bindetasche, die durch die gewinkelte Molekülgeometrie ermöglicht wird, eine wichtige Funktion erfüllen könnte. Im Detail erscheint es so, als würde speziell dieser Molekülteil die Position von Enden angrenzender Lipidenseitenketten der Zellmembran einnehmen, die sich im Apo-Zustand in einer von S1- und S5-Domäne sowie der Porenhelix gebildeten Vertiefung befinden. Li et al. vermuteten, dass diese Lipide durch die Bindung

von Retigabin verdrängt werden, was eine erhöhte Mobilität der Spannungssensordomäne erklären könnte, die in der KryoEM Struktur beobachtet wurde. Dieser allosterische Effekt von Retigabin könnte neben Konformationsänderungen in der Porendomäne für die Retigabinwirkung auf die K_V7-Kanäle mitverantwortlich sein.[5]

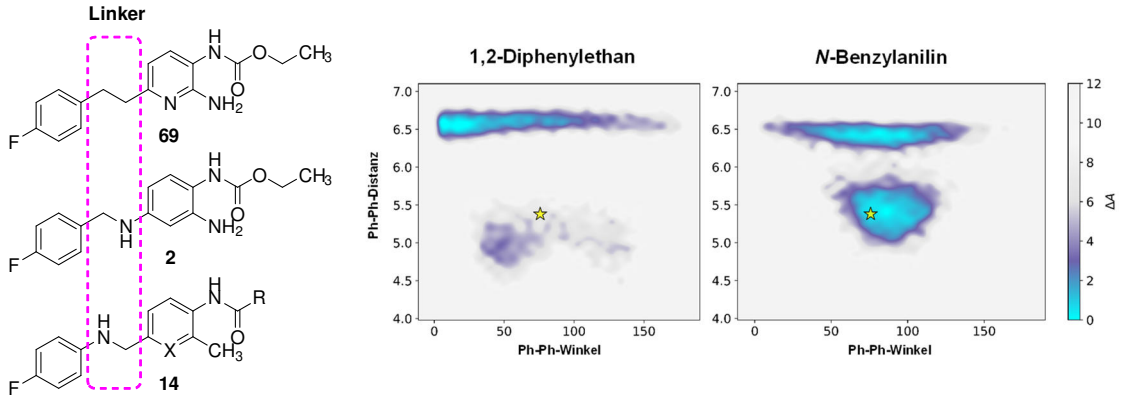

Abbildung 8. Links: Vergleichende Darstellung verschiedener Linker zwischen aromatischem Kern und 4-Fluorphenylring. Rechts: Konformationsraumanalyse von *N*-Benzylanilin und 1,2-Diphenylethan als Modellsubstanzen für die verwendeten Aminomethylen- bzw. Ethylenlinkerelemente. Der Stern markiert den Winkel und den Abstand der Phenylringe von Retigabin im gebundenen Zustand in der $K_V7.2$-Bindetasche.

Bei den in Publikation III beschriebenen Nicotinamidanaloga **55a**-**e** wurden anstelle des 4-Fluorbenzylaminrests verschiedene heterozyklische Substituenten erprobt. Auch bei diesen Strukturelementen, die ungeachtet der geringen strukturellen Ähnlichkeit noch immer in etwa die gleiche Region der Bindetasche besetzen wie der ursprüngliche 4-Fluorbenzylaminteil, fand sich ein deutlicher Einfluss der bevorzugten Molekülgeometrie auf die $K_V7.2/3$-Öffnung. In diesem Fall deuteten die vorhergesagten Bindungsposen an, dass der jeweilige zyklische Substituent nach Möglichkeit ungefähr koplanar zum zentralen Pyridinring ausgerichtet sein muss, um in die $K_V7.2/3$-Bindetasche zu passen. Diese auf Dockingergebnissen basierende Hypothese zum Bindungsmodus konnte durch die experimentellen $K_V7.2/3$-Aktivitätsdaten der strukturell eng verwandten Analoga **55a** und **58** bestätigt werden, deren EC_{50}-Werte sich signifikant um den Faktor 20 unterschieden.

Im Fall des deutlich aktiveren Morpholinanalogons **55a** begünstigt das Morpholinstickstoffatom durch Wechselwirkung mit dem elektronenarmen Pyridinring eine annähernd koplanare Ausrichtung, wenngleich der Morpholinring natürlich nicht planar ist und sich die Bezeichnung koplanar hier auf eine durch den Morpholinring gedachte Ebene bezieht. Demgegenüber bevorzugt das unterlegene Tetrahydropyrananalogon **58** aufgrund des sp^3-hybridisierten Methinkohlenstoffatoms wahrscheinlich eine gegeneinander verdrehte Anordnung von Pyridinkern und zyklischem Substituent. Diese theoretischen Überlegungen zur Molekülgeometrie konnten in Publikation III durch Dichtefunktionaltheorie-basierte Moleküldynamiksimulationen bestätigt werden. Demnach führt das Methinkohlenstoffatom anstelle des Morpholinstickstoffatoms in Hinblick auf den entsprechenden Torsionswinkel zu einer Verschiebung des energetischen Optimums vom Bereich um 0° zu ungefähr 60° bei gleichzeitiger Reduktion der Rotationsenergiebarrieren. In der Konsequenz ist für den Tetrahydropyranring von Verbindung **58** die koplanare Ausrichtung zum zentralen Pyridinring nicht wie bei einem Morpholinring fixiert. Diese fehlende Präorganisation erfordert im Verlauf der Bindung von Substanz **58** an den $K_V7.2/3$-Kanal eine zusätzliche Konformationsänderung und erhöht somit den zu erwartenden Entropieverlust, was sich

letztendlich ungünstig auf die Interaktion auswirkt. Einen Einfluss des Morpholinstickstoffatoms über die Begünstigung einer passenden Molekülgeometrie hinaus, z. B. durch die Ausbildung von direkten Wechselwirkungen mit der Bindetasche, konnte hingegen weitestgehend ausgeschlossen werden, denn das Dihydropyranderivat **57** war in Bezug auf die K_V7.2/3-Öffnung wiederum ähnlich aktiv wie das Morpholinanalogon **55a**. Im Gegensatz zum Tetrahydropyranderivat **58** nimmt der Dihydropyranring von Verbindung **57**, wie in Publikation III gezeigt wurde, durch die sich in Konjugation zum Pyridinring befindliche Doppelbindung ebenfalls bevorzugt die als günstig angenommene koplanare Konformation ein.

Der Vergleich der Analoga **55a** und **56** deutet darüber hinaus darauf hin, dass Koplanarität nicht die einzige Bedingung für einen geeigneten zyklischen Substituenten ist. Das Analogon **56** enthält eine 2,4'-Bipyridinstruktur, deren Pyridinringe zwar aller Wahrscheinlichkeit nach koplanar angeordnet sind, aber dennoch war die Verbindung um den Faktor 4,3 weniger potent als das Morpholin-analogon **55a**. Es liegt also die Vermutung nahe, dass der heterozyklische Substituent auch eine gewisse Flexibilität und Dreidimensionalität benötigt, denn für einen Morpholinring, wie er im Derivat **55a** enthalten ist, wird eine sesselartige Konformation als energetisch günstig angenommen,[145] die ebenfalls in den durch Docking und Moleküldynamiksimulationen vorhergesagten Bindungsposen des Analogons **55a** beobachtet wurde. Im Gegensatz dazu scheint die Passform des Pyridinylrests von Verbindung **56** aufgrund seiner zweidimensionalen und starren Geometrie nicht optimal zu sein, wenngleich auch bei diesem Analogon insgesamt noch immer ein guter EC_{50}-Wert von 0,5 µM erreicht wurde.

Zusammenfassend lässt sich konstatieren, dass geeignete zyklische Substituenten, die beide Anforderungen erfüllen, d. h., koplanar zum zentralen Aromaten ausgerichtet sind und durch ihre Flexibilität annähernd eine Sesselkonformation ermöglichen, dem ursprünglichen 4-Fluorbenzylaminrest von Flupirtin und Retigabin eindeutig überlegen sind. In diesem Zusammenhang sind konkret das Morpholinanalogon **55a**, das Piperidinderivat **55e** und die Dihydropyranverbindung **57** zu nennen, die hinsichtlich der K_V7.2/3-Öffnung teilweise deutlich potenter waren als das entsprechende direkte 4-Fluorbenzylaminanalogon **55f**. Im Fall des Piperidinderivats **55e** ermöglichte die Methylengruppe anstelle des Morpholinsauerstoffatoms sogar eine weitere Steigerung der Potenz um ca. das Dreifache. Vermutlich verbessert hier der lipophilere Piperidinring die Interaktion mit der von F240, F305 und L338 gebildeten hydrophoben Vertiefung der K_V7.2/3-Bindetasche, die von den zyklischen Substituenten besetzt wird.

4.2.3 Einfluss potentieller Ligand-Lipid-Interaktionen auf die K_V7.2/3-Öffnung

Die Bindestelle von Retigabin und verwandter Substanzen befindet sich, wie in Kapitel 1.2.1 erläutert, in der Transmembranregion des K_V7-Kanals an der Protein-Lipid-Grenzfläche. Potenzielle K_V7-Öffner müssen also in der Lage sein, sich in diese Grenzschicht zu integrieren, d. h., sie müssen nicht nur gut in die Bindetasche passen, sondern auch in adäquater Weise mit den angrenzenden Lipidseitenketten wechselwirken können, da ein gewisser Molekülteil zwangsläufig in Richtung der Lipidmatrix orientiert ist. Solche Ligand-Lipid-Wechselwirkungen wurden bisher als Einflussfaktoren der Arzneimittelaktivität unterschätzt, aber sie gewinnen zunehmend an Bedeutung für das Wirkstoffdesign, da eine wachsende Zahl von intramembranären Bindungsstellen durch Röntgen-kristallographie und Kryoelektronenmikroskopie entdeckt werden.[146] Ein bekanntes und treffendes

Beispiel für ausgeprägte Ligand-Lipid-Wechselwirkungen in einer intramembranären Bindetasche ist Ivacaftor, das zur Klasse der CFTR-Potentiatoren gehört (CFTR = Cystic Fibrosis Transmembrane Conductance Regulator). Das Molekül besitzt zwei *tert*-Butylgruppen, die mit Lipiden der angrenzenden Membran interagieren und gleichzeitig den polaren Teil des Liganden, der für die Wechselwirkung mit der CFTR-Bindestelle über Wasserstoffbrückenbindungen verantwortlich ist, gegen die Phospholipid-Grenzfläche abschirmen.[147]

Ein prinzipiell vergleichbares Bindungsverhalten wie bei Ivacaftor wird ungeachtet des unterschiedlichen Zielproteins auch für die hier synthetisierten K_V7-Öffner angenommen. Polare Wechselwirkungen der Analoga mit der Bindetasche finden, wie in Kapitel 4.2.1 erläutert, wahrscheinlich insbesondere über die Amidfunktion statt. Eine Abschirmung dieses eher hydrophilen Strukturbereichs gegen die angrenzende Lipidschicht ist speziell durch geeignete ortho-Substituenten relativ zur Amidgruppe möglich. Hier ist jedoch zu beachten, dass der zentrale aromatische Ring in zwei verschieden Orientierungen in der Bindetasche liegen kann. Dockingresultate aus den Publikationen I und III lassen vermuten, dass kleinere ortho-Substituenten, wie z. B. eine Methylgruppe, bevorzugt der Proteinseite zugewandt sind. Werden die Reste jedoch größer, ist diese Ausrichtung nicht mehr möglich mit der Folge, dass der zentrale Aromat durch Rotation um die Längsachse des Moleküls umgekehrt orientiert in der Bindetasche liegt und die entsprechenden Substituenten somit in Richtung Lipidschicht deuten. Ein geeigneter, d. h. sterisch anspruchsvoller und möglichst lipophiler, ortho-Substituent konnte auf diese Weise in mehreren Fällen wahrscheinlich durch Verbesserung der Ligand-Lipid-Wechselwirkung die K_V7.2/3-Öffnungsaktivität der betreffenden Analoga verbessern. Diese Beobachtung wurde prinzipiell für beide in dieser Arbeit betrachteten Grundstrukturen gemacht, wie die in Abbildung 9 dargestellten Beispiele verdeutlichen. Um diese Hypothese zum Einfluss von Ligand-Lipid-Interaktionen zu stützen, wurden in Publikation III zudem Moleküldynamiksimulationen mit einem K_V7.2/3-Kanal durchgeführt, der in eine artifizielle Membran eingebettet ist. Diese Simulationen bestätigten die angenommene Ausrichtung der Analoga in der Bindetasche mit Zuwendung der lipophilen ortho-Substituenten zur Membran. Ihre räumliche Nähe zu angrenzenden Lipidresten lässt Interaktionen über hydrophobe Wechselwirkungen plausibel erscheinen, die dazu beitragen können, die Bindung der entsprechenden Analoga in der K_V7.2/3-Bindetasche zu verbessern.

Neben der ortho-Position der Amidfunktion konnte auch in anderen Molekülbereichen beobachtet werden, dass lipophilere Strukturelemente häufig zu einer verbesserten K_V7.2/3-Öffnung führten. So bewirkte z. B., wie bereits erwähnt, der Austausch des Morpholinsubstituenten von Analogon **55a** gegen einen Piperidinrest in Verbindung **55e** eine Verringerung des EC_{50}-Wertes um den Faktor 2,9. Auch der Ersatz des Pyridinrings von Derivat **37a** durch einen Phenylring im Fall der Substanz **29b** oder der Wechsel der Butanamidseitenkette von Verbindung **37a** gegen eine 3,3-Dimethylbutanamidseitenkette bei Analogon **37b** verbesserte die Potenz um das 7,1-Fache respektive 7,2-Fache. Aufgrund dieser und weiterer ähnlicher Beobachtungen wurde der Einfluss der Lipophilie auf die K_V7.2/3-Aktivität in der Folge näher untersucht, indem für alle Analoga log$D_{7,4}$-Werte bestimmt wurden (siehe Tabelle 1). Eine substanzübergreifende Korrelation der Lipophilie mit der biologischen Aktivität konnte dabei allerdings nicht bestätigt werden, obwohl dies in ähnlicher Weise für einige eng mit Flupirtin verwandte Derivate in der Literatur beschrieben ist.[148] Wahrscheinlich war die strukturelle Diversität der in dieser Arbeit synthetisierten Analoga für einen solchen Zusammenhang zu groß. Die oben erwähnten Fallbeispiele legen gleichwohl die Vermutung

nahe, dass die allgemeine Lipophilie der Substanzen möglicherweise dennoch einen Einfluss auf die K_V7.2/3-Öffnung hat. Dies könnte zum einen an der insgesamt eher hydrophoben Natur der Bindetasche liegen. Denkbar wäre jedoch auch, dass ihre intramembranäre Lokalisation hier erneut eine Rolle spielt. Wie die Substanzen zu ihrem Bindungsort am K_V7-Kanal gelangen, ist zwar bisher nicht abschließend geklärt, aber eine plausible Möglichkeit ist die Diffusion durch die Zellmembran. Dieser hypothetische Weg könnte erklären, dass lipophilere Verbindungen in vielen Fällen eine scheinbar bessere K_V7.2/3-Öffnung zeigen, die in Wirklichkeit jedoch möglicherweise nur auf einem günstigeren Membran-Wasser-Verteilungsgleichgewicht beruht, welches die lokale Konzentration des Liganden in unmittelbarer Nähe der Bindungsstelle erhöht.

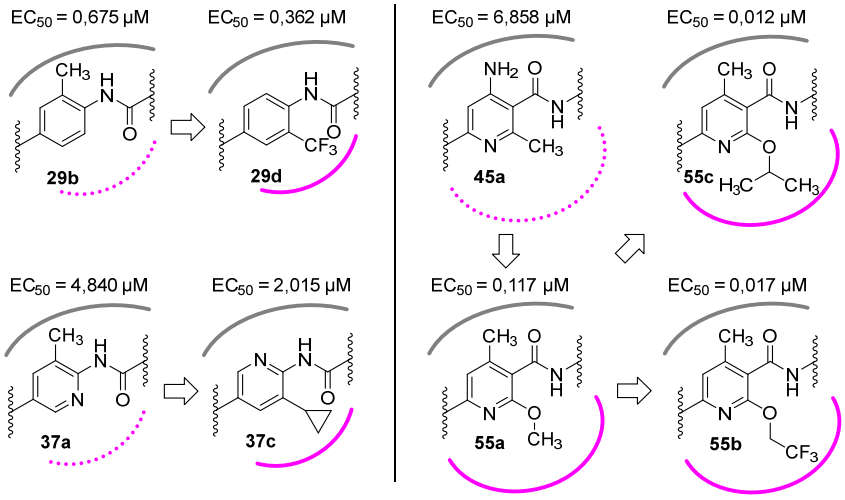

Abbildung 9. Positiver Einfluss eines sterisch anspruchsvollen, lipophilen Substituenten in ortho-Position zur Amidfunktion durch verbesserte Ligand-Lipid-Interaktionen. Für eine Trifluormethylgruppe ist in der Literatur beschrieben, dass sie raumfordernder als ein Methylrest ist und sich bioisoster zu einer Ethylgruppe verhält.[149] Graue Bögen markieren die Molekülseite, die der Bindetasche zugewandt ist, während Bögen in Fuchsia den Molekülbereich anzeigen, der mit der Lipidschicht interagiert. Eine durchgezogene Linie bedeutet gute Ligand-Lipid-Interaktionen, wohingegen eine gepunktete Linie eine mangelhafte Abschirmung in Richtung der Lipidschicht indiziert.

4.3 In vitro-Hepatotoxizität

Die durch Flupirtin hervorgerufenen schweren Leberschäden sind, wie bereits erwähnt, mit einer Melderate von 1,68 Fällen pro 100.000 Patientenjahren sehr seltene Ereignisse.[88] Aus diesem Grund waren klinische Studien nicht in der Lage, das Risiko für lebensgefährliche hepatotoxische Reaktionen aufzudecken, und Flupirtin galt lange Zeit als gut verträgliches Analgetikum mit nur relativ milden Nebenwirkungen.[82] Auch in standardmäßig durchgeführten in vitro-Toxizitätsassays verhält sich Flupirtin unauffällig, andernfalls wäre es nicht in die klinische Erprobung gelangt. Das verdeutlichen vor allem auch die in dieser Arbeit für Flupirtin bestimmten LD_{50}-Werte, welche im Bereich von 500 µM liegen und somit therapeutisch relevante Konzentrationen je nach Dosierung ca. um den Faktor 100–300 überschreiten.[104] Im Allgemeinen ist idiosynkratische Toxizität, wie sie für Flupirtin vermutet wird, aufgrund der multifaktoriellen Ursachen und individuellen Risikofaktoren in einem in vitro-Toxizitätsmodell nur sehr schwer zu reproduzieren.[150] Trotz aller Bemühungen auch seitens der pharmazeutischen Industrie existiert derzeit kein universelles Modell, das diese Form der Leberschädigung zuverlässig vorhersagt, was sich darin widerspiegelt, dass idiosynkratische Hepatotoxizität nach wie vor einer der beiden häufigsten Gründe für Marktrücknahmen, Anwendungseinschränkungen und Projektabbrüche ist.[151,152] Dementspre-

chend erfasst der in dieser Arbeit verwendete MTT-Assay ebenfalls nur die intrinsische, dosisbezogene Toxizität einer Verbindung. Die Ergebnisse sind sehr wahrscheinlich nicht prädiktiv für die idiosynkratische Toxizität von Flupirtin, da eine Beteiligung des Immunsystems ebenso wenig berücksichtigt wird wie eine intensive Metabolisierung der Substanzen.[153] Die toxikologische Untersuchung durch den MTT-Assay ist daher nicht zur Verifizierung der Hypothese des durchgeführten Wirkstoffdesigns zu verstehen, sondern sie diente der Identifizierung von intrinsischen toxikologischen Risiken der neuen Analoga, die es auszuschließen gilt, bevor etwa eine Testung im Tiermodell möglich wäre.

Die in vitro-Toxizitätsdaten der synthetisierten Derivate waren insgesamt ähnlich heterogen wie die K_V7.2/3-Aktivitätsdaten, doch während eindeutige Struktur-Aktivitäts-Beziehungen aufgestellt werden konnten, war es nicht möglich, klare Struktur-Toxizitäts-Beziehungen abzuleiten. Allgemein lässt sich jedoch festhalten, dass die beiden Grundstrukturen **14** und **15** kein generelles toxikologisches Risiko bergen. Bei Betrachtung der LD_{25}-Werte finden sich sowohl Substanzen, die im Vergleich mit Flupirtin besser abschnitten als auch Analoga, für welche kleinere LD_{25}-Werte bestimmt wurden. Es ist jedoch zu beachten, dass die absoluten LD-Werte für sich allein wenig aussagekräftig sind. Dies verdeutlichen in der Literatur veröffentlichte und ebenfalls mittels MTT-Assay bestimmte LD_{50}-Werte von verschiedenen hepatotoxischen Arzneistoffen, die sich über einen großen Konzentrationsbereich von 25 µM bis 20 mM erstrecken.[154] Deutlich relevanter ist daher die Relation von toxischer Konzentration zu therapeutisch effektiver Konzentration, also die therapeutische Breite. Zur vorläufigen Abschätzung der therapeutischen Breite wurde daher für die Analoga das Verhältnis aus LD_{25}-Wert und EC_{50}-Wert berechnet. Die in Tabelle 1 enthaltenen LD_{25}/EC_{50}-Quotienten sind für viele Analoga noch deutlich günstiger als für Flupirtin, welches bereits selbst keine ausgeprägte Toxizität zeigte. Bei den in Publikation I behandelten Substanzen mit invertierter Aminomethylenfunktion erreichte z. B. Verbindung **29a** einen Wert von 875 im Vergleich zu einem Verhältnis von 40, welches für Flupirtin errechnet wurde. Bei den Nicotinamidanaloga aus Publikation II bzw. III erwies sich das Derivat **55c** mit einem LD_{25}/EC_{50}-Quotienten von 1250 als noch unkritischer und übertraf damit sogar Retigabin. Diese Ergebnisse sind jedoch nur ein vorläufiger Indikator für die therapeutische Breite, da sie lediglich auf in vitro-Werten basieren. Bei möglichen Testungen im Tiermodell können etwa pharmakokinetische Einflussfaktoren das Verhältnis von Toxizität zu Aktivität noch deutlich verschieben. Vorerst kann jedoch konstatiert werden, dass einige toxikologisch unauffällige Substanzen erhalten wurden, bei denen die biologisch aktive und die zellschädigende Konzentration um zwei bis drei Größenordnungen getrennt sind.

Die bei der in vitro-Toxizitätstestung beobachtete mäßige Wasserlöslichkeit einiger Analoga könnte perspektivisch problematisch werden, wenn etwa funktionelle in vivo-Studien durchgeführt werden sollen. Andererseits sind die für eine weitere Charakterisierung in Frage kommenden Verbindungen ausnahmslos im nanomolaren Bereich aktiv, sodass nur sehr geringe Konzentrationen notwendig wären. Zudem wirkt sich die im Vergleich zu Flupirtin und Retigabin leicht erhöhte Lipophilie der Substanzen eventuell positiv auf das Gehirn-zu-Plasma-Konzentrationsverhältnis aus, welches insbesondere bei Epilepsiemodellen eine relevante Einflussgröße für die in vivo-Aktivität darstellt.[100] Für den Fall, dass dennoch eine Verbesserung der Wasserlöslichkeit notwendig ist, bietet sich eine Salzbildung an, denn die meisten Substanzen verfügen über entsprechende basische Strukturelemente.

4.4 Untersuchungen zur Oxidierbarkeit

Für die Nicotinamid- und Benzamidanaloga kann eine direkte Oxidation zu chinoiden Strukturen bedingt durch das gegebene Substitutionsmuster des aromatischen Kerns weitestgehend ausgeschlossen werden. Auch bei den Carba-Analoga mit invertierter Aminofunktion ist eine Bildung von Chinondiiminen oder Azachinondiiminen durch die Grundstruktur verhindert. Allerdings wäre hier die Entstehung von weniger häufig beschriebenen Chinoniminmethid-Metaboliten theoretisch denkbar. Aus diesem Grund war für diese Substanzklasse in Publikation I das oxidative Verhalten Gegenstand weiterer Untersuchungen. Cyclovoltammetrische Messungen ergaben für die entsprechenden Analoga ein sehr konsistentes Bild. Während Flupirtin und Retigabin bereits bei Potenzialen von 260 bzw. 306 mV oxidiert wurden, waren die Oxidationspotenziale der Carba-Analoga ohne Ausnahme größer als 600 mV. Somit können diese Verbindungen, verglichen mit Flupirtin und Retigabin, als deutlich oxidationsstabiler angesehen werden.

Die verringerte Oxidationsempfindlichkeit schließt jedoch nicht unbedingt die Entstehung von chinoiden Oxidationsprodukten aus, daher wurde zusätzlich das Risiko der Analoga, entsprechende Metabolite zu bilden, mit einer in silico-Methode untersucht. Die Molekülchinonbildungsscores, die für Flupirtin und Retigabin erhalten wurden, lagen mit 0,94 bzw. 0,91 nahe dem Maximalwert von 1,00 und bestätigen somit die Hypothese, dass die Wirkstoffe zur Bildung von chinoiden Oxidationsprodukten neigen (Tabelle 2). Alle Carba-Analoga hatten hingegen verglichen mit Flupirtin und Retigabin reduzierte Risikoscores, wobei jedoch ein eindeutiger Einfluss des zentralen aromatischen Rings erkennbar war. Das Pyridinanalogon **21** hatte mit 0,87 noch einen relativ hohen MQS-Wert, der deutlich über dem Grenzwert von 0,52 lag. Somit ist für diese Verbindung trotz reduzierter Oxidationsempfindlichkeit noch immer die enzymatische Bildung von chinoiden Metaboliten zu befürchten. Die Phenylanaloga **29a**-**d** hatten hingegen bereits deutlich reduzierte MQS-Werte, wobei die Substanz **29a** auch wie gefordert den Grenzwert unterschritt. Den günstigsten Einfluss auf das Risiko für chinoide Metabolite scheint jedoch der invertierte Pyridinring der Analoga **37a**-**c** zu haben, denn die MQS-Werte dieser Verbindungen lagen ausnahmslos sehr deutlich unter 0,52.

Unter Berücksichtigung dieser subkritischen in silico-Risikoscores und der erheblich verringerten Oxidationsempfindlichkeit, die bei der Cyclovoltammetrie deutlich wurde, ist die Bildung von Chinoniminmethid-Oxidationsprodukten für die Analoga **29a** und **37a**-**c** somit sehr unwahrscheinlich. Zusätzliche Sicherheit könnten hier in Zukunft in vitro-Untersuchungen mit enzymatisch vermittelter Oxidation bringen, welche darauf abzielen, reaktive Metabolite indirekt über das Auftreten von Glutathionkonjugaten nachzuweisen, ähnlich wie es für Flupirtin von Methling et al. durchgeführt wurde.[102] Eine solche experimentelle Bestätigung der Designhypothese wäre auch für die Nicotinamidanaloga wünschenswert, obwohl ihre Grundstruktur keine Möglichkeit zur direkten Bildung von chinoiden Metaboliten vermuten lässt. In der Literatur ist jedoch beispielsweise beschrieben, dass selbst allgemeinhin als metabolisch inert angenommene fluorierte Aromaten in seltenen Fällen durch oxidative ipso-Substitution zu chinoiden Strukturen oxidiert werden können.[155] Unabhängig vom oxidativen Verhalten ist für alle Carba-Analoga die Umsetzung zu farbigen Phenaziniumverbindungen, wie sie für Retigabin beschrieben sind, aufgrund ihrer Struktur unmöglich, sodass Gewebeverfärbungen, die zur Marktrücknahme von Retigabin führten, im Fall beider Grundstrukturen nicht zu befürchten sind.

5 Zusammenfassung und Ausblick

Im Rahmen dieser Arbeit wurden erfolgreich Carba-Analoga von Flupirtin und Retigabin mit verschiedenen Grundstrukturen synthetisiert und für eine Charakterisierung hinsichtlich der K_V7.2/3-Öffnungsaktivität bereitgestellt. Aufbauend auf den erhaltenen Daten war es möglich Struktur-Wirkungs-Beziehungen abzuleiten, die beispielsweise die zentrale Bedeutung der Amidfunktion und die Rolle der Konformation bestimmter Molekülbereiche umfassen. Darüber hinaus deuten Aktivitätsdaten und Moleküldynamiksimulationen auf einen nicht unerheblichen Beitrag von Ligand-Lipid-Interaktionen bei der Bindung der Analoga in der K_V7.2/3-Bindetasche hin. Diese und andere in den Publikationen I-III enthaltene Erkenntnisse zu Struktur-Wirkungs-Beziehungen bieten zusammengenommen eine wertvolle Basis, um eine weitere rationale Optimierung der Grundstrukturen zu ermöglichen, falls dies etwa in Hinblick auf physikochemische Eigenschaften oder die bisher nicht erfasste K_V7-Subtypselektivität erforderlich sein sollte.

Während für die Nicotinamid- und Benzamidanaloga die direkte Bildung von chinoiden Metaboliten bereits durch die Grundstruktur weitestgehend ausgeschlossen ist, lässt die durchgeführte Untersuchung des Oxidationsverhaltens für die Carba-Analoga mit invertierter Aminomethylen-gruppe den vorläufigen Schluss zu, dass auch für die Verbindungen **29a** und **37a**-**c** in dieser Hinsicht nur ein geringes Risiko besteht. Im Fall beider Grundstrukturen wurden zudem Substanzen erhalten, die eine sehr potente K_V7.2/3-Öffnungsaktivität offenbarten und sich diesbezüglich den K_V7-Öffnern vom Triaminoaryltyp teilweise deutlich überlegen zeigten. Darüber hinaus erwiesen sich einige der im nanomolaren Bereich aktiven Analoga im in vitro-Hepatotoxizitätsassay als unbedenklich in den Konzentrationen, die jeweils für die K_V7.2/3-Öffnung erforderlich waren.

Unter Berücksichtigung der bisher erhobenen Daten hinsichtlich Aktivität, Toxizität und Oxidationsverhalten empfehlen sich insbesondere die Verbindungen mit invertierter Aminomethylenfunktion **29a** bzw. **37b** sowie die Nicotinamidderivate **55b**/**c** als geeignete Kandidaten für eine weitergehende Charakterisierung. Diesbezüglich ist zunächst auszuschließen, dass die genannten Analoga für die Arzneimittelsicherheit kritische Ionenkanäle wie K_V7.1 oder hERG beeinflussen, die dafür bekannt sind, kardiale Nebenwirkungen zu vermitteln. Bei entsprechenden positiven Resultaten der im Moment noch andauernden Selektivitätstestungen sind nachfolgend auch funktionelle Studien im Tiermodell geplant, um einen analgetischen und/oder antikonvulsiven Effekt in vivo zu bestätigen.

6 Literaturverzeichnis

(1) Abbott, G. W. KCNQs: ligand- and voltage-gated potassium channels. *Front. Physiol.*, **2020**, *11*, 583.

(2) Schwake, M.; Jentsch, T. J.; Friedrich, T. A carboxy-terminal domain determines the subunit specificity of KCNQ K^+ channel assembly. *EMBO Rep.*, **2003**, *4* (1), 76–81.

(3) Schwake, M.; Athanasiadu, D.; Beimgraben, C.; Blanz, J.; Beck, C.; Jentsch, T. J.; Saftig, P.; Friedrich, T. Structural determinants of M-type KCNQ (K_V7) K^+ channel assembly. *J. Neurosci.*, **2006**, *26* (14), 3757–3766.

(4) Jentsch, T. J. Neuronal KCNQ potassium channels: physiology and role in disease. *Nat. Rev. Neurosci.*, **2000**, *1* (1), 21–30.

(5) Li, X.; Zhang, Q.; Guo, P.; Fu, J.; Mei, L.; Lv, D.; Wang, J.; Lai, D.; Ye, S.; Yang, H.; Guo, J. Molecular basis for ligand activation of the human KCNQ2 channel. *Cell Res.*, **2021**, *31* (1), 52–61.

(6) Miceli, F.; Soldovieri, M. V.; Iannotti, F. A.; Barrese, V.; Ambrosino, P.; Martire, M.; Cilio, M. R.; Taglialatela, M. The voltage-sensing domain of $K_V7.2$ channels as a molecular target for epilepsy-causing mutations and anticonvulsants. *Front. Pharmacol.*, **2011**, *2*, 2.

(7) Haitin, Y.; Attali, B. The C-terminus of K_V7 channels: a multifunctional module. *J. Physiol.*, **2008**, *586* (7), 1803–1810.

(8) Delmas, P.; Brown, D. A. Pathways modulating neural KCNQ/M (K_V7) potassium channels. *Nat. Rev. Neurosci.*, **2005**, *6* (11), 850–862.

(9) Wrobel, E.; Tapken, D.; Seebohm, G. The KCNE tango - how KCNE1 interacts with $K_V7.1$. *Front. Pharmacol.*, **2012**, *3*, 142.

(10) Schroeder, B. C.; Waldegger, S.; Fehr, S.; Bleich, M.; Warth, R.; Greger, R.; Jentsch, T. J. A constitutively open potassium channel formed by KCNQ1 and KCNE3. *Nature*, **2000**, *403* (6766), 196–199.

(11) Grunnet, M.; Jespersen, T.; Rasmussen, H. B.; Ljungstrøm, T.; Jorgensen, N. K.; Olesen, S.-P.; Klaerke, D. A. KCNE4 is an inhibitory subunit to the KCNQ1 channel. *J. Physiol.*, **2002**, *542* (Pt 1), 119–130.

(12) Sanguinetti, M. C.; Curran, M. E.; Zou, A.; Shen, J.; Spector, P. S.; Atkinson, D. L.; Keating, M. T. Coassembly of K_VLQT1 and minK (IsK) proteins to form cardiac I_{Ks} potassium channel. *Nature*, **1996**, *384* (6604), 80–83.

(13) Bett, G. C. L.; Morales, M. J.; Beahm, D. L.; Duffey, M. E.; Rasmusson, R. L. Ancillary subunits and stimulation frequency determine the potency of chromanol 293B block of the KCNQ1 potassium channel. *J. Physiol.*, **2006**, *576* (Pt 3), 755–767.

(14) Neyroud, N.; Tesson, F.; Denjoy, I.; Leibovici, M.; Donger, C.; Barhanin, J.; Fauré, S.; Gary, F.; Coumel, P.; Petit, C.; Schwartz, K.; Guicheney, P. A novel mutation in the potassium channel gene KVLQT1 causes the Jervell and Lange-Nielsen cardioauditory syndrome. *Nat. Genet.*, **1997**, *15* (2), 186–189.

(15) Vallon, V.; Grahammer, F.; Volkl, H.; Sandu, C. D.; Richter, K.; Rexhepaj, R.; Gerlach, U.; Rong, Q.; Pfeifer, K.; Lang, F. KCNQ1-dependent transport in renal and gastrointestinal epithelia. *Proc. Natl. Acad. Sci. USA*, **2005**, *102* (49), 17864–17869.

(16) Grahammer, F.; Herling, A. W.; Lang, H. J.; Schmitt-Gräff, A.; Wittekindt, O. H.; Nitschke, R.; Bleich, M.; Barhanin, J.; Warth, R. The cardiac K^+ channel KCNQ1 is essential for gastric acid secretion. *Gastroenterology*, **2001**, *120* (6), 1363–1371.

(17) Grahammer, F.; Warth, R.; Barhanin, J.; Bleich, M.; Hug, M. J. The small conductance K^+ channel, KCNQ1: expression, function, and subunit composition in murine trachea. *J. Biol. Chem.*, **2001**, *276* (45), 42268–42275.

(18) Purtell, K.; Paroder-Belenitsky, M.; Reyna-Neyra, A.; Nicola, J. P.; Koba, W.; Fine, E.; Carrasco, N.; Abbott, G. W. The KCNQ1-KCNE2 K^+ channel is required for adequate thyroid I^- uptake. *FASEB J.*, **2012**, *26* (8), 3252–3259.

(19) Chadha, P. S.; Zunke, F.; Davis, A. J.; Jepps, T. A.; Linders, J. T. M.; Schwake, M.; Towart, R.; Greenwood, I. A. Pharmacological dissection of $K_V7.1$ channels in systemic and pulmonary arteries. *Br. J. Pharmacol.*, **2012**, *166* (4), 1377–1387.

(20) Barrese, V.; Stott, J. B.; Greenwood, I. A. KCNQ-encoded potassium channels as therapeutic targets. *Annu. Rev. Pharmacol. Toxicol.*, **2018**, *58*, 625–648.

(21) Bal, M.; Zhang, J.; Zaika, O.; Hernandez, C. C.; Shapiro, M. S. Homomeric and heteromeric assembly of KCNQ (K_V7) K^+ channels assayed by total internal reflection fluorescence/fluorescence resonance energy transfer and patch clamp analysis. *J. Biol. Chem.*, **2008**, *283* (45), 30668–30676.

(22) Wang, H. S.; Pan, Z.; Shi, W.; Brown, B. S.; Wymore, R. S.; Cohen, I. S.; Dixon, J. E.; McKinnon, D. KCNQ2 and KCNQ3 potassium channel subunits: molecular correlates of the M-channel. *Science*, **1998**, *282* (5395), 1890–1893.

(23) Kubisch, C.; Schroeder, B. C.; Friedrich, T.; Lütjohann, B.; El-Amraoui, A.; Marlin, S.; Petit, C.; Jentsch, T. J. KCNQ4, a novel potassium channel expressed in sensory outer hair cells, is mutated in dominant deafness. *Cell*, **1999**, *96* (3), 437–446.

(24) Li, L.; Sun, H.; Ding, J.; Niu, C.; Su, M.; Zhang, L.; Li, Y.; Wang, C.; Gamper, N.; Du, X.; Zhang, H. Selective targeting of M-type potassium $K_V7.4$ channels demonstrates their key role in the regulation of dopaminergic neuronal excitability and depression-like behaviour. *Br. J. Pharmacol.*, **2017**, *174* (23), 4277–4294.

(25) Chadha, P. S.; Jepps, T. A.; Carr, G.; Stott, J. B.; Zhu, H.-L.; Cole, W. C.; Greenwood, I. A. Contribution of $K_V7.4$/$K_V7.5$ heteromers to intrinsic and calcitonin gene-related peptide-induced cerebral reactivity. *Arterioscler. Thromb. Vasc. Biol.*, **2014**, *34* (4), 887–893.

(26) Mani, B. K.; Robakowski, C.; Brueggemann, L. I.; Cribbs, L. L.; Tripathi, A.; Majetschak, M.; Byron, K. L. $K_V7.5$ potassium channel subunits are the primary targets for PKA-dependent enhancement of vascular smooth muscle K_V7 currents. *Mol. Pharmacol.*, **2016**, *89* (3), 323–334.

(27) McCallum, L. A.; Greenwood, I. A.; Tribe, R. M. Expression and function of K_V7 channels in murine myometrium throughout oestrous cycle. *Pflugers Arch.*, **2009**, *457* (5), 1111–1120.

(28) Ipavec, V.; Martire, M.; Barrese, V.; Taglialatela, M.; Currò, D. K_V7 channels regulate muscle tone and nonadrenergic noncholinergic relaxation of the rat gastric fundus. *Pharmacol. Res.*, **2011**, *64* (4), 397–409.

(29) Jepps, T. A.; Olesen, S. P.; Greenwood, I. A.; Dalsgaard, T. Molecular and functional characterization of K_V7 channels in penile arteries and corpus cavernosum of healthy and metabolic syndrome rats. *Br. J. Pharmacol.*, **2016**, *173* (9), 1478–1490.

(30) Evseev, A. I.; Semenov, I.; Archer, C. R.; Medina, J. L.; Dube, P. H.; Shapiro, M. S.; Brenner, R. Functional effects of KCNQ K^+ channels in airway smooth muscle. *Front. Physiol.*, **2013**, *4*, 277.

(31) Svalø, J.; Sheykhzade, M.; Nordling, J.; Matras, C.; Bouchelouche, P. Functional and molecular evidence for K_V7 channel subtypes in human detrusor from patients with and without bladder outflow obstruction. *PLoS One*, **2015**, *10* (2), e0117350.

(32) Tzingounis, A. V.; Heidenreich, M.; Kharkovets, T.; Spitzmaul, G.; Jensen, H. S.; Nicoll, R. A.; Jentsch, T. J. The KCNQ5 potassium channel mediates a component of the afterhyperpolarization current in mouse hippocampus. *Proc. Natl. Acad. Sci. USA*, **2010**, *107* (22), 10232–10237.

(33) Wladyka, C. L.; Kunze, D. L. KCNQ/M-currents contribute to the resting membrane potential in rat visceral sensory neurons. *J. Physiol.*, **2006**, *575* (Pt 1), 175–189.

(34) Hansen, H. H.; Waroux, O.; Seutin, V.; Jentsch, T. J.; Aznar, S.; Mikkelsen, J. D. K_V7 channels: interaction with dopaminergic and serotonergic neurotransmission in the CNS. *J. Physiol.*, **2008**, *586* (7), 1823–1832.

(35) Brown, D. A.; Adams, P. R. Muscarinic suppression of a novel voltage-sensitive K^+ current in a vertebrate neurone. *Nature*, **1980**, *283* (5748), 673–676.

(36) Robbins, J. KCNQ potassium channels: physiology, pathophysiology, and pharmacology. *Pharmacol. Ther.*, **2001**, *90* (1), 1–19.

(37) Zaika, O.; Lara, L. S.; Gamper, N.; Hilgemann, D. W.; Jaffe, D. B.; Shapiro, M. S. Angiotensin II regulates neuronal excitability via phosphatidylinositol 4,5-bisphosphate-dependent modulation of K_V7 (M-type) K^+ channels. *J. Physiol.*, **2006**, *575* (Pt 1), 49–67.

(38) Cuevas, J.; Harper, A. A.; Trequattrini, C.; Adams, D. J. Passive and active membrane properties of isolated rat intracardiac neurons: regulation by H- and M-currents. *J. Neurophysiol.*, **1997**, *78* (4), 1890–1902.

(39) Passmore, G. M.; Selyanko, A. A.; Mistry, M.; Al-Qatari, M.; Marsh, S. J.; Matthews, E. A.; Dickenson, A. H.; Brown, T. A.; Burbidge, S. A.; Main, M.; Brown, D. A. KCNQ/M currents in sensory neurons: significance for pain therapy. *J. Neurosci.*, **2003**, *23* (18), 7227–7236.

(40) Zhou, Y.; Vo, T.; Rotstein, H. G.; McCarthy, M. M.; Kopell, N. M-current expands the range of gamma frequency inputs to which a neuronal target entrains. *J. Math. Neurosci.*, **2018**, *8* (1), 13.

(41) Lang, P. M.; Fleckenstein, J.; Passmore, G. M.; Brown, D. A.; Grafe, P. Retigabine reduces the excitability of unmyelinated peripheral human axons. *Neuropharmacology*, **2008**, *54* (8), 1271–1278.

(42) Koyama, S.; Appel, S. B. Characterization of M-current in ventral tegmental area dopamine neurons. *J. Neurophysiol.*, **2006**, *96* (2), 535–543.

(43) Battefeld, A.; Tran, B. T.; Gavrilis, J.; Cooper, E. C.; Kole, M. H. P. Heteromeric K_V7.2/7.3 channels differentially regulate action potential initiation and conduction in neocortical myelinated axons. *J. Neurosci.*, **2014**, *34* (10), 3719–3732.

(44) Miceli, F.; Cilio, M. R.; Taglialatela, M.; Bezanilla, F. Gating currents from neuronal K_V7.4 channels: general features and correlation with the ionic conductance. *Channels*, **2009**, *3* (4), 277–286.

(45) Peters, H. C.; Hu, H.; Pongs, O.; Storm, J. F.; Isbrandt, D. Conditional transgenic suppression of M channels in mouse brain reveals functions in neuronal excitability, resonance and behavior. *Nat. Neurosci.*, **2005**, *8* (1), 51–60.

(46) Gu, N.; Vervaeke, K.; Hu, H.; Storm, J. F. K_V7/KCNQ/M and HCN/h, but not K_{Ca}2/SK channels, contribute to the somatic medium after-hyperpolarization and excitability control in CA1 hippocampal pyramidal cells. *J. Physiol.*, **2005**, *566* (Pt 3), 689–715.

(47) Brown, D. A.; Passmore, G. M. Neural KCNQ (K_V7) channels. *Br. J. Pharmacol.*, **2009**, *156* (8), 1185–1195.

(48) Soldovieri, M. V.; Miceli, F.; Taglialatela, M. Driving with no brakes: molecular pathophysiology of K_V7 potassium channels. *Physiology*, **2011**, *26* (5), 365–376.

(49) Borgini, M.; Mondal, P.; Liu, R.; Wipf, P. Chemical modulation of K_V7 potassium channels. *RSC Med. Chem.*, **2021**, *12* (4), 483–537.

(50) Peña, F.; Alavez-Pérez, N. Epileptiform activity induced by pharmacologic reduction of M-current in the developing hippocampus in vitro. *Epilepsia*, **2006**, *47* (1), 47–54.

(51) Padilla, K.; Wickenden, A. D.; Gerlach, A. C.; McCormack, K. The KCNQ2/3 selective channel opener ICA-27243 binds to a novel voltage-sensor domain site. *Neurosci. Lett.*, **2009**, *465* (2), 138–142.

(52) Schenzer, A.; Friedrich, T.; Pusch, M.; Saftig, P.; Jentsch, T. J.; Grötzinger, J.; Schwake, M. Molecular determinants of KCNQ (K_V7) K^+ channel sensitivity to the anticonvulsant retigabine. *J. Neurosci.*, **2005**, *25* (20), 5051–5060.

(53) Tatulian, L.; Delmas, P.; Abogadie, F. C.; Brown, D. A. Activation of expressed KCNQ potassium currents and native neuronal M-type potassium currents by the anti-convulsant drug retigabine. *J. Neurosci.*, **2001**, *21* (15), 5535–5545.

(54) Wang, C. K.; Lamothe, S. M.; Wang, A. W.; Yang, R. Y.; Kurata, H. T. Pore- and voltage sensor-targeted KCNQ openers have distinct state-dependent actions. *J. Gen. Physiol.*, **2018**, *150* (12), 1722–1734.

(55) Rivera-Arconada, I.; Roza, C.; Lopez-Garcia, J. A. Enhancing M currents: a way out for neuropathic pain? *Front. Mol. Neurosci.*, **2009**, *2*, 10.

(56) Wickenden, A. D.; McNaughton-Smith, G. K_V7 channels as targets for the treatment of pain. *Curr. Pharm. Des.*, **2009**, *15* (15), 1773–1798.

(57) Hayashi, H.; Iwata, M.; Tsuchimori, N.; Matsumoto, T. Activation of peripheral KCNQ channels attenuates inflammatory pain. *Mol. Pain.*, **2014**, *10*, 15.

(58) Rivera-Arconada, I.; Martinez-Gomez, J.; Lopez-Garcia, J. A. M-current modulators alter rat spinal nociceptive transmission: an electrophysiological study in vitro. *Neuropharmacology*, **2004**, *46* (4), 598–606.

(59) Roza, C.; Lopez-Garcia, J. A. Retigabine, the specific KCNQ channel opener, blocks ectopic discharges in axotomized sensory fibres. *Pain*, **2008**, *138* (3), 537–545.

(60) Dost, R.; Rostock, A.; Rundfeldt, C. The anti-hyperalgesic activity of retigabine is mediated by KCNQ potassium channel activation. *Naunyn Schmiedebergs Arch. Pharmacol.*, **2004**, *369* (4), 382–390.

(61) Gordon, R.; Sofia, R. D.; Diamantis, W. Effect of flupirtine maleate on the nociceptive pathway, EEG, evoked potentials and polysynaptic reflexes in laboratory animals. *Postgrad. Med. J.*, **1987**, *63 Suppl 3*, 49–55.

(62) Nickel, B. The antinociceptive activity of flupirtine: a structurally new analgesic. *Postgrad. Med. J.*, **1987**, *63 Suppl 3*, 19–28.

(63) Ahuja, V.; Mitra, S.; Kazal, S.; Huria, A. Comparison of analgesic efficacy of flupirtine maleate and ibuprofen in gynaecological ambulatory surgeries: a randomized controlled trial. *Indian J. Anaesth.*, **2015**, *59* (7), 411–415.

(64) Li, C.; Ni, J.; Wang, Z.; Li, M.; Gasparic, M.; Terhaag, B.; Uberall, M. A. Analgesic efficacy and tolerability of flupirtine vs. tramadol in patients with subacute low back pain: a double-blind multicentre trial. *Curr. Med. Res. Opin.*, **2008**, *24* (12), 3523–3530.

(65) Ringe, J. D.; Miethe, D.; Pittrow, D.; Wegscheider, K. Analgesic efficacy of flupirtine in primary care of patients with osteoporosis related pain. A multivariate analysis. *Arzneimittelforschung*, **2003**, *53* (7), 496–502.

(66) Abd-Elsayed, A.; Jackson, M.; Gu, S. L.; Fiala, K.; Gu, J. Neuropathic pain and K_V7 voltage-gated potassium channels: the potential role of K_V7 activators in the treatment of neuropathic pain. *Mol. Pain.*, **2019**, *15*, 1744806919864256.

(67) Tober, C.; Rostock, A.; Rundfeldt, C.; Bartsch, R. D-23129: a potent anticonvulsant in the amygdala kindling model of complex partial seizures. *Eur. J. Pharmacol.*, **1996**, *303* (3), 163–169.

(68) Rostock, A.; Tober, C.; Rundfeldt, C.; Bartsch, R.; Engel, J.; Polymeropoulos, E. E.; Kutscher, B.; Löscher, W.; Hönack, D.; White, H.S.; Wolf, H. H. D-23129: a new anticonvulsant with a broad spectrum activity in animal models of epileptic seizures. *Epilepsy Res.*, **1996**, *23* (3), 211–223.

(69) Roeloffs, R.; Wickenden, A. D.; Crean, C.; Werness, S.; McNaughton-Smith, G.; Stables, J.; McNamara, J. O.; Ghodadra, N.; Rigdon, G. C. In vivo profile of ICA-27243 *N*-(6-chloro-pyridin-3-yl)-3,4-difluoro-benzamide, a potent and selective KCNQ2/Q3 ($K_V7.2/K_V7.3$) activator in rodent anticonvulsant models. *J. Pharmacol. Exp. Ther.*, **2008**, *326* (3), 818–828.

(70) Jankovic, S.; Ilickovic, I. The preclinical discovery and development of ezogabine for the treatment of epilepsy. *Expert Opin. Drug Discov.*, **2013**, *8* (11), 1429–1437.

(71) Porter, R. J.; Partiot, A.; Sachdeo, R.; Nohria, V.; Alves, W. M. Randomized, multicenter, dose-ranging trial of retigabine for partial-onset seizures. *Neurology*, **2007**, *68* (15), 1197–1204.

(72) Friedman, A. K.; Juarez, B.; Ku, S. M.; Zhang, H.; Calizo, R. C.; Walsh, J. J.; Chaudhury, D.; Zhang, S.; Hawkins, A.; Dietz, D. M.; Murrough, J. W.; Ribadeneira, M.; Wong, E. H.; Neve, R. L.;

Han, M.-H. KCNQ channel openers reverse depressive symptoms via an active resilience mechanism. *Nat. Commun.*, **2016**, *7*, 11671.

(73) Tan, A.; Costi, S.; Morris, L. S.; van Dam, N. T.; Kautz, M.; Whitton, A. E.; Friedman, A. K.; Collins, K. A.; Ahle, G.; Chadha, N.; Do, B.; Pizzagalli, D. A.; Iosifescu, D. V.; Nestler, E. J.; Han, M.-H.; Murrough, J. W. Effects of the KCNQ channel opener ezogabine on functional connectivity of the ventral striatum and clinical symptoms in patients with major depressive disorder. *Mol. Psychiatry*, **2020**, *25* (6), 1323–1333.

(74) Vigil, F. A.; Bozdemir, E.; Bugay, V.; Chun, S. H.; Hobbs, M.; Sanchez, I.; Hastings, S. D.; Veraza, R. J.; Holstein, D. M.; Sprague, S. M.; M Carver, C.; Cavazos, J. E.; Brenner, R.; Lechleiter, J. D.; Shapiro, M. S. Prevention of brain damage after traumatic brain injury by pharmacological enhancement of KCNQ (K_V7, "M-type") K^+ currents in neurons. *J. Cereb. Blood Flow Metab.*, **2020**, *40* (6), 1256–1273.

(75) Ren, J.; Guo, J.; Zhu, S.; Wang, Q.; Gao, R.; Zhao, C.; Feng, C.; Qin, C.; He, Z.; Qin, C.; Wang, Z.; Zang, L. The role of potassium channels in chronic stress-induced brain injury. *Biol. Pharm. Bull.*, **2021**, *44* (2), 169–180.

(76) Bierbower, S. M.; Choveau, F. S.; Lechleiter, J. D.; Shapiro, M. S. Augmentation of M-type (KCNQ) potassium channels as a novel strategy to reduce stroke-induced brain injury. *J. Neurosci.*, **2015**, *35* (5), 2101–2111.

(77) Sampath, D.; Lam, P. M.; Laoprasert, M.; Diaz, M. J.; Busquet, N.; White, A. M.; Gonzalez, M. I.; Raol, Y. H. Effects of a potassium channel opener on brain injury and neurologic outcomes in an animal model of neonatal hypoxic-ischemic injury. *Pediatr. Res.*, **2020**, *88* (2), 202–208.

(78) Dörr, J.; Wernecke, K.-D.; Würfel, J.; Bellmann-Strobl, J.; Siffrin, V.; Sättler, M. B.; Simons, M.; Linsa, A.; Tumani, H.; Paul, F. Disease modification in multiple sclerosis by flupirtine - results of a randomized placebo controlled phase II trial. *Front. Neurol.*, **2018**, *9*, 842.

(79) Wainger, B. J.; Macklin, E. A.; Vucic, S.; McIlduff, C. E.; Paganoni, S.; Maragakis, N. J.; Bedlack, R.; Goyal, N. A.; Rutkove, S. B.; Lange, D. J.; Rivner, M. H.; Goutman, S. A.; Ladha, S. S.; Mauricio, E. A.; Baloh, R. H.; Simmons, Z.; Pothier, L.; Kassis, S. B.; La, T.; Hall, M.; Evora, A.; Klements, D.; Hurtado, A.; Pereira, J. D.; Koh, J.; Celnik, P. A.; Chaudhry, V.; Gable, K.; Juel, V. C.; Phielipp, N.; Marei, A.; Rosenquist, P.; Meehan, S.; Oskarsson, B.; Lewis, R. A.; Kaur, D.; Kiskinis, E.; Woolf, C. J.; Eggan, K.; Weiss, M. D.; Berry, J. D.; David, W. S.; Davila-Perez, P.; Camprodon, J. A.; Pascual-Leone, A.; Kiernan, M. C.; Shefner, J. M.; Atassi, N.; Cudkowicz, M. E. Effect of ezogabine on cortical and spinal motor neuron excitability in amyotrophic lateral sclerosis: a randomized clinical trial. *JAMA Neurol.*, **2021**, *78* (2), 186–196.

(80) Kornhuber, J.; Maler, M.; Wiltfang, J.; Bleich, S.; Degner, D.; Rüther, E. Neuronale Kaliumkanalöffnung durch Flupirtin. *Fortschr. Neurol. Psychiatr.*, **1999**, *67* (10), 466–475.

(81) Darius, H.; Schrör, K. The action of flupirtine on prostaglandin formation and platelet aggregation in vitro. *Arzneimittelforschung*, **1985**, *35* (1), 55–59.

(82) Uberall, M. A.; Mueller-Schwefe, G. H. H.; Terhaag, B. Efficacy and safety of flupirtine modified release for the management of moderate to severe chronic low back pain: results of SUPREME, a prospective randomized, double-blind, placebo- and active-controlled parallel-group phase IV study. *Curr. Med. Res. Opin.*, **2012**, *28* (10), 1617–1634.

(83) Göbel, H.; Schmid, J.; Heinze, A.; Pergande, G. Reduktion der spastischen Muskeltonuserhöhung bei Multipler Sklerose durch das Nonopioidanalgetikum Flupirtin. Eine randomisierte, doppelblinde Cross-over-Studie. *Schmerz*, **1999**, *13* (5), 324–331.

(84) Popovici, F.; Dorostkar, M.; Boehm, S. The non-opioid analgesic flupirtine is a modulator of $GABA_A$ receptors involved in pain sensation. *BMC Pharmacol.*, **2008**, *8* (S1).

(85) Klawe, C.; Maschke, M. Flupirtine: pharmacology and clinical applications of a nonopioid analgesic and potentially neuroprotective compound. *Expert Opin. Pharmacother.*, **2009**, *10* (9), 1495–1500.

(86) Puls, F.; Agne, C.; Klein, F.; Koch, M.; Rifai, K.; Manns, M. P.; Borlak, J.; Kreipe, H. H. Pathology of flupirtine-induced liver injury: a histological and clinical study of six cases. *Virchows Arch.*, **2011**, *458* (6), 709–716.

(87) Michel, M. C.; Radziszewski, P.; Falconer, C.; Marschall-Kehrel, D.; Blot, K. Unexpected frequent hepatotoxicity of a prescription drug, flupirtine, marketed for about 30 years. *Br. J. Clin. Pharmacol.*, **2012**, *73* (5), 821–825.

(88) European Medicines Agency. Assessment report for flupirtine containing medicinal products. https://www.ema.europa.eu/en/documents/referral/flupirtine-containing-medicines-article-107i-procedure-prac-assessment-report_en.pdf. 2013 (Zuletzt geprüft am 25.08.22).

(89) Yadav, N. K.; Shukla, T.; Upmanyu, N.; Pandey, S. P.; Khan, M. A.; Jain, D. K. Concise review: therapeutic potential of flupirtine maleate. *J. Drug Delivery Ther.*, **2019**, *9* (1-s), 467–471.

(90) Ciliberto, M. A.; Weisenberg, J. L.; Wong, M. Clinical utility, safety, and tolerability of ezogabine (retigabine) in the treatment of epilepsy. *Drug Healthc. Patient Saf.*, **2012**, *4*, 81–86.

(91) Schrøder, R. L.; Jespersen, T.; Christophersen, P.; Strøbæk, D.; Jensen, B. S.; Olesen, S.-P. KCNQ4 channel activation by BMS-204352 and retigabine. *Neuropharmacology*, **2001**, *40* (7), 888–898.

(92) Wickenden, A. D.; Zou, A.; Wagoner, P. K.; Jegla, T. Characterization of KCNQ5/Q3 potassium channels expressed in mammalian cells. *Br. J. Pharmacol.*, **2001**, *132* (2), 381–384.

(93) Treven, M.; Koenig, X.; Assadpour, E.; Gantumur, E.; Meyer, C.; Hilber, K.; Boehm, S.; Kubista, H. The anticonvulsant retigabine is a subtype selective modulator of $GABA_A$ receptors. *Epilepsia*, **2015**, *56* (4), 647–657.

(94) Verma, A.; Kumar, R.; Kumar, M. Ezogabine: development and role in the management of epileptic seizures. *Mini Rev. Med. Chem.*, **2013**, *13* (5), 697–705.

(95) Clark, S.; Antell, A.; Kaufman, K. New antiepileptic medication linked to blue discoloration of the skin and eyes. *Ther. Adv. Drug. Saf.*, **2015**, *6* (1), 15–19.

(96) Brickel, N.; Hewett, K.; Rayner, K.; McDonald, S.; De'Ath, J.; Daniluk, J.; Joshi, K.; Boll, M. C.; Tiamkao, S.; Vorobyeva, O.; Cooper, J. Safety of retigabine in adults with partial-onset seizures after long-term exposure: focus on unexpected ophthalmological and dermatological events. *Epilepsy Behav.*, **2020**, *102*, 106580.

(97) Brickel, N.; Gandhi, P.; VanLandingham, K.; Hammond, J.; DeRossett, S. The urinary safety profile and secondary renal effects of retigabine (ezogabine): a first-in-class antiepileptic drug that targets KCNQ (K_V7) potassium channels. *Epilepsia*, **2012**, *53* (4), 606–612.

(98) Provence, A.; Angoli, D.; Petkov, G. V. K_V7 channel pharmacological activation by the novel activator ML213: role for heteromeric $K_V7.4/K_V7.5$ channels in guinea pig detrusor smooth muscle function. *J. Pharmacol. Exp. Ther.*, **2018**, *364* (1), 131–144.

(99) Barrese, V.; Miceli, F.; Soldovieri, M. V.; Ambrosino, P.; Iannotti, F. A.; Cilio, M. R.; Taglialatela, M. Neuronal potassium channel openers in the management of epilepsy: role and potential of retigabine. *Clin. Pharmacol.*, **2010**, *2*, 225–236.

(100) Zhou, P.; Zhang, Y.; Xu, H.; Chen, F.; Chen, X.; Li, X.; Pi, X.; Wang, L.; Zhan, L.; Nan, F.; Gao, Z. P-retigabine: an N-propargyled retigabine with improved brain distribution and enhanced antiepileptic activity. *Mol. Pharmacol.*, **2015**, *87* (1), 31–38.

(101) Nissenkorn, A.; Kornilov, P.; Peretz, A.; Blumkin, L.; Heimer, G.; Ben-Zeev, B.; Attali, B. Personalized treatment with retigabine for pharmacoresistant epilepsy arising from a pathogenic variant in the KCNQ2 selectivity filter. *Epileptic Disord.*, **2021**, *23* (5), 695–705.

(102) Methling, K.; Reszka, P.; Lalk, M.; Vrana, O.; Scheuch, E.; Siegmund, W.; Terhaag, B.; Bednarski, P. J. Investigation of the in vitro metabolism of the analgesic flupirtine. *Drug. Metab. Dispos.*, **2009**, *37* (3), 479–493.

(103) Scheuch, E.; Methling, K.; Bednarski, P. J.; Oswald, S.; Siegmund, W. Quantitative LC-MS/MS determination of flupirtine, its N-acetylated and two mercapturic acid derivatives in man. *J. Pharm. Biomed. Anal.*, **2015**, *102*, 377–385.

(104) Siegmund, W.; Modess, C.; Scheuch, E.; Methling, K.; Keiser, M.; Nassif, A.; Rosskopf, D.; Bednarski, P. J.; Borlak, J.; Terhaag, B. Metabolic activation and analgesic effect of flupirtine in healthy subjects, influence of the polymorphic NAT2, UGT1A1 and GSTP1. *Br. J. Clin. Pharmacol.*, **2015**, *79* (3), 501–513.

(105) Klopčič, I.; Dolenc, M. S. Chemicals and drugs forming reactive quinone and quinone imine metabolites. *Chem. Res. Toxicol.*, **2019**, *32* (1), 1–34.

(106) Nicoletti, P.; Werk, A. N.; Sawle, A.; Shen, Y.; Urban, T. J.; Coulthard, S. A.; Bjornsson, E. S.; Cascorbi, I.; Floratos, A.; Stammschulte, T.; Gundert-Remy, U.; Nelson, M. R.; Aithal, G. P.; Daly, A. K. HLA-DRB1*16: 01-DQB1*05: 02 is a novel genetic risk factor for flupirtine-induced liver injury. *Pharmacogenet. Genomics*, **2016**, *26* (5), 218–224.

(107) Yun, J.; Adam, J.; Yerly, D.; Pichler, W. J. Human leukocyte antigens (HLA) associated drug hypersensitivity: consequences of drug binding to HLA. *Allergy*, **2012**, *67* (11), 1338–1346.

(108) Waddington, J. C.; Meng, X.; Illing, P. T.; Tailor, A.; Adair, K.; Whitaker, P.; Hamlett, J.; Jenkins, R. E.; Farrell, J.; Berry, N.; Purcell, A. W.; Naisbitt, D. J.; Park, B. K. Identification of flucloxacillin-haptenated HLA-B*57:01 ligands: evidence of antigen processing and presentation. *Toxicol. Sci.*, **2020**, *177* (2), 454–465.

(109) Andrade, R. J.; Chalasani, N.; Björnsson, E. S.; Suzuki, A.; Kullak-Ublick, G. A.; Watkins, P. B.; Devarbhavi, H.; Merz, M.; Lucena, M. I.; Kaplowitz, N.; Aithal, G. P. Drug-induced liver injury. *Nat. Rev. Dis. Primers*, **2019**, *5* (1), 58.

(110) Kaplowitz, N. Acetaminophen hepatoxicity: what do we know, what don't we know, and what do we do next? *Hepatology*, **2004**, *40* (1), 23–26.

(111) Hempel, R.; Schupke, H.; McNeilly, P. J.; Heinecke, K.; Kronbach, C.; Grunwald, C.; Zimmermann, G.; Griesinger, C.; Engel, J.; Kronbach, T. Metabolism of retigabine (D-23129), a novel anticonvulsant. *Drug. Metab. Dispos.*, **1999**, *27* (5), 613–622.

(112) Groseclose, M. R.; Castellino, S. An investigation into retigabine (ezogabine) associated dyspigmentation in rat eyes by MALDI imaging mass spectrometry. *Chem. Res. Toxicol.*, **2019**, *32* (2), 294–303.

(113) Howells, L.; Godfrey, M.; Sauer, M. J. Melanin as an adsorbent for drug residues. *Analyst*, **1994**, *119* (12), 2691–2693.

(114) Hernandez, C. C.; Tarfa, R. A.; Miguel I Limcaoco, J.; Liu, R.; Mondal, P.; Hill, C.; Keith Duncan, R.; Tzounopoulos, T.; Stephenson, C. R. J.; O'Meara, M. J.; Wipf, P. Development of an automated screen for K_V7.2 potassium channels and discovery of a new agonist chemotype. *Bioorg. Med. Chem. Lett.*, **2022**, *71*, 128841.

(115) Bloms-Funke, P.; Bankstahl, M.; Bankstahl, J.; Kneip, C.; Schröder, W.; Löscher, W. The novel dual-mechanism K_V7 potassium channel/TSPO receptor activator GRT-X is more effective than the K_V7 channel opener retigabine in the 6-Hz refractory seizure mouse model. *Neuropharmacology*, **2022**, *203*, 108884.

(116) Aleo, M. D.; Aubrecht, J.; D Bonin, P.; Burt, D. A.; Colangelo, J.; Luo, L.; Schomaker, S.; Swiss, R.; Kirby, S.; C Rigdon, G.; Dua, P. Phase I study of PF-04895162, a K_V7 channel opener, reveals unexpected hepatotoxicity in healthy subjects, but not rats or monkeys: clinical evidence of disrupted bile acid homeostasis. *Pharmacol. Res. Perspect.*, **2019**, *7* (1), e00467.

(117) Amato, G.; Roeloffs, R.; Rigdon, G. C.; Antonio, B.; Mersch, T.; McNaughton-Smith, G.; Wickenden, A. D.; Fritch, P.; Suto, M. J. *N*-Pyridyl and pyrimidine benzamides as KCNQ2/Q3 potassium channel openers for the treatment of epilepsy. *ACS Med. Chem. Lett.*, **2011**, *2* (6), 481–484.

(118) Zhang, Y.-M.; Xu, H.-Y.; Hu, H.-N.; Tian, F.-Y.; Chen, F.; Liu, H.-N.; Zhan, L.; Pi, X.-P.; Liu, J.; Gao, Z.-B.; Nan, F.-J. Discovery of HN37 as a potent and chemically stable antiepileptic drug candidate. *J. Med. Chem.*, **2021**, *64* (9), 5816–5837.

(119) Grupe, M.; Bentzen, B. H.; Benned-Jensen, T.; Nielsen, V.; Frederiksen, K.; Jensen, H. S.; Jacobsen, A.-M.; Skibsbye, L.; Sams, A. G.; Grunnet, M.; Rottländer, M.; Bastlund, J. F. In vitro and in vivo characterization of Lu AA41178: a novel, brain penetrant, pan-selective K_V7 potassium channel opener with efficacy in preclinical models of epileptic seizures and psychiatric disorders. *Eur. J. Pharmacol.*, **2020**, *887*, 173440.

(120) Musella, S.; Carotenuto, L.; Iraci, N.; Baroli, G.; Ciaglia, T.; Nappi, P.; Basilicata, M. G.; Salviati, E.; Barrese, V.; Vestuto, V.; Pignataro, G.; Pepe, G.; Sommella, E.; Di Sarno, V.; Manfra, M.; Campiglia, P.; Gomez-Monterrey, I.; Bertamino, A.; Taglialatela, M.; Ostacolo, C.; Miceli, F. Beyond retigabine: design, synthesis, and pharmacological characterization of a potent and chemically stable neuronal K_V7 channel activator with anticonvulsant activity. *J. Med. Chem.*, **2022**, *65* (16), 11340–11364.

(121) Vernier, J.-M.; De La Rosa, M. A.; Chen, H.; Wu, J. Z.; Larson, G. L.; Cheney, I. W.; Valeant Pharmaceuticals. Derivatives of 4-(*N*-azacycloalkyl) anilides as potassium channel modulators, **2012**, US 8293911 B2.

(122) Wurm, K. W.; Bartz, F.-M.; Schulig, L.; Bodtke, A.; Bednarski, P. J.; Link, A. Carba analogues of flupirtine and retigabine with improved oxidation resistance and reduced risk of quinoid metabolite formation. *ChemMedChem*, **2022**, e202200262.

(123) Bock, C.; Surur, A. S.; Beirow, K.; Kindermann, M. K.; Schulig, L.; Bodtke, A.; Bednarski, P. J.; Link, A. Sulfide analogues of flupirtine and retigabine with nanomolar K_V7.2/K_V7.3 channel opening activity. *ChemMedChem*, **2019**, *14* (9), 952–964.

(124) Surur, A. S.; Bock, C.; Beirow, K.; Wurm, K.; Schulig, L.; Kindermann, M. K.; Siegmund, W.; Bednarski, P. J.; Link, A. Flupirtine and retigabine as templates for ligand-based drug design of K_V7.2/3 activators. *Org. Biomol. Chem.*, **2019**, *17* (18), 4512–4522.

(125) Konishi, K.; Fukami, T.; Ogiso, T.; Nakajima, M. In vitro approach to elucidate the relevance of carboxylesterase 2 and N-acetyltransferase 2 to flupirtine-induced liver injury. *Biochem. Pharmacol.*, **2018**, *155*, 242–251.

(126) Bak-Jensen, H. H.; Hertel, K. P.; H. Lundbeck A/S. Use of KCNQ potassium channel openers for reducing symptoms of or treating disorders or conditions wherein the dopaminergic system is disrupted, **2009**, WO2009015667A1.

(127) Greve, D. R.; Rottlaender, M.; Watson, W. P.; H. Lundbeck A/S. Substituted aniline derivatives, **2004**, WO2004080950A1.

(128) Zhao, H.; Fu, H.; Qiao, R. Copper-catalyzed direct amination of ortho-functionalized haloarenes with sodium azide as the amino source. *J. Org. Chem.*, **2010**, *75* (10), 3311–3316.

(129) Tron, G. C.; Minassi, A.; Sorba, G.; Fausone, M.; Appendino, G. Icilio Guareschi and his amazing "1897 reaction". *Beilstein J. Org. Chem.*, **2021**, *17*, 1335–1351.

(130) Wurm, K. W.; Bartz, F.-M.; Schulig, L.; Bodtke, A.; Bednarski, P. J.; Link, A. Modifications of the triaminoaryl metabophore of flupirtine and retigabine aimed at avoiding quinone diimine formation. *ACS Omega*, **2022**, *7* (9), 7989–8012.

(131) Yap, J. L.; Hom, K.; Fletcher, S. Ortho-selectivity in the nucleophilic aromatic substitution (S_NAr) reactions of 3-substituted, 2,6-dichloropyridines with alkali metal alkoxides. *Tetrahedron Lett.*, **2011**, *52* (32), 4172–4176.

(132) Kühnert, S.; Bahrenberg, G.; Kless, A.; Schroder, W.; Lucas, S.; Grünenthal GmbH. Substituted 6-amino-nicotinamides as KCNQ2/3 modulators, **2012**, US 2012/0258947 Al.

(133) Yeung, K.-S.; Farkas, M. E.; Kadow, J. F.; Meanwell, N. A. A base-catalyzed, direct synthesis of 3,5-disubstituted 1,2,4-triazoles from nitriles and hydrazides. *Tetrahedron Lett.*, **2005**, *46* (19), 3429–3432.

(134) Antczak, M. I.; Zhang, Y.; Wang, C.; Doran, J.; Naidoo, J.; Voruganti, S.; Williams, N. S.; Markowitz, S. D.; Ready, J. M. Inhibitors of 15-prostaglandin dehydrogenase to potentiate tissue repair. *J. Med. Chem.*, **2017**, *60* (9), 3979–4001.

(135) Palermo, M. G. Novel one-pot cyclization of ortho substituted benzonitriles to 3-amino-1,2-benzisoxazoles. *Tetrahedron Lett.*, **1996**, *37* (17), 2885–2886.

(136) Gangloff, A. R.; Litvak, J.; Shelton, E. J.; Sperandio, D.; Wang, V. R.; Rice, K. D. Synthesis of 3,5-disubstituted-1,2,4-oxadiazoles using tetrabutylammonium fluoride as a mild and efficient catalyst. *Tetrahedron Lett.*, **2001**, *42* (8), 1441–1443.

(137) Davis, M.; Stamper, B. D. TAMH: a useful in vitro model for assessing hepatotoxic mechanisms. *Biomed. Res. Int.*, **2016**, *2016*, 4780872.

(138) Ramirez, T.; Strigun, A.; Verlohner, A.; Huener, H.-A.; Peter, E.; Herold, M.; Bordag, N.; Mellert, W.; Walk, T.; Spitzer, M.; Jiang, X.; Sperber, S.; Hofmann, T.; Hartung, T.; Kamp, H.; van Ravenzwaay, B. Prediction of liver toxicity and mode of action using metabolomics in vitro in HepG2 cells. *Arch. Toxicol.*, **2018**, *92* (2), 893–906.

(139) Mosmann, T. Rapid colorimetric assay for cellular growth and survival: application to proliferation and cytotoxicity assays. *J. Immunol. Methods*, **1983**, *65* (1-2), 55–63.

(140) Madsen, K. G.; Olsen, J.; Skonberg, C.; Hansen, S. H.; Jurva, U. Development and evaluation of an electrochemical method for studying reactive phase-I metabolites: correlation to in vitro drug metabolism. *Chem. Res. Toxicol.*, **2007**, *20* (5), 821–831.

(141) Rodríguez-Cid, L.; Sentellas, S.; Saurina, J. Voltammetric and electrogeneration approaches for the assessment of the oxidative drug metabolism. *Anal. Bioanal. Chem.*, **2018**, *410* (8), 2229–2239.

(142) Hughes, T. B.; Swamidass, S. J. Deep learning to predict the formation of quinone species in drug metabolism. *Chem. Res. Toxicol.*, **2017**, *30* (2), 642–656.

(143) Chen, L.; He, Y.; Wang, X.; Ge, J.; Li, H. Ventricular voltage-gated ion channels: detection, characteristics, mechanisms, and drug safety evaluation. *Clin. Transl. Med.*, **2021**, *11* (10), e530.

(144) Obergrussberger, A.; Friis, S.; Brüggemann, A.; Fertig, N. Automated patch clamp in drug discovery: major breakthroughs and innovation in the last decade. *Expert Opin. Drug Discov.*, **2021**, *16* (1), 1–5.

(145) Xie, M.; Zhu, G.; Hu, Y.; Gu, H. Conformations of morpholine in liquid and adsorbed on gold nanoparticles explored by raman spectroscopy and theoretical calculations. *J. Phys. Chem. C*, **2011**, *115* (42), 20596–20602.

(146) Payandeh, J.; Volgraf, M. Ligand binding at the protein-lipid interface: strategic considerations for drug design. *Nat. Rev. Drug Discov.*, **2021**, *20* (9), 710–722.

(147) Liu, F.; Zhang, Z.; Levit, A.; Levring, J.; Touhara, K. K.; Shoichet, B. K.; Chen, J. Structural identification of a hotspot on CFTR for potentiation. *Science*, **2019**, *364* (6446), 1184–1188.

(148) Seydel, J. K.; Schaper, K. J.; Coats, E. A.; Cordes, H. P.; Emig, P.; Engel, J.; Kutscher, B.; Polymeropoulos, E. E. Synthesis and quantitative structure-activity relationships of anticonvulsant 2,3,6-triaminopyridines. *J. Med. Chem.*, **1994**, *37* (19), 3016–3022.

(149) Jagodzinska, M.; Huguenot, F.; Candiani, G.; Zanda, M. Assessing the bioisosterism of the trifluoromethyl group with a protease probe. *ChemMedChem*, **2009**, *4* (1), 49–51.

(150) Kenna, J. G.; Uetrecht, J. Do in vitro assays predict drug candidate idiosyncratic drug-induced liver injury risk? *Drug. Metab. Dispos.*, **2018**, *46* (11), 1658–1669.

(151) Segovia-Zafra, A.; Di Zeo-Sánchez, D. E.; López-Gómez, C.; Pérez-Valdés, Z.; García-Fuentes, E.; Andrade, R. J.; Lucena, M. I.; Villanueva-Paz, M. Preclinical models of idiosyncratic drug-induced liver injury (iDILI): moving towards prediction. *Acta Pharm. Sin. B*, **2021**, *11* (12), 3685–3726.

(152) Kullak-Ublick, G. A.; Andrade, R. J.; Merz, M.; End, P.; Benesic, A.; Gerbes, A. L.; Aithal, G. P. Drug-induced liver injury: recent advances in diagnosis and risk assessment. *Gut*, **2017**, *66* (6), 1154–1164.

(153) Donato, M. T.; Lahoz, A.; Castell, J. V.; Gómez-Lechón, M. J. Cell lines: a tool for in vitro drug metabolism studies. *Curr. Drug Metab.*, **2008**, *9* (1), 1–11.

(154) Tham, N. T. T.; Hwang, S.-R.; Bang, J.-H.; Yi, H.; Park, Y.-I.; Kang, S.-J.; Kang, H.-G.; Kim, Y.-S.; Ku, H.-O. High-content analysis of in vitro hepatocyte injury induced by various hepatotoxicants. *J. Vet. Sci.*, **2019**, *20* (1), 34–42.

(155) Gunduz, M.; Argikar, U. A.; Kamel, A.; Colizza, K.; Bushee, J. L.; Cirello, A.; Lombardo, F.; Harriman, S. Oxidative ipso substitution of 2,4-difluoro-benzylphthalazines: identification of a rare stable quinone methide and subsequent GSH conjugate. *Drug. Metab. Dispos.*, **2012**, *40* (11), 2074–2080.

7 Publikationen

7.1 Publikation I

Carba Analogues of Flupirtine and Retigabine with Improved Oxidation Resistance and Reduced Risk of Quinoid Metabolite Formation

Konrad W. Wurm, Frieda-Marie Bartz, Lukas Schulig, Anja Bodtke, Patrick J. Bednarski, Andreas Link

ChemMedChem **2022**, e202200262.
DOI: 10.1002/cmdc.202200262

Beiträge der Autoren

Konrad W. Wurm	Planung und Durchführung der Synthesen Analytische Charakterisierung Erstellen des Manuskripts
Frieda-Marie Bartz	Biologische Testung
Lukas Schulig	Durchführung von Modelling und Moleküldynamiksimulationen
Anja Bodtke	Durchführung der HRMS- und NMR-Messungen
Patrick J. Bednarski	Korrektur des Manuskripts
Andreas Link	Anleitung bei der Bearbeitung des Projekts Erstellen des Manuskripts

_____ _____

Konrad Wurm Andreas Link

ChemMedChem

Research Article
doi.org/10.1002/cmdc.202200262

Chemistry Europe
European Chemical Societies Publishing

www.chemmedchem.org

Carba Analogues of Flupirtine and Retigabine with Improved Oxidation Resistance and Reduced Risk of Quinoid Metabolite Formation

Konrad W. Wurm,[a] Frieda-Marie Bartz,[a] Lukas Schulig,[a] Anja Bodtke,[a] Patrick J. Bednarski,[a] and Andreas Link*[a]

The K_V7 potassium channel openers flupirtine and retigabine have been valuable options in the therapy of pain and epilepsy. However, as a result of adverse reactions, both drugs are currently no longer in therapeutic use. The flupirtine-induced liver injury and the retigabine linked tissue discolouration do not appear related at first glance; nevertheless, both events can be attributed to the triaminoaryl scaffold, which is affected by oxidation leading to elusive reactive quinone diimine or azaquinone diimine metabolites. Since the mechanism of action, i.e. K_V7 channel opening, seems not to be involved in toxicity, this study aimed to further develop safer replacements for flupirtine and retigabine. In a ligand-based design strategy, replacing amino substituents of the triaminoaryl core with alkyl substituents led to carba analogues with improved oxidation resistance and negligible risk of quinoid metabolite formation. In addition to these improved safety features, some of the novel analogues exhibited significantly improved $K_V7.2/3$ channel opening activity, indicated by an up to 13-fold increase in potency and an efficacy of up to 176% compared to flupirtine, thus being attractive candidates for further development.

Introduction

K_V7 channels (KCNQ channels) are homo- or heterotetrameric, non-inactivating, voltage-dependent potassium channels with slow gating kinetics.[1] Their activation causes an outward-directed potassium flow, which in turn leads to a more negative cell membrane potential and thus increases the threshold for new action potentials.[2] The resulting current is commonly referred to as the M-current, which is fundamentally involved in controlling neuronal excitability in both the central and peripheral nervous systems.[3] The possibility of slowing excessive neuronal excitation by activating $K_V7.2/3$ sub-type channels makes them an attractive target for drug development in some areas with unmet medical needs, including pharmacoresistant epilepsy,[4] different types of pain,[5] and depression.[6] While strong evidence exists for the clinical value as analgesic and antiepileptic, only preclinical data suggest an additional antidepressant potential to date.

Flupirtine (**1**, Figure 1) was the first approved drug to act as an opener of $K_V7.2/3$ channels, although it was only identified as such several years after its discovery as a non-opioid and non-steroidal analgesic.[7] It has been in therapeutic use in humans for more than 30 years, and over this time, the drug was considered a well-tolerated analgesic with relatively mild side effects until the first reports of hepatotoxic reactions under flupirtine treatment were published in 2011 and 2012, respectively.[8,9] The severe but sporadic hepatotoxic events (reporting rate 1.68 cases/100,000 patient-years) initially forced the responsible authorities to impose restrictions on use and, after these proved insufficient, to withdraw the authorization of

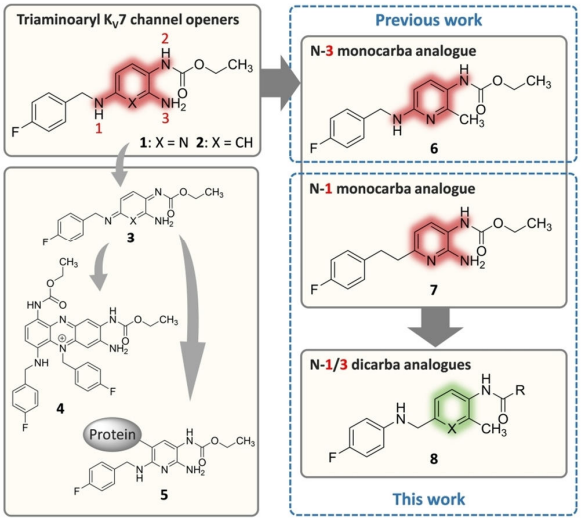

Figure 1. Structures of flupirtine (**1**) and retigabine (**2**), the proposed toxification pathway to phenazinium salt **4** in the case of retigabine, and hapten-protein adducts **5** in the case of flupirtine via azaquinone diimines or quinone diimines **3**, and selected structural modifications carried out in previous work (**6**) and this work (**7**, **8**).

[a] K. W. Wurm, F.-M. Bartz, Dr. L. Schulig, Dr. A. Bodtke, Prof. Dr. P. J. Bednarski, Prof. Dr. A. Link
Institute of Pharmacy, University of Greifswald
Friedrich-Ludwig-Jahn-Str. 17, 17489 Greifswald (Germany)
Fax: (+49) (0)3834 4204895
E-mail: link@uni-greifswald.de

Supporting information for this article is available on the WWW under https://doi.org/10.1002/cmdc.202200262

ChemMedChem
Research Article
doi.org/10.1002/cmdc.202200262
Chemistry Europe
European Chemical Societies Publishing

flupirtine-containing medications.[10] As an alarming consequence of this withdrawal, metamizole is being increasingly used to replace flupirtine in Germany despite its known association with blood dyscrasias, yielding a growing number of reports of metamizole-induced neutropenia.[11]

Retigabine (**2**, USAN: ezogabine), a close structural analogue of flupirtine, was approved in 2011 for adjunctive treatment of partial-onset seizures in adult patients with epilepsy where other appropriate medicines were insufficiently effective.[12] However, shortly after approval, it became clear that retigabine treatment occasionally resulted in blue discolouration of the skin and ocular tissues.[13] Since the consequences and the reversibility of these discolourations were initially unclear, the FDA issued a boxed warning.[14] Although additional investigations did not indicate that the pigment changes in the eyes affect vision, the manufacturer discontinued retigabine in 2017 because of limited and declining use.[15]

However, the side effects of flupirtine and retigabine responsible for failure seem to be no class effects of K_V7.2/3 channel openers in general. In both cases, the adverse drug reactions are likely resulting from the drug-specific metabolism, which affects especially the oxidation-sensitive triaminoaryl metabophore. Concerning flupirtine, an *in vitro* trapping study using peroxidase mediated oxidation was able to detect glutathione conjugates, which are suggested to indicate the formation of reactive azaquinone diimine metabolites such as **3**.[16] Additional evidence for the formation of reactive electrophilic metabolites of flupirtine was provided by a clinical study; after administration of flupirtine to healthy human subjects, mercapturic acid derivatives of the drug were detected in the urine, which are also likely to result from azaquinone diimine metabolites.[17,18] Since a connection between the formation of reactive quinoid metabolites and hepatotoxicity is well known and has been demonstrated for several drugs in the past,[19] the supposed reactive azaquinone diimine metabolites are very likely to be involved in flupirtine-induced liver injury. Furthermore, the rarity of the reported hepatotoxic reactions and the lack of a dose-dependency suggest the contribution of an additional component to the pathomechanism of flupirtine-associated hepatotoxicity. Since genetic polymorphisms of metabolizing enzymes could be largely ruled out as a cause,[18] the theory of a possible involvement of the adaptive immune system came into focus, supported by two case studies. A histological investigation concluded that clinical and histological features raise the possibility of immune-mediated toxicity, and a genome-wide association study identified a certain human leukocyte antigen gene as a genetic risk factor for flupirtine-induced hepatotoxicity.[9,20] Considering both the formation of reactive azaquinone diimine metabolites and the possible involvement of the immune system, a hapten mechanism becomes likely. After binding to an endogenous carrier protein, azaquinone diimine metabolites of flupirtine may form hapten-protein adducts such as **5** that are able to trigger toxic autoimmune responses. The resulting immune-mediated idiosyncratic reactions are typically very rare, not dose-related, and often occur with a delay,[21] as observed in the case of flupirtine-associated hepatotoxicity.

In contrast, the hepatic metabolism of retigabine is not dominated by oxidation but by phase II reactions, particularly N-glucuronidation. In fact, there is no evidence of hepatic metabolism to reactive quinone diimine metabolites or any possible hepatotoxic effects of retigabine at therapeutic doses.[12,22] However, in a reaction associated with the presence of melanin, retigabine appears to be oxidized in other tissue types, such as ocular tissues, yielding quinone diimines **3**, which subsequently tend to dimerize. The resulting dimers can be oxidized further and thus form phenazinium structures such as **4**, identified by MALDI imaging mass spectrometry in rat eyes (but not albino rats lacking melanin) after retigabine treatment. These compounds are presumed to be responsible for the blue tissue discolouration caused by retigabine.[23]

Since the oxidation to reactive metabolites is likely to be the reason for the adverse drug reactions in the cases of flupirtine and retigabine, this work aimed to modify the oxidation labile triaminoaryl metabophore of the two failed K_V7 channel openers to prevent the formation of quinone diimine or azaquinone diimine metabolites. The starting point for the structural modifications carried out in the present study was the N-3 monocarba analogue **6** synthesized in our previous work (for the numbering of the nitrogen atoms, see Figure 1).[24] Other analogues with methyl substitution at the primary amine site have also been described elsewhere (not shown).[25,26,27] In the case of analogue **6**, the removal of the primary amino function from the central pyridine ring and its replacement with a methyl group resulted in a compound that was equipotent to flupirtine, had a slightly attenuated liver cell toxicity *in vitro*, and was less sensitive to oxidation, indicated by an increased anodic peak potential in cyclovoltammetric measurements. In this work, following a ligand-based design strategy, the different N-1 monocarba analogue **7** was prepared, in which a methylene group replaces the secondary amino function of flupirtine to investigate possible advantageous properties in analogy to **6**. In the next step, the N-1/3 dicarba analogues **8** and related compounds with an inverted secondary amino function and a methyl group instead of the primary amino moiety were synthesized since the N-1 or N-3 monocarba analogues **6** and **7**, despite increased oxidation stability of **6**, still bear the risk of azaquinone diimine formation. In contrast, the N-1/3 dicarba analogues **8** only have one nitrogen atom directly attached to the central aromatic ring. Thus, metabolism to quinone diimines or azaquinone diimines can be excluded by design. In particular, similar retigabine analogues with scaffold **8** (X=CH) have already been described in patent literature,[25,28] as have structurally related tetrahydroquinoline and tetrahydroisoquinoline derivatives.[29] Nevertheless, this work provides a comprehensive investigation of the underlying structure-activity relationships and further safety relevant properties such as oxidation behaviour or *in vitro* hepatotoxicity, which are currently missing.

ChemMedChem
Research Article
doi.org/10.1002/cmdc.202200262
Chemistry Europe
European Chemical Societies Publishing

Results and Discussion

Design and synthesis of N-1 monocarba analogues

As depicted in Scheme 1, the starting material for the synthesis of the N-1 monocarba analogue **7** was commercially available 2,6-dichloro-3-nitropyridine (**12**). The initial step introduced a primary amino function through a nucleophilic substitution reaction with ammonia, yielding aminopyridine **13**. The reaction proceeded regioselectively at the 2-position as previously reported by Kinarivala et al.[30] A halogen exchange was then carried out to obtain the aryl bromide **14** as a more reactive starting material for the subsequent Sonogashira reaction to synthesize the coupling product **15**. 4-Fluorophenylacetylene (**11**) used for the coupling reaction was synthesized starting from 1-bromo-4-fluorobenzene (**9**) also via a Sonogashira reaction by using trimethylsilylacetylene as an alkyne component to obtain the corresponding coupling product **10**. The subsequent cleavage of the trimethylsilyl protective group yielded the free terminal alkyne **11**. An alternative synthetic strategy for the preparation of **15** via intermediates **17** and **18**, investigated in a first attempt, failed in the last step since no product formation took place under standard Sonogashira coupling conditions. After the successfully conducted cross-coupling reaction for C–C bond formation, a reduction of **15** was carried out by catalytic hydrogenation with Pd/C as a catalyst, in which both the triple bond and the nitro group were reduced simultaneously. The resulting *ortho*-diamine **19** was not isolated but reacted directly with ethyl chloroformate under an inert atmosphere to obtain the final compound **7**.

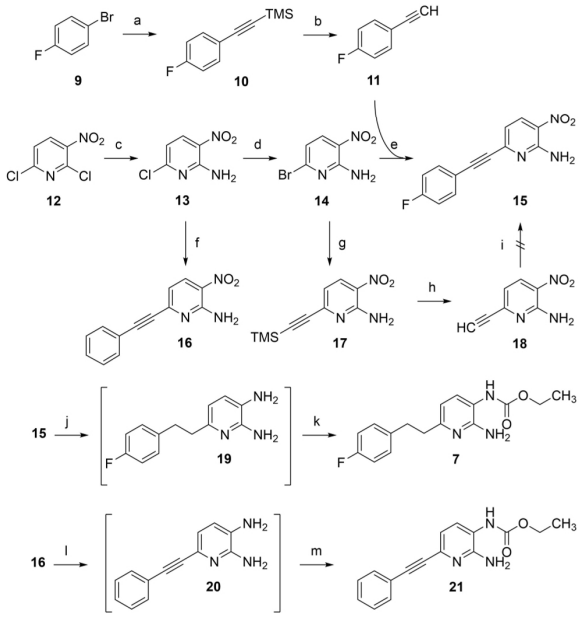

Scheme 1. Synthesis of N-1 monocarba analogues **7** and **21**: a) trimethylsilylacetylene, CuI, $Pd(PPh_3)_4$, TEA, 60 °C, 16 h, 99%; b) K_2CO_3, MeOH, RT, 5 h, 85%; c) NH_3, EtOH, 0 °C–RT, 21 h, 83%; d) HBr, AcOH, 100 °C, 8 h, 93%; e) CuI, $Pd(PPh_3)_4$, TEA, DMF, 60 °C, 6 h, 80%; f) phenylacetylene, CuI, $Pd(PPh_3)_4$, TEA, DMF, 60 °C, 1 h, 38%; g) trimethylsilylacetylene, CuI, $Pd(PPh_3)_4$, TEA, DMF, 60 °C, 0.5 h, 74%; h) K_2CO_3, MeOH, RT, 0.5 h, 75%; i) 1-bromo-4-fluorobenzene, CuI, $Pd(PPh_3)_4$, TEA, DMF, 60 °C; j) H_2, Pd/C, EtOAc, 40 °C, 40 h; k) ethyl chloroformate, THF, TEA, RT, 4 h, 25%; l) Fe, AcOH, 50 °C, 1 h; m) ethyl chloroformate, THF, TEA, RT, 7 h, 30%.

In addition to the envisioned N-1 monocarba analogue **7**, the synthetic route also offered the opportunity to synthesize a more linear and less flexible alkyne derivative **21**, enabling further exploration of the binding site. In this case, the 4-fluoro substituent was omitted to simplify the synthesis, using commercially available phenylacetylene instead of 4-fluorophenylacetylene. However, this is not expected to negatively affect the activity since a flupirtine derivative without a 4-fluoro substituent was approximately as active as the parent compound itself in the maximum electroshock seizure test, suggesting that the 4-fluoro substituent is not relevant for $K_V7.2/3$ opening.[31] To further shorten the synthesis by one step, the Sonogashira coupling was carried out starting from the aryl chloride **13**, which, however, led to a significantly reduced yield of 38% compared to previously performed Sonogashira couplings (74–99% yield), demonstrating the superiority of a preceding chloride to bromide exchange in the reactant as it was done for the synthesis of carba analogue **7**. The subsequent reduction of **16** was performed with iron in acetic acid as a reducing agent instead of catalytic hydrogenation with Pd/C since only the nitro group and not the triple bond should be reduced selectively. The final step in preparing the alkyne carba analogue **21** was the carbamate formation, which was carried out as described for the synthesis of **7** without prior isolation of the diamino intermediate **20**.

Design and synthesis of N-1/3 dicarba analogues

Since the N-1 and N-3 monocarba analogues **6**, **7** and **21** may have beneficial properties but still bear the risk of oxidative azaquinone diimine formation, the next step, as mentioned in the introduction, was the synthesis of N-1/3 dicarba analogues that only have one nitrogen atom left attached to the central aromatic ring. Designing these N-1/3 dicarba analogues, the secondary amino function was not entirely replaced by a hydrocarbon linker but inverted to retain drug-like physicochemical properties in terms of avoiding an increase in lipophilicity. Furthermore, in the case of the first compound of this series (**27**, Scheme 2), the ethyl carbamate of flupirtine and retigabine has been replaced by a 2-methylpropyl carbamate since docking suggested space for more bulky carbamate side chains and the 2-methylpropyl moiety in this position proved to be slightly superior to the ethyl residue in a series of retigabine analogues described in the literature.[32]

The synthesis of N-1/3 dicarba analogue **27** was carried out starting from the commercially available pyridine derivative **22**. In the first step, the nitrile function was introduced via a modified version of the typically copper-catalyzed Rosenmund-von Braun reaction by using a palladium catalyst and $Zn(CN)_2$ instead of CuCN. The nitro group of the resulting compound **23** was reduced with $SnCl_2$ to obtain the aminopyridine **24**, which was subsequently reacted with 2-methylpropyl chloroformate,

ChemMedChem
Research Article
doi.org/10.1002/cmdc.202200262
Chemistry Europe
European Chemical Societies Publishing

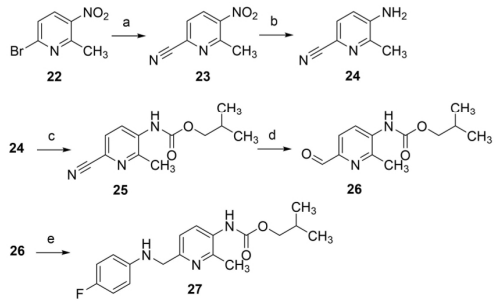

Scheme 2. Synthesis of N-1/3 dicarba analogue **27**: a) $Zn(CN)_2$, $Pd(PPh_3)_4$, DMF, 70 °C, 24 h, 96%; b) Fe, AcOH, $CaCl_2$, EtOH, RT, 2 h, 71%; c) isobutyl chloroformate, TEA, 4-DMAP, DCM, RT, 4 d, 34%; d) DIBAL–H, DCM, −85 °C, 4 h, 23%; e) 1. 4-fluoroaniline, DCM, RT, 5 h, 2. $NaBH_4$, MeOH, RT, 1 h, 82%.

yielding the carbamate **25**. In the following reaction step, the nitrile group of **25** was reduced with diisobutylaluminum hydride (DIBAL–H), which initially led to an imine intermediate (not shown) and, after acidic workup, provided the corresponding aldehyde **26**. Finally, reductive amination with 4-fluoroaniline and $NaBH_4$ was performed to obtain the desired N-1/3 dicarba analogue **27**.

In previous work, several amide derivatives of flupirtine and retigabine were found to be superior compared to carbamate analogues in terms of channel-opening activity.[24,33] In addition, it was shown that the carbamate function of flupirtine is affected by esterase-mediated cleavage, which in turn means that amide derivatives could have improved metabolic stability.[16,34] For this reason, amide derivatives of N-1/3 dicarba analogues were intended to be synthesized in the next step. Simultaneously with the introduction of an amide group, another structural change affecting the central aromatic ring was made. Since retigabine has a 7-fold increased potency compared to its pyridine congener flupirtine, the following N-1/3 dicarba amide analogues have a central phenyl ring to aim for improved biological activity (Scheme 3). In the course of these structural modifications, in addition to various N-1/3 dicarba analogues, a derivative was synthesized that bears a fluoro substituent instead of the methyl group (**35c**). Technically speaking, this compound cannot be referred to as an N-1/3 dicarba analogue but serves the same purpose of avoiding quinone diimine formation and should therefore be included as a related dideaza derivative here, too.

The syntheses of N-1/3 dicarba amide analogues containing a central phenyl ring usually began with 4-bromoanilines **31a-c**. In the case of a 2,6-dimethylated derivative, the bromoaniline **31a** was prepared by bromination of the corresponding aniline **30**. The bromoanilines were then converted into the nitriles **32a-c** in a Rosenmund-von Braun reaction using CuCN in a dual function as a catalyst and cyanide source. In the case of a trifluoromethylated analogue, the synthesis was carried out differently, starting from the nitrobenzene **28**, which was first converted into the nitrile **29** and then reduced to the aniline **32d** with $SnCl_2$. In this case, the Rosenmund-von Braun reaction was again performed in a palladium-catalyzed version providing

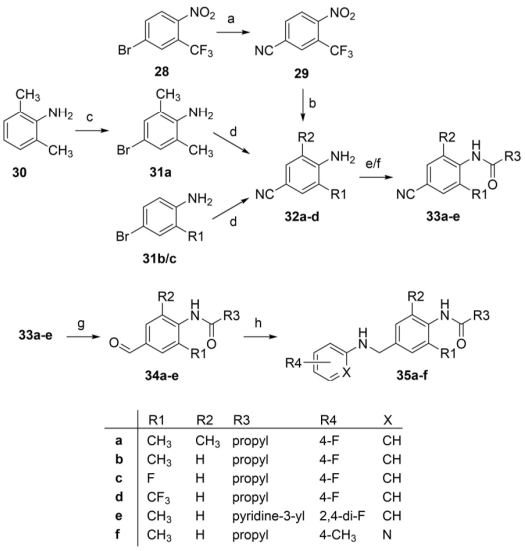

	R1	R2	R3	R4	X
a	CH_3	CH_3	propyl	4-F	CH
b	CH_3	H	propyl	4-F	CH
c	F	H	propyl	4-F	CH
d	CF_3	H	propyl	4-F	CH
e	CH_3	H	pyridine-3-yl	2,4-di-F	CH
f	CH_3	H	propyl	4-CH_3	N

Scheme 3. Synthesis of N-1/3 dicarba analogues **35a-f**: a) $Zn(CN)_2$, $Pd(OAc)_2$, PPh_3, DMF, 100 °C, 1.5 h, 83%; b) $SnCl_2$, EtOAc, 70 °C, 0.5 h, 99%; c) Br_2, DCM, −78 °C–RT, 1 h, 96%; d) CuCN, NMP, 170 °C, 7–8 h, 42–47%; e) 1. acyl chloride, TEA, 4-DMAP, THF, 0 °C, 0.5 h, 2. RT/70 °C, 16 h–7 d, 56–74% (**33a,d**); f) 1. acyl chloride, TEA, DCM, RT, 1 h, 2. RT/40 °C, 3–89 h, 67–88% (**33b,c,e**); g) Ni, HCOOH, 80 °C, 6–8 h, 37–88%; h) 1. amine, molecular sieves, toluene, 120 °C, 4–8 h, 2. $NaBH_4$, MeOH, 1,4-dioxane, 0 °C–RT, 17 h, 42–73%.

a better yield (83%) compared to the copper-catalyzed procedure used before (43–47%). The next step was an amide coupling for all derivatives. Since the 4-aminobenzonitriles **32a-d** used as reactants proved to be unreactive amine components due to the electron-withdrawing properties of the cyano group and the steric hindrance by ortho substituents, it was partially necessary to apply elevated temperatures of up to 70 °C, long reaction times of up to seven days, or additional use of a catalyst (4-DMAP). The nitrile function of the amides **33a-e** obtained in this way was subsequently reduced to obtain the corresponding aldehydes **34a-e** by using nickel in formic acid. Finally, reductive amination with sodium borohydride and different aniline reactants was carried out to prepare the desired N-1/3 dicarba analogues **35a-f**.

A total of six derivatives (**35a-f**) were synthesized in this series of N-1/3 dicarba analogues with amide substituent and a central phenyl ring, some of which have additional structural changes. Instead of the methyl group, a trifluoromethyl group or, as already mentioned, a fluoro substituent was introduced in compounds **35c** and **35d**, respectively. In addition, a pyridine ring was evaluated both as an alternative bulkier amide substituent in the case of **35e** and a more hydrophilic replacement of the 4-fluorophenyl ring in analogue **35f**. In the case of **35f**, the putatively metabolically most labile position of the pyridine ring was substituted with a methyl group. Moreover, a second ortho methyl group has already proven to be beneficial for the activity of some analogues of flupirtine and retigabine known from the literature and was therefore attached to the central ring of **35a**.[27,35]

ChemMedChem
Research Article
doi.org/10.1002/cmdc.202200262
Chemistry Europe
European Chemical Societies Publishing

Since it was expected that the N-1/3 dicarba analogues **35 a**–**e** with clog*S* values in the range of −3.94 to −4.63 are considerably less soluble in water than flupirtine and retigabine (clog*S* = −3.16/−3.41),[36] it was investigated whether the secondary amino group allows salt formation. With compound **35 d** as an example, it was successfully shown that a stable hydrochloride salt could be prepared. However, it was not verified whether salts of weaker acids, such as maleic acid, which was used for salt formation in the case of flupirtine, are also possible.

While it was an obvious choice to replace the basic heterocycle of flupirtine with a phenyl ring, as in the case of N-1/3 dicarba analogues **35 a**–**f**, the pyridine ring has attractive physicochemical features. For this reason, it was investigated whether an inverted pyridine ring, which is rotated by 180° relative to the substitution pattern of flupirtine, might be favourable. In the following, a synthetic route is presented, leading to these novel N-1/3 dicarba analogues with amide substituent and inverted pyridine ring (**43 a**–**c**, Scheme 4). Since the methyl group is introduced in the last reaction step, the synthetic pathway also offered the possibility of replacing the methyl group with variable hydrocarbon residues.

The syntheses of the N-1/3 dicarba analogues with an inverted pyridine ring were carried out starting from 6-aminonicotinic acid (**36**), which was esterified in the first reaction step to obtain the ethyl ester **37**. The subsequent bromination was performed by reacting **37** with *N*-bromosuccinimide, yielding compound **38**. To obtain the aldehyde **40**, a two-step procedure was carried out. In the first step, $LiAlH_4$ was used to reduce the ethyl ester **38** to the corresponding alcohol **39**, which was then reoxidized in the second step by using activated MnO_2, yielding the desired aldehyde **40**. This reduction-oxidation procedure was followed by the synthesis of the amides **41 a**/**b** carried out by employing the corresponding acyl chlorides. Subsequently, the aldehyde group of the resulting amides was coupled with 4-fluoroaniline in a reductive amination procedure to obtain the secondary amines **42 a**/**b**. Due to their structural similarity to the N-1/3 dicarba analogues, which also prevents oxidation to azaquinone diimines, one of the bromo intermediates (**42 a**) was also subjected to biological testing. In the last step, the methyl group was introduced via a Suzuki reaction with trimethylboroxine as the methyl source, a cheaper and fairly soluble anhydride alternative for methylboronic acid, thus yielding the final compounds **43 a**/**b**. In the case of compound **43 b**, a bulkier 3,3-dimethylbutanamide substituent was introduced as an amide sidechain. This 3,3-dimethylbutanamide moiety is contained, for example, as a structural element in Lu AA41178, a K_V7 channel opener that demonstrated efficacy in preclinical models of epileptic seizures and psychiatric disorders but is not devoid of the risk of azaquinone diimine formation.[35] In addition, compound **43 c** with a cyclopropyl substituent instead of the methyl group was synthesized to evaluate possible space for a sterically more demanding hydrocarbon moiety in this part of the scaffold. The synthesis was conducted analogously to the methyl compounds by using cyclopropylboronic acid. The cyclopropyl residue in this particular case has the advantage of not increasing the lipophilicity as much as other branched hydrocarbon residues, such as a 2-propyl group, because of the increased π-character of its C–C bonds.[37] Unfortunately, all Suzuki couplings carried out resulted in only poor to moderate yields (15–43 %). This was partly due to the formation of various by-products. The debrominated compound **44** could be isolated and characterized as one of these by-products in the synthesis of **43 a** and **43 b**, respectively.

Sterically demanding amide sidechains, such as the already mentioned 3,3-dimethylbutanamide moiety but also benzamides, or phenylacetic acid amides, have proven advantageous in several amide-type $K_V7.2/3$ channel openers derived from flupirtine and retigabine.[24,35,38] Consequently, these amide residues are also of interest for the N-1/3 dicarba analogues. However, an increase in lipophilicity, which is associated with these bulky amide moieties, should be avoided as far as possible to ensure at least a moderate aqueous solubility of the relatively lipophilic N-1/3 dicarba analogues. For this reason, it was investigated whether less lipophilic but still bulky heterocycles are tolerated as part of the amide sidechain. A first attempt to introduce a heteroaromatic amide substituent was compound **35 e**, which has a pyridine ring incorporated in the nicotinamide structure. In the following, a modified synthesis strategy is presented, which was established to couple other aromatic and non-aromatic heterocycles to the amide sidechain (Scheme 5).

The starting material was the above-mentioned compound **32 b**, the amino group of which was protected in the first step by reaction with phthalic anhydride, forming the phthalimide **45**. Afterwards, the corresponding aldehyde **46** was synthesized analogously to compounds **34 a**–**e** by treating the nitrile with Raney nickel in formic acid. The reductive amination procedure with sodium borohydride, which had previously been used, was unsuccessful in this case since it led to a reductive ring-opening

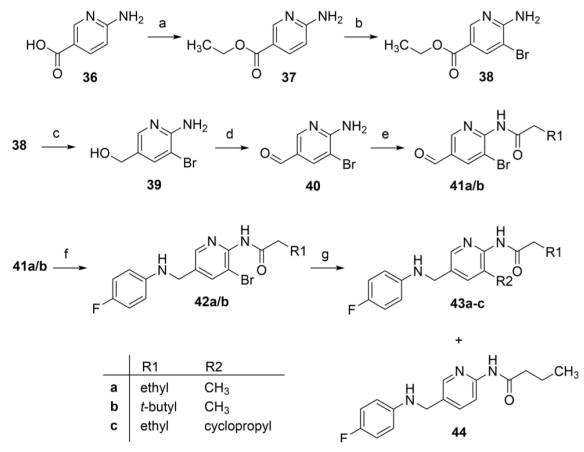

Scheme 4. Synthesis of N-1/3 dicarba analogues **43 a**-**c**: a) EtOH, $SOCl_2$, 90 °C, 18 h, 88 %; b) NBS, THF, 0 °C–RT, 17 h, 77 %; c) $LiAlH_4$, THF, RT, 5 h, 54 %; d) MnO_2, toluene, 80 °C, 2 h, 41 %; e) acyl chloride, DIPEA, DCM, 0 °C–RT, 16.5–24.5 h 48–50 %; f) 1. 4-fluoroaniline, toluene, molecular sieves, 120 °C, 5 h, 2. $NaBH_4$, MeOH, 1,4-dioxane, 0 °C, 17 h, 57–74 %; g) trimethylboroxine or cyclopropylboronic acid, $Pd(PPh_3)_4$, Na_2CO_3, 1,4-dioxane, H_2O, 140 °C, μW irradiation, 75 min, 15–43 %.

ChemMedChem
Research Article
doi.org/10.1002/cmdc.202200262
Chemistry Europe
European Chemical Societies Publishing

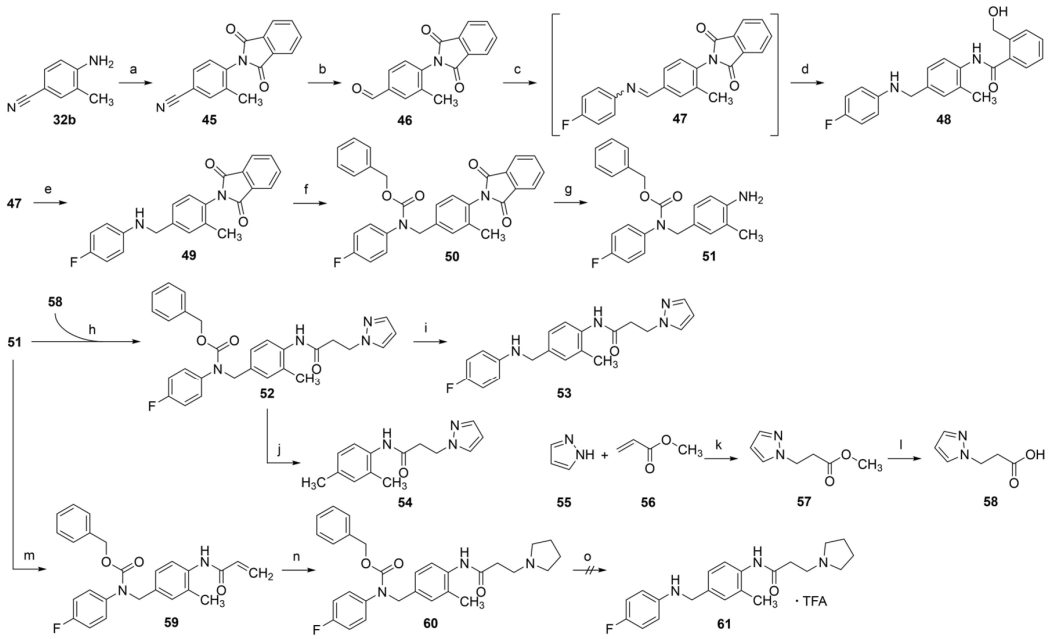

Scheme 5. Synthesis of N-1/3 dicarba analogues **48** and **53**: a) Phthalic anhydride, AcOH, 130 °C, 5 h, 83%; b) Ni, HCOOH, 80 °C, 6 h, 81%; c) 4-fluoroaniline, molecular sieves, toluene, 120 °C, 6 h; d) $NaBH_4$, MeOH, 1,4-dioxane, 0 °C–RT, 17 h, 68% (c + d); e) H_2, Pd/C, EtOAc, RT, 6 h, 67% (c + e); f) Cbz-Cl, DIPEA, DCM, RT, 4 h, 84%; g) N_2H_4, H_2O, THF, RT, 16 h, 98%; h) DIC, HOBt, DMF, RT, 16 h, 69%; i) HBr, AcOH, RT, 2 h, 89%; j) H_2, Pd/C, EtOAc, RT, 20 min, 61%; k) DBU, MeCN, RT, 16 h, 76%; l) KOH, H_2O, MeOH, RT, 16 h, 74%; m) acyl chloride, DIPEA, DCM, 0 °C, 2.5 h, 94%; n) pyrrolidine, EtOH, 60 °C, 7 h, 87%; o) H_2, Pd/C, MeOH, RT, 2 h, 50%.

of the phthalimide structure yielding **48**. Alternatively, a catalytic hydrogenation procedure with Pd/C as a catalyst was applied for the reductive amination to obtain the desired product **49**. Reductive cleavage of the benzylamine partial structure, as initially feared, was not observed under these conditions. The resulting secondary amine **49** was then protected by reacting the amino group with benzyl chloroformate, forming the benzyl carbamate **50**. Subsequently, the phthalimide protective group was cleaved by hydrazine. The resulting aniline **51** could then be modified by the attachment of different amide sidechains. Compound **52** with a 3-(1*H*-pyrazol-1-yl)propanamide sidechain was realized by coupling the corresponding carboxylic acid **58** with DIC and HOBt as coupling reagents. The required carboxylic acid **58** was synthesized from 1*H*-pyrazole and methyl acrylate via an aza-Michael addition and subsequent hydrolysis of the resulting ester **57**. Finally, the Cbz group of **52** had to be removed to release the secondary amino group. The first attempt of a reductive cleavage of the protecting group failed because the cleavage also affected the benzylamine partial structure, yielding **54**. Alternatively, the deprotection was realized by applying an acidic cleavage protocol utilising HBr in acetic acid to obtain the final compound **53**. The undesired reaction product **48**, which arose as a result of the reductive ring-opening of the phthalimide structure, was also subjected to biological testing since it represents an N-1/3 dicarba analogue with a bulky but not too lipophilic amide sidechain.

As a second heterocycle-containing amide sidechain, a 3-(pyrrolidin-1-yl)propanamide moiety was considered. For this purpose, compound **51** was reacted with acryloyl chloride to give the corresponding acrylamide **59**. The pyrrolidine moiety was then introduced again via an aza-Michael addition, yielding **60**. Finally, the Cbz group was cleaved hydrogenolytically by using Pd/C as a catalyst. The resulting product had to be purified by preparative RP-HPLC and was obtained as the trifluoroacetic acid salt after lyophilization of the product containing fraction. In contrast to the undesired conversion of **52** to **54**, ^{1}H-NMR spectroscopic data suggest the benzylamine partial structure was not or, considering the moderate yield, at least only partially cleaved under these conditions. Unfortunately, the resulting trifluoroacetic acid salt was found to be highly hygroscopic, transforming from an amorphous solid to a sticky resin within minutes after contact with air. A hydrochloride salt, which was stable and non-hygroscopic in the case of analogue **35d**, was also evaluated here but proved to be similarly hygroscopic as the trifluoroacetic acid salt, and the free base turned out to be a viscous oil that did not solidify. Therefore, compound **61** was excluded from further characterization and biological testing.

ChemMedChem
Research Article
doi.org/10.1002/cmdc.202200262
Chemistry Europe
European Chemical Societies Publishing

Evaluation of K_V7.2/3 opening activity

The K_V7 channel opening activity was tested on HEK-293 cells overexpressing the K_V7.2/3 channel. For this purpose, a commercially available assay was applied, which uses the permeability of potassium channels for thallium ions. In this assay, a thallium-sensitive fluorescent dye is used, which, when bound to Tl^+ passed through potassium channels, produces a fluorescent signal. The intensity of the signal is proportional to the number of open potassium channels and therefore provides information about the functional activity of the K_V7.2/3 channels. The corrected fluorescence intensity as a function of the compound concentration was used to determine the EC_{50} values, which express the concentration required to reach the half-maximal fluorescence signal. Moreover, the efficacy was determined, which is the percentage of the maximal fluorescence signal induced by a compound relative to the maximal fluorescence signal induced by flupirtine. A representative dose-response curve is shown in Figure 4. For a summary of the activity data, see Table 1.

In contrast to the N-1 monocarba analogue **6**, which served as the initial inspiration for synthesizing other carba analogues, the N-1 monocarba analogue **7** proved considerably less potent than flupirtine; up to a concentration of 20 μM, the concentration-response curve of **7** (not shown) rose slightly without reaching a maximum and always remained below the curve of flupirtine. An exact EC_{50} value could not be determined. However, the compound was clearly less active than flupirtine. The alkyne derivative **21** was completely inactive even up to a concentration of 20 μM. Both results were not necessarily to be expected since a recently published cryogenic electron microscopy (cryo-EM) structure of K_V7.2 in complex with retigabine does not indicate any specific interactions of the secondary amino group of retigabine with the binding site.[39] However, the *N*-benzylaniline partial structure of retigabine appears to be in an angled, synclinal conformation in the bound state (Figure 2B), which suggests conformational causes may be responsible for the drastic loss in activity of the N-1 monocarba analogues **7** and **21**. This is obvious in the case of the alkyne derivative **21**, as it is built linearly due to the acetylene linker and consequently differs significantly from the angled conformation described for retigabine in the bound state. In contrast to **21**, a synclinal conformation similar to retigabine would theoretically be conceivable for compound **7**. However, the crystal structure of 1,2-diphenylethane (Figure 2A),[40] as a simplified model for the ethylene linker of **7**, suggests that a straight, antiperiplanar conformation might be energetically preferred. In contrast, the crystal structure of *N*-benzylaniline (Figure 2C) reveals an angled, synclinal conformation due to the aniline nitrogen atom geometry,[41] thus resembling the conformation of retigabine in the bound state (Figure 2B). These assumptions regarding the conformation were supported by molecular dynamics simulations, which more closely reflect the conformational states in solution. As can be seen in Figure 2, the Helmholtz free energy landscape of *N*-benzylaniline shows a minimum in the region matching the ring angle and ring distance of retigabine bound to K_V7.2, whereas this specific conformation is clearly energetically unfavourable for 1,2-diphenylethane. Applied to the current carba analogues, these findings imply that methyleneamino linked compounds such as flupirtine and retigabine are conformationally preorganized. In contrast, derivatives with an ethylene linker such as carba analogue **7** bind rather poorly to the binding site since the entropic costs of conformational reordering may be higher than for methyleneamino linked compounds.

Table 1. K_V7.2/3 channel opening activity, *in vitro* toxicity, and log$D_{7.4}$ values of the synthesized analogues **7–53** in comparison to flupirtine and retigabine.[a]

Entry	Log$D_{7.4}$	HEK-293 EC_{50}[b] [μM]	Efficacy [%]	TAMH LD_{50}[c] [μM]	TAMH LD_{25}[d] [μM]	HEP-G2 LD_{50}[c] [μM]	HEP-G2 LD_{25}[d] [μM]
Flu	2.1	1.837 ± 0.844	100	487 ± 51	103 ± 47	547 ± 111	74 ± 40
Ret	2.1	0.249 ± 0.052	119 ± 7	> 400	> 400	> 400	269 ± 166
7	3.0	> 10.000	–	> 63	25 ± 7	> 63	27 ± 16
21	3.0	–[e]	–[e]	> 125	63 ± 12	> 125	> 125
27	3.4	4.123 ± 3.945	94 ± 15	> 250	76 ± 15	> 250	136 ± 38
35 a	3.0	0.143 ± 0.020	143 ± 7	> 125	> 125	> 125	> 125
35 b	2.9	0.675 ± 0.276	176 ± 14	> 125	> 125	> 125	88 ± 9
35 c	3.0	1.505 ± 0.364	167 ± 16	> 63	> 63	> 63	> 63
35 d	3.0	0.362 ± 0.093	156 ± 14	> 125	> 125	> 125	75 ± 17
35 e	3.0	–[e]	–[e]	> 125	41 ± 11	107 ± 16	61 ± 7
35 f	2.3	7.858 ± 2.167	70 ± 9	> 125	> 125	> 125	> 125
42 a	2.7	5.454 ± 1.696	163 ± 23	> 63	> 63	> 63	> 63
43 a	2.3	4.840 ± 2.907	89 ± 32	> 125	110 ± 54	> 125	46 ± 24
43 b	3.0	0.677 ± 0.419	153 ± 12	> 125	> 125	> 125	66 ± 27
43 c	2.8	2.015 ± 1.195	138 ± 20	> 125	76 ± 52	> 125	55 ± 17
48	2.9	–[e]	–[e]	> 125	70 ± 10	84 ± 6	80 ± 7
53	2.9	2.361 ± 0.543	144 ± 42	> 63	> 63	> 63	> 63

[a] Log$D_{7.4}$ values were estimated by applying an HPLC-based method. EC_{50} values were determined in HEK-293 cells overexpressing the K_V7.2/3 channel. LD values were obtained by MTT assay after 24 h of exposure. EC_{50} and LD values are means with corresponding standard deviations of at least three independent determinations. [b] Required concentration to reach half-maximal K_V7.2/3 channel opening activity. [c] Required concentration to reduce cell viability by 50% compared to untreated controls. [d] Required concentration to reduce cell viability by 25% compared to untreated controls. [e] Inactive up to a concentration of 20 μM.

ChemMedChem
Research Article
doi.org/10.1002/cmdc.202200262
Chemistry Europe
European Chemical Societies Publishing

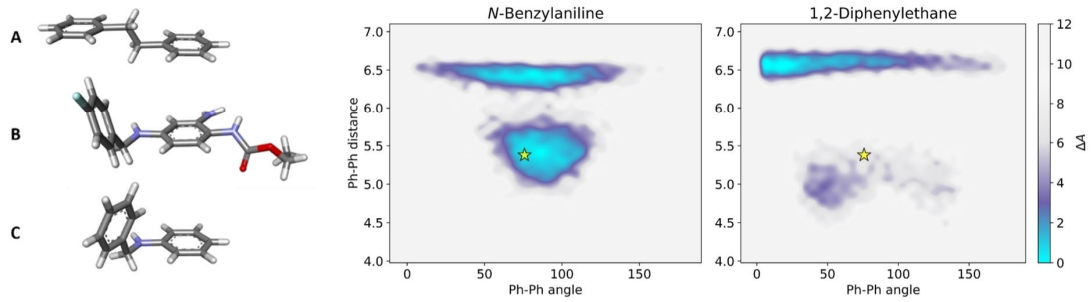

Figure 2. Left: Crystal structures of 1,2-diphenylethane (A) and *N*-benzylaniline (C) in comparison to the conformation of retigabine in the bound state (B) obtained from a cryo-EM structure of $K_V7.2$ in complex with retigabine. Right: Helmholtz free energy landscapes for the conformational space analysis of *N*-benzylaniline and 1,2-diphenylethane in octan-1-ol, as representative scaffolds for the investigated ligand structures. The star denotes the corresponding ring angle and ring distance in retigabine bound to $K_V7.2$.

In contrast to the N-1 monocarba analogues **7** and **21**, several N-1/3 dicarba analogues and structurally related compounds showed a significantly increased $K_V7.2/3$ opening activity compared to flupirtine, with analogue **35 a** exceeding retigabine in both terms of potency and efficacy. Overall, the small series of N-1/3 dicarba analogues synthesized in the present study provided valuable insights into the structure-activity relationships of this substance class, which will be discussed below.

The inverted methyleneamino linker of the N-1/3 dicarba analogues, instead of a possible ethylene linker as investigated in the case of N-1 monocarba analogue **7**, was originally chosen in order to retain balanced and drug-like lipophilicity. In retrospect, this turned out to be positive in two ways since, in addition to the lipophilicity, the biological activity was also not negatively affected, as in the case of the ethylene linker of **7**. Presumably, the inverted methyleneamino linker of the N-1/3 dicarba analogues also favours an angled conformation like the original linker of flupirtine and retigabine since it is still an *N*-benzylaniline partial structure, albeit inverted.

In order to investigate the binding mode of the N-1/3 dicarba analogues and to shed light on the possible role of the inverted methyleneamino linker, a molecular docking study was performed. Figure 3 shows the docking poses of retigabine compared to selected analogues (**27**, **35 d**, and **43 c**). As can be seen, the general orientation in the binding pocket, as well as the conformation of the N-1/3 dicarba analogues, is roughly comparable to retigabine. However, a significant difference is a newly occurring hydrogen bond interaction with the backbone carbonyl oxygen atom of W236, which is enabled by the inversion of the secondary amino group.

In line with our previous findings concerning N-3 monocarba analogue **6**, the methyl group as a replacement for the primary amino function of flupirtine and retigabine is also well-tolerated in the N-1/3 dicarba analogues, although the above-mentioned cryo-EM structure of $K_V7.2$ in complex with retigabine suggests the primary amino group may be involved in hydrogen bonds to S342 and F305. Possibly, these interactions are not mandatory for the activity, or alternatively, their loss is compensated by other effects, such as the increased compound lipophilicity. A replacement of the primary amino

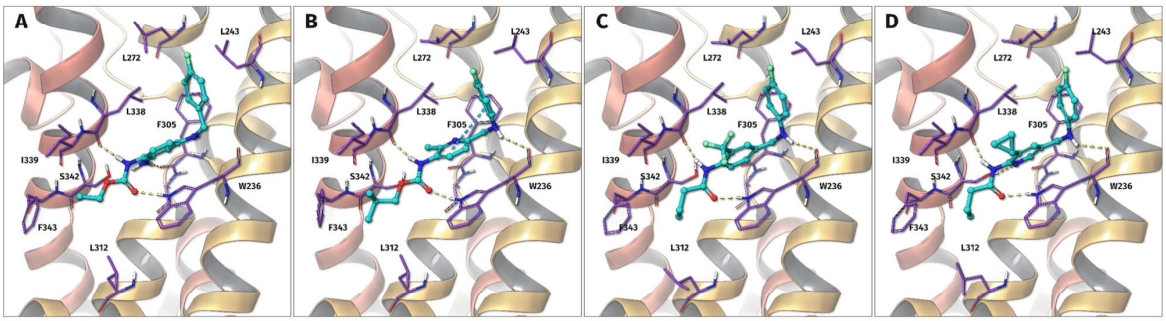

Figure 3. Predicted induced-fit docking poses of retigabine (A), **27** (B), **35 d** (C), and **43 c** (D) in the binding pocket of the heterotetrameric $K_V7.2/3$ potassium channel. The hydrogen bonds (yellow dashed lines) of the carbamate group are mostly preserved for all compounds, while the alkyl chain binds to a larger hydrophobic pocket. Inverting the secondary amine nitrogen atom position results in a hydrogen bond interaction with the backbone carbonyl oxygen atom of W236. The hydrogen bond interactions to S342 and F305, formed by flupirtine and retigabine, are not mandatory for activity. The primary amino group can therefore be replaced by hydrophobic substituents to form interactions with a small pocket between I339 and L338. An inversion of the pyridine ring realized in **43 c** enables the pyridine nitrogen atom to act as a hydrogen bond acceptor for S342.

ChemMedChem
Research Article
doi.org/10.1002/cmdc.202200262
Chemistry Europe
European Chemical Societies Publishing

function with a methyl group or other non-polar substituents along with additional structural changes generally led to more lipophilic compounds as reflected by higher log$D_{7.4}$ values throughout all N-1/3 dicarba analogues compared to flupirtine and retigabine (Table 1). A possible correlation between increased lipophilicity and improved activity was already observed in our previous work but could not be clearly proven since other structural features aside from the compound lipophilicity also affect the activity.[33] Nevertheless, lipophilicity seems to be a relevant variable influencing activity, and a possible reason might be the location of the K_V7.2/3 binding site, which is situated in the area where the channel is embedded in the cell membrane. It has not yet been clarified how ligands find their way to the binding pocket. However, a plausible possibility is that potential K_V7 openers first have to diffuse into the lipid double layer in order to reach their site of action, which requires a certain degree of lipophilicity.

Halogen substituents to replace the methyl group were also tolerated. However, as revealed by comparing the activity data of **35 b** and **35 c**, a smaller fluoro substituent was inferior to a methyl group. In contrast, the comparison of **42 a** and **43 a** suggests a larger bromo substituent has a similar to slightly superior effect on the K_V7.2/3 opening activity compared to a methyl group. The likewise electron-withdrawing trifluoromethyl residue was clearly superior to both the fluoro substituent and the methyl group, as the comparison of **35 b**, **35 c**, and **35 d** demonstrates. Furthermore, the binding site appears to offer space for bulkier hydrocarbon residues than a methyl group. The introduction of a cyclopropyl moiety in compound **43 c** led to a 2.4-fold increase in potency and an increase in efficiency of 49% compared to the corresponding methyl analogue **43 a**. In this case, too, the improvement in activity is possibly related to an increase in lipophilicity since the log$D_{7.4}$ value increased at the same time from 2.3 to 2.8 when a cyclopropyl residue replaced the methyl group. Moreover, molecular docking reveals a slightly different binding pose of **43 c**. As shown in Figures 3C and 3D, larger lipophilic substituents than a methyl group such as the cyclopropyl moiety as well as the trifluoromethyl group, which is suggested to be about as bulky as an ethyl residue,[42] face away from the binding site. This is contrary to a methyl group (Figure 3B), which is oriented in the opposite direction, thus occupying a lipophilic pocket between I339 and L338 that might be too small for larger substituents. However, the orientation of sterically more demanding substituents facing away from the binding pocket and the resulting marginal rotation of the central aromatic ring may be advantageous, as suggested by the increased potency of **35 d** and **43 c** compared to **35 b** and **43 a**.

As with several analogues known from the literature, an additional methyl group in ortho position to the amide function proved advantageous.[27,35] The resulting compound **35 a**, with an EC_{50} value of 0.143 μM, was the most active in the present set of substances, clearly reflected by the left-shifted concentration-activity curve in comparison to flupirtine displayed in Figure 4. This is in analogy with our recently published series of inverted amide derivatives of flupirtine and retigabine with benzamide/nicotinamide scaffold, where an additional ortho

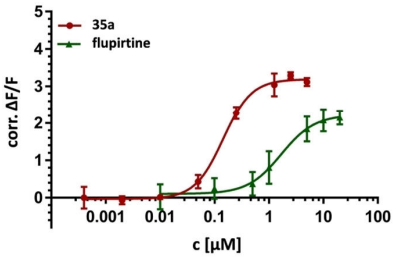

Figure 4. Comparison of the concentration-activity curves of **35 a** and flupirtine.

methyl group even made the difference from complete inactivity to submicromolar activity (not shown).[43] As we have demonstrated, the positive effect of the methyl group and the resulting ortho disubstitution is probably attributed to steric interactions, which force the amide group to rotate out of the plane, favouring a dihedral angle that is in good agreement with the predicted dihedral angle in the bound state. However, the positive effect on the activity is not quite as pronounced for anilide **35 a** as for the previously published benzamide/nicotinamide series. Nevertheless, the methyl group in **35 a** led to a 4.7-fold increase in potency compared to **35 b**, lacking the additional ortho methyl group.

In agreement with experience made with previously prepared analogues of flupirtine and retigabine bearing different scaffolds, an exchange of the carbamate function for an amide group was possible without drastically impairing the activity.[24,33] This was confirmed by molecular docking since the hydrogen bonds of the carbamate group of flupirtine and retigabine are preserved for amide derivatives (Figure 3C/D). Similar to the ethoxycarbonylamino sidechain, the butanoylamino side chain of **35 d** and **43 c** binds to a larger hydrophobic pocket, which apparently offers additional space for sterically more demanding amide residues. In line with this observation, a bulky and lipophilic side chain was found to increase the activity of the N-1/3 dicarba analogues further since it presumably enables a better fit in the corresponding hydrophobic cavity. This becomes evident when comparing **43 a** and **43 b**, where a 3,3-dimethylbutanoylamino side-chain caused a 7.2-fold increase in potency compared to a butanoylamino sidechain and, at the same time, increased the log$D_{7.4}$ value from 2.3 to 3.0. In contrast, a bulky but less lipophilic amide moiety such as the 3-(1*H*-pyrazol-1-yl)propanoylamino residue of **53**, which left the log$D_{7.4}$ value unchanged compared to a butanoylamino sidechain (**35 a**), seems not to be an adequate amide residue to occupy the hydrophobic cavity since it led to a 3.5-fold decrease in potency.

The incorporation of a pyridine ring or a benzyl alcohol moiety into the lateral molecule parts also proved problematic and led to inactive (**35 e**, **48**) or weakly active substances (**35 f**). While docking suggests the benzyl alcohol moiety of **48** does not fit the binding pocket at all, the pyridine rings of **35 e** and **35 f** principally fit but may weaken hydrophobic interactions in the area of the lateral lipophilic pockets, which seem vital for a

ChemMedChem
Research Article
doi.org/10.1002/cmdc.202200262
Chemistry Europe
European Chemical Societies Publishing

sufficient binding. Possibly, the same applies to **53**, where a 3-(1*H*-pyrazol-1-yl)propanoylamino side chain had a detrimental effect on the activity, too, as mentioned above. However, in the case of **53**, at least a fair K_V7.2/3 opening activity was retained.

If at all, a pyridine ring is most likely to be tolerated in the central part of the molecule (**27**, **42 a**, **43 a**–**c**), although it became clear that a more lipophilic phenyl ring is superior here, too, leading to substances with increased potency (**35 a**–**d**). However, through further structural modifications, such as a bulky, lipophilic amide sidechain, the potent compound **43 b** with an EC_{50} value of 0.677 μM could be obtained despite the presence of a pyridine ring as the central molecule part. Interestingly, the orientation of the pyridine nitrogen atom relative to the substitution pattern may be of certain importance here. An inverted pyridine ring as in **43 a**–**c** seems to be advantageous for binding since docking suggests the nitrogen atom can act as a hydrogen bond acceptor for S342 in this type of compounds (Figure 3B vs 3D). However, this observation could not be clearly confirmed by activity data since direct comparison of **27** and **43 a** with regard to the influence of the inverted pyridine ring is not valid due to the different carbamate/amide side chains.

Evaluation of in vitro hepatotoxicity

Idiosyncratic toxicity, as suspected for flupirtine-induced liver injury, is an ongoing challenge in drug discovery since it is still very difficult to predict in an *in vitro* assay due to the multifactorial causes.[44] Some experimental assays have been developed to evaluate idiosyncratic hepatotoxicity, but they include complex procedures and are partly not sufficiently validated.[45] Furthermore, too little is known for sure about the pathomechanism of flupirtine-induced liver injury to select an appropriate model for idiosyncratic hepatotoxicity. For these reasons, the toxicity evaluation of the newly synthesized compounds was limited to determining the general toxicity in cultured liver cells by using a standard MTT based cell viability assay, which, however, does not consider the possible involvement of an immunological component in the flupirtine-induced hepatotoxicity as mentioned in the introduction. Nevertheless, the resulting toxicity data are highly relevant since the focus of our work is on the development of safe K_V7.2/3 openers, and consequently, the new carba scaffolds have to be examined for potential toxicological risks. The human and mouse cell lines Hep-G2 and TAMH, respectively, that were used for the assay are of hepatic origin and well established for *in vitro* hepatotoxicity testing.[46] The detection of cell viability with the MTT assay is based on the mitochondrial reduction of the yellow, water-soluble 3-(4,5-dimethylthiazol-2-yl)-2,5-diphenyltetrazolium bromide (MTT) to a blue-violet, water-insoluble formazan in living cells, which can be quantified by colourimetric measurement.[47] A limiting factor in the toxicity testing was the aqueous solubility of the substances; most of the compounds proved to have only low to moderate toxicity, and as a result, LD_{50} values could only be determined in some cases since the required high concentrations could not be achieved without the substances precipitating. For this reason, LD_{25} values were calculated that indicate the concentration at which cell viability was reduced to 75 % (Table 1).

To our knowledge, no hepatotoxic effect is known for retigabine, and this was also observed in the MTT assay. LD_{50} values could not be determined but are above 400 μM and therefore considered as uncritical. The same applies to flupirtine with LD_{50} values of around 500 μM. Although LD_{25} values in the range of 74–103 μM were calculated, these should not be assessed as critical either since the peak plasma concentration after oral administration of 400 mg flupirtine was determined as 1.6 μM (modified release dosage form once daily for 8 days).[18] Considering this value as a relevant physiological concentration range, it becomes clear that flupirtine itself may exhibit only very mild, if any, acute hepatotoxicity at therapeutic dosing; otherwise, it would have hardly been approved as an analgesic. Despite this apparent lack of *in vitro* toxicity, flupirtine proved to be severely hepatotoxic for a very small number of patients. However, as already mentioned, other influencing factors that are not considered in an artificial *in vitro* toxicity assay may contribute to the pathomechanism.

Similar to flupirtine and retigabine, most of the novel carba and N-1/3 dicarba analogues demonstrated a rather uncritical level of *in vitro* hepatotoxicity. When comparing the LD_{25} values, predominantly, some of the less active or inactive substances performed slightly worse than flupirtine. This particularly affected the N-1 monocarba analogue **7** and the inactive N-1/3 dicarba analogues **35 e** and **48**, which both share an aromatic amide sidechain as a common structural feature. However, most of the remaining N-1/3 dicarba analogues, including the submicromolar active compounds **35 b**, **d**, and **43 b**, exhibited a weakly pronounced and uncritical level of liver cell toxicity comparable to flupirtine. The most active compound **35 a**, with LD_{25} values above 125 μM in both cell lines, tends to be slightly less toxic than flupirtine. It must also be taken into account that the last-mentioned substances demonstrated superior potency and efficacy compared to flupirtine. Consequently, these analogues may have a wider therapeutic safety window when considering the similar uncritical level of toxicity. In addition, they could potentially be effective at reduced doses, thus further minimizing the risk of toxic reactions since a high daily dose is generally considered a risk factor for oral drugs to induce hepatotoxicity.[48] In conclusion, the *in vitro* toxicity data confirmed our initial design strategy to develop safer K_V7.2/3 channel openers. In addition to ortho or para nitrogen atoms, an aniline moiety was also avoided, which is generally considered harmful since it can potentially be metabolized to toxic *N*-hydroxylamine and nitroso metabolites.[49] Therefore, two structural alerts were simultaneously removed by the redesign of flupirtine and retigabine to N-1/3 dicarba analogues.

Evaluation of oxidizability

Oxidation stability is a key characteristic for new analogues of flupirtine and retigabine since the oxidation-sensitive triami-

ChemMedChem
Research Article
doi.org/10.1002/cmdc.202200262
Chemistry Europe
European Chemical Societies Publishing

noaryl scaffold seems to be the main weak point of both drugs. For this reason, all newly synthesized compounds were examined for their oxidizability. While flupirtine is probably oxidized enzymatically, the oxidation of retigabine is supposed to take place via a melanin-associated reaction, or at least melanin may function as an adsorbent for oxidation products.[50] Since two different oxidation mechanisms have to be considered, cyclic voltammetry seemed a practicable solution to evaluate the general oxidizability of the novel analogues. This method has already been used to investigate the electrochemical behaviour of other oxidatively toxified drugs such as paracetamol or diclofenac.[51] Furthermore, a recent study concluded that electrochemical oxidation is a suitable approach for a preliminary investigation of the oxidative behaviour of drug candidates since the profile of generated oxidation products is roughly comparable to *in vitro* microsomal incubation.[52]

Figure 5 shows a representative cyclic voltammogram of compound **35a** versus retigabine. The anodic peak potentials, which are marked by dashed lines, indicate that **35a** with an oxidation potential of 633 mV is significantly more oxidation-stable compared to retigabine ($E_{p.a.}$ 260 mV) and flupirtine ($E_{p.a.}$ 306 mV, not shown), respectively. This trend is consistent for all carba analogues (Table 2), confirming the initial design strategy of replacing amino substituents with alkyl substituents to reduce oxidation sensitivity. For three derivatives (**35e**, **48**, **53**), however, no anodic peak potential could be determined. In contrast to the other analogues, these compounds have an aromatic amide sidechain; this structural feature might be the reason for the apparent lack of anodic peak potentials since the large planar molecular fraction may lead to reduced aqueous solubility, hence making it impossible to obtain a cyclic voltammogram.

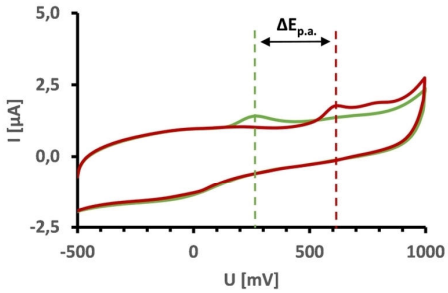

Figure 5. Cyclic voltammograms of retigabine (green) and the N-1/3 dicarba analogue **35a** (red) in 0.1 M Tris-HCl buffer (pH 7.4) with anodic peak potential values ($E_{p.a.}$) indicated by dashed lines.

Table 2. Investigations on the oxidizability of flupirtine, retigabine, and the synthesized carba analogues **7–53**, including anodic peak potentials ($E_{p.a.}$) determined by cyclic voltammetry and *in silico* molecule quinone formation scores (MQS) predicted by XenoSite.

Entry	$E_{p.a.}$ [mV][a]	MQS	Entry	$E_{p.a.}$ [mV][a]	MQS
Flu	306	0.91	35e	–[b]	0.91
Ret	260	0.94	35f	850	0.51
7	628	0.93	42a	668	0.28
21	553	0.93	43a	678	0.42
27	648	0.87	43b	663	0.45
35a	633	0.50	43c	678	0.34
35b	618	0.57	48	–[b]	0.33
35c	643	0.73	53	–[b]	0.55
35d	663	0.56			

[a] The cyclic voltammetry measurements were carried out in a 0.1 M Tris-HCl buffer (pH 7.4) in a potential range from −0.5 to 1.0 V with 5 mV voltage steps and a sweep rate of 0.1 V/s. [b] No oxidation was observed in the specified potential range.

A very early hypothesis of ours, according to which low oxidation potentials correlate with good $K_V7.2/3$ opening activity and vice versa, could not be confirmed since all N-1/3 dicarba analogues showed improved oxidation stability, and at the same time, some derivatives were significantly more potent than flupirtine.[53]

A reduced tendency towards oxidation, indicated by higher anodic peak potentials in cyclic voltammetry, does not inevitably exclude the formation of quinoid metabolites, as it does not allow any conclusions to be drawn about the type of oxidation products formed. Therefore, the propensity of the carba analogues to form quinoid metabolites was investigated in more detail. Considering the N-1/3 dicarba scaffold of analogues **27**–**53**, oxidation to quinone diimines or azaquinone diimines is impossible due to the lack of ortho or para amino substituents. As a result, no phenazinium-like dimers can be formed, which are suspected of being responsible for the blue tissue discolouration in the case of retigabine. However, the formation of different quinoid metabolites such as quinone imine methides would still be theoretically conceivable, which, although they cannot form coloured phenazinium structures, can possibly trigger hepatotoxic reactions similar to the azaquinone diimine oxidation products of flupirtine. To evaluate the possibility of quinoid metabolite formation in general, XenoSite was used, which is an *in silico* method based on a deep learning approach that allows for predicting the formation of different quinone species in drug metabolism.[54] The predicted molecule quinone formation scores (MQS) are included in Table 2, whereby the developer of XenoSite defined a value of 0.52 as the cut-off above a molecule is likely to form quinoid metabolites.

As can be seen, flupirtine and retigabine have high molecule quinone formation scores of 0.91 and 0.94, respectively. Together with the low oxidation potentials determined by cyclic voltammetry, these results support the initial hypothesis that quinoid metabolites may be a factor in the adverse drug reactions of flupirtine and retigabine. While cyclic voltammetry revealed a reduction in oxidation sensitivity to comparable levels for all carba analogues except **21** and **35f**, *in silico* risk prediction for quinoid metabolite formation yielded more differentiated results. The N-1 monocarba analogues **7** and **21** demonstrated MQS values above 0.9 and were thus in the range of flupirtine and retigabine. Therefore, they are also likely to form quinone diimine metabolites despite an overall reduced sensitivity to oxidation indicated by higher anodic peak potentials. In contrast, all N-1/3 dicarba analogues have significantly reduced MQS values except compound **35e**,

ChemMedChem
Research Article
doi.org/10.1002/cmdc.202200262
Chemistry Europe
European Chemical Societies Publishing

whereby a visual inspection of the graphical output of XenoSite showed that the high MQS value of **35e** is not associated with the central phenyl ring. Surprisingly, XenoSite predicted oxidation of the 2,4-difluoroaniline ring of **35e**, which was actually assumed to be metabolically stable. However, the literature shows that in some cases, fluorinated aromatic compounds can also be metabolized to quinoid structures by oxidative ipso substitution.[55] The data of the other N-1/3 dicarba analogues indicate that the central aromatic ring itself has a crucial impact on the risk for quinoid metabolite formation. A central pyridine ring, as in flupirtine derivative **27**, is still associated with a relatively high risk (MQS 0.87), whereas a phenyl ring significantly reduces the molecule quinone formation score to 0.51–0.73. An inverted pyridine ring seems to be the best choice since the MQS values of the concerning compounds **42a**–**43c** are, without exception, well below the cut-off of 0.52. Despite the slightly less favourable central phenyl ring, the MQS of the most active compound **35a** is also below the cut-off value. In conclusion, the formation of quinoid metabolites is improbable in the latter cases, including the submicromolar active compounds **35a** and **43b**.

Conclusion

With the aim of developing safer replacements for flupirtine and retigabine, the oxidation-sensitive triaminoaryl metabophore was successfully transformed into an oxidation-stable carba scaffold by replacing amino substituents with alkyl groups while maintaining good $K_V7.2/3$ opening activity. Particularly, the N-1/3 dicarba analogues **35a** and **43b** exhibited submicromolar activity and no critical toxicity *in vitro*. In addition, they showed improved oxidation stability and *in silico* predictions indicate a negligible risk for the formation of quinoid metabolites. Consequently, **35a** and **43b** represent excellent candidates for further development and characterization. This includes an *in vitro* metabolism study to confirm the absence of reactive metabolites and an investigation of channel selectivity, both of which are subject to future research.

Experimental Section

Chemistry

Unless otherwise stated, all solvents and reagents were purchased from commercial suppliers (Sigma Aldrich, VWR, TCI and ABCR) and used without further purification. All anhydrous solvents were obtained from Acros Organics, except THF, which was dried by refluxing over sodium and benzophenone (until a permanent dark blue colouration was evident), followed by distillation under anhydrous conditions. Microwave-assisted syntheses were conducted using an Anton Paar Monowave 300 reactor operated in closed vessel mode. An integrated IR sensor was used for temperature control, and the stirring speed was set to 600 rpm. A Bruker Avance III device was used to record ^{1}H-NMR (400 MHz) and ^{13}C-NMR (100 MHz) spectra. The chemical shifts were measured using the internal standard tetramethylsilane (TMS) in deuterated solvents and reported in parts per million (ppm). The coupling constants (*J*) are reported in Hz, and the splitting patterns are abbreviated as follows: br = broad, s = singlet, d = doublet, t = triplet, q = quartet, m = multiplet, and combinations thereof. MIR spectra were recorded with an ALPHA FT-IR instrument from Bruker Optics coupled with a diamond ATR accessory unit. A Bruker Elute UHPLC with Bruker compact QTOF-MS, a Bruker maXis LC-QTOF-MS or a Shimadzu LCMS-IT-TOF system, each operated with ESI ionization, were used to obtain the HRAM-MS data. The melting points were measured with an automated Büchi Melting Point M-565 apparatus. HPLC analysis (at 220 nm, using the 100% method) determined the purity of all final compounds to be >95%. Preparative and analytical HPLC procedures were conducted using Shimadzu devices CBM-20 A, LC-20AP, SIL-20 A, FRC-10 A with SPD 20 A UV/Vis detector. For analytical separation, a LiChroCART (250× 4 mm) and for preparative scale separation, a Hibar RT (250× 25 mm) HPLC column was used, both containing LiChrospher 100 RP-18e (5 μm). A mobile phase consisting of methanol/water (75:25) with 0.1% formic acid was used unless stated otherwise. Thin-layer chromatography (TLC) was performed on silica gel 60 F_{254} aluminium plates obtained from Merck. Column chromatography was carried out using a glass column and silica gel 60 from Carl Roth with a particle size of 20–45 μm. Purification by flash chromatography was conducted using 25 g or 50 g Biotage SNAP KP-SIL columns, which were run with the Sepacore system from Büchi. Alternatively, an Interchim puriFlash XS 520Plus system in combination with 80 g puriFlash 30SI-HP or 25 g puriFlash 15SI-HP columns was used.

General procedure (**Sonogashira reaction**): $Pd(PPh_3)_4$ (0.05 equiv.) and CuI (0.05 equiv.) were set under an argon atmosphere in a three-necked round bottom flask. Aryl halide (2.0–3.6 mmol, 0.1 mmol/mL) and alkyne (1.5–2.7 equiv., see individual procedures) were dissolved in a mixture of triethylamine and DMF (1:2.5, v/v). The resulting solution was degassed using the freeze pump thaw method and added to the mixture of $Pd(PPh_3)_4$ and CuI. The resulting solution was stirred at 60 °C. After complete conversion (0.5–6 h), the reaction was quenched by the addition of water (100 mL), and the mixture was extracted with DCM (2×100 mL). The combined organic phases were extracted with water (3× 100 mL), dried over Na_2SO_4, filtrated, and concentrated under reduced pressure to obtain the crude product.

General procedure (**Rosenmund-von Braun reaction**): The aryl bromide reactant (32.0–62.0 mmol, 0.8 mmol/mL) and CuCN (2.0 equiv.) were dissolved in NMP. The reaction mixture was stirred at 170 °C. After complete conversion (7–8 h), it was allowed to cool to room temperature. Ethyl acetate (600 mL) was added, and the resulting suspension was filtered through a pad of celite. The filtrate was extracted with an aq. 3.5% NH_3 solution (2×300 mL), washed with brine, dried over Na_2SO_4, filtrated, and concentrated under reduced pressure to obtain the crude product.

General procedure (nitrile reduction): The nitrile reactant (2.6–10.0 mmol, 0.1 mmol/mL) was dissolved in 98% formic acid, a Raney nickel suspension in water (50%, 0.8 mL per mmol nitrile reactant) was added, and the mixture was stirred at 80 °C. After complete conversion (6–8 h), it was filtered through a pad of celite, which was subsequently rinsed with ethyl acetate (100 mL). The combined filtrates were concentrated under reduced pressure. The resulting residue was suspended in ethyl acetate (50–190 mL) and filtrated. The filtrate was extracted with an equal volume of a saturated aq. $NaHCO_3$ solution. Thereafter, the organic phase was washed with brine, dried over Na_2SO_4, filtrated, and concentrated under reduced pressure to obtain the crude product.

General procedure (reductive amination): The aldehyde reactant (1.1–4.8 mmol, 0.1 mmol/mL) was suspended in dry toluene. 4 Å molecular sieves (1.0 g/mL) and the amine reactant (1.1–1.2 equiv.,

ChemMedChem
Research Article
doi.org/10.1002/cmdc.202200262
Chemistry Europe
European Chemical Societies Publishing

see individual procedures) were added. The resulting reaction mixture was stirred at 120 °C. After complete conversion (4–8 h), it was filtered hot to remove the molecular sieves. The filtrate was cooled to room temperature and concentrated under reduced pressure. The residue was dissolved in a mixture of 1,4-dioxane and methanol (4:1, v/v) to a concentration of 0.1 mmol/mL. The mixture was cooled to 0 °C, and sodium borohydride (5.0 equiv.) was added in portions over a period of 1 h under stirring. Afterwards, the mixture was allowed to warm to room temperature and stirred for 16 h. The reaction was quenched by adding 50–220 mL of water, and the mixture was extracted with an equal volume of ethyl acetate. The organic phase was washed with brine, dried over Na_2SO_4, filtrated, and concentrated under reduced pressure to obtain the crude product.

General procedure (Suzuki reaction): In a microwave vessel, the aryl bromide reactant (1.2–1.3 mmol, 0.3 mmol/mL) was dissolved in 1,4-dioxane. A 2 M aq. solution of Na_2CO_3 (2.8 equiv.), $Pd(PPh_3)_4$ (0.1 equiv.), and boronic acid or boronic acid anhydride (2.0 equiv.) were added. Argon was passed through the reaction mixture for 30 min. Afterwards, the mixture was heated in a microwave reactor at 140 °C in a closed vessel under an atmosphere of argon. After 75 min, water (100 mL) was added, and the aq. mixture was extracted with ethyl acetate (100 mL). The organic phase was washed with brine, dried over Na_2SO_4, filtrated, and concentrated under reduced pressure to obtain the crude product.

Ethyl [2-amino-6-(4-fluorophenethyl)pyridin-3-yl]carbamate (7): Compound **15** (411 mg, 1.60 mmol) and Pd/C (10% Pd, 50% water wet, 200 mg) were suspended in ethyl acetate (40 mL). The suspension was carefully set under a hydrogen atmosphere (balloon pressure) and stirred at 40 °C. After 16 h, another 200 mg of Pd/C were added. Afterwards, stirring was continued for 24 h at 40 °C under a hydrogen atmosphere. After completion of the reaction, the catalyst was filtered off, and the filtrate was concentrated under reduced pressure. The resulting residue was dissolved in 20 mL of THF, and triethylamine (445 μL, 3.20 mmol, 2.0 equiv.) was added. The reaction was set under an argon atmosphere, and a solution of ethyl chloroformate (304 μL, 3.20 mmol, 2.0 equiv.) in 2 mL of THF was added dropwise over 30 min. After stirring at room temperature for an additional 4 h, the reaction mixture was partitioned between 100 mL of ethyl acetate and 100 mL of water. The organic phase was extracted with water (2×100 mL), washed with brine, dried over Na_2SO_4, filtrated, and concentrated under reduced pressure. The crude residue was purified by silica gel column chromatography (ethyl acetate/*n*-hexane 3:2) and subsequent recrystallization (methanol/water) to obtain **7** as a colourless solid (120 mg, 0.40 mmol, 25%): $R_f = 0.23$ (ethyl acetate/*n*-hexane 1:1); mp: 154 °C; ^{1}H-NMR (400 MHz, DMSO-d_6): δ(ppm) = 8.57 (s, 1H), 7.44 (d, $J = 6.6$ Hz, 1H), 7.28–7.18 (m, 2H), 7.12–7.02 (m, 2H), 6.41 (d, $J = 7.8$ Hz, 1H), 5.70 (s, 2H), 4.10 (q, $J = 7.1$ Hz, 2H), 2.94–2.85 (m, 2H), 2.80–2.71 (m, 2H),1.23 (t, $J = 7.1$ Hz, 3H); ^{13}C-NMR (100 MHz, DMSO-d_6): δ(ppm) = 160.6 (d, $J = 241.0$ Hz), 154.5, 152.3, 137.8 (d, $J = 3.0$ Hz), 131.0, 130.0, 130.0 (d, $J = 7.9$ Hz), 116.4, 114.8 (d, $J = 20.9$ Hz), 110.9, 60.3, 38.7, 34.2, 14.5; IR (ATR): $\tilde{\nu}$ = 3417, 3329 (m, ν_{N-H}), 3036 (w, ν_{C-H}), 1686 (s, $\nu_{C=O}$) 1652 (m, δ_{N-H}); ESI-HRMS (*m/z*): calcd. for $[C_{16}H_{18}N_3O_2F+H]^+$ 304.1456, found 304.1447; cpd purity (220 nm): 100%.

[(4-Fluorophenyl)ethynyl]trimethylsilane (10): $Pd(PPh_3)_4$ (347 mg, 0.30 mmol, 0.05 equiv.) and CuI (57 mg, 0.30 mmol, 0.05 equiv.) were set under an argon atmosphere in a three-necked round bottom flask. 1-Bromo-4-fluorobenzene (660 μL, 6.00 mmol) and ethynyl(trimethyl)silane (1020 μL, 7.20 mmol, 1.2 equiv.) were dissolved in 18 mL of triethylamine. The resulting solution was degassed using the freeze pump thaw method and added to the mixture of $Pd(PPh_3)_4$ and CuI. The resulting solution was stirred at 60 °C for 16 h under an argon atmosphere. Subsequently, the reaction was quenched by adding water (100 mL), and the mixture was extracted with *n*-hexane (100 mL). The organic phase was washed with brine, dried over Na_2SO_4, filtrated, and concentrated under reduced pressure. The crude residue was purified by silica gel column chromatography with *n*-hexane as mobile phase, which yielded **10** as a colourless liquid (1.14 g, 6.0 mmol, 99%): $R_f = 0.83$ (*n*-hexane); ^{1}H-NMR (400 MHz, DMSO-d_6): δ(ppm) = 7.56–7.47 (m, 2H), 7.27–7.16 (m, 2H), 0.23 (s, 9H); ^{13}C-NMR (100 MHz, DMSO-d_6): δ(ppm) = 162.1 (d, $J = 248.1$ Hz), 133.9 (d, $J = 8.6$ Hz), 118.6 (d, $J = 3.4$ Hz), 115.9 (d, $J = 22.1$ Hz), 104.0, 93.8, −0.2; IR (ATR): $\tilde{\nu}$ = 2161 (w, $\nu_{C\equiv C}$).

1-Ethynyl-4-fluorobenzene (11): Compound **10** (1.22 g, 6.3 mmol) and K_2CO_3 (1.76 g, 12.7 mmol, 2.0 equiv.) were dissolved in 19 mL of methanol. The reaction mixture was set under an argon atmosphere and stirred at room temperature. After 5 h, 50 mL of water were added, and the pH of the solution was adjusted to 4–5 by the addition of a 1 M aq. HCl solution. Afterwards, the resulting solution was extracted with diethyl ether (3×50 mL). The combined organic phases were washed with brine, dried over Na_2SO_4, filtrated, and concentrated under reduced pressure. The resulting orange liquid (645 mg, 5.37 mmol, 85%) was used for the following reaction without characterization or further purification.

6-Chloro-3-nitropyridin-2-amine (13): 2,6-Dichloro-3-nitropyridine (19.30 g, 100.0 mmol) was dissolved in ethanol (200 mL). The reaction mixture was cooled to 0 °C, and ammonia gas was passed through the solution under stirring for 3 h. Afterwards, the reaction mixture was sealed and continued to stir at room temperature. After 18 h, the solution was poured into water (400 mL). The resulting precipitate was collected by filtration and washed with additional water (200 mL) and *n*-hexane (200 mL). The title compound was obtained as a yellow solid (14.41 g, 83.0 mmol, 83%): $R_f = 0.86$ (ethyl acetate/*n*-hexane 2:3); mp: 190 °C; ^{1}H-NMR (400 MHz, DMSO-d_6): δ(ppm) = 8.39 (d, $J = 8.6$ Hz, 1H), 8.25 (s, 2H), 6.77 (d, $J = 8.7$ Hz, 1H); ^{13}C-NMR (100 MHz, DMSO-d_6): δ(ppm) = 155.0, 153.4, 138.3, 126.1, 112.0; MIR (ATR): $\tilde{\nu}$ = 3442 (w, ν_{N-H}), 3157 (w, ν_{C-H}), 1552 (m, δ_{N-H}), 1552 (m, ν_{N-O}).

6-Bromo-3-nitropyridin-2-amine (14): Compound **13** (750 mg, 4.32 mmol) was suspended in 10 mL of an HBr solution in acetic acid (33%). The resulting reaction mixture was stirred for 8 h at 100 °C. The reaction was cooled to 0 °C and adjusted to pH 7 with an aq. NaOH solution (10%). The resulting precipitate was filtered off and washed with water to obtain the title compound as a yellow solid (878 mg, 4.03 mmol, 93%): $R_f = 0.70$ (ethyl acetate/*n*-hexane 1:4); mp: 242 °C; ^{1}H-NMR (400 MHz, DMSO-d_6): δ(ppm) = 8.26 (d, $J = 8.6$ Hz, 1H), 8.26 (s, 2H), 6.90 (d, $J = 8.5$ Hz, 1H); ^{13}C-NMR (100 MHz, DMSO-d_6): δ(ppm) = 153.4, 146.9, 137.7, 126.4, 115.8; IR (ATR): $\tilde{\nu}$ = 3444 (w, ν_{N-H}), 3147 (w, ν_{C-H}), 1629 (m, δ_{N-H}), 1552 (m, ν_{N-O}).

6-[(4-Fluorophenyl)ethynyl]-3-nitropyridin-2-amine (15): The synthesis was conducted from **14** (436 mg, 2.00 mmol) and **11** (645 mg, 5.37 mmol, 2.7 equiv.) according to the general procedure (Sonogashira reaction). The crude residue was further purified by silica gel column chromatography (ethyl acetate/*n*-hexane 1:4) and subsequent recrystallization (ethyl acetate) to obtain **15** as a gold-coloured solid (411 mg, 1.60 mmol, 80%): $R_f = 0.66$ (ethyl acetate/*n*-hexane 1:3); mp: 224 °C; ^{1}H-NMR (400 MHz, DMSO-d_6): δ(ppm) = 8.42 (d, $J = 8.5$ Hz, 1H), 8.03 (s, 2H), 7.75–7.67 (m, 2H), 7.38–7.29 (m, 2H), 6.96 (d, $J = 8.5$ Hz, 1H); ^{13}C-NMR (100 MHz, DMSO-d_6): δ(ppm) = 162.9 (d, $J = 250.0$ Hz), 153.5, 147.6, 135.8, 134.6 (d, $J = 8.9$ Hz), 126.3, 117.1 (d, $J = 3.3$ Hz), 116.3 (d, $J = 22.3$ Hz), 115.7, 90.7, 87.9; IR (ATR): $\tilde{\nu}$ = 3469 (w, ν_{N-H}), 3097 (w, ν_{C-H}), 2217 (w, $\nu_{C\equiv C}$), 1613 (m, δ_{N-H}), 1598 (m, ν_{N-O}).

ChemMedChem
Research Article
doi.org/10.1002/cmdc.202200262
Chemistry Europe
European Chemical Societies Publishing

3-Nitro-6-(phenylethynyl)pyridin-2-amine (**16**): The synthesis was carried out from **13** (521 mg, 3.00 mmol) and ethynylbenzene (659 μL, 6.00 mmol, 2.0 equiv.) according to the general procedure (Sonogashira reaction). The crude residue was further purified by silica gel column chromatography (ethyl acetate/*n*-hexane 1:7) and subsequent recrystallization (ethyl acetate) to obtained **16** as an orange solid (274 mg, 1.15 mmol, 38%): R_f = 0.70 (ethyl acetate/*n*-hexane 1:3); mp: decomp.; ^{1}H-NMR (400 MHz, DMSO-d_6): δ(ppm) = 8.42 (d, *J* = 8.5 Hz, 1H), 8.04 (s, 2H), 7.67–7.60 (m, 2H), 7.53–7.46 (m, 3H,), 6.97 (d, *J* = 8.5 Hz, 1H); ^{13}C-NMR (100 MHz, DMSO-d_6): δ(ppm) = 153.7, 147.7, 135.7, 132.0, 130.2, 129.0, 126.3, 120.6, 115.7, 91.7, 88.1; IR (ATR): $\tilde{\nu}$ = 3467 (w, ν_{N-H}), 3099 (w, ν_{C-H}), 2209 (w, $\nu_{C\equiv C}$), 1626 (m, δ_{N-H}), 1565 (m, ν_{N-O}).

3-Nitro-6-[(trimethylsilyl)ethynyl]pyridin-2-amine (**17**): The synthesis was conducted from **14** (630 mg, 3.63 mmol) and ethynyl(trimethyl)silane (775 μL, 5.45 mmol, 1.5 equiv.) according to the general procedure (Sonogashira reaction). The purification was carried out by silica gel column chromatography (ethyl acetate/*n*-hexane 1:9) and subsequent recrystallization (ethyl acetate) to obtain **17** as a gold-coloured solid (634 mg, 2.69 mmol, 74%): R_f = 0.62 (ethyl acetate/*n*-hexane 1:9); mp: 164 °C; ^{1}H-NMR (400 MHz, DMSO-d_6): δ(ppm) = 8.36 (d, *J* = 8.5 Hz, 1H), 7.99 (s, 2H), 6.83 (d, *J* = 8.5 Hz, 1H), 0.25 (s, 9H); ^{13}C-NMR (100 MHz, DMSO-d_6): δ(ppm) = 153.4, 147.0, 135.8, 126.5, 115.5, 103.1, 97.9, −0.61; IR (ATR): $\tilde{\nu}$ = 3472 (m, ν_{N-H}), 3133, 2962 (w, ν_{C-H}), 1617 (m, δ_{N-H}), 1563 (m, ν_{N-O}).

6-Ethynyl-3-nitropyridin-2-amine (**18**): Compound **17** (574 mg, 2.44 mmol) and K_2CO_3 (674 mg, 4.88 mmol, 2.0 equiv.) were dissolved in 20 mL of methanol. The reaction was stirred at room temperature. After 30 min, water (50 mL) was added. The pH of the resulting solution was adjusted to 7 by the addition of a 1 M aq. HCl solution. Subsequently, the neutralized solution was extracted with ethyl acetate (3×50 mL). The combined organic phases were washed with brine, dried over Na_2SO_4, filtrated, and concentrated to dryness under reduced pressure. The title compound was obtained as a brown solid (299 mg, 1.83 mmol, 75%): R_f = 0.54 (ethyl acetate/*n*-hexane 1:3); mp: decomp.; ^{1}H-NMR (400 MHz, DMSO-d_6): δ(ppm) = 8.38 (d, *J* = 8.5 Hz, 1H), 7.99 (s, 2H), 6.87 (d, *J* = 8.5 Hz, 1H), 4.63 (s, 1H); ^{13}C-NMR (100 MHz, DMSO-d_6): δ(ppm) = 153.4, 147.0, 135.8, 126.7, 115.7, 83.5, 82.0; IR (ATR): $\tilde{\nu}$ = 3464 (w, ν_{N-H}), 3087 (w, ν_{C-H}), 2106 (w, $\nu_{C\equiv C}$), 1624 (m, δ_{N-H}), 1568 (m, ν_{N-O}).

Ethyl [2-amino-6-(phenylethynyl)pyridin-3-yl]carbamate (**21**): Compound **16** (239 mg, 1.00 mmol) and iron powder (670 mg, 12.00 mmol, 12.0 equiv.) were suspended in acetic acid (20 mL). The reaction mixture was set under an argon atmosphere and stirred for 1 h at 50 °C. Subsequently, the reaction was cooled to 0 °C and adjusted to pH 7 with an aq. NaOH solution (10%). The resulting aqueous mixture was extracted with DCM (3×50 mL). The combined organic phases were dried over Na_2SO_4, filtrated, and concentrated under reduced pressure. The resulting residue was dissolved in 20 mL of THF, and triethylamine (333 μL, 2.40 mmol, 2.4 equiv.) was added. The reaction was again set under an argon atmosphere, and a solution of ethyl chloroformate (115 μL, 1.20 mmol, 1.2 equiv.) in 2 mL of THF was added dropwise over 30 min. After stirring at room temperature for an additional 6.5 h, the reaction mixture was partitioned between 100 mL of ethyl acetate and 100 mL of water. The organic phase was extracted with water (2×100 mL), washed with brine, dried over Na_2SO_4, filtrated, and concentrated under reduced pressure. The crude residue was purified by silica gel column chromatography (ethyl acetate/*n*-hexane 1:1) to obtain **21** as an off-white solid (85 mg, 0.30 mmol, 30%): R_f = 0.45 (ethyl acetate/*n*-hexane 1:1); mp: 152 °C; ^{1}H-NMR (400 MHz, DMSO-d_6): δ(ppm) = 8.83 (s, 1H), 7.75 (d, *J* = 7.9 Hz, 1H), 7.58–7.49 (m, 2H), 7.48–7.38 (m, 3H), 6.86 (d, *J* = 7.9 Hz, 1H), 6.10 (s, 2H), 4.14 (q, *J* = 7.1 Hz, 2H), 1.26 (t, *J* = 7.1 Hz, 3H); ^{13}C-NMR (100 MHz, DMSO-d_6): δ(ppm) = 154.1, 151.9, 134.6, 131.4, 128.9, 128.8, 128.5, 122.0, 119.5, 116.4, 89.7, 86.2, 60.6, 14.5; IR (ATR): $\tilde{\nu}$ = 3457, 3281 (m, ν_{N-H}), 3142, 2978 (w, ν_{C-H}), 1690 (s, $\nu_{C=O}$), 1620 (m, δ_{N-H}); ESI-HRMS (*m/z*): calcd. for $[C_{16}H_{15}N_3O_2+H]^+$ 282.1237, found 282.1235; cpd purity (220 nm): 100%.

6-Methyl-5-nitropicolinonitrile (**23**): 6-Bromo-2-methyl-3-nitropyridine (2.82 g, 13.0 mmol), $Pd(PPh_3)_4$ (451 mg, 0.39 mmol, 0.03 equiv.), and zinc cyanide (2.14 g, 18.2 mmol, 1.4 equiv.) were dissolved in DMF (20 mL). The reaction mixture was set under an argon atmosphere and stirred at 70 °C. After 24 h, it was cooled to room temperature and quenched by adding water (100 mL). The resulting aq. suspension was extracted with ethyl acetate (100 mL). The organic phase was extracted with water (2×100 mL), washed with brine, dried over Na_2SO_4, filtrated, and concentrated under reduced pressure. The crude residue was purified by silica gel column chromatography (ethyl acetate/*n*-hexane 1:4) to obtain **23** as a yellow oil (2.03 g, 12.4 mmol, 96%): R_f = 0.74 (ethyl acetate/*n*-hexane 1:3); ^{1}H-NMR (400 MHz, DMSO-d_6): δ(ppm) = 8.66 (d, *J* = 8.3 Hz, 1H), 8.22 (dd, *J* = 8.3, 0.7 Hz, 1H), 2.77 (s, 3H); ^{13}C-NMR (100 MHz, DMSO-d_6): δ(ppm) = 154.4, 147.3, 134.6, 134.6, 127.9, 116.2, 22.8; IR (ATR): $\tilde{\nu}$ = 3085, 2991 (w, ν_{C-H}), 1593 (m, ν_{N-O}).

5-Amino-6-methylpicolinonitrile (**24**): Compound **23** (163 mg, 1.00 mmol), iron powder (670 mg, 12.00 mmol, 12.0 equiv.), and calcium chloride (1.33 g, 12.0 mmol, 12.0 equiv.) were suspended in acetic acid (1 mL) and ethanol (6 mL). The reaction mixture was stirred for 2 h at room temperature. Afterwards, the suspension was filtered through a pad of celite, which was subsequently rinsed with ethanol. The combined filtrates were concentrated under reduced pressure. The crude residue was purified by silica gel column chromatography (ethyl acetate/*n*-hexane 1:1) to obtain **24** as a yellow solid (95 mg, 0.71 mmol, 71%): R_f = 0.34 (ethyl acetate/*n*-hexane 1:1); mp: 197 °C; ^{1}H-NMR (400 MHz, DMSO-d_6): δ(ppm) = 7.48 (d, *J* = 8.3 Hz, 1H), 6.92 (d, *J* = 8.3 Hz, 1H), 6.14 (s, 2H), 2.28 (s, 3H); ^{13}C-NMR (100 MHz, DMSO-d_6): δ(ppm) = 146.1, 144.5, 128.1, 119.2, 117.8, 116.7, 20.4; IR (ATR): $\tilde{\nu}$ = 3445 (m, ν_{N-H}), 3191, 2941 (w, ν_{C-H}), 2215 (m, $\nu_{C\equiv N}$), 1646 (m, δ_{N-H}).

Isobutyl (6-cyano-2-methylpyridin-3-yl)carbamate (**25**): Compound **24** (1.94 g, 14.6 mmol) and *N,N*-dimethylpyridin-4-amine (89 mg, 0.73 mmol, 0.05 equiv.) were dissolved in DCM (100 mL). Triethylamine (4.08 mL, 29.2 mmol, 2.0 equiv.) and isobutyl chloroformate (3.81 mL, 29.2 mmol, 2.0 equiv.) were added successively, and the reaction was stirred at room temperature. After 24, 48, and 72 h, an additional equivalent isobutyl chloroformate (1.90 mL, 14.6 mmol) was added. After 96 h in total, the reaction mixture was concentrated under reduced pressure, and the crude residue was purified by silica gel column chromatography (ethyl acetate/*n*-hexane 1:1) to obtain **25** as a colourless solid (1.17 g, 5.0 mmol, 34%): R_f = 0.54 (ethyl acetate/*n*-hexane 1:3); mp: 106 °C; ^{1}H-NMR (400 MHz, DMSO-d_6): δ(ppm) = 9.44 (s, 1H), 8.16 (d, *J* = 8.4 Hz, 1H), 7.85 (d, *J* = 8.4 Hz, 1H), 3.93 (d, *J* = 6.7 Hz, 2H), 2.50 (s, 3H), 2.05–1.86 (m, 1H), 0.94 (d, *J* = 6.7 Hz, 6H); ^{13}C-NMR (100 MHz, DMSO-d_6): δ(ppm) = 154.0, 152.1, 136.9, 129.1, 127.2, 125.8, 117.7, 70.9, 27.5, 21.1, 18.8; IR (ATR): $\tilde{\nu}$ = 3336 (m, ν_{N-H}), 3053 (w, ν_{C-H}), 2235 (w, $\nu_{C\equiv N}$), 1729 (s, $\nu_{C=O}$).

Isobutyl (6-formyl-2-methylpyridin-3-yl)carbamate (**26**): Compound **25** (300 mg, 1.29 mmol) was dissolved in dry DCM (20 mL). The resulting solution was set under an argon atmosphere and cooled to −85 °C. 3.86 mL of a 1 M solution of DIBAL in *n*-hexane (3.9 mmol, 3.0 equiv.) were dissolved in dry DCM (20 mL) and added dropwise to the reaction mixture over a period of 1 h while maintaining the temperature at −85 °C. Afterwards, the reaction was continued to stir at −85 °C. After 2 h, an additional 1.29 mL of the 1 M DIBAL solution in *n*-hexane (1.3 mmol, 1.0 equiv.) was added dropwise. The reaction was stirred for 1 h at −85 °C and then quenched by adding a 1 M aq. HCl solution (20 mL).

ChemMedChem
Research Article
doi.org/10.1002/cmdc.202200262
Chemistry Europe
European Chemical Societies Publishing

Subsequently, the mixture was allowed to warm to room temperature and stirred vigorously for 1 h. Afterwards, the phases were separated, and the aq. phase was extracted with DCM (2×50 mL). The combined organic phases were dried over Na_2SO_4, filtrated, and concentrated under reduced pressure. The crude residue was purified by silica gel column chromatography (ethyl acetate/*n*-hexane 1:1) to obtain **26** as a slightly yellow solid (70 mg, 0.30 mmol, 23%): R_f = 0.73 (ethyl acetate/*n*-hexane 1:1); mp: 102 °C; ^{1}H-NMR (400 MHz, DMSO-d_6): δ(ppm) = 9.87 (d, *J* = 0.8 Hz, 1H), 9.39 (s, 1H), 8.17 (d, *J* = 8.3 Hz, 1H), 7.80 (d, *J* = 8.4 Hz, 1H), 3.93 (d, *J* = 6.7 Hz, 2H), 2.56 (s, 3H), 2.03–1.89 (m, 1H), 0.95 (d, *J* = 6.7 Hz, 6H); ^{13}C-NMR (100 MHz, DMSO-d_6): δ(ppm) = 192.6, 154.1, 150.5, 147.0, 137.3, 129.3, 120.2, 70.8, 27.5, 21.1, 18.9; IR (ATR): $\tilde{\nu}$ = 3298 (w, ν_{N-H}), 2958 (w, ν_{C-H}), 1733 (s, $\nu_{C=O}$), 1682 (m, δ_{N-H}).

Isobutyl (6-{[(4-fluorophenyl)amino]methyl}-2-methylpyridin-3-yl)carbamate (**27**): Compound **26** (65 mg, 0.28 mmol) and 4-fluoroaniline (29 μL, 0.30 mmol, 1.1 equiv.) were dissolved in dry DCM (15 mL). After stirring at room temperature for 5 h, the reaction mixture was concentrated under reduced pressure. The residue was dissolved in methanol (20 mL), and sodium borohydride (47 mg, 1.38 mmol, 5.0 equiv.) was added in portions over 30 min at room temperature. The reaction kept stirring at room temperature for another 30 min. Thereafter, water (20 mL) was added, and subsequently, methanol was removed under reduced pressure. A brown precipitate formed, which was filtered off and washed with water. The crude product was recrystallized from methanol/water to obtain **27** as an off-white solid (75 mg, 0.23 mmol, 82%): R_f = 0.41 (ethyl acetate/*n*-hexane 1:1); mp: 123 °C; ^{1}H-NMR (400 MHz, DMSO-d_6): δ(ppm) = 8.99 (s, 1H), 7.63 (d, *J* = 8.2 Hz, 1H), 7.14 (d, *J* = 8.2 Hz, 1H), 6.93–6.82 (m, 2H), 6.57–6.48 (m, 2H), 6.22 (t, *J* = 6.1 Hz, 1H), 4.24 (d, *J* = 6.1 Hz, 2H), 3.85 (d, *J* = 6.7 Hz, 2H), 2.41 (s, 3H), 1.98–1.83 (m, 1H), 0.91 (d, *J* = 6.7 Hz, 6H); ^{13}C-NMR (100 MHz, DMSO-d_6): δ(ppm) = 155.0, 154.6, 154.3 (d, *J* = 229 Hz), 151.4, 145.1, 132.5, 130.9, 118.5, 115.2 (d, *J* = 21.9 Hz), 112.9 (d, *J* = 7.3 Hz), 70.3, 48.6, 27.6, 20.9, 18.9; IR (ATR): $\tilde{\nu}$ = 3380, 3280 (w, ν_{N-H}), 2928 (w, ν_{C-H}), 1688 (s, $\nu_{C=O}$). ESI-HRMS (*m/z*): calcd. for $[C_{18}H_{22}N_3O_2F + H]^+$ 332.1769, found 332.1754; cpd purity (220 nm): 100%.

4-Nitro-3-(trifluoromethyl)benzonitrile (**29**): $Pd(OAc)_2$ (45 mg, 0.20 mmol, 0.2 equiv.) and triphenylphoshine (polymer bound, 3 mmol/g, 150 mg, 0.45 mmol, 0.5 equiv) were suspended in DMF (3 mL) and set under an argon atmosphere. The mixture was stirred at room temperature. After 1.5 h, $Zn(CN)_2$ (235 mg, 2.00 mmol, 2.0 equiv.) and a solution of 4-bromo-1-nitro-2-(trifluormethyl)benzene (270 mg, 1.00 mmol) in DMF (2 mL) were added. Thereafter, the reaction mixture was stirred at 100 °C under an atmosphere of argon. After 1.5 h, the suspension was cooled to room temperature, poured into ethyl acetate (100 mL), and filtrated. The filtrate was extracted with water (3×100 mL), washed with brine, dried over Na_2SO_4, filtrated again, and concentrated under reduced pressure. The crude residue was purified by flash chromatography (mobile phase: ethyl acetate/*n*-hexane with 10–20% ethyl acetate) to obtain **29** as a colourless solid (180 mg, 0.83 mmol, 83%): R_f = 0.66 (ethyl acetate/*n*-hexane 1:3); mp: 89 °C; ^{1}H-NMR (400 MHz, DMSO-d_6): δ(ppm) = 8.69 (d, *J* = 1.8 Hz, 1H), 8,52 (dd, *J* = 8.4, 1.8 Hz, 1H), 8.38 (d, *J* = 8.4 Hz, 1H); ^{13}C-NMR (100 MHz, DMSO-d_6): δ(ppm) = 149.3, 139.1, 132.6 (q, *J* = 5.1 Hz), 126.2, 122.2 (q, *J* = 34.3 Hz), 121.3 (q, *J* = 273.3 Hz), 116.2, 116.2; IR (ATR): $\tilde{\nu}$ = 3057, 2921 (w, ν_{C-H}), 2239 (w, $\nu_{C\equiv N}$), 1539 (s, ν_{N-O}).

4-Bromo-2,6-dimethylaniline (**31a**): 2,6-Dimethylaniline (7.87 g, 65.0 mmol) was dissolved in DCM (200 mL), and the resulting solution was cooled to −78 °C. A solution of bromine (3.49 mL, 69.2 mmol, 1.1 equiv.) in DCM (20 mL) was slowly added to the mixture over a period of 30 min while maintaining the temperature at −78 °C. Subsequently, the cooling was removed. After the solution was warmed to room temperature, the reaction was quenched by adding a 10% aq. solution of $NaHSO_3$ (8 mL) to the mixture. Afterwards, a saturated solution of Na_2CO_3 (100 mL) was added. The organic layer was separated, dried over Na_2SO_4, filtrated, and concentrated under reduced pressure. The crude residue was purified by silica gel column chromatography (ethyl acetate/*n*-hexane 1:4) to obtain **31a** as a dark red oil (12.46 g, 62.3 mmol, 96%): R_f = 0.79 (ethyl acetate/*n*-hexane 1:1); ^{1}H-NMR (400 MHz, DMSO-d_6): δ(ppm) = 6.96 (s, 2H), 4.69 (s, 2H), 2.06 (s, 6H); ^{13}C-NMR (100 MHz, DMSO-d_6): δ(ppm) = 143.7, 129.6, 123.0, 106.1, 17.5; IR (ATR): $\tilde{\nu}$ = 3425 (w, ν_{N-H}), 2974 (w, ν_{C-H}), 1627 (m, δ_{N-H}).

4-Amino-3,5-dimethylbenzonitrile (**32a**): The synthesis was conducted from **31a** (12.40 g, 62.0 mmol) according to the general procedure (Rosenmund-von Braun reaction). The purification was carried out by silica gel column chromatography (ethyl acetate/*n*-hexane 2:3) to obtain **32a** as a dark red solid (3.81 g, 26.1 mmol, 42%): R_f = 0.62 (ethyl acetate/*n*-hexane 1:1); mp: 116 °C; ^{1}H-NMR (400 MHz, DMSO-d_6): δ(ppm) = 7.21 (s, 2H), 5.57 (s, 2H), 2.09 (s, 6H); ^{13}C-NMR (100 MHz, DMSO-d_6): δ(ppm) = 149.2, 131.4, 120.8, 120.8, 95.6, 17.4; IR (ATR): $\tilde{\nu}$ = 3477 (m, ν_{N-H}), 2965 (w, ν_{C-H}), 2206 (m, $\nu_{C\equiv N}$), 1631 (s, δ_{N-H}).

4-Amino-3-methylbenzonitrile (**32b**): The synthesis was carried out from 4-bromo-2-methylaniline (10.15 g, 54.6 mmol) in accordance with the general procedure (Rosenmund-von Braun reaction). The crude residue was further purified by silica gel column chromatography (ethyl acetate/*n*-hexane 2:3) and subsequent recrystallization (methanol/water) to obtain **32b** as an off-white solid (3.22 g, 24.3 mmol, 45%): R_f = 0.60 (ethyl acetate/*n*-hexane 2:3); mp: 94 °C; ^{1}H-NMR (400 MHz, DMSO-d_6): δ(ppm) = 7.33–7.24 (m, 2H), 6.64 (d, *J* = 8.2 Hz, 1H), 5.89 (s, 2H), 2.05 (s, 3H); ^{13}C-NMR (100 MHz, DMSO-d_6): δ(ppm) = 151.2, 133.5, 131.1, 121.2, 120.7, 113.4, 95.8, 17.0; IR (ATR): $\tilde{\nu}$ = 3400 (w, ν_{N-H}), 2944 (w, ν_{C-H}), 2216 (m, $\nu_{C\equiv N}$), 1646 (s, δ_{N-H}).

4-Amino-3-fluorobenzonitrile (**32c**): The synthesis was conducted from 4-bromo-2-fluoroaniline (6.00 g, 31.6 mmol) according to the general procedure (Rosenmund-von Braun reaction). The purification was carried out by silica gel column chromatography (ethyl acetate/*n*-hexane 3:7) and subsequent recrystallization (toluene/*n*-hexane) to obtain **32c** as an orange solid (2.02 g, 14.8 mmol, 47%): R_f = 0.81 (ethyl acetate/*n*-hexane 1:1); mp: 88 °C; ^{1}H-NMR (400 MHz, DMSO-d_6): δ(ppm) = 7.48 (dd, *J* = 11.7, 1.9 Hz, 1H), 7.29 (dd, *J* = 8.3, 1.8 Hz, 1H), 6.78 (dd, *J* = 9.0, 8.4 Hz 1H), 6.21 (s, 2H); ^{13}C-NMR (100 MHz, DMSO-d_6): δ(ppm) = 148.9 (d, *J* = 239.4 Hz), 141.8 (d, *J* = 12.7 Hz), 129.9 (d, *J* = 2.5 Hz), 119.4 (d, *J* = 2.6 Hz), 118.5 (d, *J* = 21.3 Hz), 115.6 (d, *J* = 5.5 Hz), 95.4 (d, *J* = 8.5 Hz); IR (ATR): $\tilde{\nu}$ = 3443 (w, ν_{N-H}), 2221 (m, $\nu_{C\equiv N}$), 1633 (s, δ_{N-H}).

4-Amino-3-(trifluoromethyl)benzonitrile (**32d**): Compound **29** (1.20 g, 5.6 mmol) was dissolved in ethyl acetate (50 mL). $SnCl_2$ (6.26 g, 27.8 mmol, 5.0 equiv.) was added, and the reaction mixture was stirred at 70 °C. After 30 min, it was cooled to room temperature and a saturated aq. $NaHCO_3$ solution (100 mL) was added. The phases were separated, and the aq. phase was extracted with ethyl acetate (2×100 mL). The combined organic phases were washed with brine, dried over Na_2SO_4, filtrated, and concentrated under reduced pressure. The crude residue was purified by silica gel column chromatography (ethyl acetate/*n*-hexane 3:2) to obtained **32d** as a slightly yellow solid (1.02 g, 5.5 mmol, 99%): R_f = 0.79 (ethyl acetate/*n*-hexane 1:1); mp: 105 °C; ^{1}H-NMR (400 MHz, DMSO-d_6): δ(ppm) = 9.50 (s, 1H), 9.25 (s, 1H), 7.90 (d, *J* = 1.9 Hz, 1H), 7.85 (dd, *J* = 8.7, 1.9 Hz, 1H), 7.33 (d, *J* = 8.7 Hz, 1H); ^{13}C-NMR (100 MHz, DMSO-d_6): δ(ppm) = 150.8, 137.1, 130.7 (q, *J* = 5.7 Hz), 123,3 (q, *J* = 270.3 Hz), 118.9, 112.8, 110.1 (q, *J* = 31.7 Hz), 98.2; IR (ATR): $\tilde{\nu}$ = 3318 (m, ν_{N-H}), 2237 (m, $\nu_{C\equiv N}$), 1618 (s, δ_{N-H}).

***N*-(4-Cyano-2,6-dimethylphenyl)butyramide** (**33a**): Compound **32a** (1.50 g, 10.3 mmol) was dissolved in THF (25 mL). *N,N*-Dimeth-

ChemMedChem
Research Article
doi.org/10.1002/cmdc.202200262
Chemistry Europe
European Chemical Societies Publishing

ylpyridin-4-amine (125 mg, 1.03 mmol, 0.1 equiv.) and triethylamine (2.86 mL, 20.5 mmol, 2.0 equiv.) were added successively. The reaction mixture was cooled to 0 °C, and a solution of butanoyl chloride (1.27 mL, 12.3 mmol, 1.2 equiv.) in THF (10 mL) was added dropwise under stirring over a period of 30 min. Afterwards, the reaction mixture was allowed to warm to room temperature, and stirring was continued for 16 h. After completion of the reaction, ethyl acetate (200 mL) was added, and the mixture was successively extracted with a 2 M aq. HCl solution (200 mL) and a saturated aq. $NaHCO_3$ solution (200 mL). Afterwards, the organic phase was washed with brine, dried over Na_2SO_4, filtrated, and concentrated under reduced pressure. The crude residue was purified by silica gel column chromatography (ethyl acetate/*n*-hexane 1:1) to obtain **33a** as a colourless solid (1.63 g, 7.6 mmol, 74%): R_f = 0.45 (ethyl acetate/*n*-hexane 1:1); mp: 193 °C; ^{1}H-NMR (400 MHz, DMSO-d_6): δ(ppm) = 9.47 (s, 1H), 7.59–7.54 (m, 2H), 2.33 (t, *J* = 7.2 Hz, 2H), 2.17 (s, 6H), 1.71–1.57 (m, 2H), 0.95 (t, *J* = 7.4 Hz, 3H); ^{13}C-NMR (100 MHz, DMSO-d_6): δ(ppm) = 170.7, 140.3, 136.8, 131.2, 118.8, 108.7, 37.3, 18.7, 17.9, 13.7; IR (ATR): $\tilde{\nu}$ = 3250 (m, ν_{N-H}), 2963 (w, ν_{C-H}), 2223 (m, $\nu_{C\equiv N}$), 1651 (s, $\nu_{C=O}$).

***N*-(4-Cyano-2-methylphenyl)butyramide** (**33b**): Compound **32b** (1.50 g, 11.4 mmol) was dissolved in DCM (20 mL), and triethylamine (3.16 mL, 22.7 mmol, 2.0 equiv.) was added in one portion. A solution of butanoyl chloride (1.76 mL, 17.0 mmol, 1.5 equiv.) in DCM (10 mL) was added dropwise under stirring over a period of 1 h. Afterwards, the reaction mixture was stirred for 3 h at 40 °C. After completion of the reaction, DCM (100 mL) was added, and the mixture was successively extracted with a 2 M aq. HCl solution (100 mL) and a saturated aq. $NaHCO_3$ solution (100 mL). Subsequently, the organic phase was washed with brine, dried over Na_2SO_4, filtrated, and concentrated under reduced pressure. The crude residue was purified by flash chromatography (ethyl acetate/*n*-hexane with 20–50% ethyl acetate) to obtain **33b** as a slightly yellow solid (2.02 g, 10.0 mmol, 88%): R_f = 0.58 (ethyl acetate/*n*-hexane 2:3); mp: 106 °C; ^{1}H-NMR (400 MHz, DMSO-d_6): δ(ppm) = 9.39 (s, 1H), 7.81 (d, *J* = 8.3 Hz, 1H), 7.68 (dd, *J* = 1.8, 0.9 Hz, 1H), 7.61 (dd, *J* = 8.4, 2.0 Hz, 1H), 2.39 (t, *J* = 7.3 Hz, 2H), 2.26 (s, 3H), 1.70–1.56 (m, 2H), 0.93 (t, *J* = 7.4 Hz, 3H); ^{13}C-NMR (100 MHz, DMSO-d_6): δ(ppm) = 171.6, 141.2, 134.0, 131.4, 130.1, 124.0, 119.0, 106.3, 37.9, 18.6, 17.6, 13.6; IR (ATR): 3399 (m, ν_{N-H}), 2979 (w, ν_{C-H}), 2216 (m, $\nu_{C\equiv N}$), 1646 (s, $\nu_{C=O}$).

***N*-(4-Cyano-2-fluorophenyl)butyramide** (**33c**): Compound **32c** (700 mg, 5.14 mmol) was dissolved in DCM (20 mL), and triethylamine (1070 µL, 7.71 mmol, 1.5 equiv.) was added in one portion. A solution of butanoyl chloride (798 µL, 7.71 mmol, 1.5 equiv.) in DCM (20 mL) was added dropwise under stirring over a period of 1 h. The reaction mixture was stirred at room temperature. After 24 h, additional amounts of triethylamine (1070 µL, 7.71 mmol, 1.5 equiv.) and butanoyl chloride (798 µL, 7.71 mmol, 1.5 equiv.) were added, and the reaction was continued for 24 h. Afterwards, DCM (100 mL) was added, and the mixture was extracted successively with a 2 M aq. HCl solution (100 mL) and a saturated aq. $NaHCO_3$ solution (100 mL). The organic phase was washed with brine, dried over Na_2SO_4, filtrated, and concentrated under reduced pressure. The crude residue was purified by silica gel column chromatography (ethyl acetate/*n*-hexane 3:7) to obtain **33c** as an orange solid (715 mg, 3.47 mmol, 67%): R_f = 0.81 (ethyl acetate/*n*-hexane 1:1); mp: 89 °C; ^{1}H-NMR (400 MHz, DMSO-d_6): δ(ppm) = 10.03 (s, 1H), 8.26 (pseudo-t, *J* = 8.2 Hz, 1H), 7.86 (dd, *J* = 11.1, 1.9 Hz, 1H), 7.66–7.60 (m, 1H), 2.41 (t, *J* = 7.3 Hz, 2H), 1.64–1.52 (m, 2H), 0.89 (t, *J* = 7.4 Hz, 3H); ^{13}C-NMR (100 MHz, DMSO-d_6): δ(ppm) = 172.3, 151.7 (d, *J* = 247.3 Hz), 131.6 (d, *J* = 11.1 Hz), 129.3 (d, *J* = 3.5 Hz), 123.0 (d, *J* = 2.7 Hz), 119.3 (d, *J* = 23.4 Hz), 117.9 (d, *J* = 2.6 Hz), 105.7 (d, *J* = 9.4 Hz), 37.8, 18.4, 13.5; IR (ATR): $\tilde{\nu}$ = 3320 (w, ν_{N-H}), 2232 (m, $\nu_{C\equiv N}$), 1698 (s, $\nu_{C=O}$).

***N*-[4-Cyano-2-(trifluoromethyl)phenyl]butyramide** (**33d**): Compound **32d** (300 mg, 1.61 mmol) was dissolved in THF (20 mL). Triethylamine (453 µL, 3.22 mmol, 2.0 equiv.) and *N,N*-dimethylpyridin-4-amine (20 mg, 0.16 mmol, 0.1 equiv.) were added. The reaction mixture was cooled to 0 °C, and a solution of butanoyl chloride (333 µL, 3.33 mmol, 2.0 equiv.) in THF (20 mL) was added dropwise under stirring over a period of 30 min. Thereafter, the reaction mixture was stirred at 70 °C. After 7 d, the reaction was terminated. Ethyl acetate (100 mL) was added, and the mixture was extracted successively with a 2 M aq. HCl solution (100 mL) and a saturated aq. $NaHCO_3$ solution (100 mL). Subsequently, the organic phase was washed with brine, dried over Na_2SO_4, filtrated, and concentrated under reduced pressure. The crude residue was purified by silica gel column chromatography (ethyl acetate/*n*-hexane 1:3) to obtain **33d** as a colourless solid (230 mg, 0.90 mmol, 56%): R_f = 0.79 (ethyl acetate/*n*-hexane 1:1); mp: 107 °C; ^{1}H-NMR (400 MHz, DMSO-d_6): δ(ppm) = 9.71 (s, 1H), 8.28 (d, *J* = 1.9 Hz, 1H), 8.13 (dd, *J* = 8.4, 1.9 Hz, 1H), 7.81 (d, *J* = 8.2 Hz, 1H), 2.38 (t, *J* = 7.3 Hz, 2H), 1.68–1.54 (m, 2H), 0.92 (t, *J* = 7.4 Hz, 3H); ^{13}C-NMR (100 MHz, DMSO-d_6): δ(ppm) = 172.2, 139.9, 136.6, 131.0 (q, *J* = 5.0 Hz), 130.0, 124.2 (q, *J* = 30.0 Hz), 122.6 (q, *J* = 272.0 Hz), 117.5, 108.7, 37.5, 18.5, 13.4; IR (ATR): $\tilde{\nu}$ = 3273 (m, ν_{N-H}), 3072, 2964 (w, 2237 ν_{C-H}), 2235 (m, $\nu_{C\equiv N}$), 1671 (s, $\nu_{C=O}$) 1618 (m, δ_{N-H}).

***N*-(4-Cyano-2-methylphenyl)nicotinamide** (**33e**): Compound **32b** (700 mg, 5.30 mmol) was dissolved in DCM (40 mL), and triethylamine (1111 µL, 7.95 mmol, 1.5 equiv.) was added in one portion. Subsequently, pyridine-3-carbonyl chloride (1.50 g, 10.6 mmol, 2.0 equiv.) was added in small portions under stirring over a period of 1 h. Afterwards, the reaction mixture was stirred at room temperature. After 65 h, another portion of pyridine-3-carbonyl chloride (750 mg, 5.3 mmol, 1.0 equiv.) was added, and the reaction was stirred at 40 °C. After 24 h, DCM (100 mL) was added, and the mixture was extracted with a saturated aq. $NaHCO_3$ solution (3× 100 mL). Afterwards, the organic phase was washed with brine, dried over Na_2SO_4, filtrated, and freed from solvent under reduced pressure. The crude residue was purified by flash chromatography (100% ethyl acetate) to obtain **33e** as a colourless solid (857 mg, 3.61 mmol, 68%): R_f = 0.54 (ethyl acetate/*n*-hexane 2:3); mp: 191 °C; ^{1}H-NMR (400 MHz, DMSO-d_6): δ(ppm) = 10.25 (s, 1H), 9.14 (dd, *J* = 2.4, 0.9 Hz, 1H), 8.80 (dd, *J* = 4.8, 1.7 Hz, 1H), 8.32 (ddd, *J* = 7.9, 2.3, 1.7 Hz, 1H), 7.83–7.77 (m, 1H), 7.76–7.67 (m, 2H), 7.60 (ddd, *J* = 7.9, 4.8, 0.9 Hz, 1H), 2.34 (d, *J* = 0.8 Hz, 3H); ^{13}C-NMR (100 MHz, DMSO-d_6): δ(ppm) = 164.7, 152.9, 149.3, 141.2, 136.1, 134.7, 134.6, 130.6, 130.3, 126.7, 124.0, 119.3, 108.5, 18.1; IR (ATR): 3300 (m, ν_{N-H}), 3028, 2997 (w, ν_{C-H}), 2228 (m, $\nu_{C\equiv N}$), 1655 (s, $\nu_{C=O}$).

***N*-(4-Formyl-2,6-dimethylphenyl)butyramide** (**34a**): The synthesis was conducted from **33a** (1.40 g, 6.5 mmol) according to the general procedure (nitrile reduction). The purification was carried out by silica gel column chromatography (ethyl acetate/*n*-hexane 1:1) to obtain **34a** as an off-white solid (1.26 g, 5.7 mmol, 88%): R_f = 0.38 (ethyl acetate/*n*-hexane 1:1); mp: 136 °C; ^{1}H-NMR (400 MHz, DMSO-d_6): δ(ppm) = 9.92 (s, 1H), 9.45 (s, 1H), 7.61 (s, 2H), 2.34 (t, *J* = 7.3 Hz, 2H), 2.22 (s, 6H), 1.72–1.58 (m, 2H), 0.96 (t, *J* = 7.4 Hz, 3H); ^{13}C-NMR (100 MHz, DMSO-d_6): δ(ppm) = 192.5, 170.6, 141.4, 136.1, 134.0, 128.8, 37.4, 18.8, 18.2, 13.7; IR (ATR): $\tilde{\nu}$ = 3245 (m, ν_{N-H}), 2958 (w, ν_{C-H}), 1693, 1647 (s, $\nu_{C=O}$).

***N*-(4-Formyl-2-methylphenyl)butyramide** (**34b**): The synthesis was carried out from **33b** (2.02 g, 10.0 mmol) in accordance with the general procedure (nitrile reduction). The crude residue was further purified by silica gel column chromatography (ethyl acetate/*n*-hexane 1:1) to obtain **34b** as an off-white solid (1.52 g, 7.4 mmol, 74%): R_f = 0.71 (ethyl acetate); mp: 79 °C; ^{1}H-NMR (400 MHz, DMSO-d_6): δ(ppm) = 9.89 (s, 1H), 9.37 (s, 1H), 7.85 (d, *J* = 8.2 Hz, 1H), 7.74 (d, *J* = 1.6 Hz, 1H), 7.71 (dd, *J* = 8.2, 2.0 Hz, 1H), 2.40 (t, *J* = 7.3 Hz, 2H), 2.31 (s, 3H), 1.71–1.57 (m, 2H), 0.94 (t, *J* = 7.4 Hz, 3H); ^{13}C-NMR

ChemMedChem
Research Article
doi.org/10.1002/cmdc.202200262
Chemistry Europe
European Chemical Societies Publishing

(100 MHz, DMSO-d_6): δ(ppm) = 192.4, 172.0, 142.9, 132.7, 132.1, 131.1, 128.2, 124.1, 38.4, 19.1, 18.3, 14.1; IR (ATR): $\tilde{\nu}$ = 3288 (m, ν_{N-H}), 2965 (w, ν_{C-H}), 1698, 1653 (s, $\nu_{C=O}$).

***N*-(2-Fluoro-4-formylphenyl)butyramide** (**34c**): The synthesis was conducted from **33c** (650 mg, 3.15 mmol) according to the general procedure (nitrile reduction). The purification was carried out by silica gel column chromatography (ethyl acetate/*n*-hexane 3 : 7) to obtain **34c** as an off-white solid (483 mg, 2.31 mmol, 73 %): R_f = 0.56 (ethyl acetate/*n*-hexane 3 : 7); mp: 87 °C; ^{1}H-NMR (400 MHz, DMSO-d_6): δ(ppm) = 9.99 (s, 1H), 9.88 (d, *J* = 1.9 Hz, 1H), 8.32 (dd, *J* = 8.6, 7.5 Hz, 1H), 7.77–7.68 (m, 2H), 2.43 (t, *J* = 7.3 Hz, 2H), 1.67–1.55 (m, 2H), 0.90 (t, *J* = 7.4 Hz, 3H); ^{13}C-NMR (100 MHz, DMSO-d_6): δ(ppm) = 191.0 (d, *J* = 2.1 Hz), 172.2, 152.5 (d, *J* = 247.5 Hz), 132.4 (d, *J* = 11.5 Hz), 132.1 (d, *J* = 5.5 Hz), 126.8 (d, *J* = 2.9 Hz), 122.5 (d, *J* = 2.1 Hz), 115.2 (d, *J* = 19.8 Hz), 37.9, 18.4, 13.5; IR (ATR): $\tilde{\nu}$ = 3313 (m, ν_{N-H}), 3012, 2962 (w, ν_{C-H}), 1706, 1672 (s, $\nu_{C=O}$), 1609 (s, δ_{N-H}).

***N*-[4-Formyl-2-(trifluoromethyl)phenyl]butyramide** (**34d**): The synthesis was carried out from **33d** (673 mg, 2.63 mmol) in accordance with the general procedure (nitrile reduction). The crude residue was further purified by silica gel column chromatography (ethyl acetate/*n*-hexane 1 : 3) to obtain **34d** as a colourless solid (372 mg, 1.44 mmol, 55 %): R_f = 0.76 (ethyl acetate/*n*-hexane 1 : 1); mp: 70 °C; ^{1}H-NMR (400 MHz, DMSO-d_6): δ(ppm) = 10.04 (s, 1H), 9.68 (s, 1H), 8.25 (d, *J* = 1.9 Hz, 1H), 8.16 (dd, *J* = 8.1, 1.7 Hz, 1H), 7.84 (d, *J* = 8.2 Hz, 1H), 2.39 (t, *J* = 7.3 Hz, 2H), 1.69–1.55 (m, 2H), 0.93 (t, *J* = 7.4 Hz, 3H); ^{13}C-NMR (100 MHz, DMSO-d_6): δ(ppm) = 191.5, 172.2, 140.7, 133.3, 132.8, 129.8, 128.2 (q, *J* = 5.1 Hz), 123.9 (q, *J* = 30.0 Hz), 123.1 (q, *J* = 272.0 Hz), 37.6, 18.5, 13.4; IR (ATR): $\tilde{\nu}$ = 3289 (m, ν_{N-H}), 2969 (w, ν_{C-H}), 1701, 1668 (s, $\nu_{C=O}$).

***N*-(4-Formyl-2-methylphenyl)nicotinamide** (**34e**): The synthesis was conducted from **33e** (781 mg, 3.29 mmol) according to the general procedure (nitrile reduction). The purification was carried out by silica gel column chromatography (100 % ethyl acetate) to obtain **34e** as a colourless solid (290 mg, 1.21 mmol, 37 %): R_f = 0.56 (ethyl acetate); mp: 156 °C; ^{1}H-NMR (400 MHz, DMSO-d_6): δ(ppm) = 10.23 (s, 1H), 9.97 (s, 1H), 9.15 (dd, *J* = 2.4, 0.9 Hz, 1H), 8.79 (dd, *J* = 4.8, 1.7 Hz, 1H), 8.33 (ddd, *J* = 7.9, 2.4, 1.7 Hz, 1H), 7.84 (d, *J* = 1.9 Hz, 1H), 7.79 (dd, *J* = 8.2, 1.9 Hz, 1H), 7.75 (d, *J* = 8.2 Hz, 1H), 7.60 (ddd, *J* = 7.9, 4.8, 0.9 Hz, 1H), 2.38 (s, 3H); ^{13}C-NMR (100 MHz, DMSO-d_6): δ(ppm) = 192.3, 164.2, 152.4, 148.8, 141.8, 135.6, 133.5, 133.4, 131.7, 129.9, 127.6, 125.9, 123.6, 17.9; IR (ATR): $\tilde{\nu}$ = 3298 (m, ν_{N-H}), 3039, 2813 (w, ν_{C-H}), 1693, 1652 (s, $\nu_{C=O}$).

***N*-(4-{[(4-Fluorophenyl)amino]methyl}-2,6-dimethylphenyl)butyramide** (**35a**): The synthesis was carried out from **34a** (250 mg, 1.14 mmol) and 4-fluoroaniline (130 μL, 1.37 mmol, 1.2 equiv.) in accordance with the general procedure (reductive amination). The crude residue was further purified by silica gel column chromatography (ethyl acetate/*n*-hexane 3 : 2) and subsequent recrystallization (methanol/water) to obtain **35a** as a colourless solid (226 mg, 0.72 mmol, 63 %): R_f = 0.72 (ethyl acetate/*n*-hexane 6 : 4); mp: 125 °C; ^{1}H-NMR (400 MHz, DMSO-d_6): δ(ppm) = 9.09 (s, 1H), 7.03 (s, 2H), 6.93–6.82 (m, 2H), 6.58–6.48 (m, 2H), 6.08 (t, *J* = 5.9 Hz, 1H), 4.12 (d, *J* = 5.9 Hz, 2H), 2.27 (t, *J* = 7.3 Hz, 2H), 2.10 (s, 6H), 1.70–1.56 (m, 2H), 0.94 (t, *J* = 7.4 Hz, 3H); ^{13}C-NMR (100 MHz, DMSO-d_6): δ(ppm) = 170.7, 154.2 (d, *J* = 230.7 Hz), 145.4, 137.8, 134.9, 134.0, 126.4, 115.1 (d, *J* = 21.8 Hz), 112.9 (d, *J* = 7.3 Hz), 46.7, 37.4, 18.9, 18.2, 13.7; IR (ATR): $\tilde{\nu}$ = 3270 (w, ν_{N-H}), 3013, 2963 (w, ν_{C-H}), 1654 (s, $\nu_{C=O}$); ESI-HRMS (*m/z*): calcd. for $[C_{19}H_{24}N_2OF+H]^+$ 315.1867, found 315.1866; cpd purity (220 nm): 100 %.

***N*-(4-{[(4-Fluorophenyl)amino]methyl}-2-methylphenyl)butyramide** (**35b**): The synthesis was conducted from **34b** (500 mg, 2.44 mmol) and 4-fluoroaniline (257 μL, 2.68 mmol, 1.1 equiv.) according to the general procedure (reductive amination). The purification was carried out by flash chromatography (ethyl acetate/*n*-hexane, 30–40 % ethyl acetate) and subsequent recrystallization (methanol/water) to obtain **35b** as a colourless solid (480 mg, 1.60 mmol, 66 %): R_f = 0.54 (ethyl acetate/*n*-hexane 2 : 3); mp: 92 °C; ^{1}H-NMR (400 MHz, DMSO-d_6): δ(ppm) = 9.17 (s, 1H), 7.27 (d, *J* = 8.1 Hz, 1H), 7.17 (d, *J* = 2.1 Hz, 1H), 7.11 (dd, *J* = 8.2, 2.1 Hz, 1H), 6.92–6.81 (m, 2H), 6.58–6.48 (m, 2H), 6.09 (t, *J* = 6.0 Hz, 1H), 4.15 (d, *J* = 5.9 Hz, 2H), 2.28 (t, *J* = 7.3 Hz, 2H), 2.15 (s, 3H), 1.68–1.54 (m, 2H), 0.93 (t, *J* = 7.4 Hz, 3H); ^{13}C-NMR (100 MHz, DMSO-d_6): δ(ppm) = 171.0, 154.2 (d, *J* = 230.7 Hz), 145.4 (d, *J* = 1.6 Hz), 136.7, 135.0, 131.8, 129.0, 125.3, 124.7, 115.1 (d, *J* = 22.0 Hz), 112.9 (d, *J* = 7.3 Hz), 46.6, 37.7, 18.8, 18.0, 13.6; IR (ATR): $\tilde{\nu}$ = 3270 (w, ν_{N-H}), 3013, 2963 (w, ν_{C-H}), 1654 (s, $\nu_{C=O}$); ESI-HRMS (*m/z*): calcd. for $[C_{18}H_{22}N_2OF+H]^+$ 301.1711, found 301.1714; cpd purity (220 nm): 100 %.

***N*-(2-Fluoro-4-{[(4-fluorophenyl)amino]methyl}phenyl)butyramide** (**35c**): The synthesis was carried out from **34c** (480 mg, 2.29 mmol) 4-fluoroaniline (242 μL, 2.52 mmol, 1.1 equiv.) in accordance with the general procedure (reductive amination). The crude residue was further purified by silica gel column chromatography (ethyl acetate/*n*-hexane 3 : 7) and subsequent recrystallization (methanol/water) to obtain **35c** as a colourless solid (508 mg, 1.67 mmol, 73 %): R_f = 0.76 (ethyl acetate/*n*-hexane 1 : 1); mp: 123 °C; ^{1}H-NMR (400 MHz, DMSO-d_6): δ(ppm) = 9.55 (s, 1H), 7.71 (pseudo-t, *J* = 8.2 Hz, 1H), 7.16 (dd, *J* = 11.8, 1.9 Hz, 1H), 7.10 (dd, *J* = 8.3, 1.9 Hz, 1H), 6.91–6.81 (m, 2H), 6.57–6.47 (m, 2H), 6.16 (t, *J* = 6.1 Hz, 1H), 4.19 (d, *J* = 6.1 Hz, 2H), 2.30 (d, *J* = 14.6 Hz, 1H), 1.62–1.50 (m, 2H), 0.89 (t, *J* = 7.4 Hz, 3H); ^{13}C-NMR (100 MHz, DMSO-d_6): δ(ppm) = 171.4, 154.4 (d, *J* = 230 Hz), 153.9 (d, *J* = 244 Hz), 145.1 (d, *J* = 1.5 Hz), 138.0 (*J* = 6.4 Hz), 124.6, 124.4, 122.7 (d, *J* = 3.1 Hz), 115.2 (d, *J* = 22.0 Hz), 113.9 (d, *J* = 20.2 Hz), 113.1 (d, *J* = 7.3 Hz), 46.1, 37.6, 18.6, 13.5; IR (ATR): $\tilde{\nu}$ = 3430, 3300 (m, ν_{N-H}), 3034, 2963 (w, ν_{C-H}), 1672 (s, $\nu_{C=O}$), 1599 (s, δ_{N-H}). ESI-HRMS (*m/z*): calcd. for $[C_{17}H_{18}F_2N_2O+H]^+$ 305.1460, found 305.1461; cpd purity (220 nm): 100 %.

***N*-(4-{[(4-Fluorophenyl)amino]methyl}-2-(trifluoromethyl)phenyl)-butyramide hydrochloride** (**35d**): The synthesis was conducted from **34d** (320 mg, 1.23 mmol) and 4-fluoroaniline (140 μL, 1.48 mmol, 1.2 equiv.) according to the general procedure (reductive amination). The purification was carried out by silica gel column chromatography (ethyl acetate/*n*-hexane 1 : 3), which yielded the product as a colourless oil. To obtain a solid, the residue was dissolved in ethyl acetate. The resulting solution was cooled to 0 °C, and HCl gas was passed through the solution for 30 min to precipitate a hydrochloride salt. The precipitate was filtered off to obtain **35d** as an off-white solid (284 mg, 0.72 mmol, 59 %): R_f = 0.74 (ethyl acetate/*n*-hexane 2 : 3); mp: 193 °C (decomp.); ^{1}H-NMR (400 MHz, MeOH-d_4): δ(ppm) = 7.83 (d, *J* = 2.0 Hz, 1H), 7.74 (dd, *J* = 8.3, 2.1 Hz, 1H), 7.66 (d, *J* = 8.3 Hz, 1H), 7.53–7.43 (m, 2H), 7.37–7.27 (m, 2H), 4.71 (s, 2H), 2.44 (t, *J* = 7.4 Hz, 2H), 1.83–1.69 (m, 2H), 1.04 (t, *J* = 7.4 Hz, 3H); ^{13}C-NMR (100 MHz, MeOH-d_4): δ(ppm) = 175.9, 164.2 (d, *J* = 250.2 Hz), 137.8, 136.0, 132.8, 131.8, 131.2, 129.9, 127.4 (q, *J* = 30.3 Hz), 126.4, 124.8 (q, *J* = 271.3 Hz), 118.4 (d, *J* = 23.7 Hz), 55.7, 39.2, 20.3, 14.1; IR (ATR): $\tilde{\nu}$ = 3286 (w, ν_{N-H}), 2973 (w, ν_{C-H}), 1666 (s, $\nu_{C=O}$); ESI-HRMS (*m/z*): calcd. for $[C_{18}H_{19}N_2OF_4+H]^+$ 355.1428, found 355.1427; cpd purity (220 nm): 99 %.

***N*-(4-{[(2,4-Difluorophenyl)amino]methyl}-2-methylphenyl)nicotinamide** (**35e**): The synthesis was carried out from **34e** (288 mg, 1.20 mmol) and 2,4-difluoroaniline (179 μL, 1.80 mmol, 1.5 equiv.) in accordance with the general procedure (reductive amination). The crude residue was further purified by silica gel column chromatography (ethyl acetate/*n*-hexane 4 : 1) and subsequent recrystallization (methanol/water) to obtain **35e** as a colourless solid (180 mg, 0.51 mmol, 42 %): R_f = 0.42 (ethyl acetate); mp: 147 °C; ^{1}H-NMR (400 MHz, DMSO-d_6): δ(ppm) = 10.01 (s, 1H), 9.15–9.09 (m, 1H), 8.76 (dd, *J* = 4.8, 1.7 Hz, 1H), 8.29 (dt, *J* = 8.1, 2.0 Hz, 1H), 7.56 (ddd, *J* = 7.9, 4.8, 0.9 Hz, 1H), 7.32–7.24 (m, 2H), 7.20 (dd, *J* = 8.1, 2.0 Hz, 1H),

ChemMedChem
Research Article
doi.org/10.1002/cmdc.202200262
Chemistry Europe
European Chemical Societies Publishing

7.07 (ddd, J = 11.9, 8.9, 2.9 Hz, 1H), 6.78 (tdd, J = 8.8, 2.9, 1.4 Hz, 1H), 6.54 (ddd, J = 10.1, 9.0, 5.6 Hz, 1H), 6.08 (td, J = 6.2, 2.0 Hz, 1H), 4.30 (d, J = 6.1 Hz, 2H), 2.22 (s, 3H); ^{13}C-NMR (100 MHz, DMSO-d_6): δ(ppm) = 163.9, 152.1, 152.8 (dd, J = 233.7, 11.0 Hz), 150.0 (dd, J = 241.2, 11.9 Hz), 148.6, 137.7, 135.4, 134.5, 133.6, 133.4 (dd, J = 11.7, 2.6 Hz), 130.1, 128.9, 126.5, 124.6, 123.5, 112.1 (dd, J = 8.8, 5.2 Hz), 110.6 (dd, J = 21.2, 3.5 Hz), 103.4 (dd, J = 26.8, 22.7 Hz), 45.9, 18.0; IR (ATR): $\tilde{\nu}$ = 3293 (m, ν_{N-H}), 1644 (s, $\nu_{C=O}$), 1590 (s, δ_{N-H}); ESI-HRMS (*m/z*): calcd. for $[C_{20}H_{18}N_3OF_2+H]^+$ 354.1408, found 354.1410; cpd purity (220 nm): 100 %.

***N*-(2-Methyl-4-{[(5-methylpyridin-2-yl)amino]methyl}phenyl)butyramide** (**35 f**): The synthesis was conducted from **34 b** (500 mg, 2.44 mmol) and 5-methylpyridin-2-amine (290 mg, 2.68 mmol, 1.1 equiv.) according to the general procedure (reductive amination). The purification was carried out by flash chromatography (ethyl acetate/*n*-hexane, 30–40 % ethyl acetate) and subsequent recrystallization (methanol/water) to obtain **35 f** as a colourless solid (480 mg, 1.51 mmol, 62 %): R_f = 0.48 (ethyl acetate/*n*-hexane 2 : 3); mp: 134 °C; ^{1}H-NMR (400 MHz, DMSO-d_6): δ(ppm) = 9.17 (s, 1H), 7.80–7.74 (m, 1H), 7.23 (d, J = 8.1 Hz, 1H), 7.19 (dd, J = 8.5, 2.4 Hz, 1H), 7.13 (d, J = 2.0 Hz, 1H), 7.07 (dd, J = 8.1, 2.1 Hz, 1H), 6.72 (t, J = 6.0 Hz, 1H), 6.41 (d, J = 8.4 Hz, 1H), 4.36 (d, J = 6.0 Hz, 2H), 2.27 (t, J = 7.3 Hz, 2H), 2.14 (s, 3H), 2.07 (s, 3H), 1.67–1.54 (m, 2H), 0.92 (t, J = 7.4 Hz, 3H); ^{13}C-NMR (100 MHz, DMSO-d_6): δ(ppm) = 170.9, 156.9, 146.9, 137.6, 137.5, 134.8, 131.7, 129.0, 125.2, 124.7, 119.7, 107.7, 44.0, 37.7, 18.8, 18.0, 17.0, 13.6; IR (ATR): $\tilde{\nu}$ = 3251 (m, ν_{N-H}), 3086, 2921 (w, ν_{C-H}), 1650 (s, $\nu_{C=O}$), 1612 (s, δ_{N-H}); ESI-HRMS (*m/z*): calcd. for $[C_{18}H_{23}N_3O+H]^+$ 298.1914, found 298.1913; cpd purity (220 nm): 100 %.

Ethyl 6-aminonicotinate (**37**): 6-Amino-3-carboxylic acid (12.50 g, 90.5 mmol) was suspended in dry ethanol (250 mL). The suspension was set under an argon atmosphere. Thionyl chloride (19.7 mL, 272 mmol, 3.0 equiv.) was added dropwise, and the suspension was stirred at 90 °C. After 18 h, the reaction mixture was concentrated under reduced pressure. The residue was dissolved in ethyl acetate (250 mL) and extracted with an aq. saturated $NaHCO_3$ solution (250 mL). The organic phase was washed with brine, dried over Na_2SO_4, filtrated, and concentrated to dryness under reduced pressure to obtain **37** as an off-white solid (13.20 g, 79.4 mmol, 88 %): R_f = 0.38 (ethyl acetate/*n*-hexane 1 : 1); mp: 153 °C; ^{1}H-NMR (400 MHz, DMSO-d_6): δ(ppm) = 8.48 (dd, J = 2.4, 0.8 Hz, 1H), 7.80 (dd, J = 8.7, 2.4 Hz, 1H), 6.79 (s, 2H), 6.43 (dd, J = 8.8, 0.8 Hz, 1H), 4.21 (q, J = 7.1 Hz, 2H), 1.26 (t, J = 7.1 Hz, 3H); ^{13}C-NMR (100 MHz, DMSO-d_6): δ(ppm) = 165.2, 162.5, 151.0, 137.5, 113.5, 107.0, 59.8, 14.3; IR (ATR): $\tilde{\nu}$ = 3409 (m, ν_{N-H}), 2977 (w, ν_{C-H}), 1687 (s, $\nu_{C=O}$), 1597 (s, δ_{N-H}).

Ethyl 6-amino-5-bromonicotinate (**38**): Compound **37** (7.80 g, 46.9 mmol) was dissolved in dry THF (70 mL). The solution was set under an argon atmosphere and cooled to 0 °C. NBS (8.77 g, 49.3 mmol, 1.1 equiv.) was added in portions under stirring. Afterwards, the cooling was removed, and the mixture was stirred at room temperature with the exclusion of light. After 17 h, the mixture was poured into an ice-cold saturated aq. $NaHCO_3$ solution (200 mL), which was subsequently extracted with ethyl acetate (3 × 200 mL). The combined organic phases were washed with brine, dried over Na_2SO_4, filtrated, and concentrated under reduced pressure. The crude residue was purified by silica gel column chromatography (ethyl acetate/*n*-hexane 3 : 7) to obtain **38** as an off-white solid (8.80 g, 35.9 mmol, 77 %): R_f = 0.71 (ethyl acetate/*n*-hexane 1 : 1); mp: 129 °C; ^{1}H-NMR (400 MHz, DMSO-d_6): δ(ppm) = 8.48 (d, J = 2.0 Hz, 1H), 8.06 (d, J = 2.0 Hz, 1H), 7.13 (s, 2H), 4.23 (q, J = 7.1 Hz, 2H), 1.27 (t, J = 7.1 Hz, 3H); ^{13}C-NMR (100 MHz, DMSO-d_6): δ(ppm) = 164.0, 159.1, 149.4, 140.1, 115.3, 101.9, 60.3, 14.2; IR (ATR): $\tilde{\nu}$ = 3431 (m, ν_{N-H}), 2981 (w, ν_{C-H}), 1707 (s, $\nu_{C=O}$), 1635 (s, δ_{N-H}).

(6-Amino-5-bromopyridin-3-yl)methanol (**39**): Compound **38** (3.00 g, 12.2 mmol) was set under an argon atmosphere and dissolved in dry THF (30 mL). A 2.96 mM solution of $LiAlH_4$ in THF (4.96 mL, 14.7 mmol, 1.2 equiv.) was added dropwise. The reaction mixture was stirred at room temperature. After 2 h, additional $LiAlH_4$ solution (4.96 mL, 14.7 mmol, 1.2 equiv.) was added, and stirring was continued for 3 h. Afterwards, the reaction was quenched by the addition of water (0.5 mL). The resulting precipitate was filtered off and rinsed with ethyl acetate (200 mL). The filtrate was washed with brine, dried over Na_2SO_4, filtrated, and concentrated under reduced pressure. The crude residue was purified by silica gel column chromatography (DCM/methanol 9 : 1) to obtain **39** as a yellow solid (1.35 g, 6.7 mmol, 54 %): R_f = 0.30 (ethyl acetate/*n*-hexane 3 : 1); mp: 113 °C; ^{1}H-NMR (400 MHz, DMSO-d_6): δ(ppm) = 7.86 (d, J = 2.0 Hz, 1H), 7.64 (d, J = 2.0 Hz, 1H), 6.07 (s, 2H), 5.02 (t, J = 5.7 Hz, 1H), 4.29 (d, J = 5.7 Hz, 2H); ^{13}C-NMR (100 MHz, DMSO-d_6): δ(ppm) = 155.4, 145.7, 139.4, 127.7, 102.8, 59.9; IR (ATR): 3400–3000 (b, ν_{O-H}), 3373 (m, ν_{N-H}), 2952 (w, ν_{C-H}), 1603 (s, δ_{N-H}).

6-Amino-5-bromonicotinaldehyde (**40**): Compound **39** (2.56 g, 12.6 mmol) was suspended in toluene. Activated MnO_2 (3.01 g, 34.6 mmol, 2.8 equiv.) was added in one portion, and the reaction mixture was stirred at 80 °C. After 2 h, it was filtered through a pad of celite, which was subsequently rinsed with ethyl acetate. The combined filtrates were concentrated under reduced pressure to obtain **40** as a yellow solid (1.03 g, 5.1 mmol, 41 %): R_f = 0.49 (ethyl acetate/*n*-hexane 1 : 1); mp: 177 °C; ^{1}H-NMR (400 MHz, DMSO-d_6): δ(ppm) = 9.67 (s, 1H), 8.47 (d, J = 1.9 Hz, 1H), 8.06 (d, J = 1.9 Hz, 1H), 7.40 (s, 2H); ^{13}C-NMR (100 MHz, DMSO-d_6): δ(ppm) = 188.5, 159.7, 152.6, 138.8, 123.5, 103.2; IR (ATR): $\tilde{\nu}$ = 3474 (m, ν_{N-H}), 2988 (w, ν_{C-H}), 1672 (s, $\nu_{C=O}$), 1634 (s, δ_{N-H}).

***N*-(3-Bromo-5-formylpyridin-2-yl)butyramide** (**41 a**): Compound **40** (2.00 g, 10.0 mmol) was dissolved in DCM (100 mL). DIPEA (3.47 mL, 19.9 mmol, 2.0 equiv.) was added in one portion. The reaction mixture was cooled to 0 °C, and a solution of 3,3-dimethylbutanoyl chloride (2.06 mL, 19.9 mmol, 2.0 equiv.) in DCM (20 mL) was added dropwise over a period of 30 min. The cooling was removed, and the reaction mixture was stirred at room temperature. After 16 h, additional DCM (200 mL) was added, and the solution was extracted successively with a saturated aq. $NaHCO_3$ solution (200 mL), and a 2 M aq. HCl solution (200 mL). The organic phase was washed with brine, dried over Na_2SO_4, filtrated, and concentrated under reduced pressure. The crude residue was purified by flash chromatography (ethyl acetate/*n*-hexane, 30–70 % ethyl acetate) to obtain **41 a** as a colourless solid (1.35 g, 5.0 mmol, 50 %): R_f = 0.52 (ethyl acetate/*n*-hexane 1 : 1); mp: 101 °C; ^{1}H-NMR (400 MHz, DMSO-d_6): δ(ppm) = 10.37 (s, 1H), 10.00 (s, 1H), 8.88 (d, J = 1.9 Hz, 1H), 8.48 (d, J = 1.9 Hz, 1H), 2.37 (t, J = 7.3 Hz, 2H), 1.76–1.42 (m, 2H), 0.93 (t, J = 7.4 Hz, 3H); ^{13}C-NMR (100 MHz, DMSO-d_6): δ(ppm) = 190.4, 171.3, 153.6, 149.1, 141.7, 130.1, 115.8, 37.5, 18.3, 13.6; IR (ATR): $\tilde{\nu}$ = 3248 (m, ν_{N-H}), 3052, 2963 (w, ν_{C-H}), 1687, 1670 (s, $\nu_{C=O}$).

***N*-(3-Bromo-5-formylpyridin-2-yl)-3,3-dimethylbutanamide** (**41 b**): Compound **40** (500 mg, 2.49 mmol) was dissolved in DCM (25 mL). DIPEA (866 µL, 4.98 mmol, 2.0 equiv.) was added in one portion. The reaction mixture was cooled to 0 °C, and a solution of 3,3-dimethylbutanoyl chloride (415 µL, 2.99 mmol, 1.2 equiv.) in DCM (5 mL) was added dropwise over a period of 30 min. The cooling was removed, and the reaction mixture was stirred at room temperature. After 16 h, additional 3,3-dimethylbutanoyl chloride (415 µL, 2.99 mmol, 1.2 equiv.) dissolved in DCM (5 mL) was added dropwise at 0 °C. Afterwards, stirring was continued at room temperature. After another 8 h, DCM (100 mL) was added, and the solution was extracted successively with saturated aq. $NaHCO_3$ solution (100 mL) and 2 M aq. HCl solution (100 mL). The organic

ChemMedChem
Research Article
doi.org/10.1002/cmdc.202200262
Chemistry Europe
European Chemical Societies Publishing

phase was washed with brine, dried over Na_2SO_4, filtrated, and concentrated under reduced pressure. The crude residue was purified by flash chromatography (ethyl acetate/*n*-hexane, 30–70% ethyl acetate) to obtain **41b** as slightly yellow oil (360 mg, 1.20 mmol, 48%): $R_f = 0.59$ (ethyl acetate/*n*-hexane 1:1); ^{1}H-NMR (400 MHz, DMSO-d_6): δ(ppm) = 10.34 (s, 1H), 10.01 (s, 1H), 8.89 (d, $J = 2.0$ Hz, 1H), 8.48 (d, $J = 1.9$ Hz, 1H), 2.27 (s, 2H), 1.04 (s, 9H); ^{13}C-NMR (100 MHz, DMSO-d_6): δ(ppm) = 190.4, 169.9, 153.6, 149.0, 141.8, 130.2, 116.0, 48.6, 31.0, 29.7; IR (ATR): $\tilde{\nu} = 3241$ (m, ν_{N-H}), 3050, 2905 (w, ν_{C-H}), 1689, (s, $\nu_{C=O}$).

***N*-(3-Bromo-5-{[(4-fluorophenyl)amino]methyl}pyridin-2-yl)butyramide** (**42a**): The synthesis was conducted from **41a** (1.29 g, 4.77 mmol) and 4-fluoroaniline (542 µL, 5.719 mmol, 1.2 equiv.) according to the general procedure (reductive amination). The purification was carried out by silica gel column chromatography (ethyl acetate/*n*-hexane 1:1), yielding **42a** as a colourless oil. To obtain a solid, the residue was dissolved in methanol, followed by the addition of ice-cold water to form a precipitate, which was filtered off, yielding the title compound a colourless solid (998 mg, 2.73 mmol, 57%): $R_f = 0.31$ (ethyl acetate/*n*-hexane 1:1); mp: 151 °C; ^{1}H-NMR (400 MHz, DMSO-d_6): δ(ppm) = 10.03 (s, 1H), 8.40 (d, $J = 2.0$ Hz, 1H), 8.05 (d, $J = 2.0$ Hz, 1H), 6.96–6.85 (m, 2H), 6.63–6.54 (m, 2H), 6.22 (t, $J = 6.3$ Hz, 1H), 4.28 (d, $J = 6.2$ Hz, 2H), 2.28 (t, $J = 7.3$ Hz, 2H), 1.65–1.54 (m, 2H), 0.93 (t, $J = 7.4$ Hz, 3H); ^{13}C-NMR (100 MHz, DMSO-d_6): δ(ppm) = 171.2, 154.5 (d, $J = 231.7$ Hz), 148.1, 146.5, 144.7 (d, $J = 1.5$ Hz), 140.6, 135.6, 117.3, 115.3 (d, $J = 22.0$ Hz), 113.2 (d, $J = 7.4$ Hz), 43.4, 37.2, 18.4, 13.6; IR (ATR): $\tilde{\nu} = 3239$ (m, ν_{N-H}), 2966 (w, ν_{C-H}), 1665 (s, $\nu_{C=O}$). ESI-HRMS (*m/z*): calcd. for $[C_{16}H_{17}BrFN_3O+H]^+$ 366.0612, found 366.0608; cpd purity (220 nm): 100%.

***N*-(3-Bromo-5-{[(4-fluorophenyl)amino]methyl}pyridin-2-yl)-3,3-dimethylbutanamide** (**42b**): The synthesis was carried out from **41b** (320 mg, 1.07 mmol) and 4-fluoroaniline (123 µL, 1.28 mmol, 1.2 equiv.) in accordance with the general procedure (reductive amination). The crude residue was further purified by silica gel column chromatography (ethyl acetate/*n*-hexane 1:1), yielding the product as a colourless oil. To obtain a solid, the residue was dissolved in methanol, followed by the addition of ice-cold water to form a precipitate, which was filtered off, yielding **42b** as a colourless solid (310 mg, 0.79 mmol, 74%): $R_f = 0.39$ (ethyl acetate/*n*-hexane 1:1); mp: 141 °C; ^{1}H-NMR (400 MHz, DMSO-d_6): δ(ppm) = 9.96 (s, 1H), 8.38 (d, $J = 2.1$ Hz, 1H), 8.03 (d, $J = 2.0$ Hz, 1H), 6.94–6.83 (m, 2H), 6.61–6.52 (m, 2H), 6.20 (t, $J = 6.3$ Hz, 1H), 4.26 (d, $J = 6.2$ Hz, 2H), 2.17 (s, 2H), 1.03 (s, 9H); ^{13}C-NMR (100 MHz, DMSO-d_6): δ(ppm) = 169.8, 154.5 (d, $J = 231.4$ Hz), 148.2, 146.5, 144.7, 140.6, 135.6, 117.2, 115.3 (d, $J = 22.0$ Hz), 113.2 (d, $J = 7.3$ Hz), 48.5, 43.3, 30.8, 29.7; IR (ATR): $\tilde{\nu} = 3383$, 3311 (m, ν_{N-H}), 3059, 2958 (w, ν_{C-H}), 1667 (s, $\nu_{C=O}$), 1576 (s, δ_{N-H}).

***N*-(5-{[(4-Fluorophenyl)amino]methyl}-3-methylpyridin-2-yl)butyramide** (**43a**): The synthesis was conducted from **42a** (450 mg, 1.23 mmol) and trimethylboroxine (702 µL of a 3.5 M solution in THF, 2.46 mmol, 2.0 equiv.) according to the general procedure (Suzuki reaction). The purification was carried out by flash chromatography (ethyl acetate/*n*-hexane, 60–90% ethyl acetate), yielding the product as a colourless oil. To obtain a solid, the residue was dissolved in methanol, followed by the addition of ice-cold water to form a precipitate, which was filtered off, yielding **43a** as a colourless solid (70 mg, 0.23 mmol, 19%): $R_f = 0.39$ (ethyl acetate/*n*-hexane 3:1); mp: 104 °C; ^{1}H-NMR (400 MHz, DMSO-d_6): δ(ppm) = 9.87 (s, 1H), 8.21 (d, $J = 2.2$ Hz, 1H), 7.60 (d, $J = 2.3$ Hz, 1H), 6.97–6.80 (m, 2H), 6.69–6.49 (m, 2H), 6.13 (t, $J = 6.0$ Hz, 1H), 4.21 (d, $J = 6.0$ Hz, 2H), 2.29 (t, $J = 7.3$ Hz, 2H), 2.12 (s, 3H), 1.74–1.49 (m, 2H), 0.92 (t, $J = 7.4$ Hz, 3H); ^{13}C-NMR (100 MHz, DMSO-d_6): δ(ppm) = 171.2, 154.4 (d, $J = 231.1$ Hz), 149.1, 145.1 (d, $J = 1.6$ Hz), 144.7, 138.3, 133.2, 128.3, 115.2 (d, $J = 22.0$ Hz), 113.1 (d, $J = 7.3$ Hz), 44.1, 37.3, 18.5, 17.7, 13.6; IR (ATR): $\tilde{\nu} = 3256$ (m, ν_{N-H}), 2964 (w, ν_{C-H}), 1686 (s, $\nu_{C=O}$). ESI-HRMS (*m/z*): calcd. for $[C_{17}H_{20}FN_3O+H]^+$ 302.1663, found 302.1665; cpd purity (220 nm): 99%.

***N*-(5-{[(4-Fluorophenyl)amino]methyl}-3-methylpyridin-2-yl)-3,3-dimethylbutanamide** (**43b**): The synthesis was carried out from **42b** (500 mg, 1.27 mmol) and trimethylboroxine (725 µL of a 3.5 M solution in THF, 2.54 mmol, 2.0 equiv.) in accordance with the general procedure (Suzuki reaction). The crude residue was further purified by flash chromatography (ethyl acetate/*n*-hexane, 50–80% ethyl acetate), yielding the product as a colourless oil. To obtain a solid, the residue was dissolved in methanol, followed by the addition of ice-cold water to form a precipitate, which was filtered off, yielding **43b** as a colourless solid (180 mg, 0.55 mmol, 43%): $R_f = 0.35$ (ethyl acetate/*n*-hexane 1:1); mp: 93 °C; ^{1}H-NMR (400 MHz, DMSO-d_6): δ(ppm) = 9.82 (s, 1H), 8.21 (d, $J = 2.2$ Hz, 1H), 7.61 (d, $J = 2.3$ Hz, 1H), 6.95–6.84 (m, 2H), 6.63–6.53 (m, 2H), 6.14 (t, $J = 6.0$ Hz, 1H), 4.22 (d, $J = 6.0$ Hz, 2H), 2.21 (s, 2H), 2.15 (s, 3H), 1.04 (s, 9H); ^{13}C-NMR (100 MHz, DMSO-d_6): δ(ppm) = 169.9, 154.4 (d, $J = 231.3$ Hz), 149.1, 145.1 (d, $J = 1.6$ Hz), 144.8, 138.3, 133.2, 128.4, 115.2 (d, $J = 21.9$ Hz), 113.1 (d, $J = 7.3$ Hz), 48.6, 44.1, 30.7, 29.7, 18.0; IR (ATR): $\tilde{\nu} = 3242$ (m, ν_{N-H}), 2956 (w, ν_{C-H}), 1660 (s, $\nu_{C=O}$), 1586 (w, δ_{N-H}). ESI-HRMS (*m/z*): calcd. for $[C_{19}H_{24}FN_3O+H]^+$ 330.1976, found 330.1979; cpd purity (220 nm): 99%.

***N*-(3-Cyclopropyl-5-{[(4-fluorophenyl)amino]methyl}pyridin-2-yl)butyramide** (**43c**): The synthesis was conducted from **42a** (450 mg, 1.23 mmol) and cyclopropylboronic acid (211 mg, 2.46 mmol, 2.0 equiv.) according to the general procedure (Suzuki reaction). The purification was carried out by flash chromatography (ethyl acetate/*n*-hexane, 50–90% ethyl acetate), yielding the product as a colourless oil. To obtain a solid, the residue was dissolved in methanol, followed by the addition of ice-cold water to form a precipitate, which was filtered off, yielding **43c** as a colourless solid (60 mg, 0.18 mmol, 15%): $R_f = 0.39$ (ethyl acetate/*n*-hexane 1:1); mp: 127 °C; ^{1}H-NMR (400 MHz, DMSO-d_6): δ(ppm) = 9.83 (s, 1H), 8.17 (d, $J = 2.2$ Hz, 1H), 7.34 (d, $J = 2.3$ Hz, 1H), 6.95–6.84 (m, 2H), 6.62–6.52 (m, 2H), 6.09 (t, $J = 6.2$ Hz, 1H), 4.19 (d, $J = 6.1$ Hz, 2H), 2.30 (d, $J = 7.3$ Hz, 2H), 1.95–1.84 (m, 1H), 1.65–1.53 (m, 2H), 0.92 (t, $J = 7.4$ Hz, 3H), 0.89–0.84 (m, 2H), 0.58–0.49 (m, 2H); ^{13}C-NMR (100 MHz, DMSO-d_6): δ(ppm) = 171.5, 154.4 (d, $J = 231.2$ Hz), 149.3, 145.0 (d, $J = 1.6$ Hz), 144.3, 133.8, 133.3, 133.3, 115.2 (d, $J = 22.0$ Hz), 113.2 (d, $J = 7.3$ Hz), 44.2, 37.3, 18.6, 13.7, 11.1, 7.8; IR (ATR): $\tilde{\nu} = 3262$ (m, ν_{N-H}), 3002, 2962 (w, ν_{C-H}), 1666 (s, $\nu_{C=O}$), 1584 (m, δ_{N-H}). ESI-HRMS (*m/z*): calcd. for $[C_{19}H_{22}FN_3O+H]^+$ 328.1820, found 328.1817; cpd purity (220 nm): 100%.

***N*-(5-{[(4-Fluorophenyl)amino]methyl}pyridin-2-yl)butyramide** (**44**): Compound **44** was a side product in the synthesis of **43a**. The separation from the main product by flash chromatography yielded **44** as a colourless solid (25 mg, 0.09 mmol, 7%): $R_f = 0.54$ (ethyl acetate/*n*-hexane 1:1); mp: 92 °C; ^{1}H-NMR (400 MHz, DMSO-d_6): δ(ppm) = 10.37 (s, 1H), 8.28 (d, $J = 2.5$ Hz, 1H), 8.04 (d, $J = 8.5$ Hz, 1H), 7.72 (dd, $J = 8.5$, 2.4 Hz, 1H), 6.95–6.84 (m, 2H), 6.62–6.52 (m, 2H), 6.10 (t, $J = 6.1$ Hz, 1H), 4.19 (d, $J = 6.0$ Hz, 2H), 2.34 (t, $J = 7.3$ Hz, 2H), 1.66–1.54 (m, 2H), 0.89 (t, $J = 7.4$ Hz, 3H); ^{13}C-NMR (100 MHz, DMSO-d_6): δ(ppm) = 171.9, 154.4 (d, $J = 231.1$ Hz), 151.0, 146.9, 145.1 (d, $J = 1.5$ Hz), 137.3, 130.5, 115.2 (d, $J = 21.9$ Hz), 113.2 (d, $J = 7.3$ Hz), 113.0, 44.2, 37.9, 18.4, 13.5; IR (ATR): $\tilde{\nu} = 3307$ (m, ν_{N-H}), 2965 (w, ν_{C-H}), 1672 (s, $\nu_{C=O}$), 1578 (m, δ_{N-H}).

4-(1,3-Dioxoisoindolin-2-yl)-3-methylbenzonitrile (**45**): Compound **32b** (460 mg, 3.48 mmol) and phthalic anhydride (523 mg, 3.48 mmol, 1.0 equiv.) were suspended in acetic acid (20 mL). The mixture was stirred at 130 °C. After 5 h, the reaction was poured on ice water. The precipitate was filtered off and recrystallized from methanol to obtain **45** as an off-white solid (756 mg, 2.88 mmol, 83%): $R_f = 0.76$ (ethyl acetate/*n*-hexane 1:1); mp: 211 °C; ^{1}H-NMR

ChemMedChem
Research Article
doi.org/10.1002/cmdc.202200262
Chemistry Europe
European Chemical Societies Publishing

(400 MHz, DMSO-d_6): δ(ppm) = 8.05–7.98 (m, 2H), 7.98–7.89 (m, 3H), 7.85 (ddd, *J* = 8.1, 2.0, 0.7 Hz, 1H), 7.63 (d, *J* = 8.1 Hz, 1H), 2.21 (s, 3H); ^{13}C-NMR (100 MHz, DMSO-d_6): δ(ppm) = 166.4, 138.3, 135.5, 134.9, 134.5, 131.7, 130.5, 130.4, 123.7, 118.3, 111.8, 17.3; IR (ATR): $\tilde{\nu}$ = 3074, 2926 (w, ν_{C-H}), 2233 (m, $\nu_{C\equiv N}$), 1719 (s, $\nu_{C=O}$).

4-(1,3-Dioxoisoindolin-2-yl)-3-methylbenzaldehyde (**46**): The synthesis was conducted from **45** (3.30 g, 12.6 mmol) according to the general procedure (nitrile reduction). The purification was carried out by silica gel column chromatography (ethyl acetate/*n*-hexane 2 : 3) to obtain **46** as a colourless solid (2.71 g, 10.2 mmol, 81 %): R_f = 0.72 (ethyl acetate/*n*-hexane 1 : 1); mp: 188 °C; ^{1}H-NMR (400 MHz, DMSO-d_6): δ(ppm) = 10.06 (s, 1H), 8.03–7.99 (m, 2H), 7.98–7.92 (m, 3H), 7.91–7.87 (m, 1H), 7.63 (d, *J* = 8.0 Hz, 1H), 2.25 (s, 3H); ^{13}C-NMR (100 MHz, DMSO-d_6): δ(ppm) = 192.6, 166.6, 137.6, 136.4, 136.3, 134.9, 131.7, 131.6, 130.1, 127.5, 123.7, 17.5; IR (ATR): $\tilde{\nu}$ = 3027, 2976 (w, ν_{C-H}), 1704, 1681 (s, $\nu_{C=O}$).

***N*-(4-{[(4-Fluorophenyl)amino]methyl}-2-methylphenyl)-2-(hydroxymethyl)benzamide** (**48**): The synthesis was carried out from **46** (1.20 g, 4.5 mmol) and 4-fluoroaniline (520 μL, 5.43 mmol, 1.2 equiv.) in accordance with the general procedure (reductive amination). The crude residue was further purified by silica gel column chromatography (ethyl acetate/*n*-hexane 2 : 3) and subsequent recrystallization (methanol/water), which yielded **48** as a colourless solid (1.12 g, 3.1 mmol, 68 %): R_f = 0.72 (ethyl acetate/*n*-hexane 3 : 2); mp: 144 °C; ^{1}H-NMR (400 MHz, DMSO-d_6): δ(ppm) = 9.82 (s, 1H), 7.63–7.55 (m, 2H), 7.53–7.45 (m, 1H), 7.42–7.33 (m, 2H), 7.24 (d, *J* = 2.0 Hz, 1H), 7.18 (dd, *J* = 8.3, 2.1 Hz, 1H), 6.94–6.83 (m, 2H), 6.60–6.50 (m, 2H), 6.14 (t, *J* = 6.0 Hz, 1H), 5.36 (t, *J* = 5.5 Hz, 1H), 4.69 (d, *J* = 5.5 Hz, 2H), 4.19 (d, *J* = 5.9 Hz, 2H), 2.24 (s, 3H); ^{13}C-NMR (100 MHz, DMSO-d_6): δ(ppm) = 167.3, 154.3 (d, *J* = 230.9 Hz), 145.3, 140.2, 137.5, 135.2, 134.8, 132.7, 129.9, 129.1, 127.6, 127.6, 126.7, 125.9, 124.8, 115.2 (d, *J* = 22.0 Hz), 113.0 (d, *J* = 7.3 Hz), 61.0, 46.7, 18.1; IR (ATR): $\tilde{\nu}$ = 3000–3300 (b, ν_{O-H}), 3267 (m, ν_{N-H}), 3036, 2907 (w, ν_{C-H}), 1645 (s, $\nu_{C=O}$); ESI-HRMS (*m/z*): calcd. for $[C_{22}H_{22}N_2O_2F+H]^+$ 365.1660, found 365.1658; cpd purity (220 nm): 100 %.

2-(4-{[(4-Fluorophenyl)amino]methyl}-2-methylphenyl)isoindoline-1,3-dione (**49**): Compound **46** (1.64 g, 6.2 mmol) was suspended in dry toluene (50 mL). 4 Å molecular sieves (5 g), and 4-fluoroaniline (713 μL, 7.43 mmol, 1.2 equiv.) were added. The reaction mixture was stirred at 120 °C. After 6 h, the reaction was terminated, and the mixture was filtered hot to remove the molecular sieves. The filtrate was cooled to room temperature and concentrated under reduced pressure. The residue was dissolved in ethyl acetate (50 mL). Pd/C (10 % Pd, 50 % water wet, 300 mg) was added, and the mixture was carefully set under a hydrogen atmosphere (balloon pressure). After the reaction stirred for 6 h at room temperature, the catalyst was filtered off, and the filtrate was concentrated under reduced pressure. The crude residue was purified by silica gel column chromatography (ethyl acetate/*n*-hexane 3 : 7) and subsequent recrystallization (toluene/*n*-hexane) to obtain **49** as a slightly yellow coloured solid (1.49 g, 4.1 mmol, 67 %): R_f = 0.81 (ethyl acetate/*n*-hexane 1 : 1); mp: 156 °C; ^{1}H-NMR (400 MHz, DMSO-d_6): δ(ppm) = 8.01–7.94 (m, 2H), 7.94–7.87 (m, 2H), 7.40–7.34 (m, 1H), 7.33–7.23 (m, 2H), 6.94–6.85 (m, 2H), 6.61–6.53 (m, 2H), 6.21 (t, *J* = 6.0 Hz, 1H), 4.25 (d, *J* = 6.0 Hz, 2H), 2.09 (s, 3H); ^{13}C-NMR (100 MHz, DMSO-d_6): δ(ppm) = 167.1, 154.3 (d, *J* = 231.0 Hz), 145.3 (d, *J* = 1.3 Hz), 141.3, 136.1, 134.7, 131.6, 129.4, 129.3, 129.1, 125.4, 123.5, 115.2 (d, *J* = 22.0 Hz), 112.9 (d, *J* = 7.3 Hz), 46.6, 17.5; IR (ATR): $\tilde{\nu}$ = 3399 (m, ν_{N-H}), 2976 (w, ν_{C-H}), 1720 (s, $\nu_{C=O}$); 1610 (m, δ_{N-H}).

Benzyl [4-(1,3-dioxoisoindolin-2-yl)-3-methylbenzyl](4-fluorophenyl)carbamate (**50**): Compound **49** (3.00 g, 8.3 mmol) was dissolved in DCM (200 mL). DIPEA (2.90 mL, 16.7 mmol, 2.0 equiv.) and benzyl chloroformate (1.46 mL, 10.4 mmol, 1.3 equiv.) were added, and the resulting solution was stirred at room temperature. After 4 h, the reaction mixture was concentrated under reduced pressure. The residue was purified by flash chromatography (ethyl acetate/*n*-hexane, 30–50 % ethyl acetate) to obtain **50** as an off-white solid (3.46 g, 7.0 mmol, 84 %): R_f = 0.40 (ethyl acetate/*n*-hexane 1 : 3); mp: 150 °C; ^{1}H-NMR (400 MHz, DMSO-d_6): δ(ppm) = 8.01–7.95 (m, 2H), 7.95–7.89 (m, 2H), 7.42–7.14 (m, 12H), 5.16 (s, 2H), 4.92 (s, 2H), 2.07 (s, 3H); ^{13}C-NMR (100 MHz, DMSO-d_6): δ(ppm) = 167.0, 160.1 (d, *J* = 243.7 Hz), 154.9, 138.7, 138.0, 136.5, 136.3, 134.7, 131.6, 129.8, 129.3, 128.7, 128.6 (d, *J* = 8.9 Hz), 128.4, 127.8, 127.4, 125.3, 123.5, 115.6 (d, *J* = 22.5 Hz), 66.9, 53.1, 17.47; IR (ATR): $\tilde{\nu}$ = 3031, 2973 (w, ν_{C-H}), 1695 (s, $\nu_{C=O}$).

Benzyl (4-amino-3-methylbenzyl)(4-fluorophenyl)carbamate (**51**): Compound **50** (3.40 g, 6.9 mmol) was dissolved in THF (100 mL). An 80 % hydrazine hydrate solution (8.37 mL, 137.5 mmol, 20.0 equiv.) was added, and the reaction mixture was stirred for 16 h at room temperature. After complete conversion, the volatiles were removed under reduced pressure. The residue was dissolved in DCM (200 mL), and insoluble solids were filtered off. The filtrate was concentrated under reduced pressure, and the crude residue was purified by silica gel column chromatography (ethyl acetate/*n*-hexane 1 : 1), which yielded **51** as a slightly yellow oil (2.45 g, 6.7 mmol, 98 %): R_f = 0.75 (ethyl acetate/*n*-hexane 1 : 1); ^{1}H-NMR (400 MHz, DMSO-d_6): δ(ppm) = 7.39–7.24 (m, 5H), 7.19–7.07 (m, 4H), 6.73 (d, *J* = 2.4 Hz, 1H), 6.66 (dd, *J* = 8.1, 2.1 Hz, 1H), 6.48 (d, *J* = 8.0 Hz, 1H), 5.12 (s, 2H), 4.75 (s, 2H), 4.64 (s, 2H), 1.96 (s, 3H); ^{13}C-NMR (100 MHz, DMSO-d_6): δ(ppm) = 160.1 (*J* = 243.2 Hz), 154.8, 145.8, 137.9, 136.7, 129.6, 129.2 (d, *J* = 8.4 Hz), 128.3, 127.8, 127.4, 126.1, 124.6, 120.9, 115.4 (d, *J* = 22.5 Hz), 113.8, 66.6, 53.2, 17.4; IR (ATR): $\tilde{\nu}$ = 3367 (m, ν_{N-H}), 3032, 2930 (w, ν_{C-H}), 1692 (s, $\nu_{C=O}$); 1626 (m, δ_{N-H}).

Benzyl {4-[3-(1*H*-pyrazol-1-yl)propanamido]-3-methylbenzyl}(4-fluorophenyl)carbamate (**52**): Compound **58** (423 mg, 3.02 mmol, 2.0 equiv.) was dissolved in DMF (10 mL). HOBt (510 mg, 3.77 mmol, 2.5 equiv.), DIC (591 μL, 3.77 mmol, 2.5 equiv.) and **51** (550 mg, 1.51 mmol) were added successively. The reaction mixture was stirred at room temperature. After 16 h, the solution was partitioned between ethyl acetate (100 mL) and water (100 mL). The organic phase was extracted with water (2 × 100 mL), washed with brine, dried over Na_2SO_4, filtrated, and concentrated under reduced pressure. The crude residue was purified by silica gel column chromatography (ethyl acetate/*n*-hexane 9 : 1). NMR analysis of the obtained product revealed that it contained a significant amount of diisopropyl urea as a side product of the coupling reaction. To remove the diisopropyl urea, the crude product was suspended in 30 mL of diethyl ether. Solids were filtered off, and the filtrate was concentrated under reduced pressure to obtain the product as a colourless solid. NMR analysis showed a reduction of the diisopropyl urea by a factor of 10, but the product still contained about 25 mol% (8 wt%) of diisopropyl urea based on NMR analysis. Nevertheless, the obtained product (550 mg in total containing 506 mg of the desired product, 1.04 mmol, 69 %) was used for the following reaction without further purification. ^{1}H-NMR (400 MHz, DMSO-d_6): δ(ppm) = 9.29 (s, 1H), 7.67 (d, *J* = 2.3 Hz, 1H), 7.44 (d, *J* = 2.0 Hz, 1H), 7.38–7.20 (m, 8H), 7.19–7.09 (m, 2H), 6.99 (d, *J* = 2.1 Hz, 1H), 6.95 (dd, *J* = 8.1, 2.1 Hz, 1H), 6.21 (t, *J* = 2.0 Hz, 1H), 5.13 (s, 2H), 4.79 (s, 2H), 4.40 (t, *J* = 6.8 Hz, 2H), 2.88 (t, *J* = 6.8 Hz, 2H), 2.04 (s, 3H); ^{13}C-NMR (100 MHz, DMSO-d_6): δ(ppm) = 168.5, 160.1 (d, *J* = 242.8 Hz), 154.9, 138.6, 137.8, 136.6, 135.2, 134.3, 131.7, 129.9, 129.3, 128.9, 128.3, 127.8, 127.4, 125.0, 124.9, 115.5 (d, *J* = 22.6 Hz), 104.9, 66.8, 53.0, 47.4, 36.4, 17.8.

***N*-(4-{[(4-Fluorophenyl)amino]methyl}-2-methylphenyl)-3-(1*H*-pyrazol-1-yl)propanamide** (**53**): Compound **52** (417 mg, 0.86 mmol) was suspended in a 33 wt% solution of HBr in acetic acid (10 mL) and stirred at room temperature in a sealed vessel. After 2 h, the

ChemMedChem
Research Article
doi.org/10.1002/cmdc.202200262
Chemistry Europe
European Chemical Societies Publishing

reaction mixture was poured into diethyl ether (100 mL). The resulting precipitate was filtered off. The colourless solid was washed with diethyl ether, and afterwards, partitioned between ethyl acetate (100 mL) and a saturated aq. solution of $NaHCO_3$ (100 mL). The organic phase was washed with brine, dried over Na_2SO_4, filtrated, and concentrated under reduced pressure. The crude residue was purified by silica gel column chromatography (ethyl acetate/*n*-hexane 9:1) and subsequent recrystallization (methanol/water) to obtain **53** as a colourless solid (270 mg, 0.77 mmol, 89%): R_f = 0.39 (ethyl acetate/*n*-hexane 3:1); mp: 183 °C; ^{1}H-NMR (400 MHz, DMSO-d_6): δ(ppm) = 9.30 (s, 1H), 7.67 (d, *J* = 2.2 Hz, 1H), 7.44 (d, *J* = 1.8 Hz, 1H), 7.24 (d, *J* = 8.1 Hz, 1H), 7.16 (d, *J* = 2.1 Hz, 1H), 7.11 (dd, *J* = 8.1, 2.1 Hz, 1H), 6.92–6.81 (m, 2H), 6.58–6.48 (m, 2H), 6.21 (t, *J* = 2.0 Hz, 1H), 6.09 (t, *J* = 6.0 Hz, 1H), 4.40 (t, *J* = 6.8 Hz, 2H), 4.14 (d, *J* = 5.9 Hz, 2H), 2.87 (t, *J* = 6.8 Hz, 2H), 2.07 (s, 3H); ^{13}C-NMR (100 MHz, DMSO-d_6): δ(ppm) = 168.5, 154.2 (d, *J* = 230.7 Hz), 145.4, 138.6, 136.9, 134.7, 131.8, 129.9, 129.0, 125.1, 124.7, 115.2 (d, *J* = 22.0 Hz), 112.9 (d, *J* = 7.3 Hz), 104.9, 47.5, 46.6, 36.4, 17.8; IR (ATR): $\tilde{\nu}$ = 3371, 3171 (m, ν_{N-H}), 3108, 2991 (w, ν_{C-H}), 1670 (s, $\nu_{C=O}$); 1612 (m, δ_{N-H}); ESI-HRMS (*m/z*): calcd. for $[C_{20}H_{21}FN_4O + H]^+$ 353.1771, found 353.1775; cpd purity (220 nm): 100%.

***N*-(2,4-Dimethylphenyl)-3-(1*H*-pyrazol-1-yl)propanamide** (**54**): Compound **52** (280 mg, 0.58 mmol) was dissolved in ethyl acetate (25 mL). Pd/C (10% Pd, 50% water wet, 50 mg) was added, the suspension was carefully set under a hydrogen atmosphere (balloon pressure) and stirred at room temperature. After 20 min, the reaction mixture was filtered through a pad of celite, and the filtrate was concentrated under reduced pressure. The crude residue was purified by silica gel column chromatography (ethyl acetate/*n*-hexane 9:1) and subsequent recrystallization (water), which yielded **54** as a colourless solid (86 mg, 0.35 mmol, 61%): R_f = 0.38 (ethyl acetate/*n*-hexane 3:1); mp: 118 °C; ^{1}H-NMR (400 MHz, DMSO-d_6): δ(ppm) = 9.27 (s, 1H), 7.67 (d, *J* = 1.6 Hz, 1H), 7.44 (d, *J* = 1.1 Hz, 1H), 7.17 (d, *J* = 8.0 Hz, 1H), 6.98 (d, *J* = 2.0 Hz, 1H), 6.93 (dd, *J* = 8.0, 2.1 Hz, 1H), 6.21 (t, *J* = 2.0 Hz, 1H), 4.40 (t, *J* = 6.8 Hz, 2H), 2.87 (t, *J* = 6.8 Hz, 2H), 2.23 (s, 3H), 2.05 (s, 3H); ^{13}C-NMR (100 MHz, DMSO-d_6): δ(ppm) = 168.5, 138.6, 134.2, 133.5, 131.8, 130.7, 129.9, 126.3, 125.2, 104.9, 47.5, 36.4, 20.4, 17.7; IR (ATR): $\tilde{\nu}$ = 3293 (m, ν_{N-H}), 3021, 2957 (w, ν_{C-H}), 1651 (s, $\nu_{C=O}$); 1590 (m, δ_{N-H}).

Methyl 3-(1*H*-pyrazol-1-yl)propanoate (**57**): Methyl prop-2-enate (2.27 mL, 25.0 mmol), pyrazole (1.70 g, 25.0 mmol, 1.0 equiv.) and DBU (3.73 mL, 25.0 mmol, 1.0 equiv.) were dissolved in acetonitrile (25 mL). The reaction mixture was stirred at room temperature. After 16 h, the volatiles were removed under reduced pressure, and the residue was purified by silica gel column chromatography (ethyl acetate/*n*-hexane 3:7) to obtain **57** as a colourless oil (2.93 g, 19.0 mmol, 76%): R_f = 0.46 (ethyl acetate/*n*-hexane 3:7); ^{1}H-NMR (400 MHz, DMSO-d_6): δ(ppm) = 7.69 (dd, *J* = 2.3, 0.8 Hz, 1H), 7.42 (dd, *J* = 1.9, 0.7 Hz, 1H), 6.20 (t, *J* = 2.1 Hz, 1H), 4.35 (t, *J* = 6.7 Hz, 2H), 3.59 (s, 3H), 2.86 (t, *J* = 6.7 Hz, 2H); ^{13}C-NMR (100 MHz, DMSO-d_6): δ(ppm) = 171.1, 138.7, 130.0, 105.0, 51.5, 46.7, 34.2; IR (ATR): $\tilde{\nu}$ = 2954 (w, ν_{C-H}), 1732 (s, $\nu_{C=O}$).

3-(1*H*-Pyrazol-1-yl)propanoic acid (**58**): Compound **57** (2.72 g, 17.7 mmol) was dissolved in methanol (30 mL). A solution of potassium hydroxide (3.89 g, 70.6 mmol, 4.0 equiv.) in water (10 mL) was added, and the solution was stirred at room temperature. After 16 h, the reaction mixture was acidified to pH 1–2 with conc. aq. HCl and subsequently concentrated under reduced pressure. The residue was treated with diethyl ether several times and remaining solids were filtered off. The resulting filtrate was concentrated under reduced pressure again to obtain **58** as a colourless solid (1.83 g, 13.1 mmol, 74%): R_f = 0.49 (ethyl acetate/toluene/AcOH 5:5:1); mp: 67 °C; ^{1}H-NMR (400 MHz, DMSO-d_6): δ(ppm) = 11.14 (s, 1H), 7.69 (dd, *J* = 2.3, 0.7 Hz, 1H), 7.43 (dd, *J* = 1.8, 0.7 Hz, 1H), 6.21 (t, *J* = 2.1 Hz, 1H), 4.31 (t, *J* = 6.8 Hz, 2H), 2.77 (t, *J* = 6.8 Hz, 2H); ^{13}C-NMR (100 MHz, DMSO-d_6): δ(ppm) = 172.2, 138.6, 130.1, 105.0, 46.9, 34.5; IR (ATR): $\tilde{\nu}$ = 3300–2500 (b, ν_{O-H}), 3120, 2971 (w, ν_{C-H}), 1712 (s, $\nu_{C=O}$).

Benzyl (4-acrylamido-3-methylbenzyl)(4-fluorophenyl)carbamate (**59**): Compound **51** (270 mg, 0.74 mmol) was dissolved in DCM (25 mL). DIPEA (258 µL, 1.48 mmol, 2.0 equiv.) was added in one portion. The reaction mixture was cooled to 0 °C, and a solution of prop-2-enoyl chloride (91 µL, 1.11 mmol, 1.5 equiv.) in DCM (2 mL) was added dropwise over a period of 30 min. Subsequently, stirring at 0 °C was continued. After 2 h, the reaction mixture was concentrated under reduced pressure, and the crude residue was purified by flash chromatography (ethyl acetate/*n*-hexane, 30–60% ethyl acetate) to obtain **59** as a colourless oil (290 mg, 0.69 mmol, 94%): R_f = 0.30 (ethyl acetate/*n*-hexane 3:7); ^{1}H-NMR (400 MHz, DMSO-d_6): δ(ppm) = 9.42 (s, 1H), 7.41 (d, *J* = 8.1 Hz, 1H), 7.38–7.20 (m, 7H), 7.20–7.10 (m, 2H), 7.04 (d, *J* = 2.1 Hz, 1H), 6.99 (dd, *J* = 8.1, 2.1 Hz, 1H), 6.52 (dd, *J* = 17.0, 10.2 Hz, 1H), 6.23 (dd, *J* = 17.1, 2.0 Hz, 1H), 5.73 (dd, *J* = 10.2, 2.1 Hz, 1H), 5.14 (s, 2H), 4.81 (s, 2H), 2.14 (s, 3H); ^{13}C-NMR (100 MHz, DMSO-d_6): δ(ppm) = 163.2, 160.1 (d, *J* = 243.5 Hz), 154.9, 137.9, 136.6, 135.1, 134.4, 131.7, 131.5, 129.4, 128.9, 128.4, 127.8, 127.4, 126.5, 125.1, 124.8, 115.5 (d, *J* = 22.6 Hz), 66.8, 53.0, 17.9; IR (ATR): $\tilde{\nu}$ = 3271 (m, ν_{N-H}), 3031, 2953 (w, ν_{C-H}), 1687, 1663 (s, $\nu_{C=O}$).

Benzyl (4-fluorophenyl){3-methyl-4-[3-(pyrrolidin-1-yl)propanamido]benzyl}carbamate (**60**): Compound **59** (280 mg, 0.67 mmol) was dissolved in ethanol (25 mL). Pyrrolidine (98 µL, 1.34 mmol, 2.0 equiv.) was added in one portion, and the reaction mixture was stirred at 60 °C. After 7 h, the solution was concentrated under reduced pressure, and the crude residue was purified by silica gel column chromatography (DCM/methanol 95:5) to obtain **60** as a colourless oil (285 mg, 0.58 mmol, 87%): R_f = 0.73 (DCM/methanol 9:1); ^{1}H-NMR (400 MHz, DMSO-d_6): δ(ppm) = 9.98 (s, 1H), 7.64 (d, *J* = 8.2 Hz, 1H), 7.39–7.18 (m, 7H), 7.18–7.09 (m, 2H), 7.00 (d, *J* = 2.1 Hz, 1H), 6.95 (dd, *J* = 8.2, 2.1 Hz, 1H), 5.14 (s, 2H), 4.78 (s, 2H), 2.72 (t, *J* = 6.5 Hz, 2H), 2.61–2.41 (m, 6H), 2.12 (s, 3H), 1.79–1.65 (m, 4H); ^{13}C-NMR (100 MHz, DMSO-d_6): δ(ppm) = 170.2, 160.1 (d, *J* = 243.4 Hz), 154.9, 137.8, 136.6, 135.9, 133.1, 129.3, 129.2, 129.0, 128.4, 127.8, 127.4, 125.2, 122.8, 115.5 (d, *J* = 22.6 Hz), 66.8, 53.2, 52.9, 51.5, 35.2, 23.1, 17.6; IR (ATR): $\tilde{\nu}$ = 1698 (s, $\nu_{C=O}$).

***N*-(4-{[(4-Fluorophenyl)amino]methyl}-2-methylphenyl)-3-(pyrrolidin-1-yl)propanamide 2,2,2-trifluoroacetate** (**61**): Compound **60** (480 mg, 0.98 mmol) was dissolved in methanol (25 mL). Pd/C (10% Pd, 50% water wet, 200 mg) was added, the suspension was carefully set under a hydrogen atmosphere (balloon pressure) and stirred at room temperature. After 2 h, the reaction mixture was filtered through a pad of celite. The filtrate was concentrated under reduced pressure. The crude residue was purified by silica gel column chromatography (DCM/methanol 95:5) and successive preparative HPLC (Hibar RT 250–25 column, mobile phase methanol/water 1:1 with 0.1% TFA). The title compound was obtained as a colourless solid, which turned into an orange oil after contact with air (230 mg, 0.49 mmol, 50%): ^{1}H-NMR (400 MHz, MeOH-d_4): δ(ppm) = 7.55 (d, *J* = 8.2 Hz, 1H), 7.20–7.35 (m, 7H), 4.52 (s, 2H), 3.78–3.68 (m, 2H), 3.58 (t, *J* = 6.8 Hz, 2H), 3.24–3.11 (m, 2H), 3.30 (t, *J* = 6.8 Hz, 2H), 2.31 (s, 3H), 2.23–2.14 (m, 2H), 2.14–2.03 (m, 2H).

LogD$_{7.4}$ estimation

The log$D_{7.4}$ estimation was carried out as previously reported by means of a standard HPLC-based method, which was established in accordance with guideline OPPTS 830.7570 of the United States Environmental Protection Agency.[43] Briefly, the HPLC analysis was performed with a Phenomenex Luna 5 µm Phenyl-Hexyl 100 Å column (150×4.6 mm) as stationary phase and a mixture of

ChemMedChem
Research Article
doi.org/10.1002/cmdc.202200262
Chemistry Europe
European Chemical Societies Publishing

methanol (75%) and 10 mM Tris/HCl buffer (25%) at pH 7.4 as mobile phase (flow rate 1.0 mL/min). In the first step, the capacity factors of seven reference substances were determined from their retention times (acetophenone, benzene, ethyl benzoate, benzophenone, phenyl benzoate, diphenyl ether, bibenzyl) with uracil used as a dead-time marker. The reference substances were taken from a list of recommended standards included in the above-mentioned guideline and cover the required log$D_{7.4}$ range of 1.7–4.8. The logarithm of the capacity factors of the reference substances was then plotted against the corresponding log*P* values taken from the mentioned guideline to obtain a calibration function. For non-ionizable compounds like the reference substances used for calibration, log*P* values can be considered equivalent to the log$D_{7.4}$ values. To obtain a reference mixture, 2 mg of the reference substances were each dissolved in 1 mL of methanol, and 50 μL aliquots of each reference solution were subsequently combined. The reference mixture was measured before and after the substances to be tested, and the mean retention time from both measurements was used to calculate the calibration function. The calibration function was then used to determine the log$D_{7.4}$ values from the corresponding retention times for each substance to be tested. The compounds of interest were injected as a solution in methanol (2 mg/mL), and the retention time was determined as the mean value from two measurements.

Cyclic Voltammetry

The cyclic voltammetry measurements were carried out as described elsewhere.[24,33] Briefly, a 797 VA Computrace device from Metrohm was used with a three-electrode cell setup consisting of a glassy carbon working electrode, a platinum auxiliary electrode, and an Ag/AgCl reference electrode. To prepare the test solutions, 2 mg of each substance were suspended in 10 mL of a 0.1 M Tris-HCl buffer (pH 7.4) and dissolved under ultrasonic treatment. If a substance did not dissolve completely, the insoluble residues were separated. Before each measurement, the cell containing the test solution was flushed with nitrogen for 150 s. The cyclic voltammograms were recorded in a potential range from −0.5 to 1.0 V with 5 mV voltage steps and a sweep rate of 0.1 V/s. After each measurement, the glassy carbon working electrode was cleaned by using an aluminum oxide suspension and a polishing cloth.

Evaluation of K_V7.2/3 channel opening activity

The FLIPR Potassium Assay Kit (Molecular Devices, CA, USA) was used to determine the K_V7.2/3 channel opening activity of the test compounds in accordance with the manufacturer's instructions. The culturing of the HEK-293 cells transfected with KCNQ2/3 (SB Drug Discovery, Glasgow, UK) and the data processing were carried out as described in earlier work.[24,33] In short, 60,000 cells per well were seeded into black-walled 96-well plates with a clear bottom (4titude Vision Plates from Azenta Life Sciences). After incubation for 24 h, 100 μL of loading buffer containing 5 mM probenecid was added to obtain a total volume of 200 μL. Subsequently, the plates were incubated in the dark for 1 h at room temperature. A serial dilution of the test compounds in DMSO was prepared, added to the wells, and incubation was continued for 30 min. Control wells contained the loading buffer with a DMSO concentration corresponding to the substance samples (1% (v/v)). Fluorimetric measurements were conducted at extinction/emission wavelengths of 485 nm and 535 nm, respectively, with an Infinite F200 Pro plate reader (Tecan). The background fluorescence (baseline) was measured for 20 s. Subsequently, a stimulus buffer (25 mM K^+, 15 mM Tl^+) was added to each well, and the fluorescence intensity was recorded for 2.5 min. The measured fluorescence intensity changes were normalized by dividing with the average baseline signal (F/F_0) at each time point of signal acquisition. A correction was then performed by determining the difference between the normalized control signal and the normalized baseline signal (average value of 1) and subtracting the result from the F/F_0 value at each time point at a given concentration (corr. $\triangle F/F_0$). To obtain a dose-response curve, the maximal corr. $\Delta F/F_0$ values were plotted against the logarithmic compound concentration. The EC_{50} value for each compound was calculated as a relative value with GraphPad Prism 6 (La Jolla, CA, USA) by determining the inflexion point of the sigmoidal curve. The corresponding E_{max} value indicated the intrinsic activity of a compound and was determined relative to flupirtine by defining the maximum corr. $\Delta F/F_0$ value of flupirtine as 100%. The EC_{50} and E_{max} values are the means of at least three independent experiments ± standard deviation (SD).

Hepatic Cell Viability Assay

The cell culture of the TAMH and HEP–G2 cells and the MTT assay used to evaluate the cell viability were performed as previously described in detail.[24,33] Briefly, for the TAMH mouse liver cell line, 20,000 cells/well grown in serum-free DMEM/F12 medium supplemented with 5% PANEXIN NTA, 10 mM nicotinamide and 10 μg/mL gentamicin sulfate were seeded into 96 well plates. In the case of the HEP–G2 human hepatoma cell line, 15,000 cells/well grown in RPMI 1640 (PAN Biotech), supplemented with 10% heat-inactivated fetal bovine serum and 1% penicillin/streptomycin, were seeded into 96-well plates. For both cell lines, the following incubation was carried out at 37 °C in 5% CO_2 atmosphere for 24 h. Solutions of test compounds in DMSO were serially diluted into the corresponding culture medium to obtain 5–9 compound concentrations with 1% DMSO (v/v). The resulting serial dilutions were used to replace the medium in the wells. Additional wells were used for control and contained the same number of cells and 1% (v/v) DMSO without test compounds. To determine the background optical density (OD), wells without cells were used, which were treated analogously to the control wells. After 24 h of incubation, the respective medium was removed and fresh medium supplemented with 10% (v/v) of a 2.5 mg/mL solution of 3-(4,5-dimethylthiazol-2-yl)-2,5-diphenyltetrazolium bromide (MTT) was added. After an additional 4 h of incubation, the culture medium in each well was carefully replaced with 50 μL of DMSO to dissolve the formazan crystals. Subsequently, ODs were measured at 570 nm using a SpectraMax 190 microplate reader. To determine the cell viability, the ODs of the test compound (T) and control (C) wells were corrected by subtracting the bank value. The calculated $T/C_{corr.}$-ratios were then plotted against the logarithmic compound concentration. The data analysis was performed by using GraphPad Prism 6. After interpolation of a sigmoidal standard curve the LD_{50} and LD_{25} values represented the concentrations that reduced cell viability to 50 or 75%, respectively. If no reduction of cell viability to 75% was observed at the highest possible concentration, the LD_{25} was reported as higher than the highest tested concentration. The determined LD_{50} and LD_{25} values are the means of at least three independent experiments ± standard deviation (SD).

Molecular docking

The heterotetrameric structure of the K_V7.2/3 potassium channel was taken from an in-house library and is published elsewhere.[43] In brief, the prepared structure of the homotetrameric K_V7.2 potassium channel with retigabine (PDB 7CR2) was used as a template for an energy-based homology modelling within the Multiple Sequence Viewer in Maestro (Schrödinger, LLC, NY, USA).[39] All compounds were prepared by the Ligand Preparation tool and

ChemMedChem
Research Article
doi.org/10.1002/cmdc.202200262
Chemistry Europe
European Chemical Societies Publishing

docked with Glide (version 94137) by using an induced fit approach (standard sampling protocol, 20 protein conformations per ligand).[56] The bounding box was placed onto the bound retigabine ligand structure, and an implicit membrane was applied to the transmembrane region. Finally, all ligand poses were visually compared and analyzed.

T-REMD simulations

The 3D structures of 1,2-diphenylethane and *N*-benzylaniline were generated from their corresponding 2D structures and solvated in a cubic box of octan-1-ol with an edge length of 3.5 nm. OPLS4 force field parameters were assigned,[57] and all simulations were performed with Desmond (version 6.9.137 with GPU support).[58] Both systems were minimized for 100 ps and equilibrated by using a standard relaxation protocol provided by Schrodinger, followed by 5 ns of NPT simulation at a temperature of 300 K, 1 atm pressure and a timestep of 2 ps. Temperature and pressure in all simulations were maintained by a Langevin thermostat and barostat, respectively. Short-range van der Waals and electrostatic interaction cutoffs were set to 1 nm, including a 0.1 nm switching function. The temperature replica exchange simulations (T-REMD) were started from the last frame of the previous equilibration simulation and performed in an NVT ensemble for 50 ns.[59] In total, eight replica were distributed on a temperature range (evenly spaced log scale) between 300 and 330 K. Exchange attempts were performed every 500 fs and snapshots were saved every 5 ps. The baseline trajectory (10.000 structures) was analyzed with custom scripts using the Schrodinger Python API to calculate ring angles and distances.

Acknowledgements

KWW and FMB are funded by grants DFG LI 765/7-2 and DFG BE 1287/6-2 awarded to AL and PJB by the Deutsche Forschungsgemeinschaft (DFG - German Research Foundation). We thank Ms. Anne Schüttler and Ms. Maria Hühr for excellent technical assistance. Open Access funding enabled and organized by Projekt DEAL.

Conflict of Interest

The authors declare no conflict of interest.

Data Availability Statement

The data that support the findings of this study are available in the supplementary material of this article.

Keywords: drug design · flupirtine · ion channels · K_V7 · retigabine

[1] a) F. Miceli, M. R. Cilio, M. Taglialatela, F. Bezanilla, *Channels* **2009**, *3*, 277; b) A. Battefeld, B. T. Tran, J. Gavrilis, E. C. Cooper, M. H. P. Kole, *J. Neurosci.* **2014**, *34*, 3719.
[2] a) J. Robbins, *Pharmacol. Ther.* **2001**, *90*, 1; b) H. Wulff, N. A. Castle, L. A. Pardo, *Nat. Rev. Drug Discovery* **2009**, *8*, 982.
[3] a) D. A. Brown, G. M. Passmore, *Br. J. Pharmacol.* **2009**, *156*, 1185; b) J. Cuevas, A. A. Harper, C. Trequattrini, D. J. Adams, *J. Neurophysiol.* **1997**, *78*, 1890; c) O. Zaika, L. S. Lara, N. Gamper, D. W. Hilgemann, D. B. Jaffe, M. S. Shapiro, *J. Physiol.* **2006**, *575*, 49.
[4] A. Nissenkorn, P. Kornilov, A. Peretz, L. Blumkin, G. Heimer, B. Ben-Zeev, B. Attali, *Epileptic Disord.* **2021**, *23*, 695.
[5] a) L. Djouhri, M. I. Malki, A. Zeidan, K. Nagi, T. Smith, *J. Drug Targeting* **2019**, *27*, 1118; b) F. Zhang, S. Liu, L. Jin, L. Tang, X. Zhao, T. Yang, Y. Wang, B. Huo, R. Liu, H. Li, *Pharmacology* **2020**, 1.
[6] S. Costi, M.-H. Han, J. W. Murrough, *CNS Drugs* **2022**, *36*, 207.
[7] J. Kornhuber, M. Maler, J. Wiltfang, S. Bleich, D. Degner, E. Rüther, *Fortschr. Neurol. Psychiatr.* **1999**, *67*, 466.
[8] a) M. C. Michel, P. Radziszewski, C. Falconer, D. Marschall-Kehrel, K. Blot, *Br. J. Clin. Pharmacol.* **2012**, *73*, 821; b) V. K. Naguri, R. B. Komaram, T. V. Sagar, *Asian J. Pharm. Clin. Res.* **2019**, *84*.
[9] F. Puls, C. Agne, F. Klein, M. Koch, K. Rifai, M. P. Manns, J. Borlak, H. H. Kreipe, *Virchows Arch.* **2011**, *458*, 709.
[10] a) "Assessment report for flupirtine containing medicinal products", can be found under https://www.ema.europa.eu/en/documents/referral/flupirtine-containing-medicines-article-107i-procedure-prac-assessment-report en.pdf, **2013**; b) "Withdrawal of pain medicine flupirtine endorsed: serious liver problems continued to be reported despite previous restrictions", can be found under https://www.ema.europa.eu/en/documents/press-release/withdrawal-pain-medicine-flupirtine-endorsed en.pdf, **2018**.
[11] D. Rudin, J. Spoendlin, A. L. Cismaru, E. Liakoni, N. Bonadies, U. Amstutz, C. R. Meier, S. Krähenbühl, M. Haschke, *Eur. J. Intern. Med.* **2019**, *68*, 36.
[12] M. A. Ciliberto, J. L. Weisenberg, M. Wong, *Drug, Healthc. Patient Saf.* **2012**, *4*, 81.
[13] a) S. Clark, A. Antell, K. Kaufman, *Ther. Adv. Drug Saf.* **2015**, *6*, 15; b) T. Garin Shkolnik, H. Feuerman, E. Didkovsky, I. Kaplan, R. Bergman, L. Pavlovsky, E. Hodak, *JAMA Dermatol.* **2014**, *150*, 984.
[14] "FDA Drug Safety Communication: Anti-seizure drug Potiga (ezogabine) linked to retinal abnormalities and blue skin discoloration", can be found under http://wayback.archive-it.org/7993/20170112031636/http://www.fda.gov/Drugs/DrugSafety/ucm349538.htm, **2013**.
[15] a) N. Brickel, K. Hewett, K. Rayner, S. McDonald, J. De'Ath, J. Daniluk, K. Joshi, M. C. Boll, S. Tiamkao, O. Vorobyeva, J. Cooper, *Epilepsy Behav.* **2020**, *102*, 106580; b) "FDA Drug Safety Communication: FDA determines 2013 labeling adequate to manage risk of retinal abnormalities, potential vision loss, and skin discoloration with anti-seizure drug Potiga (ezogabine); requires additional study", can be found under http://wayback.archive-it.org/7993/20170112031551/http://www.fda.gov/Drugs/DrugSafety/ucm451166.htm, **2015**.
[16] K. Methling, P. Reszka, M. Lalk, O. Vrana, E. Scheuch, W. Siegmund, B. Terhaag, P. J. Bednarski, *Drug Metab. Dispos.* **2009**, *37*, 479.
[17] E. Scheuch, K. Methling, P. J. Bednarski, S. Oswald, W. Siegmund, *J. Pharm. Biomed. Anal.* **2015**, *102*, 377.
[18] W. Siegmund, C. Modess, E. Scheuch, K. Methling, M. Keiser, A. Nassif, D. Rosskopf, P. J. Bednarski, J. Borlak, B. Terhaag, *Br. J. Clin. Pharmacol.* **2015**, *79*, 501.
[19] I. Klopčič, M. S. Dolenc, *Chem. Res. Toxicol.* **2019**, *32*, 1.
[20] P. Nicoletti, A. N. Werk, A. Sawle, Y. Shen, T. J. Urban, S. A. Coulthard, E. S. Bjornsson, I. Cascorbi, A. Floratos, T. Stammschulte, U. Gundert-Remy, M. R. Nelson, G. P. Aithal, A. K. Daly, *Pharmacogenet. Genomics* **2016**, *26*, 218.
[21] R. J. Andrade, N. Chalasani, E. S. Björnsson, A. Suzuki, G. A. Kullak-Ublick, P. B. Watkins, H. Devarbhavi, M. Merz, M. I. Lucena, N. Kaplowitz, G. P. Aithal, *Nat. Rev. Dis. Primers* **2019**, *5*, 58.
[22] R. Hempel, H. Schupke, P. J. McNeilly, K. Heinecke, C. Kronbach, C. Grunwald, G. Zimmermann, C. Griesinger, J. Engel, T. Kronbach, *Drug Metab. Dispos.* **1999**, *27*, 613.
[23] M. R. Groseclose, S. Castellino, *Chem. Res. Toxicol.* **2019**, *32*, 294.
[24] A. S. Surur, C. Bock, K. Beirow, K. Wurm, L. Schulig, M. K. Kindermann, W. Siegmund, P. J. Bednarski, A. Link, *Org. Biomol. Chem.* **2019**, *17*, 4512.
[25] H. H. Bak-Jensen, K. P. Hertel (H. Lundbeck A/S), WO2009015667A1, **2009**.
[26] a) N. Khanzhin, M. Rottländer, A. Ritzen, W. P. Watson (H. Lundbeck A/S), WO2004082677, **2004**; b) F. Nan, M. Li, Z. Gao, Y. Zhang, H. Hu, H. Xu, H. Liu, X. Pi (Shanghai Institute of Materia Medica), WO2015165352A1, **2015**; c) C. W. Tornoe, M. Rottlaender, D. R. Greve, N. Khanzhin, A. Ritzen, W. P. Watson (H. Lundbeck A/S), WO2006029623A1, **2006**.
[27] Y.-M. Zhang, H.-Y. Xu, H.-N. Hu, F.-Y. Tian, F. Chen, H.-N. Liu, L. Zhan, X.-P. Pi, J. Liu, Z.-B. Gao, F.-J. Nan, *J. Med. Chem.* **2021**, *64*, 5816.

ChemMedChem
Research Article
doi.org/10.1002/cmdc.202200262
Chemistry Europe
European Chemical Societies Publishing

[28] D. R. Greve, M. Rottlaender, W. P. Watson (H. Lundbeck A/S), WO2004080950A1, **2004**.
[29] a) H. Chen, B. Liang, Z. Zhao, W. Cao, W. Xu, Q. Li, J. Wang, P. Zhang, Z. Jiang, G. Zhang, C. Gao, H. Gong, G. Zuo (Simcere Pharmaceutical Group Limited), WO2014048165A1, **2014**; b) B. Liang, G. Liu, H. Chen (Shanghai Zhimeng Pharmaceutical Tech Co Ltd), CN114057641 A, **2022**.
[30] N. Kinarivala, R. Patel, R.-M. Boustany, A. Al-Ahmad, P. C. Trippier, *J. Med. Chem.* **2017**, *60*, 9739.
[31] J. K. Seydel, K. J. Schaper, E. A. Coats, H. P. Cordes, P. Emig, J. Engel, B. Kutscher, E. E. Polymeropoulos, *J. Med. Chem.* **1994**, *37*, 3016.
[32] L. Wang, G.-H. Qiao, H.-N. Hu, Z.-B. Gao, F.-J. Nan, *ACS Med. Chem. Lett.* **2019**, *10*, 27.
[33] C. Bock, A. S. Surur, K. Beirow, M. K. Kindermann, L. Schulig, A. Bodtke, P. J. Bednarski, A. Link, *ChemMedChem* **2019**, *14*, 952.
[34] K. Konishi, T. Fukami, T. Ogiso, M. Nakajima, *Biochem. Pharmacol.* **2018**, *155*, 242.
[35] M. Grupe, B. H. Bentzen, T. Benned-Jensen, V. Nielsen, K. Frederiksen, H. S. Jensen, A.-M. Jacobsen, L. Skibsbye, A. G. Sams, M. Grunnet, M. Rottländer, J. F. Bastlund, *Eur. J. Pharmacol.* **2020**, *887*, 173440.
[36] a) A. Daina, O. Michielin, V. Zoete, *Sci. Rep.* **2017**, *7*, 42717; b) J. S. Delaney, *J. Chem. Inf. Comput. Sci.* **2004**, *44*, 1000.
[37] T. T. Talele, *J. Med. Chem.* **2016**, *59*, 8712.
[38] S. Yang, D. Lu, P. Ouyang, *Bioorg. Med. Chem. Lett.* **2018**, *28*, 3004.
[39] X. Li, Q. Zhang, P. Guo, J. Fu, L. Mei, D. Lv, J. Wang, D. Lai, S. Ye, H. Yang, J. Guo, *Cell Res.* **2021**, *31*, 52.
[40] J. Harada, K. Ogawa, *Struct. Chem.* **2001**, *12*, 243.
[41] R. Betz, C. McCleland, H. Marchand, *Acta Crystallogr. Sect. E* **2011**, *67*, 1195.
[42] M. Jagodzinska, F. Huguenot, G. Candiani, M. Zanda, *ChemMedChem* **2009**, *4*, 49.
[43] K. W. Wurm, F.-M. Bartz, L. Schulig, A. Bodtke, P. J. Bednarski, A. Link, *ACS Omega* **2022**, *7*, 7989.
[44] A. D. Roth, M.-Y. Lee, *BioMed Res. Int.* **2017**, *2017*, 9176937.
[45] a) J. G. Kenna, J. Uetrecht, *Drug Metab. Dispos.* **2018**, *46*, 1658; b) A. A. Elzagallaai, M. J. Rieder, *Br. J. Clin. Pharmacol.* **2015**, *80*, 889.
[46] a) M. Davis, B. D. Stamper, *BioMed Res. Int.* **2016**, *2016*, 4780872; b) T. Ramirez, A. Strigun, A. Verlohner, H.-A. Huener, E. Peter, M. Herold, N. Bordag, W. Mellert, T. Walk, M. Spitzer, X. Jiang, S. Sperber, T. Hofmann, T. Hartung, H. Kamp, B. van Ravenzwaay, *Arch. Toxicol.* **2018**, *92*, 893.
[47] T. Mosmann, *J. Immunol. Methods* **1983**, *65*, 55.
[48] Z. Weng, K. Wang, H. Li, Q. Shi, *Oncotarget* **2015**, *6*, 17031.
[49] A. F. Stepan, D. P. Walker, J. Bauman, D. A. Price, T. A. Baillie, A. S. Kalgutkar, M. D. Aleo, *Chem. Res. Toxicol.* **2011**, *24*, 1345.
[50] L. Howells, M. Godfrey, M. J. Sauer, *Analyst* **1994**, *119*, 2691.
[51] a) K. G. Madsen, J. Olsen, C. Skonberg, S. H. Hansen, U. Jurva, *Chem. Res. Toxicol.* **2007**, *20*, 821; b) K. G. Madsen, C. Skonberg, U. Jurva, C. Cornett, S. H. Hansen, T. N. Johansen, J. Olsen, *Chem. Res. Toxicol.* **2008**, *21*, 1107.
[52] L. Rodríguez-Cid, S. Sentellas, J. Saurina, *Anal. Bioanal. Chem.* **2018**, *410*, 2229.
[53] C. J. Lemmerhirt, M. Rombach, A. Bodtke, P. J. Bednarski, A. Link, *ChemMedChem* **2015**, *10*, 368.
[54] T. B. Hughes, S. J. Swamidass, *Chem. Res. Toxicol.* **2017**, *30*, 642.
[55] M. Gunduz, U. A. Argikar, A. Kamel, K. Colizza, J. L. Bushee, A. Cirello, F. Lombardo, S. Harriman, *Drug Metab. Dispos.* **2012**, *40*, 2074.
[56] R. A. Friesner, R. B. Murphy, M. P. Repasky, L. L. Frye, J. R. Greenwood, T. A. Halgren, P. C. Sanschagrin, D. T. Mainz, *J. Med. Chem.* **2006**, *49*, 6177.
[57] C. Lu, C. Wu, D. Ghoreishi, W. Chen, L. Wang, W. Damm, G. A. Ross, M. K. Dahlgren, E. Russell, C. D. von Bargen, R. Abel, R. A. Friesner, E. D. Harder, *J. Chem. Theory Comput.* **2021**, *17*, 4291.
[58] K. J. Bowers, E. Chow, H. Xu, R. O. Dror, M. P. Eastwood, B. A. Gregersen, J. L. Klepeis, I. Kolossvary, M. A. Moraes, F. D. Sacerdoti, J. K. Salmon, Y. Shan, D. E. Shaw, in *SC '06: Proceedings of the 2006 ACM/IEEE conference on Supercomputing* (Ed.: B. Horner-Miller), ACM Press, New York, USA, **2006**, 84-es.
[59] R. Qi, G. Wei, B. Ma, R. Nussinov, *Methods Mol. Biol.* **2018**, *1777*, 101.

Manuscript received: May 11, 2022
Revised manuscript received: June 7, 2022
Accepted manuscript online: June 10, 2022
Version of record online: July 7, 2022

7.2 Publikation II

Modifications of the Triaminoaryl Metabophore of Flupirtine and Retigabine Aimed at Avoiding Quinone Diimine Formation

Konrad W. Wurm, Frieda-Marie Bartz, Lukas Schulig, Anja Bodtke, Patrick J. Bednarski, Andreas Link

ACS Omega **2022**, *7*, 7989–8012.
DOI: 10.1021/acsomega.1c07103

Beiträge der Autoren

Konrad W. Wurm	Planung und Durchführung der Synthesen Analytische Charakterisierung Erstellen des Manuskripts
Frieda-Marie Bartz	Biologische Testung
Lukas Schulig	Durchführung von Modelling und Moleküldynamiksimulationen
Anja Bodtke	Durchführung der HRMS- und NMR-Messungen
Patrick J. Bednarski	Korrektur des Manuskripts
Andreas Link	Anleitung bei der Bearbeitung des Projekts Erstellen des Manuskripts

_____ _____

Konrad Wurm Andreas Link

ACS OMEGA

http://pubs.acs.org/journal/acsodf

Article

Modifications of the Triaminoaryl Metabophore of Flupirtine and Retigabine Aimed at Avoiding Quinone Diimine Formation

Konrad W. Wurm, Frieda-Marie Bartz, Lukas Schulig, Anja Bodtke, Patrick J. Bednarski, and Andreas Link*

Cite This: *ACS Omega* 2022, 7, 7989−8012

Read Online

ACCESS | Metrics & More | Article Recommendations | Supporting Information

ABSTRACT: The potassium channel opening drugs flupirtine and retigabine have been withdrawn from the market due to occasional drug-induced liver injury (DILI) and tissue discoloration, respectively. While the mechanism underlying DILI after prolonged flupirtine use is not entirely understood, evidence indicates that both drugs are metabolized in an initial step to reactive *ortho*- and/or *para*-azaquinone diimines or *ortho*- and/or *para*-quinone diimines, respectively. Aiming to develop safer alternatives for the treatment of pain and epilepsy, we have attempted to separate activity from toxicity by employing a drug design strategy of avoiding the detrimental oxidation of the central aromatic ring by shifting oxidation toward the formation of benign metabolites. In the present investigation, an alternative retrometabolic design strategy was followed. The nitrogen atom, which could be involved in the formation of both *ortho*- or *para*-quinone diimines of the lead structures, was shifted away from the central ring, yielding a substitution pattern with nitrogen substituents in the meta position only. Evaluation of $K_V7.2/3$ opening activity of the 11 new specially designed derivatives revealed surprisingly steep structure−activity relationship data with inactive compounds and an activity cliff that led to the identification of an apparent "magic methyl" effect in the case of *N*-(4-fluorobenzyl)-6-[(4-fluorobenzyl)amino]-2-methoxy-4-methylnicotinamide. This flupirtine analogue showed potent $K_V7.2/3$ opening activity, being six times as active as flupirtine itself, and by design is devoid of the potential for azaquinone diimine formation.

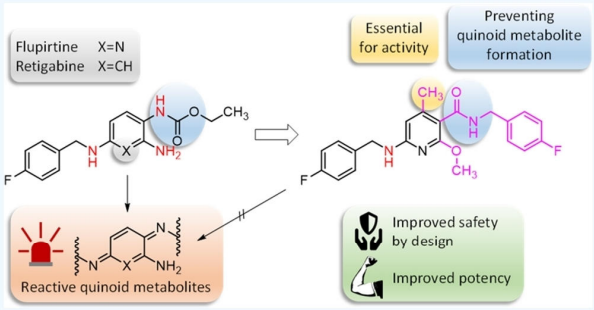

INTRODUCTION

Reactive drug metabolites are well-known causes of drug-induced liver injury (DILI) and other adverse drug reactions and are thus an important determinant of drug toxicity and failure.[1,2] Of 68 drugs that were retroactively recalled due to idiosyncratic toxicity or addressed in boxed warnings by the Food and Drug Administration, an association with the formation of reactive metabolites was found in 62−69% of the cases.[3] Two current examples that reflect this problem are the K_V7 channel openers flupirtine (**1**) and retigabine (**2**, USAN: ezogabine). The structural closely related compounds with a triaminoaryl scaffold are oxidized to reactive quinone diimine or azaquinone diimine metabolites (**5**) under different conditions and with different consequences (Figure 1).

In the case of flupirtine, oxidation is mainly catalyzed enzymatically and leads to rare but severe hepatotoxic reactions.[4−6] The pathomechanism underlying the toxicity of flupirtine has not been fully clarified. An in vitro assay showed the formation of glutathione conjugates after enzymatic oxidation by peroxidases,[5] and in a clinical study, mercapturic acid derivatives were detected in the urine of healthy human subjects treated with flupirtine,[7] both of which are indicators for the formation of reactive azaquinone diimine metabolites (**5**). After covalent binding to endogenous macromolecules, reactive metabolites such as azaquinone diimines can either directly cause cellular damage or form haptens (**6**) that are able to trigger toxic autoimmune responses.[8] The rarity of the hepatotoxic reactions under flupirtine treatment as well as the lack of a clear dose dependency rather suggests the hapten hypothesis and the involvement of the adaptive immune system. This assumption is backed by histological findings and the identification of a certain human leukocyte antigen gene as a genetic risk factor for flupirtine-induced hepatotoxicity.[9,10] The hypothesis that pharmacogenetic causes, such as polymorphisms of metabolizing enzymes, contribute to flupirtine-induced hepatotoxicity could not be confirmed in a clinical study.[7]

In contrast, the oxidation of retigabine does not take place hepatically but probably in a reaction catalyzed by or in

Received: December 16, 2021
Accepted: February 8, 2022
Published: February 25, 2022

https://doi.org/10.1021/acsomega.1c07103
ACS Omega 2022, 7, 7989−8012

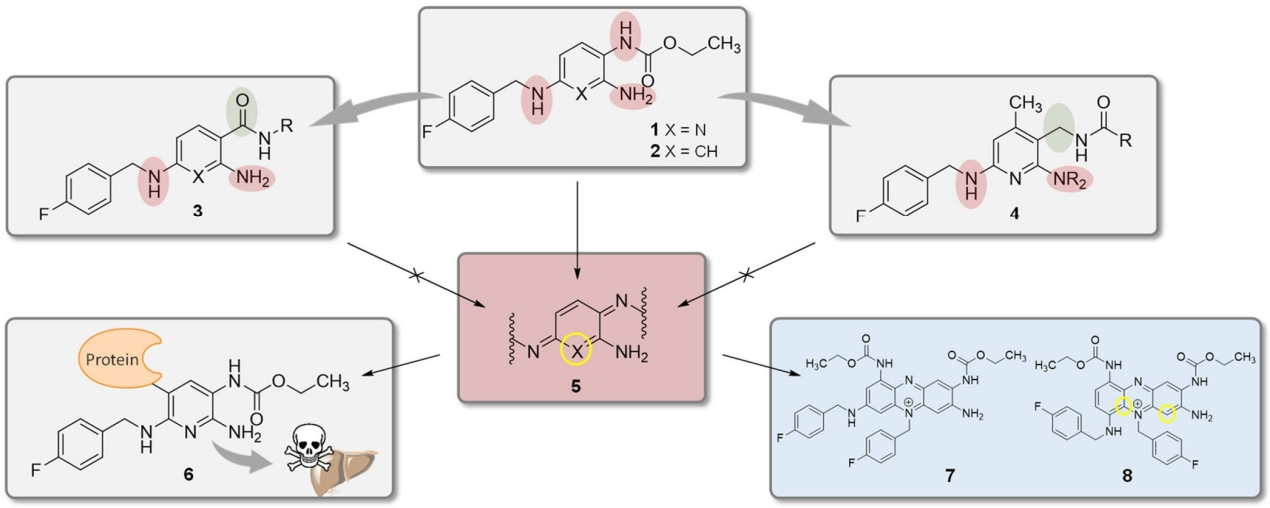

Figure 1. Structures of flupirtine (**1**) and retigabine (**2**), their proposed toxification pathway to phenazinium salts (**7**, **8**), and hapten-protein adducts **6** via quinone diimines **5**, and selected structural modifications carried out in this work (type **3** and **4**).

association with melanin.[11,12] Via quinone diimines as intermediates, retigabine can dimerize to phenazinium structures (**7**, **8**), which are suspected of causing blue discoloration of various tissues.[12,13] For these retigabine dimers, Groseclose et al. postulate compound **7** as a possible structure based on high-resolution and high-accuracy mass spectrometry data. In our opinion, however, isomer **8** is more likely to be formed because the formation of this structure is not associated with a carbamate migration to the free primary amino group. Flupirtine dimers are also known in the literature, but their structure is clearly different. Essentially, the structure of these dimers can be described as a flupirtine molecule linked to the pyridine ring of another flupirtine molecule via its amino group.[5] Cyclization and oxidation to a phenazinium-like structure comparable to **8** were not observed. A hypothetical flupirtine analogue of dimer **8** would contain the two former pyridine nitrogen atoms at the positions highlighted with yellow circles in Figure 1, which would result in a highly unlikely direct connection of the positively charged phenazinium nitrogen atom with another positively charged nitrogen atom. Furthermore, in contrast to retigabine, there is no evidence that the reported dimers of flupirtine are responsible for the reported adverse drug reaction. In Summary, the blue tissue discoloration caused by retigabine as well as the hepatotoxicity of flupirtine finally led to the withdrawal of the respective drugs from the market, which is regrettable since their mechanism of action is unique, meaning that the proven therapeutical potential of K_V7 channel openers is currently underexploited.[14,15]

K_V7 channels (also referred to as KCNQ channels) are voltage-dependent homo- or heterotetrameric potassium channels distributed in both the central and peripheral nervous systems.[16−18] Their activation is accompanied by a potassium efflux, as a result of which the membrane potential of neurons is hyperpolarized, leading to reduced transmission of action potentials.[19] The important role of K_V7 channels in controlling neuronal excitability makes them validated targets in the treatment of pain and epilepsy.[20] As a consequence, the failure of the two existing K_V7 channel openers flupirtine and retigabine, which were in therapeutic use in humans, left a treatment gap that has not yet been filled. Flupirtine was a valuable alternative to non-steroidal anti-inflammatory drugs and weak opioids because it caused neither gastrointestinal bleeding nor adverse effects such as addiction, constipation, or respiratory depression, notoriously associated with opioids.[21] Retigabine has been shown to be effective for the adjunctive treatment of partial-onset seizures, and no adequate replacement for retigabine is available, especially in epilepsy forms where pathogenesis is based on a mutation of the K_V7 channels.[22,23] In addition to these approved indications, K_V7 channel openers are supposed to have therapeutic potential in other medical areas, such as amyotrophic lateral sclerosis, traumatic brain injuries, or depression.[24−26]

Because the adverse drug reactions caused by flupirtine and retigabine are not related to the mechanism of action, it appeared promising to investigate chemical modifications of these clinically validated, drug-like leads in a retrometabolic drug design approach. In previous work, sulfide analogues (Figure 2A) were synthesized for this purpose in order to redirect the oxidation by shifting the highest occupied molecular orbital from the central aromatic ring to the sulfide substituent and thus avoiding the formation of quinone diimine metabolites.[27] In the present study, we follow the alternative approach of changing the substitution pattern of the central aromatic ring in such a way that there are no longer two nitrogen atoms in the ortho or para position, removing the possibility for unwanted oxidative formation of quinone diimines. This is an advantage over the recently reported clinical candidate HN37 (Figure 2C), where the para-substitution pattern is identical to the lead structure **2**, and thus, the formation of charged *para*-quinone diimines is not fully excluded, per se.[28] Since amide derivatives have proven to be very active in our previous work (Figure 2B), inverted amide derivatives were synthesized in which the carbonyl carbon atom is directly attached to an optionally methylated, central aromatic ring instead of the nitrogen atom (**3**, Figure 1).[27,29] Another approach was the insertion of a methylene spacer to separate the carbamate/amide nitrogen atom from the central pyridine ring (**4**, Figure 1). A small set of substances was synthesized for both strategies in order to verify whether the applied retrometabolic drug design approach can lead to active K_V7 channel openers.

https://doi.org/10.1021/acsomega.1c07103
ACS Omega 2022, 7, 7989−8012

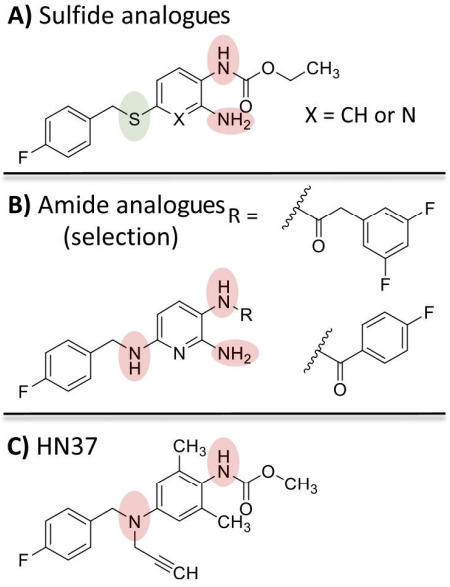

Figure 2. (A) Sulfide analogues of flupirtine (**1**) and retigabine (**2**) synthesized in a previous work.[27] (B) Selection of amide analogues (not inverted) synthesized in a recent structure−activity relationship (SAR) study.[29] (C) HN37, a drug candidate under clinical trial in China.[28]

RESULTS AND DISCUSSION

Analogue design and synthesis. As mentioned above, in the case of the inverted amide scaffold (**3**), the formation of azaquinone diimines is not possible due to the meta position of the remaining amino substituents. In order to verify this hypothesis and exclude a risk for the formation of other quinoid metabolite species, the compounds were evaluated with XenoSite. XenoSite is a deep learning approach to predict the formation of quinone species in the drug metabolism, which considers both one- and two-step quinone formation and enables accurate quinone formation predictions in non-obvious cases. It is able to predict atom pairs that form quinones with an area under the curve (AUC) accuracy of 97.6% and identify molecules that form quinones with 88.2% AUC.[30] A visualization of the results of compound **36b** as a representative example for this substance class is contained in Table 1, which underlines that in contrast to flupirtine and retigabine, no risk for the formation of quinoid metabolites is to be feared for the inverted amide scaffold.

When initially designing the inverted amide analogues, only the amide side chain was varied in order to keep as closely as possible to the structure of flupirtine and retigabine. For the design of the side chains, we partly used findings from an earlier SAR study that examined, inter alia, non-inverted amide derivatives of flupirtine and retigabine.[29] Both aliphatic and aromatic side chains were evaluated in the present work. Mainly a fluorobenzyl substituent was used as an aromatic amide side chain since similar residues proved successful in the previous work mentioned above (Figure 2B). Aliphatic side chains, such as a butyramide residue, in particular, have also proven to be active in the case of the non-inverted amide derivatives. The *N*-propylamide and *N*-butylamide side chains used in the following are meant to be analogues of the butyramide side chain of the non-inverted amide derivatives

Table 1. XenoSite-Predicted Probabilities for the Formation of Quinoid Metabolites of Flupirtine (1), Retigabine (2), a Representative Inverted Amide Analogue (36b), and a Representative Methylene Spacer Analogue (66)

Entry	Atom quinone formation scores	Pair quinone formation scores	Scale
Flupirtine (**1**)	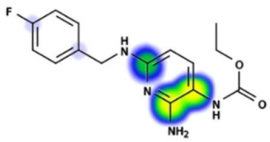	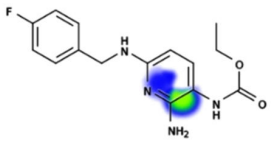	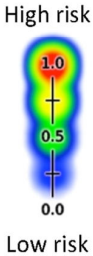
Retigabine (**2**)		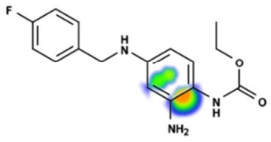	
Inverted amide analogues (**36b**)	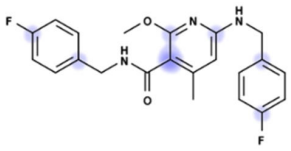	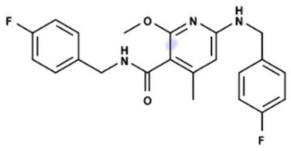	
Methylene spacer analogues (**66**)	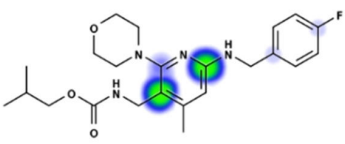	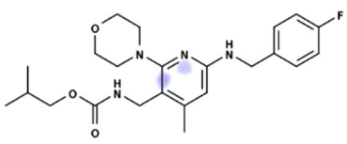	

https://doi.org/10.1021/acsomega.1c07103
ACS Omega 2022, 7, 7989−8012

Scheme 1. Synthesis of Compound 17 as a Representative of Target Modification Type 3[a]

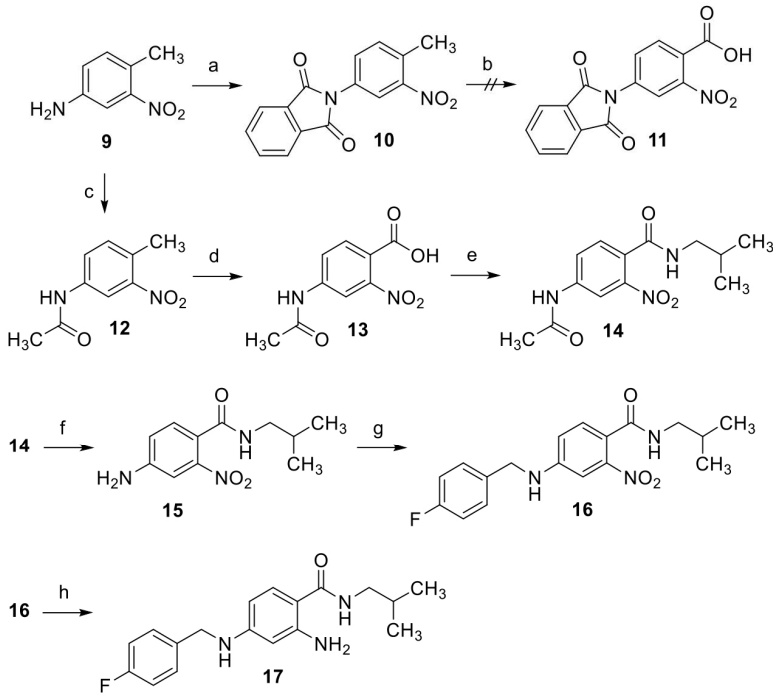

[a](a) Phthalic anhydride, TEA, toluene, 120 °C, 4 h, 82%; (b) $KMnO_4$, H_2O, 80 °C; (c) acetic anhydride, AcOH, RT, 15 min, 87%; (d) $KMnO_4$, H_2O, 80 °C, 5 h, 52%; (e) isobutylamine, CDI, THF, RT, 17 h, 74%; (f) HCl, H_2O, 100 °C, 2 h, 96%, (g) (1) 4-fluorobenzaldehyde, toluene, 120 °C, 5 h (2) $NaBH_4$, 1,4-dioxane, MeOH, RT, 1.5 h, 37%; (h) $SnCl_2$, EtOAc, 80 °C, 30 min, 68%.

and were of interest because they more closely resemble the ethyl carbamate structure of flupirtine and retigabine compared to the aromatic substituents. In addition, a branched 2-methylpropyl side chain was also used since findings from the non-inverted amide analogues suggest that bulkier substituents in the amide region lead to improved activity.

A retigabine derivative with a 2-methylpropyl amide side chain (**17**) was realized in a six-step synthesis (Scheme 1). The starting material was the commercially available compound **9**, whose amino group was protected in the first step. Both inclusion of the amino function into a phthalimido group and acetylation were evaluated as possible protecting strategies in **10** and **12**, respectively. However, only the acetamido group proved to be functional since the phthalimido group was not stable in the subsequent $KMnO_4$ oxidation to carboxylic acid **13**. After the oxidation step, the amide coupling was carried out by using 1,1′-carbonyldiimidazole (CDI) as a coupling reagent. The acetylamino group of the resulting benzamide **14** was then deacetylated by acidic hydrolysis of the acetanilide function, yielding **15**. This was followed by reductive amination to obtain compound **16**, and in the end, a reduction of the nitro group with $SnCl_2$ was carried out to give the target compound **17**.

An inverted amide analogue of flupirtine was obtained in a shorter, three-step synthesis (Scheme 2). 2,6-Dichloronicotinic acid (**18**) was the starting material in this route. In the first step of the synthesis, the primary amino group was introduced regioselectively in position 2. This was achieved in a copper-catalyzed, Ullmann-type reaction with sodium azide as a nitrogen source. In accordance with the mechanism proposed in the literature, the reaction is assumed to proceed via a five-membered, cyclic transition state formed after oxidative addition, which involves the carboxyl group as well as the copper ion and explains the observed regioselectivity. An aryl azide, formed as an intermediate after reductive elimination, was reduced directly in situ to the corresponding primary amine **19**.[31] It is also possible to introduce the amino group through a simple nucleophilic substitution with ammonia. However, this variant turned out to be inferior to the copper-catalyzed reaction since it was not as regioselective. This made a chromatographic separation of the regioisomers necessary and resulted in a significantly lower yield of only 57% compared to 87% for the copper-catalyzed reaction. In the next step, the amide coupling was carried out as described for the synthesis of retigabine derivative **17** with CDI as the coupling reagent, yielding **20**. The final nucleophilic substitution reaction to introduce the 4-fluorobenzylamino residue gave compound **21** but unfortunately in a poor yield of 16%; 4-

Scheme 2. Synthesis of Compound 21 as a Representative of Target Modification Type 3[a]

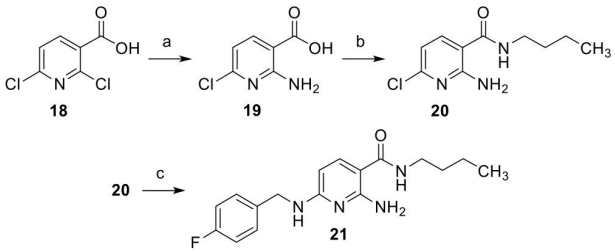

[a](a) NaN_3, CuI, ethylenediamine, K_2CO_3, EtOH, 95 °C, 11.5 h, 87%; (b) *n*-butylamine, CDI, DCM, RT, 48 h, 55%; (c) 4-fluorobenzylamine, 160 °C, 3 h, 16%.

https://doi.org/10.1021/acsomega.1c07103
ACS Omega 2022, 7, 7989−8012

fluorobenzylamine is only a moderate nucleophile and, moreover, presumably decomposes at the high temperature required for the reaction.

In addition to the synthesis of the two inverted amide derivatives with minimal structural changes in comparison to lead **1** and **2**, the next step was to introduce advantageous substructures inspired by derivatives of flupirtine and retigabine known from the literature. For example, the effect of an additional methyl group in the ortho position to the amide function was investigated, which is included in several potent K_V7 channel openers (not shown).[28,32] Furthermore, a replacement of the primary amino group by an alkoxy residue and the introduction of a fluorinated phenyl ring into the amide side chain proved to be advantageous for the $K_V7.2/3$ channel opening activity in our previous work.[29] Both structural changes were also applied to the inverted amide derivatives. However, the 4-fluorobenzylaminoaryl scaffold incorporated in flupirtine and retigabine was kept unchanged in all synthesized compounds.

As depicted in Scheme 3, the syntheses of two methoxy-substituted derivatives with an aliphatic or aromatic amide side

Scheme 3. Synthesis of Compounds 28a and b[a]

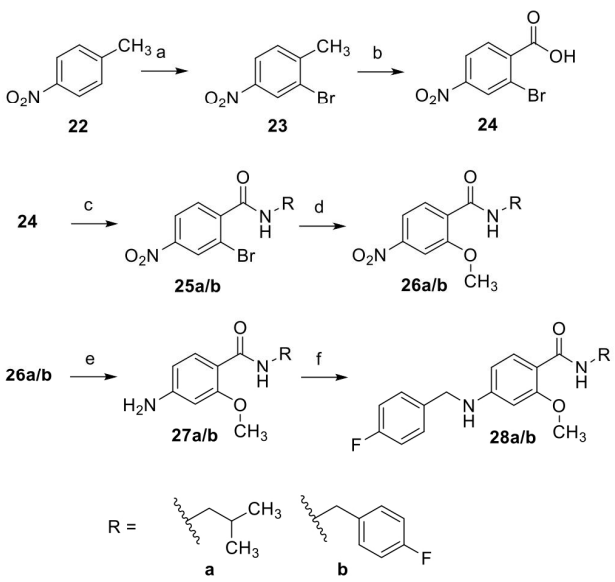

[a](a) Br_2, Fe, 80 °C, 1.5 h, 55%; (b) $KMnO_4$, H_2O, pyridine, 100 °C, 17 h, 18%; (c) (1) $SOCl_2$, toluene, 120 °C, 2.5−8 h, (2) isobutylamine or 4-fluorobenzylamine, (TEA), DCM, 0 °C to RT, 2.5−16 h, 42−72%; (d) MeOH, K_2CO_3, CuI, ethylenediamine, N_2, 95 °C, 15 h, 46−51%; (e) $SnCl_2$, EtOAc, 80 °C, 30 min, 98−100%; (f) (1) 4-fluorobenzaldehyde, toluene, 120 °C, 5−7 h, (2) $NaBH_4$, 1,4-dioxane, MeOH, RT, 17−24 h, 41−69%.

chain were conducted starting from 4-nitrotoluene (**22**). After regioselective bromination, the methyl group of **23** was oxidized to a carboxyl group with $KMnO_4$ as the oxidizing agent to obtain **24**. This was followed by the amide coupling in which the acyl chloride was formed in situ by reaction with thionyl chloride and subsequently reacted with the corresponding amines to give the desired amides **25a/b**. The methoxy function was introduced in a copper-catalyzed C−O cross-coupling reaction with methanol in a dual function as a solvent and reactant. Finally, the aromatic nitro compound **26a/b** was reduced to aniline **27a/b**, followed by reductive amination, which provided the target compounds **28a/b**.

An additional methyl group in the ortho position to the amide function could easily be introduced by the Guareschi reaction, in which acetoacetic ester reacts with cyanoacetamide in a condensation reaction to form a pyridine derivative. The resulting dihydroxypyridine **31** was subsequently chlorinated by treatment with phosphoryl chloride, yielding **32** (Scheme 4). Thereafter, the nitrile group was hydrolyzed to obtain carboxylic acid **33**. This worked best with a mixture of concentrated sulfuric acid and concentrated nitric acid. While such mixtures are known nitrating agents, nitration of the electron-poor pyridine ring was not to be expected here. The subsequent introduction of the methoxy group was achieved by nucleophilic substitution with sodium methoxide produced in situ by the reaction of sodium hydride with methanol. As described in the literature for similar cases, the substitution reaction proceeded regioselectively with the exclusive formation of product **34** substituted at position 2.[33] Yap et al. suggest that this regioselectivity could be explained by the formation of a six-membered, cyclic transition state involving the carboxyl group and the sodium methoxide, which favors position 2.[33] In the next step, the amide coupling was again carried out via an acyl chloride, which in contrast to the synthesis of **25a/b** was not generated with thionyl chloride but with oxalyl chloride. Finally, the 4-fluorobenzylamino residue was introduced as described for **21** by using microwave heating instead of conventional heating in order to obtain the final compounds **36a/b**. The low yields of 7−20% can be partly explained by ether cleavage, resulting in the formation of a byproduct identified as **37** in the case of the synthesis of **36b**.

An ethyl group was also evaluated as an alternative to the methoxy group; Scheme 5 shows the synthesis of a corresponding compound. The starting point was commercially available ester **38**. A reduction of the nitro group with $SnCl_2$ and subsequent reductive amination of **39** with $NaBH_4$ gave the 4-fluorobenzylamino-substituted compound **40**. After Boc protection of the amino group, the coupling of trimethylsilylacetylene was performed via a Sonogashira reaction to yield **42**. The trimethylsilyl protective group was then selectively cleaved with K_2CO_3 in order to subsequently reduce the resulting terminal alkyne by catalytic hydrogenation to obtain **44**. This was followed by hydrolysis of the methyl ester under alkaline conditions. The amide coupling, which gave **46**, was performed with a coupling reagent. Since the previously used methods for amide coupling via acyl chlorides or CDI resulted in yields that could be improved (42−72%), 1-[bis(dimethylamino)methylene]-1*H*-1,2,3-triazolo[4,5-*b*]-pyridinium 3-oxide hexafluorophosphate (HATU) was evaluated here as an alternative coupling reagent, which enabled a good yield of 78%. The use of CDI instead of HATU would, however, probably also have been possible. In the last step, the Boc protective group was cleaved with trifluoroacetic acid (TFA), and final product **47** was isolated by precipitation of the hydrochloride salt.

As illustrated in Figure 3, the second retrometabolic drug design approach was the introduction of a methylene spacer between the carbamate or amide nitrogen atom and the central aromatic ring in **50**. The analogues with a methylene spacer here differed to a greater extent from flupirtine and retigabine in terms of their substituents since two morpholino-substituted flupirtine derivatives with nanomolar EC_{50} values (**48**, **49**) synthesized in a previous work served as templates (Figure

https://doi.org/10.1021/acsomega.1c07103
ACS Omega 2022, 7, 7989−8012

Scheme 4. Synthesis of Compounds 36a and b[a]

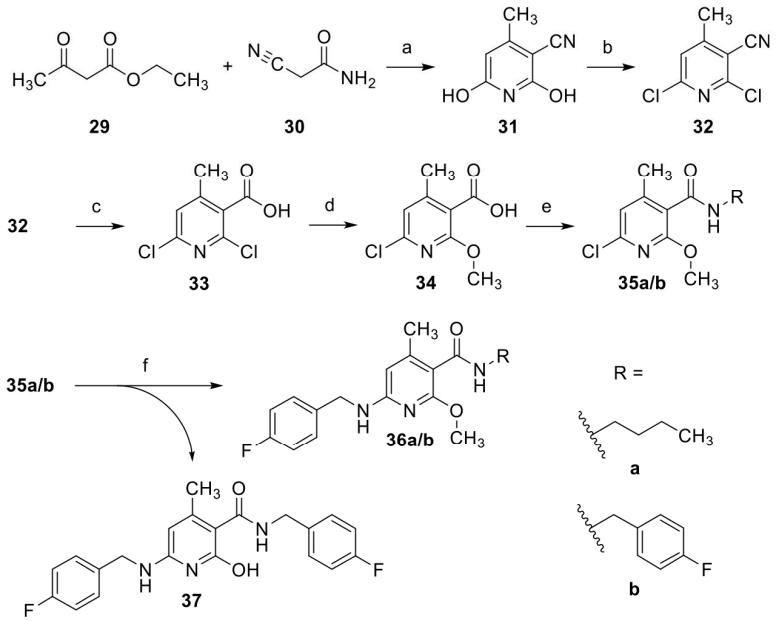

[a](a) KOH, MeOH, 65 °C, 2 h, 75%; (b) benzyltrimethylammonium chloride, $POCl_3$, 90 °C, 16 h, 55%; (c) H_2SO_4, HNO_3, 105 °C, 2 h, 77%; (d) MeOH, NaH, THF, 0−70 °C, 7 h, 96%; (e) (1) $(COCl)_2$, DMF, THF, 0 °C to RT, 2−3 h, (2) *n*-butylamine or 4-fluorobenzylamine, (TEA), DCM or THF, 0 °C to RT, 16 h, 53−61%; (f) 4-fluorobenzylamine, 165 °C, microwave, 1 h, 7−23%.

Scheme 5. Synthesis of Compound 47[a]

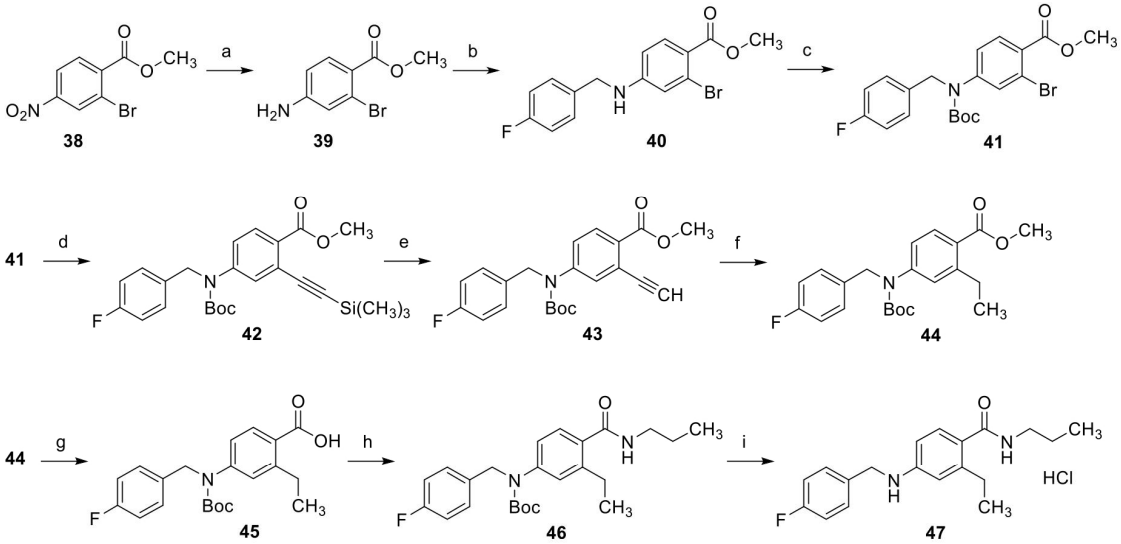

[a](a) $SnCl_2$, EtOAc, 70 °C, 4 h, 91%; (b) (1) 4-fluorobenzaldehyde, toluene, 120 °C, 8 h, (2) $NaBH_4$, 1,4-dioxane, MeOH, 0 °C to RT, 17 h, 87%; (c) Boc_2O, TEA, 4-DMAP, DCM, RT, 16 h, 87%; (d) trimethylsilylacetylene, CuI, $Pd(PPh_3)_4$, TEA, DMF, 60 °C, 4 h, 76%; (e) K_2CO_3, MeOH, RT, 1 h, 84%; (f) H_2, Pd/C, MeOH, 40 °C, 16 h, 86%; (g) KOH, MeOH, H_2O, 40 °C 24 h, 91%; (h) *n*-propylamine, HATU, DIPEA, DMF, RT, 8 h, 78%; (i) (1) TFA, DCM, RT, 6 h, (2) HCl, EtOAc, 0 °C, 30 min, 90%.

3).[29] As already described for the inverted amides, an additional methyl group was introduced in position 4 of the pyridine ring. A similar retrometabolic drug design approach was used successfully in the development of atenolol (**52**) from practolol (**51**). In order to prevent the formation of a toxic *N*-hydroxyaniline metabolite after cleavage of the anilide structure, an analogously functioning methylene spacer was introduced in **52**.[34,35] In contrast to the compounds synthesized here, however, the amide was additionally inverted. The introduction of a methylene spacer in **50** prevents the formation of azaquinone diimine metabolites due to the meta position of the remaining amino substituents. These compounds were also tested with XenoSite for the risk of quinoid metabolite formation.[30] A visualization of the results of compound **66** as a representative example for this scaffold is contained in Table 1. The risk for the formation of quinoid

https://doi.org/10.1021/acsomega.1c07103
ACS Omega 2022, 7, 7989−8012

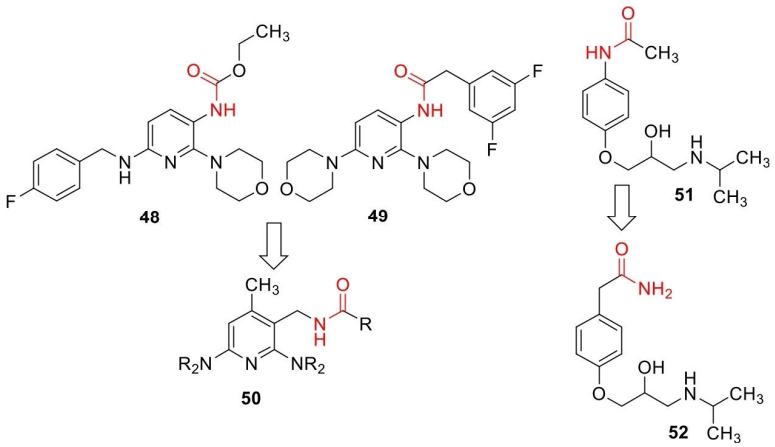

Figure 3. Design of flupirtine analogues containing a methylene spacer (**48**, **49**, **50**) and structural changes made in atenolol (**52**) compared to practolol (**51**).

Scheme 6. Synthesis of Compound 55a−66 as a Representative of Target Modification Type 4[a]

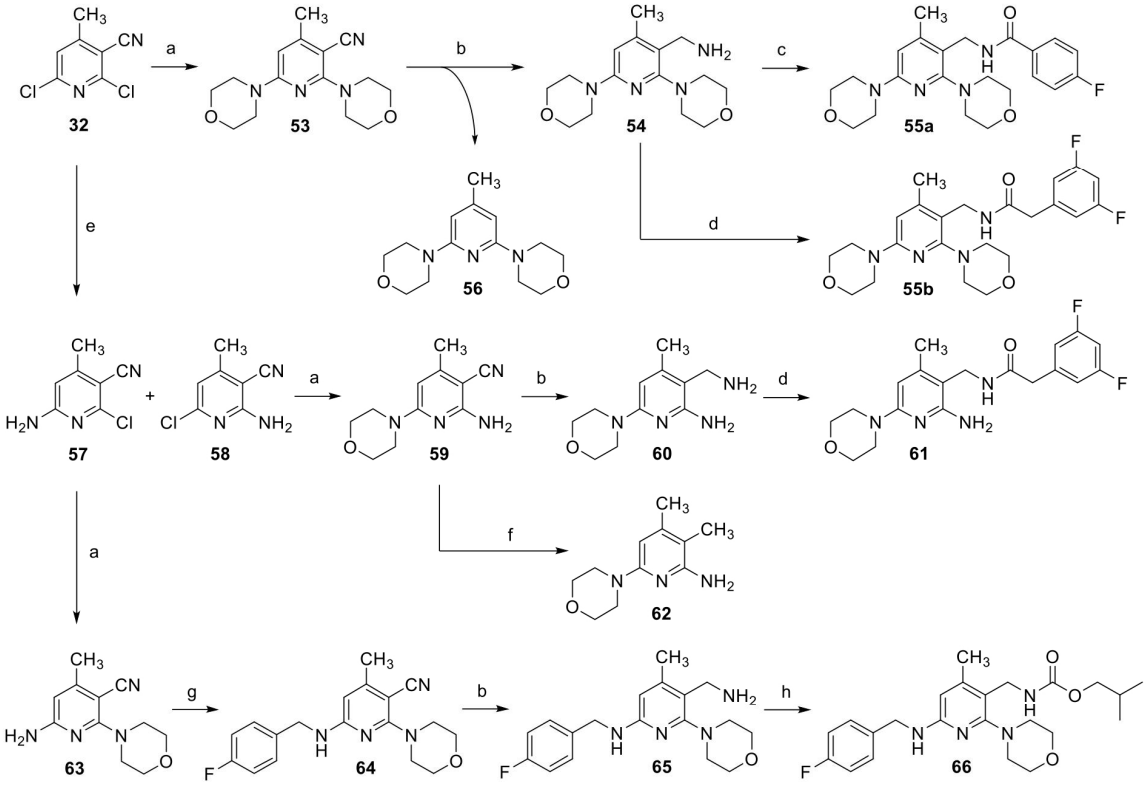

[a](a) Morpholine, 2-propanol, 170 °C, pressure reactor, 3−5 h, 82−89%; (b) Ni, H_2, NH_3, MeOH, 50 °C, 5−6 h, 34−52%; (c) 4-fluorobenzoyl chloride, TEA, DCM, 0 °C to RT, 16 h, 79%; (d) 2-(3,5-difluorophenyl)acetic acid, CDI, THF, RT, 18 h, 69−84%; (e) NH_3, 2-propanol, 70 °C, pressure reactor, 9 h, 14% (**57**), 20% (**58**); (f) H_2, Pd/C, MeOH, 40 °C, 48 h, 79%.; (g) (1) 4-fluorobenzaldehyde, DCM, RT, 16 h, (2) MeOH, $NaBH_3CN$, RT, 25 h, 42%; (h) isobutyl chloroformate, TEA, DCM, 0 °C to RT, 16 h, 64%.

metabolites is significantly reduced compared to flupirtine and retigabine but not completely excluded as with the inverted amide scaffold. The formation of an azaquinone imine methide metabolite is theoretically conceivable in this case, although not very likely, as suggested by the in silico prediction.

As described in Scheme 6, the syntheses of the compounds with methylene spacers were carried out starting from nitrile **32**. Different amino substituents were introduced via nucleophilic substitution reactions. The introduction of the second amino substituent required high temperatures, which made the use of a pressure reactor necessary. The pressure reactor was also used to introduce the primary amino function of **57** and **58** by heating chloropyridine **32** in a saturated solution of ammonia in 2-propanol. The resulting mixture of isomers was then separated by chromatography. Since the regioisomers could not be clearly assigned on the basis of their

https://doi.org/10.1021/acsomega.1c07103
ACS Omega 2022, 7, 7989−8012

^{1}H- and ^{13}C NMR spectra, a heteronuclear multiple bond correlation (HMBC) spectrum was recorded in each case, which is contained in the Supporting Information. This enabled the isomers to be differentiated since in the case of isomer **57**, a coupling between the protons of the amino group and the CH carbon atom of the pyridine ring was visible, which was missing in the HMBC spectrum of isomer **58**. The 4-fluorobenzylamino-substituted intermediate **64** was obtained via reductive amination of **63**. After both amino substituents had been introduced, the nitrile group was reduced to a primary amino group in each case. The first attempt to carry out the reduction of **59** by means of catalytic hydrogenation with the use of Pd/C as a catalyst failed and instead gave compound **62**. As a consequence, Raney nickel was used as an alternative catalyst, and ammonia was added to the reaction mixture. With this reduction procedure, the desired primary amines **54**, **60**, and **65** could be obtained. However, byproducts were formed in all the reactions. Upon reduction of **53**, a specific byproduct was isolated and identified as compound **56**. In the last step, the primary amino group was acylated or carbamylated; this was done either by coupling the corresponding carboxylic acid with CDI as the coupling reagent (**55b**/**61**) or by reaction with 4-fluorobenzoyl chloride and isobutyl chloroformate, respectively (**55a**/**66**).

Biological Evaluation. To evaluate the biological activity, the synthesized analogues were tested on HEK293 cells overexpressing the $K_V7.2/3$ channel. The measurement was carried out in a fluorescence-based assay in which a thallium-sensitive dye generated the fluorescence signal. Due to its similarity to potassium, thallium can also pass through K_V7 channels. The intensity of the fluorescence signal correlates with the amount of intracellular thallium and thus with the ability of the compounds to open K_V7 channels. To determine the potency, the fluorescence intensity was measured as a function of the compound concentration. The efficacy was determined relative to the maximum fluorescence signal induced by flupirtine. A representative concentration−activity curve is shown in Figure 4. For a summary of the activity data, see Table 2.

The two inverted amide analogues **17** and **21** with structural changes affecting only the amide side chain were found to be inactive in the biological testing. Inactive in this context means that no channel opening activity was detected up to a concentration of 10 μM. Even the compounds in which the primary amino group was replaced with a methoxy function (**28a**/**b**) turned out to be inactive. This is noteworthy because previous work had shown alkoxy substitution to be very beneficial for activity.[29] The ethyl substituent in place of the primary amino group in compound **47** also did not result in any improvement in terms of activity. In addition, the experimentally determined log $D_{7.4}$ values of the three last-mentioned analogues (**28a**/**b**, **47**) are in the range of 3.2−4.3, that is, compared to flupirtine and retigabine, whose log $D_{7.4}$ value is 2.1, the compounds are thus significantly more lipophilic. Increased lipophilicity, specifically indicated by log $D_{7.4}$ values greater than 3.5, has proven advantageous in terms of activity in the past but was not confirmed in the present cases.[27] This initially raised concerns that the change to the inverted amide scaffold is a too severe structural intervention to maintain $K_V7.2/3$ channel opening activity.

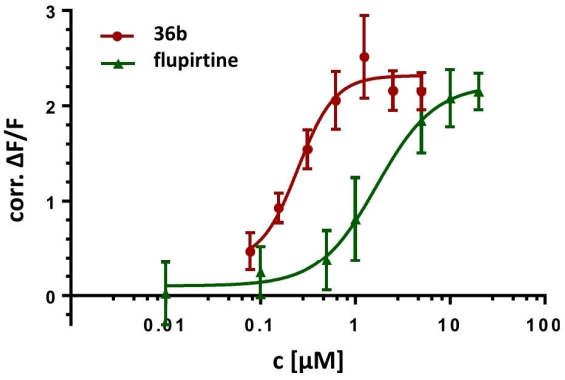

Figure 4. Comparison of the concentration−activity curves of **36b** and flupirtine (**1**).

Surprisingly, the two analogues with an additional methyl group in position 4 of the pyridine ring (**36a**/**b**) were found to be quite active, whereby **36b** with an EC_{50} value of 0.310 μM is even about six times more potent than flupirtine with similar efficacy. Figure 4 shows the direct comparison of the concentration−activity curves of **36b** and flupirtine, illustrating the improved activity of **36b**.

Of particular interest is the comparison between compound **36b** with nanomolar potency and compound **28b**, which is inactive up to a concentration of 10 μM (Figure 5). Both analogues differ in two structural features, one of which is a central phenyl ring present in compound **28b** instead of a pyridine ring incorporated in compound **36b**. However, this difference was not expected to have a negative effect on the activity of **28b** since, in the case of **1** and **2**, the phenyl ring in **2** has even improved potency and efficacy compared to **1**, rendering retigabine (**2**) the more active analogue of flupirtine (**1**). The key difference is, therefore, probably the additional methyl group of **36b**, causing the switch from inactive to active; such a significant difference in biological activity between two compounds resulting from a single structural modification is generally referred to as an activity cliff.[36] Since the modification is a methyl group, it can additionally be referred to as a "magic methyl" effect in this particular case. However, it cannot be excluded that other ortho substituents instead of the methyl group would produce a comparable effect. For this reason, we choose the term "apparent magic methyl effect" in the following. Different causes are discussed to be responsible for such effects.[37−39] For compound **36b**, since the methyl group is attached to an aromatic ring in the ortho position to an amide function, it may be for steric reasons, in combination with the methoxy group flanking the amide function on the other side, that a rotation of the amide group out of the plane of the aromatic ring occurs. On one hand, this may lead to a change in the distribution of electrons between the ring and the amide group. On the other hand, a twisted conformation may better fit the binding pocket's active conformation, thus decreasing the conformational reordering required upon binding.[37] A beneficial conformational pre-organization through an increase in shape complementarity between the unbound substrate and the active site of the protein in the bound state caused by an ortho methyl group has been described, for example, in the binding of an inhibitor (**66**) to the p38α MAP3 kinase, where the corresponding conformational information provided by an X-ray structure has been published.[40] A similar drastic improvement in activity through an ortho magic methyl group in the vicinity of an

https://doi.org/10.1021/acsomega.1c07103
ACS Omega 2022, 7, 7989−8012

Table 2. K_V7.2/3 Channel Opening Activity, In Vitro Toxicity, and log $D_{7.4}$ Values of the Synthesized Compounds 17−66 in Comparison to Flupirtine (1) and Retigabine (2)[a]

		HEK-293 cells		TAMH cells		HEP-G2 cells	
entry	log $D_{7.4}$	EC_{50}[b] [μM]	efficacy [%]	LD_{50}[c] [μM]	LD_{25}[d] [μM]	LD_{50}[c] [μM]	LD_{25}[d] [μM]
1	2.1	1.837 ± 0.844	100	487 ± 51	103 ± 47	547 ± 111	74 ± 40
2	2.1	0.147 ± 0.012[f]	134 ± 16[f]	>400[f]	>400[f]	>400[f]	269 ± 166[f]
17	2.7	[e]		>125	>125	>125	56 ± 40
21	2.9	[e]		149 ± 7	145 ± 7	149 ± 11	148 ± 11
28a	3.8	[e]		>63	43 ± 27	42 ± 7	31 ± 13
28b	4.3	[e]		>8	>8	>8	>8
36a	3.7	3.515 ± 0.724	65 ± 9	>63	17 ± 1	>63	24 ± 1
36b	4.1	0.310 ± 0,119	105 ± 12	>63	>63	>16	>16
47	3.2	[e]		>125	140 ± 14	77 ± 15	60 ± 9
55a	3.5	[e]		>31	22 ± 7	>31	22 ± 6
55b	3.5	[e]		>250	24 ± 5	>250	20 ± 7
61	2.6	[e]		>63	>63	>63	>63
66	4.8	[e]		>125	52 ± 61	>125	24 ± 27

[a]log $D_{7.4}$ values were estimated by using an HPLC-based method. EC_{50} values were obtained in HEK293 cells overexpressing K_V7.2/3 channels. LD values were determined by the MTT assay after 24 h exposure. EC_{50} and LD values are means and SDs of ≥3 independent determinations, respectively. [b]Concentration required to reach half-maximal channel opening activity. [c]Concentration required to reduce cell viability by 50% compared to untreated controls. [d]Concentration required to reduce cell viability by 25% compared to untreated controls. [e]Inactive up to a concentration of 10 μM. [f]Retigabine (2) values were taken from our recently published work.[27]

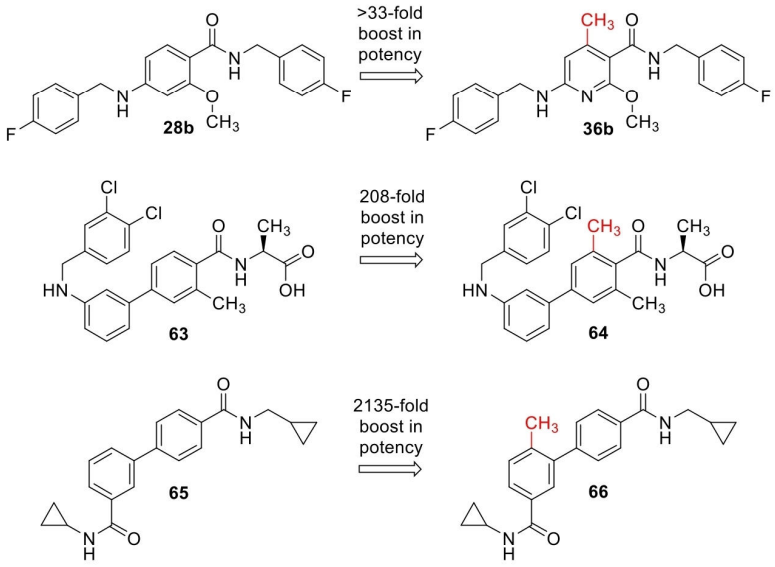

Figure 5. Drastically improved activity by additional *ortho* methyl groups in present example (**36b**) and literature cases of an $S1P_1$ antagonist (**64**) and an inhibitor of the p38α MAP3 kinase (**66**).

amide function was discovered, for example, in the development of an $S1P_1$ antagonist (**64**).[41]

Compound **36a** is a structural analogue of **36b**, which differs only in the replacement of the benzylic amide side chain with an unbranched aliphatic side chain. However, this modification is associated with a significant loss of potency by a factor of 11 and a drop of efficacy to 65%. On one hand, this could be due to the reduced lipophilicity; on the other hand, it would also be conceivable that an aromatic or at least sterically more demanding side chain ensures a better affinity for the K_V7.2/3 channel binding pocket.

Regrettably, the second retrometabolic design approach, which was based on the insertion of a methylene spacer, was unsuccessful. The four synthesized compounds (**55a/b**, **61**, **66**) were invariably inactive at a concentration of up to 10 μM in spite of the potentially advantageous methyl group. If it is taken into account that the double morpholino-substituted derivative **49**, which served as the lead structure for two of the analogues, had an EC_{50} value of 0.011 μM, the inactivity of compounds **55a/b**, **61**, and **66** indicates that the introduction of the methylene spacer was responsible for drastically impaired affinity for the binding pocket.

In addition to the activity, basic toxicological properties of the newly synthesized compounds were also investigated by using the 3-(4,5-dimethylthiazol-2-yl)-2,5-diphenyltetrazolium bromide (MTT) cell viability assay on mouse TAMH and human HEP-G2 hepatic cell lines (see Table 2). Both cell lines are established for the evaluation of hepatotoxicity.[42,43] However, it should be noted that the values determined are not predictive for idiosyncratic toxicity since no direct dose−

https://doi.org/10.1021/acsomega.1c07103
ACS Omega 2022, 7, 7989−8012

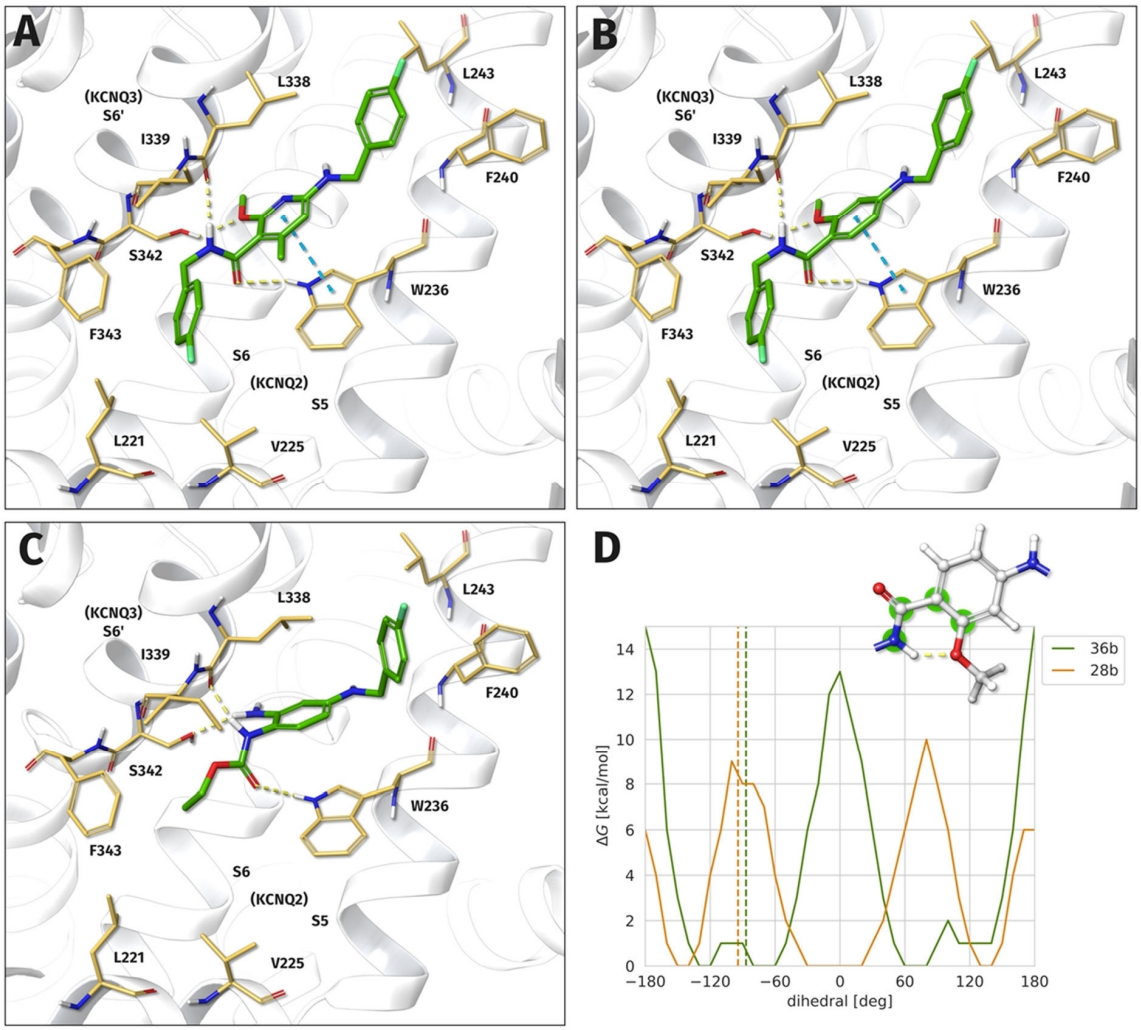

Figure 6. Predicted binding modes of **36b** (A) and **28b** (B) in comparison to retigabine (**2**, C) in the S5, S6, S6′-binding pocket of the heterotetrameric $K_V7.2/3$ potassium channel. For **36b**, an improved binding free energy was determined compared to **28b** ($|\Delta\Delta G| = 1.261$ kcal/mol). All three compounds form hydrogen bonds to W236, L338, and S342 as well as hydrophobic interactions on both sides. Replacing the carbamate group of **2** with an amide slightly displaces the center aromatic ring, which then additionally forms a $\pi-\pi$ interaction with W236. A bulky hydrophobic group at the amide substituent is able to occupy the hydrophobic cavity of L221, V225, and F343. The ortho methyl group of **36b** significantly increases the rotational energy barrier of the amide group (D, dihedral atoms highlighted in green), predicted by REMD simulations in TIP3P water. The dihedral values for the binding modes are represented as dashed lines. For **28b**, planar conformations are stabilized by an intramolecular hydrogen bond, while for conformations with a dihedral value of around (−)150°, both oxygen atoms can be bridged by a water molecule. Compared to **36b**, the binding mode dihedral value is energetically unfavorable. The Gibbs-free-energy values were estimated by Boltzmann inversion of the corresponding dihedral frequencies.

effect relationship can be observed for this type of toxicity.[44] These toxic reactions typically occur even at subcritical concentrations and after a latency period as it was also observed for the flupirtine-induced hepatotoxicity, where evidence supports the theory of immune-mediated toxicity following hapten-protein adduct formation.[5,6,9,10] This is also underlined by the results of the cell viability assay, where the drug flupirtine itself does not appear to be acutely hepatotoxic with LD_{50} values in the range of 500 μM. Retigabine showed even weaker cytotoxicity compared to flupirtine, although the in silico prediction revealed a very high probability of forming quinone diimine metabolites (Table 1). This is not a contradiction since the metabolization to quinone diimines probably requires different conditions in the case of retigabine. In contrast to flupirtine, which undergoes mainly the oxidative hepatic metabolism, retigabine is mostly *N*-glucuronidated, as has been shown earlier.[5] However, as already mentioned, Groseclose and Castellino provided clear albeit indirect evidence for the oxidation of retigabine to quinone diimines.[12] The reaction is probably not catalyzed by liver enzymes but possibly linked to the presence of melanin, and thus, the resulting reactive quinone diimine metabolites (Figure 1) do not primarily affect the liver but other organs such as the skin and eyes.

Despite the moderate to low in vitro toxicity of flupirtine and retigabine, it is relevant how the new analogues perform in a toxicity test since intrinsic, dose-related hepatotoxicity must also be avoided when developing new analogues of flupirtine and retigabine. A limitation in the in vitro toxicity testing was the occasional poor water solubility of the analogues. For many

https://doi.org/10.1021/acsomega.1c07103
ACS Omega 2022, 7, 7989−8012

compounds, it was not possible to determine an LD_{50} value up to the solubility limit. For this reason and to enable comparability, in addition to the more common LD_{50} values, LD_{25} values were calculated, which express the concentration that reduced the cell viability to 75%. When comparing the LD_{25} values, most analogues were found to be more toxic compared with flupirtine and retigabine. Unfortunately, no LD_{25} value could be determined for the most active compound **36b** due to its poor aqueous solubility. Exceptions were the inverted amide analogues **17**, **21**, and **47**, which had higher LD_{25} values than flupirtine and retigabine, especially with the TAMH cell line. Since these substances are also the three least lipophilic analogues, apart from **61**, the main reason for the impaired toxicity of several other compounds is perhaps the increased lipophilicity compared to flupirtine and retigabine. The results are in agreement with the literature that suggests a connection between increased lipophilicity and increased risk for DILI.[45,46] However, it should also be noted that a certain degree of lipophilicity of the substances is necessary in order to enable the penetration of the blood−brain barrier through passive diffusion.[47] Since this initial work was only about a proof of concept of the retrometabolic design approach, balancing the lipophilicity was not yet the main focus of our research and remains an optimization approach for further work to improve water solubility and toxicological properties.

Finally, basic pharmacokinetic properties and the drug-likeness of the most active compound **36b** were estimated with in silico methods. Using SwissADME,[48] the drug-likeness of **36b** according to the Lipinski rules was evaluated as given. Other drug-likeness criteria (Ghose, Veber, Egan) are fully met as well. As the log *P* value and other key figures such as the calculated low ratio of sp^3 hybridized carbon atoms (0.18) suggest, SwissADME classified **36b** as moderately to poorly water-soluble with a predicted log *S* value in the range from −8.9 to −5.0. This is in line with our experience from biological testing, where a maximum concentration of 63 μM could be achieved in the MTT assay without compound **36b** precipitating in the assay buffer. Furthermore, the substance is classified as blood−brain barrier permeant by SwissADME, which is crucial for the effect on K_V7 channels in the central nervous system. In addition, high gastrointestinal absorption and no impairment by the P-glycoprotein transporter are predicted, which should positively affect bioavailability. The metabolic stability was estimated with PredMS,[49] which is a random forest model for predicting the metabolic stability of drug candidates in human liver microsomes. According to the PredMS algorithm, **36b** is assessed as being metabolically stable (≥50% remaining at 30 min).

Computational Chemistry. The elaboration of a hypothetical binding mode and a more detailed investigation of the apparent magic methyl effect in the case of **36b** were carried out by means of a molecular docking study. The basis for the intended simulations was the recently published cryogenic electron microscopy (Cryo-EM) structure of a homotetrameric $K_V7.2$ channel in complex with retigabine.[50] To obtain conclusive docking results, the model of a heterotetrameric $K_V7.2/3$ channel was created by homology modeling based on the mentioned Cryo-EM data since the channel opening activity was also tested on the Kv7.2/3 channel subtype.

The binding poses of compounds **28b** and **36b** predicted from molecular docking are shown in Figure 6 in comparison with retigabine (**2**). The binding of all three substances is characterized by hydrophobic interactions of the lateral molecule parts and hydrogen bonds in the central area to amino acids W236, L338, and S342. However, replacing the ethyl carbamate of retigabine with an inverted amide structure appears to cause a slight shift of the central aromatic ring, which allows for an additional $\pi-\pi$-interaction with W236. It can also be seen that a bulky amide side chain enables a better fit in the area of the hydrophobic cavity formed by L221, V225, and F343, which could explain the improved activity of the *N*-(4-fluorobenzyl)nicotinamide analogue **36b** in comparison to the *N*-butylnicotinamide analogue **36a**.

No specific interaction of the additional methyl group with the binding site was observed in the predicted docking pose of **36b**. However, the amide function of **28b** and **36b** is clearly rotated by approximately 90° in relation to the central aromatic ring. Both findings support the hypothesis of an apparent magic methyl effect caused by a conformational preorganization of the ligand in the case of **36b**. Additional evidence was provided by a replica-exchange molecular dynamics simulation performed to calculate the rotational energy barrier of the amide group. The results are visualized in Figure 6D, which shows the one-dimensional Gibbs-free-energy landscape of **28b** and **36b** as a function of the dihedral angle. As can be seen, planar conformations are energetically favorable for compound **28b** since these are also stabilized by an intramolecular hydrogen bond involving the amide function and the adjacent methoxy group. In contrast, the additional methyl group and the resulting ortho-disubstitution of the amide function in the case of **36b** lead to an energetic preference for a dihedral angle of approximately 90°. This dihedral angle matches the conformation in the bound state obtained from molecular docking, thus improving the binding energy of **36b** by reducing the entropic cost of conformational reordering required for this interaction.

■ CONCLUSIONS

In conclusion, it can be stated that the concept of a retrometabolic drug design could be successfully applied to flupirtine (**1**) and retigabine (**2**). Unfortunately, the strategy to insert a methylene spacer failed, but replacing the carbamate group of **1** and **2** with an inverted amide resulted in a compound (**36b**) six times as potent as flupirtine. However, further structural modifications, such as the introduction of an essential methyl group, which is postulated to cause an improved binding by conformational preorganization, were necessary to obtain active compounds. Additional work is required to balance compound lipophilicity by addition of an ionizable/polar moiety in order to obtain substances with attenuated toxicological properties while at the same time maintaining the improved $K_V7.2/3$ channel opening activity of **36b**. If these changes are successfully implemented, the inverted amide scaffold represents a promising approach to obtain safer replacements for flupirtine and retigabine, which, as a result of their structural design, are not at risk of forming reactive quinone diimine metabolites.

■ EXPERIMENTAL SECTION

Chemistry. All solvents and reagents were obtained from commercial suppliers (Sigma Aldrich, VWR, or ABCR) and were used without purification. Anhydrous solvents were purchased from Acros Organics, except tetrahydrofuran (THF), which was dried by refluxing over sodium and benzophenone (until a permanent dark-blue coloration was

https://doi.org/10.1021/acsomega.1c07103
ACS Omega 2022, 7, 7989−8012

visible), followed by distillation under anhydrous conditions. Microwave-assisted syntheses were performed using an Anton Paar Monowave 300 reactor operated in the closed vessel mode using G10-vials with a 6 mL total capacity; temperature control was performed by means of an integrated IR sensor, and the stirring speed was 600 rpm. NMR spectra were recorded with a Bruker Avance III device at 400 MHz (^{1}H NMR) and 100 MHz (^{13}C NMR). Chemical shifts were referenced to tetramethylsilane as an internal standard in deuterated solvents and reported in parts per million (ppm). Coupling constants (J) are reported in Hz using the abbreviations br = broad, s = singlet, d = doublet, t = triplet, q = quartet, m = multiplet, and combinations thereof. Mid-infrared spectra were recorded on an ALPHA FT-IR instrument from Bruker Optics equipped with a diamond attenuated total reflectance (ATR) accessory unit and are indicated in terms of absorption frequency [cm^{-1}]. HRAM-MS data were measured using a Shimadzu LCMS-IT-TOF or a Bruker maXis LC-QTOF-MS system, each with electrospray ionization (ESI). Melting points were measured using a Melting Point M-565 apparatus from Büchi. The purity of the final compounds was determined by high-performance liquid chromatography (HPLC) (applying the 100% method at 220 nm). All final compounds are >95% pure by HPLC analysis. Preparative and analytical HPLC procedures were performed using Shimadzu devices CBM-20A, LC-20A P, SIL-20A, and FRC-10A with an SPD 20A UV/vis detector and an ELSD-LT II. In the analytical mode, a LiChroCART (250 × 4 mm) was used, and in the preparative mode, a Hibar RT (250 × 25 mm) HPLC column was used, both containing LiChrospher 100 RP-18e (5 μm). An eluent of methanol/water (75:25) with 0.1% formic acid was used unless stated otherwise. Thin-layer chromatography was executed on silica gel 60 F_{254} aluminum plates purchased from Merck. Column chromatography was performed on a glass column using silica gel 60 from Carl Roth with a particle size of 20−45 μm. For flash chromatography, the Sepacore system from Büchi was used in combination with 25 or 50 g Biotage SNAP columns.

General Procedure A: Reductive Amination. The amine component (1.0 equiv, 22−142 mmol/L) was suspended in dry toluene. 4 Å molecular sieves (0.1 g/mL) and 4-fluorobenzaldehyde (1.0−1.2 equiv) were added. The reaction mixture was stirred at 120 °C for 5−8 h. Afterward, it was filtered hot to remove the molecular sieves. The filtrate was cooled to room temperature and concentrated under reduced pressure. The residue was dissolved in 25 mL of a mixture of 1,4-dioxane and methanol (4:1). The resulting solution was cooled to 0 °C, and sodium borohydride (2.8−5.0 equiv) was added in portions over a period of 1 h under stirring. Thereafter, stirring at room temperature was continued for 16 h before the reaction was quenched by adding 100 mL of water. The resulting mixture was extracted with ethyl acetate (250 mL). The organic phase was washed with brine, dried over Na_2SO_4, filtrated, and concentrated under reduced pressure. The crude residue was purified by silica gel column chromatography to obtain the title compound.

General Procedure B: Reduction of Nitrile Functions to Primary Amino Groups. The nitrile compound (30−50 mmol/L) was dissolved in a saturated solution of ammonia in methanol (30 mL). 500 mg of a Raney nickel suspension in water (50%) was washed with methanol and added to the reaction mixture. The suspension was carefully set under a hydrogen atmosphere (balloon pressure) and stirred at 50 °C. After 6 h, the catalyst was removed by filtration, and the filtrate was concentrated under reduced pressure. The resulting residue was dissolved in ethyl acetate and filtrated through a pad of silica gel, which was subsequently rinsed with additional 250 mL of ethyl acetate. The obtained filtrate contained a side product. Afterward, the silica gel pad was rinsed with 100 mL of a mixture of methanol and conc. aq ammonia solution (9:1) to elute the desired product. The filtrate was concentrated under reduced pressure to obtain the title compound.

2-(4-Methyl-3-nitrophenyl)isoindoline-1,3-dione (10). 4-Methyl-3-nitroaniline (16.76 g, 110.2 mmol), phthalic anhydride (19.58 g, 132.2 mmol, 1.2 equiv), and triethylamine (TEA) (18.32 mL, 132.2 mmol, 1.2 equiv) were dissolved in toluene (300 mL). The mixture was stirred at 120 °C, and water was removed by using a Dean−Stark apparatus. After 4 h, it was cooled to room temperature, and the resulting precipitate was filtered off. The filter cake was washed successively with a saturated aq $NaHCO_3$ solution and boiling ethyl acetate. Afterward, the resulting solid was recrystallized from dimethyl sulfoxide (DMSO) and washed with water to obtain **10** as a colorless solid (25.34 g, 89.8 mmol, 82%): R_f = 0.69 (ethyl acetate/*n*-hexane 1:1); mp 231 °C; ^{1}H NMR (400 MHz, DMSO-d_6): δ (ppm) = 8.18 (d, J = 2.1 Hz, 1H); 8.00 (m, 2H), 7.93 (m, 2H), 7.77 (dd, J = 8.2, 2.1 Hz, 1H), 7.68 (dd, J = 8.1, 1.0 Hz, 1H), 2.59 (s, 3H); ^{13}C NMR (100 MHz, DMSO-d_6): δ (ppm) = 166.6, 148.6, 134.9, 133.2, 132.7, 132.0, 131.5, 130.7, 123.6, 123.0, 19.4; IR (ATR): $\tilde{\nu}$ = 2990 (w, ν_{C-H}), 1728 (s, $\nu_{C=O}$), 1531 (m, ν_{N-O}).

***N*-(4-Methyl-3-nitrophenyl)acetamide (12).** 4-Methyl-3-nitroaniline (11.85 g, 77.9 mmol) was dissolved in a mixture of acetic anhydride (29.4 mL, 311.5 mmol, 4.0 equiv) and acetic acid (95 mL). The reaction mixture was stirred at room temperature. After 15 min, acetic acid and excessive acetic anhydride were removed under reduced pressure. The resulting residue was recrystallized (ethanol/water) to obtain **12** as a beige solid (13.13 g, 67.6 mmol, 87%): R_f = 0.31 (ethyl acetate/*n*-hexane 1:1); mp 150 °C; ^{1}H NMR (400 MHz, DMSO-d_6): δ (ppm) = 10.30 (s, 1H), 8.36 (d, J = 2.3 Hz, 1H), 7.70 (dd, J = 8.3, 2.3 Hz, 1H), 7.42 (d, J = 8.4 Hz, 1H), 2.46 (s, 3H), 2.07 (s, 3H); ^{13}C NMR (100 MHz, DMSO-d_6): δ (ppm) = 168.9, 148.6, 138.2, 126.9, 133.0, 123.5, 114.1, 24.0, 19.1; IR (ATR): $\tilde{\nu}$ = 3353 (m, ν_{N-H}), 3042, 2993 (w, ν_{C-H}), 1673 (s, $\nu_{C=O}$), 1600 (m, δ_{N-H}); 1524 (s, ν_{N-O}).

4-Acetamido-2-nitrobenzoic Acid (13). *N*-(4-Methyl-3-nitrophenyl)acetamide (13.00 g, 66.9 mmol) was suspended in water and stirred at 80 °C. $KMnO_4$ was added in eight portions at 30 min intervals (in total 33.85 g, 214.2 mmol, 3.2 equiv). After the last addition, the reaction mixture was continued to stir for 1 h at 80 °C. Afterward, the reaction mixture was cooled to room temperature, and the pH was adjusted to 11−12 by the addition of a 10% aq NaOH solution. Thereafter, a conc. aq H_2O_2 solution was added until the violet color of the mixture disappeared. The resulting brown precipitate was filtered off, and the filtrate was cooled to 0 °C. By the addition of conc. aq HCl to the filtrate, the product was precipitated and subsequently filtered off to obtain **13** as a colorless solid (7.81 g, 34.8 mmol, 52%): R_f = 0.32 (ethyl acetate/toluene/AcOH 5:5:1); mp 223 °C; ^{1}H NMR (400 MHz, DMSO-d_6): δ (ppm) = 13.57 (s, 1H), 10.61 (s, 1H), 8.19 (d, J = 2.0 Hz, 1H), 7.86 (d, J = 8.5 Hz, 1H), 7.78 (dd, J = 8.5, 2.1 Hz, 1H), 2.11 (s, 3H); ^{13}C NMR (100 MHz, DMSO-d_6): δ (ppm) = 169.5, 165.1, 149.8, 142.8, 131.4, 121.3, 119.9, 112.8, 24.1; IR

https://doi.org/10.1021/acsomega.1c07103
ACS Omega 2022, 7, 7989−8012

(ATR): $\tilde{\nu}$ = 3346 (m, ν_{N-H}), 3300−2500 (b, ν_{O-H}), 1720, 1671 (s, $\nu_{C=O}$), 1613 (m, δ_{N-H}); 1528 (s, ν_{N-O}).

4-Acetamido-*N*-isobutyl-2-nitrobenzamide (14). 4-Acetamido-2-nitrobenzoic acid (500 mg, 2.23 mmol) was dissolved in THF (20 mL). CDI (722 mg, 4.46 mmol, 2.0 equiv) was added in one portion, and the mixture was stirred at room temperature. After 1 h, isobutylamine (670 μL, 6.69 mmol, 3.0 equiv) was added, and the reaction mixture was stirred at room temperature for additional 16 h. Afterward, ethyl acetate (100 mL) was added. The resulting solution was extracted successively with a saturated aq $NaHCO_3$ solution (100 mL) and a 2 M aq HCl solution (100 mL). The organic phase was washed with brine, dried over Na_2SO_4, filtrated, and concentrated under reduced pressure. The crude residue was purified by recrystallization (methanol/water) to obtain **14** as a light-yellow solid (460 mg, 1.65 mmol, 74%): R_f = 0.50 (ethyl acetate/*n*-hexane 4:1); mp 186 °C; ^{1}H NMR (400 MHz, DMSO-d_6): δ (ppm) = 10.49 (s, 1H), 8.57 (t, J = 5.9 Hz, 1H), 8.31 (d, J = 2.1 Hz, 1H), 7.80 (dd, J = 8.4, 2.1 Hz, 1H), 7.53 (d, J = 8.3 Hz, 1H), 3.02 (dd, J = 6.8, 5.9 Hz, 2H), 2.10 (s, 3H), 1.80 (m, 1H), 0.90 (d, J = 6.7 Hz, 6H); ^{13}C NMR (100 MHz, DMSO-d_6): δ (ppm) = 169.3, 165.2, 147.6, 140.8, 129.7, 126.9, 122.4, 113.5, 46.7, 28.0, 24.1, 20.2; IR (ATR): $\tilde{\nu}$ = 3257 (m, ν_{N-H}), 2969 (w, ν_{C-H}), 1679, 1631 (s, $\nu_{C=O}$), 1603 (m, δ_{N-H}); 1539 (s, ν_{N-O}).

4-Amino-*N*-isobutyl-2-nitrobenzamide (15). 4-Acetamido-*N*-isobutyl-2-nitrobenzamide (800 mg, 2.86 mmol) was suspended in a 20% aq HCl solution (50 mL). The mixture was stirred at 100 °C. After 2 h, it was cooled to 0 °C, and KOH pellets were added to adjust the pH to 7. The resulting aq suspension was extracted with ethyl acetate (2 × 100 mL). The combined organic phases were washed with brine, dried over Na_2SO_4, filtrated, and concentrated under reduced pressure. The crude residue was purified by recrystallization (methanol/water) to obtain **15** as a yellow solid (650 mg, 2.74 mmol, 96%): R_f = 0.64 (ethyl acetate/*n*-hexane 1:1); mp 155 °C; ^{1}H NMR (400 MHz, DMSO-d_6): δ (ppm) = 8.32 (t, J = 5.8 Hz, 1H), 7.27 (d, J = 8.4 Hz, 1H), 6.97 (d, J = 2.3 Hz, 1H), 6.76 (dd, J = 8.4, 2.3 Hz, 1H), 6.04 (s, 2H), 2.97 (dd, J = 6.9, 5.9 Hz, 2H), 1.77 (m, 1H), 0.88 (d, J = 6.7 Hz, 6H); ^{13}C NMR (100 MHz, DMSO-d_6): δ (ppm) = 165.4, 150.9, 149.6, 129.9, 115.9, 118.4, 107.5, 46.5, 28.1, 20.2; IR (ATR): $\tilde{\nu}$ = 3422, 3289 (m, ν_{N-H}), 2958 (w, ν_{C-H}), 1631 (s, $\nu_{C=O}$), 1603 (m, δ_{N-H}); 1544 (m, ν_{N-O}).

4-[(4-Fluorobenzyl)amino]-*N*-isobutyl-2-nitrobenzamide (16). The synthesis was carried out according to general procedure A. 4-Amino-*N*-isobutyl-2-nitrobenzamide (260 mg, 1.10 mmol), 4-fluorobenzaldehyde (142 μL, 1.32 mmol, 1.2 equiv), toluene (50 mL), and 4 Å molecular sieves (5.0 g) were used in the first reaction step. In the second step, the reduction was performed by using 146 mg of sodium borohydride (3.85 mmol, 3.5 equiv). The purification by silica gel column chromatography (ethyl acetate/*n*-hexane 4:6) afforded **16** as a yellow solid (140 mg, 0.41 mmol, 37%): R_f = 0.33 (ethyl acetate/*n*-hexane 1:1); mp 106 °C; ^{1}H NMR (400 MHz, DMSO-d_6): δ (ppm) = 8.33 (t, J = 5.8 Hz, 1H), 7.38 (m, 2H), 7.30 (d, J = 8.5 Hz, 1H), 7.21 (t, J = 6.1 Hz, 1H), 7.16 (m, 2H), 7.0 (d, J = 2.3 Hz, 1H), 6.79 (dd, J = 8.5, 2.4 Hz, 1H), 4.35 (d, J = 6.0 Hz, 2H), 2.96 (dd, J = 6.9, 5.9 Hz, 2H), 1.76 (m, 1H), 0.86 (d, J = 6.7 Hz, 6H); ^{13}C NMR (100 MHz, DMSO-d_6): δ (ppm) = 165.2, 161.2 (d, J = 242.4 Hz), 150.0, 149.7, 135.0 (d, J = 3.0 Hz), 129.8, 129.1 (d, J = 8.1 Hz), 118.5, 115.2 (d, J = 21.3 Hz), 114.3, 106.4, 46.5, 45.1, 28.1, 20.1; IR (ATR): $\tilde{\nu}$ = 3286 (m, ν_{N-H}), 2959 (w, ν_{C-H}), 1626 (s, $\nu_{C=O}$), 1547 (m, ν_{N-O}).

2-Amino-4-[(4-fluorobenzyl)amino]-*N*-isobutylbenzamide (17). 4-[(4-Fluorobenzyl)amino]-*N*-isobutyl-2-nitrobenzamide (340 mg, 0.98 mmol) was dissolved in ethyl acetate (20 mL). $SnCl_2$ (929 mg, 4.90 mmol, 5.0 equiv) was added, and the mixture was stirred at 80 °C for 30 min. Afterward, it was cooled to room temperature, and a sat. aq $NaHCO_3$ solution (100 mL) was added. The resulting mixture was extracted with ethyl acetate (2 × 100 mL). The combined organic phases were washed with brine, dried over Na_2SO_4, filtrated, and concentrated under reduced pressure. The crude residue was purified by recrystallization (methanol/water) to obtain **17** as a slightly gray solid (210 mg, 0.67 mmol, 68%): R_f = 0.60 (ethyl acetate/*n*-hexane 3:2); mp 127 °C; ^{1}H NMR (400 MHz, DMSO-d_6): δ (ppm) = 7.70 (t, J = 5.8 Hz, 1H), 7.34 (m, 2H), 7.26 (d, J = 8.8 Hz, 1H), 7.13 (m, 2H), 6.34 (s, 2H), 6.15 (t, J = 6.2 Hz, 1H), 5.83 (dd, 8.7, 2.3 Hz, 1H), 5.76 (d, J = 2.3 Hz, 1H), 4.21 (d, J = 6.1 Hz, 2H), 2.95 (dd, J = 7.0, 5.8 Hz, 2H), 1.77 (m, 1H), 0.84 (d, J = 6.7 Hz, 6H); ^{13}C NMR (100 MHz, DMSO-d_6): δ (ppm) = 168.9, 161.0 (d, J = 241.8 Hz), 151.5, 151.2, 136.3 (d, J = 2.9 Hz), 129.1, 128.8 (d, J = 8.0 Hz), 114.9 (d, J = 21.1 Hz), 104.2, 101.6, 97.0, 46.1, 45.2, 28.1, 20.2; IR (ATR): $\tilde{\nu}$ = 3419, 3288 (m, ν_{N-H}), 3040, 2964 (w, ν_{C-H}), 1619 (s, $\nu_{C=O}$), 1590 (m, δ_{N-H}); ESI-HRMS: calcd for $[C_{18}H_{22}N_3OF + H]^+$, 316.1820; found, 316.1810; cpd purity (220 nm): 100%.

2-Amino-6-chloronicotinic Acid (19). Procedure A: 2,6-dichloronicotinic acid (1.00 g, 5.2 mmol) was dissolved in conc. aq ammonia solution (30 mL). The mixture was stirred in a sealed vessel at 130 °C. After 8 h, the reaction mixture was cooled to 0 °C and adjusted to pH 7 with a 6 M aq HCl solution. The formed precipitate was filtered off and purified by silica gel column chromatography using diethyl ether as the mobile phase. The title compound was obtained as a colorless solid (506 mg, 2.95 mmol, 57%). Procedure B: 2,6-dichloronicotinic acid (384 mg, 2.00 mmol) was dissolved in ethanol (30 mL). CuI (76 mg, 0.40 mmol, 0.2 equiv), K_2CO_3 (553 mg, 4.00 mmol, 2.0 equiv), NaN_3 (520 mg, 8.00 mmol, 4.0 equiv), and ethylenediamine (27 μL, 0.40 mmol, 0.2 equiv) were added. The mixture was set under an atmosphere of argon and stirred at 95 °C. After 11.5 h, it was cooled to room temperature, and water (30 mL) was added. Subsequently, the resulting solution was neutralized by the addition of a 1 M aq HCl solution. The resulting mixture was extracted with ethyl acetate (3 × 100 mL). The combined organic phases were washed with brine, dried over Na_2SO_4, filtrated, and concentrated under reduced pressure. The crude residue was purified by silica gel column chromatography [dichloromethane (DCM)/MeOH 9:1] to obtain **19** as a colorless solid (300 mg, 1.74 mmol, 87%): R_f = 0.69 (toluene/ethyl acetate/AcOH 5:5:1); mp decomp.; ^{1}H NMR (400 MHz, DMSO-d_6): δ (ppm) = 13.14 (s, 1H), 8.03 (d, J = 8.1 Hz, 1H), 7.55 (s, 2H), 6.63 (d, J = 8.1 Hz, 1H); ^{13}C NMR (100 MHz, DMSO-d_6): δ (ppm) = 167.9, 159.7, 153.2, 143.2, 111.0, 104.5; IR (ATR): $\tilde{\nu}$ = 3446, 3281 (m, ν_{N-H}), 3300−2500 (b, ν_{O-H}), 1672 (s, $\nu_{C=O}$), 1624 (m, δ_{N-H}).

2-Amino-*N*-butyl-6-chloronicotinamide (20). 2-Amino-6-chloronicotinic acid (310 mg, 1.81 mmol) was suspended in DCM (20 mL). CDI (322 mg, 1.99 mmol, 1.1 equiv) was added in one portion, and the mixture was stirred for 15 min at room temperature. Afterward, *n*-butylamine (179 μL, 1.81 mmol, 1.0 equiv) was added, and the mixture was continued to

https://doi.org/10.1021/acsomega.1c07103
ACS Omega 2022, 7, 7989−8012

stir at room temperature. After 24 h, another 89 μL of *n*-butylamine (0.90 mmol, 0.5 equiv) was added, and the reaction was continued under the same conditions for additional 24 h. Thereafter, the mixture was concentrated under reduced pressure. The crude residue was purified by silica gel column chromatography (ethyl acetate/*n*-hexane 1:1) and successive recrystallization (methanol/water), which yielded **20** as a colorless solid (227 mg, 1.00 mmol, 55%): R_f = 0.47 (ethyl acetate/*n*-hexane 1:3); mp 140 °C; ^{1}H NMR (400 MHz, DMSO-d_6): δ (ppm) = 8.42 (t, J = 5.6 Hz, 1H), 7.91 (d, J = 8.1 Hz, 1H), 7.47 (s, 2H), 6.62 (d, J = 8.0 Hz, 1H), 3.21 (td, J = 7.1, 5.6 Hz, 2H), 1.47 (m, 2H), 1.31 (m, 2H), 0.89 (t, J = 7.3 Hz, 3H); ^{13}C NMR (100 MHz, DMSO-d_6): δ (ppm) = 166.5, 159.0, 150.9, 139.4, 110.0, 108.4, 38.7, 31.0, 19.6, 13.7; IR (ATR): $\tilde{\nu}$ = 3454, 3292 (m, ν_{N-H}), 2959 (w, ν_{C-H}), 1621 (s, $\nu_{C=O}$), 1567 (m, δ_{N-H}).

2-Amino-*N*-butyl-6-[(4-fluorobenzyl)amino]-nicotinamide (21). 2-Amino-*N*-butyl-6-chloronicotinamide (114 mg, 0.50 mmol) was suspended in 4-fluorobenzylamine (2.86 mL, 25.00 mmol, 50.0 equiv). The mixture was stirred at 160 °C without a solvent. After 3 h, the reaction mixture was cooled to room temperature and used directly for silica gel column chromatography (ethyl acetate/*n*-hexane 1:1). The crude product was further purified by recrystallization (methanol/water), which yielded **21** as a colorless solid (25 mg, 0.08 mmol, 16%): R_f = 0.34 (ethyl acetate/*n*-hexane 1:1); mp 108 °C; ^{1}H NMR (400 MHz, DMSO-d_6): δ (ppm) = 7.73 (t, J = 5.6 Hz, 1H), 7.60 (d, J = 8.6 Hz, 1H), 7.35 (m, 2H), 7.13 (m, 3H), 7.02 (s, 2H), 5.71 (d, J = 8.6 Hz, 1H), 4.44 (d, J = 6.0 Hz, 2H), 3.15 (td, J = 7.1, 5.6 Hz, 2H), 1.44 (tt, J = 7.9, 6.4 Hz, 2H), 1.29 (m, 2H), 0.88 (t, J = 7.32 Hz, 3H); ^{13}C NMR (100 MHz, DMSO-d_6): δ (ppm) = 167.7, 161.0 (d, J = 241.8 Hz), 159.3, 159.1, 137.1, 136.7 (d, J = 3.0 Hz), 129.2 (d, J = 7.9 Hz), 114.8 (d, J = 21.1 Hz), 97.1, 96.0, 43.0, 38.4, 31.5, 19.7, 13.7; IR (ATR): $\tilde{\nu}$ = 3419, 3400, 3292, (m, ν_{N-H}), 2961 (w, ν_{C-H}), 1590 (s, $\nu_{C=O}$), 1537 (m, δ_{N-H}); ESI-HRMS: calcd for $[C_{17}H_{21}N_4OF + H]^+$, 317.1772; found, 317.1763; cpd purity (220 nm): 100%.

2-Bromo-1-methyl-4-nitrobenzene (23). A mixture of 1-methyl-4-nitrobenzene (10.00 g, 72.9 mmol) and iron powder (163 mg, 2.92 mmol, 0.04 equiv) was melted by heating to 80 °C. To the resulting melt, bromine (4.48 mL, 87.5 mmol, 1.2 equiv) was added dropwise under stirring over a period of 10 min. Afterward, the reaction mixture was continued to stir at 80 °C. After 1.5 h, a 10% aq solution of KOH (110 mL) was added. A precipitate formed, which was filtered off. The filter cake was dissolved in DCM (250 mL), and the resulting solution was extracted with water (2 × 250 mL). The organic phase was washed with brine, dried over Na_2SO_4, filtrated, and concentrated under reduced pressure. The crude residue was purified by recrystallization (ethanol) to obtain **23** as a colorless solid (8.60 g, 39.8 mmol, 55%): R_f = 0.50 (*n*-hexane); mp 80 °C; ^{1}H NMR (400 MHz, DMSO-d_6): δ (ppm) = 8.38 (d, J = 2.4 Hz, 1H), 8.16 (dd, J = 8.4, 2.4 Hz, 1H), 7.66 (dd, J = 8.4, 0.8 Hz, 1H), 2.47 (d, J = 0.6 Hz, 3H); ^{13}C NMR (100 MHz, DMSO-d_6): δ (ppm) = 146.3, 145.7, 131.8, 126.7, 124.2, 122.5, 22.6; IR (ATR): $\tilde{\nu}$ = 3094, 2961 (w, ν_{C-H}), 1517 (m, ν_{N-O}).

2-Bromo-4-nitrobenzoic Acid (24). 2-Bromo-1-methyl-4-nitrobenzene (8.50 g, 39.4 mmol) was suspended in a mixture of water (34 mL) and pyridine (68 mL). The mixture was heated to 100 °C, and $KMnO_4$ was added in 10 portions at 30 min intervals (in total 34.82 g, 220.4 mmol, 5.6 equiv). After the last 30 min interval, additional $KMnO_4$ (3.33 g, 59.0 mmol, 1.5 equiv) was added, and the reaction mixture was continued to stir for 12 h at 100 °C. Afterward, the reaction mixture was cooled to room temperature and filtered through a pad of Celite. The filtrate was cooled to 0 °C, and the product was precipitated by the addition of conc. aq HCl. The resulting precipitate was filtered off and recrystallized (ethyl acetate) to obtain **24** as a colorless solid (1.72 g, 7.0 mmol, 18%): R_f = 0.74 (*n*-butanol/AcOH/water 8:1:1); mp 127 °C; ^{1}H NMR (400 MHz, DMSO-d_6): δ (ppm) = 14.06 (s, 1H), 8.48 (d, J = 2.2 Hz, 1H), 8.22 (dd, J = 8.5, 2.2 Hz, 1H), 7.95 (d, J = 8.5 Hz, 1H); ^{13}C NMR (100 MHz, DMSO-d_6): δ (ppm) = 166.5, 148.7, 140.1, 131.1, 128.2, 122.8, 119.9; IR (ATR): $\tilde{\nu}$ = 3097 (w, ν_{C-H}), 1517 (m, ν_{N-O}).

2-Bromo-*N*-isobutyl-4-nitrobenzamide (25a). 2-Bromo-4-nitrobenzoic acid (1.00 g, 4.1 mmol) was dissolved in toluene (50 mL) and treated with thionyl chloride (650 μL, 8.95 mmol, 2.2 equiv) at room temperature. The reaction mixture was stirred at 120 °C for 8 h. Subsequently, the volatiles were removed under reduced pressure. The residue was dissolved in toluene and concentrated under reduced pressure again. The resulting oil was dissolved in DCM (20 mL) and added dropwise to a solution of isobutylamine (1223 μL, 12.21 mmol, 3.0 equiv) in DCM (20 mL) at 0 °C under stirring. Thereafter, the reaction mixture was warmed to room temperature and stirred for 16 h. Afterward, it was extracted successively with a sat. aq $NaHCO_3$ solution (50 mL) and a 1 M aq HCl solution (50 mL). The organic phase was washed with brine, dried over Na_2SO_4, filtrated, and concentrated under reduced pressure. The crude residue was purified by recrystallization (ethanol/water) to obtain **25a** as a colorless solid (880 mg, 2.92 mmol, 72%): R_f = 0.50 (ethyl acetate/*n*-hexane 3:7); mp 136 °C; ^{1}H NMR (400 MHz, DMSO-d_6): δ (ppm) = 8.66 (t, J = 5.9 Hz, 1H), 8.45 (d, J = 2.2 Hz, 1H), 8.26 (dd, J = 8.4, 2.3 Hz, 1H), 7.64 (d, J = 8.4 Hz, 1H), 3.08 (dd, J = 6.8, 5.9 Hz, 2H), 1.82 (dq, J = 13.4, 6.7 Hz, 1H), 0.93 (d, J = 6.7 Hz, 6H); ^{13}C NMR (100 MHz, DMSO-d_6): δ (ppm) = 165.9, 147.9, 145.3, 129.7, 127.4, 122.8, 119.4, 46.5, 28.0, 20.2; IR (ATR): $\tilde{\nu}$ = 3246 (m, ν_{N-H}), 3098, 2958 (w, ν_{C-H}), 1642 (s, $\nu_{C=O}$), 1592 (m, δ_{N-H}), 1519 (m, ν_{N-O}).

2-Bromo-*N*-(4-fluorobenzyl)-4-nitrobenzamide (25b). 2-Bromo-4-nitrobenzoic acid (1.50 g, 6.1 mmol) was dissolved in toluene (75 mL) and treated with thionyl chloride (974 μL, 13.41 mmol, 2.2 equiv) at room temperature. The reaction mixture was stirred at 120 °C for 2.5 h. Subsequently, the volatiles were removed under reduced pressure. The residue was dissolved in toluene and concentrated under reduced pressure again. The resulting oil was dissolved in DCM (20 mL) and added dropwise to a solution of 4-fluorobenzylamine (1046 μL, 9.15 mmol, 1.5 equiv) and TEA (1691 μL, 12.20 mmol, 2.0 equiv) in DCM (20 mL) at 0 °C under stirring. Thereafter, the reaction mixture was warmed to room temperature and stirred for 2.5 h. Afterward, it was extracted successively with a sat. aq $NaHCO_3$ solution (50 mL) and a 1 M aq HCl solution (50 mL). The organic phase was washed with brine, dried over Na_2SO_4, filtrated, and concentrated under reduced pressure. The crude residue was purified by recrystallization (ethanol/water) to obtain **25b** as a beige solid (910 mg, 2.58 mmol, 42%): R_f = 0.72 (ethyl acetate/*n*-hexane 1:1); mp 184 °C; ^{1}H NMR (400 MHz, DMSO-d_6): δ (ppm) = 9.20 (t, J = 6.0 Hz, 1H), 8.46 (d, J = 2.2 Hz, 1H), 8.28 (dd, J = 8.4, 2.2 Hz, 1H), 7.70 (d, J = 8.4 Hz, 1H), 7.42 (m, 2H), 7.19 (m, 2H), 4.47 (d, J = 5.92 Hz, 2H); ^{13}C NMR (100 MHz,

https://doi.org/10.1021/acsomega.1c07103
ACS Omega 2022, 7, 7989−8012

DMSO-d_6): δ (ppm) = 165.9, 161.3 (d, J = 242.6 Hz), 148.1, 144.6, 134.8 (d, J = 3.0 Hz), 129.8, 129.4 (d, J = 8.1 Hz), 127.5, 122.8, 119.5, 115.1 (d, J = 21.4 Hz), 41.8; IR (ATR): $\tilde{\nu}$ = 3256 (m, ν_{N-H}), 3075, 2941 (w, ν_{C-H}), 1638 (s, $\nu_{C=O}$), 1588 (m, δ_{N-H}), 1521 (m, ν_{N-O}).

***N*-Isobutyl-2-methoxy-4-nitrobenzamide (26a).** 2-Bromo-*N*-isobutyl-4-nitrobenzamide (1.20 g, 4.0 mmol) was dissolved in methanol (20 mL). CuI (76 mg, 0.40 mmol, 0.1 equiv), K_2CO_3 (1.10 g, 8.0 mmol, 2.0 equiv), and ethane-1,2-diamine (13 μL, 0.20 mmol, 0.05 equiv) were added. Subsequently, the reaction mixture was set under a nitrogen atmosphere and stirred at 95 °C. After 15 h, it was filtered hot, and the resulting filtrate was concentrated under reduced pressure. The crude residue was purified by silica gel column chromatography (ethyl acetate/*n*-hexane 3:7) and successive recrystallization (methanol/water) to obtain **26a** as a colorless solid (460 mg, 1.82 mmol, 46%): R_f = 0.65 (ethyl acetate/*n*-hexane 3:7); mp 101 °C; ^{1}H NMR (400 MHz, DMSO-d_6): δ (ppm) = 7.87 (m, 1H), 8.34 (t, J = 5.6 Hz, 1H), 7.86 (s, 1H), 7.75 (m, 1H), 3.97 (s, 3H), 3.10 (dd, J = 6.9, 6.0 Hz, 2H), 1.82 (m, 1H), 0.91 (d, J = 6.7 Hz, 6H); ^{13}C NMR (100 MHz, DMSO-d_6): δ (ppm) = 164.0, 156.8, 149.1, 130.5, 131.3, 115.4, 106.7, 56.5, 46.5, 28.0, 20.0; IR (ATR): $\tilde{\nu}$ = 3314 (m, ν_{N-H}), 3118, 2956 (w, ν_{C-H}), 1642 (s, $\nu_{C=O}$), 1545 (m, δ_{N-H}), 1517 (m, ν_{N-O}).

***N*-(4-Fluorobenzyl)-2-methoxy-4-nitrobenzamide (26b).** The synthesis was carried out as described for **26a**. 2-Bromo-*N*-(4-fluorobenzyl)-4-nitrobenzamide (800 mg, 2.27 mmol), methanol (25 mL), CuI (43 mg, 0.40 mmol 0.1 equiv), K_2CO_3 (627 mg, 4.54 mmol, 2.0 equiv), and ethane-1,2-diamine (7.6 μL, 0.11 mmol, 0.05 equiv) were used. The title compound was obtained as a colorless solid (350 mg, 1.15 mmol, 51%): R_f = 0.58 (ethyl acetate/*n*-hexane 1:1); mp 104 °C; ^{1}H NMR (400 MHz, DMSO-d_6): δ (ppm) = 8.93 (t, J = 6.0 Hz, 1H), 7.88 (m, 2H), 7.82 (d, J = 8.9 Hz, 1H), 7.38 (m, 2H), 7.17 (m, 2H), 4.47 (d, J = 6.1 Hz, 2H), 3.99 (s, 3H); ^{13}C NMR (100 MHz, DMSO-d_6): δ (ppm) = 164.1, 161.2 (d, J = 242.1 Hz), 157.0, 149.3, 135.4 (d, J = 3.0 Hz), 130.7, 130.5, 129.0 (d, J = 8.1 Hz), 115.4, 115.0 (d, J = 21.3 Hz), 106.9, 56.6, 41.9; IR (ATR): $\tilde{\nu}$ = 3372 (m, ν_{N-H}), 3013, 2946 (w, ν_{C-H}), 1641 (s, $\nu_{C=O}$), 1605 (m, δ_{N-H}), 1508 (m, ν_{N-O}).

4-Amino-*N*-isobutyl-2-methoxybenzamide (27a). *N*-Isobutyl-2-methoxy-4-nitrobenzamide (440 mg, 1.74 mmol) was dissolved in ethyl acetate (35 mL). $SnCl_2$ (1.65 g, 8.7 mmol, 5.0 equiv) was added, and the mixture was stirred at 80 °C for 30 min. Afterward, it was cooled to room temperature, and a sat. aq $NaHCO_3$ solution (100 mL) was added. The resulting mixture was extracted with ethyl acetate (2 × 100 mL). The combined organic phases were washed with brine, dried over Na_2SO_4, filtrated, and concentrated under reduced pressure to obtain **27a** as a brown oil (380 mg, 1.71 mmol, 98%): R_f = 0.78 (ethyl acetate); ^{1}H NMR (400 MHz, DMSO-d_6): δ (ppm) = 7.81 (t, J = 5.8 Hz, 1H), 7.60 (d, J = 8.4 Hz, 1H), 6.24 (d, J = 2.0 Hz, 1H), 6.19 (dd, J = 8.4, 2.0 Hz, 1H), 5.68 (s, 2H), 3.82 (s, 3H), 3.09 (dd, J = 6.8, 5.8 Hz, 2H), 1.78 (m, 1H), 0.88 (d, J = 6.7 Hz, 6H); ^{13}C NMR (100 MHz, DMSO-d_6): δ (ppm) = 164.7, 158.8, 153.1, 132.5, 109.2, 106.1, 96.1, 55.5, 46.2, 28.1, 20.1; IR (ATR): $\tilde{\nu}$ = 3402, 3339, 3222, (m, ν_{N-H}), 2957 (w, ν_{C-H}), 1628 (s, $\nu_{C=O}$), 1595 (s, δ_{N-H}).

4-Amino-*N*-(4-fluorobenzyl)-2-methoxybenzamide (27b). The synthesis was carried out as described for **27a**. *N*-(4-Fluorobenzyl)-2-methoxy-4-nitrobenzamide (300 mg, 0.99 mmol) and $SnCl_2$ (935 mg, 4.93 mmol, 5.0 equiv) were used. The title compound was obtained as a brown solid (280 mg, 1.02 mmol, 100%): R_f = 0.35 (ethyl acetate/*n*-hexane 6:4); mp 126 °C; ^{1}H NMR (400 MHz, DMSO-d_6): δ (ppm) = 8.35 (t, J = 6.1 Hz, 1H), 7.63 (d, J = 8.5 Hz, 1H), 7.32 (m, 2H), 7.13 (m, 2H), 6.24 (d, J = 2.0 Hz, 1H), 6.19 (dd, J = 8.6, 2.0 Hz, 1H), 5.72 (s, 2H), 4.44 (d, J = 6.1 Hz, 2H), 3.81 (s, 3H); ^{13}C NMR (100 MHz, DMSO-d_6): δ (ppm) = 164.9, 161.0 (d, J = 241.7 Hz), 159.1, 153.3, 136.6 (d, J = 2.9 Hz), 132.6, 129.0 (d, J = 8.0 Hz), 114.9 (d, J = 21.1 Hz), 108.7, 106.1, 95.9, 55.4, 41.7; IR (ATR): $\tilde{\nu}$ = 3446, 3392, 3346 (m, ν_{N-H}), 1627 (s, $\nu_{C=O}$), 1588 (m, δ_{N-H}).

4-[(4-Fluorobenzyl)amino]-*N*-isobutyl-2-methoxybenzamide (28a). The synthesis was carried out according to general procedure A. 4-Amino-*N*-isobutyl-2-methoxybenzamide (360 mg, 1.62 mmol), 4-fluorobenzaldehyde (209 μL, 1.94 mmol, 1.2 equiv), toluene (30 mL), and 4 Å molecular sieves (3.0 g) were used in the first reaction step. In the second step, the reduction was performed by using 258 mg of sodium borohydride (6.80 mmol, 4.2 equiv). The purification by silica gel column chromatography (ethyl acetate/*n*-hexane 7:3) afforded **28a** as a colorless solid (220 mg, 0.67 mmol, 41%): R_f = 0.59 (ethyl acetate/*n*-hexane 7:3); mp 154 °C; ^{1}H NMR (400 MHz, DMSO-d_6): δ (ppm) = 7.80 (t, J = 5.8 Hz, 1H), 7.61 (d, J = 8.5 Hz, 1H), 7.39 (m, 2H), 7.15 (m, 2H), 6.83 (t, J = 6.1 Hz, 1H), 6.25 (d, J = 2.1 Hz, 1H), 6.22 (dd, J = 8.5, 2.1 Hz, 1H), 4.31 (d, J = 6.0 Hz, 2H), 3.80 (s, 3H), 3.08 (dd, J = 6.8, 5.9 Hz, 2H), 1.77 (m, 1H), 0.87 (d, J = 6.7 Hz, 6H); ^{13}C NMR (100 MHz, DMSO-d_6): δ (ppm) = 164.7, 161.1 (d, J = 242.0 Hz), 158.7, 152.3, 135.8 (d, J = 3.1 Hz), 132.3, 129.1 (d, J = 8.1 Hz), 115.0 (d, J = 21.2 Hz), 109.6, 104.5, 95.0, 55.5, 46.2, 45.3, 28.1, 20.1; IR (ATR): $\tilde{\nu}$ = 3404, 3299 (m, ν_{N-H}), 3068, 2954 (w, ν_{C-H}), 1629 (s, $\nu_{C=O}$), 1593 (s, δ_{N-H}); ESI-HRMS: calcd for $[C_{19}H_{23}N_2O_2F + H]^+$, 331.1816; found, 331.1803; cpd purity (220 nm): 100%.

***N*-(4-Fluorobenzyl)-4-[(4-fluorobenzyl)amino]-2-methoxybenzamide (28b).** The synthesis was carried out according to general procedure A. 4-Amino-*N*-(4-fluorobenzyl)-2-methoxybenzamide (250 mg, 0.91 mmol), 4-fluorobenzaldehyde (196 μL, 1.08 mmol, 1.2 equiv), toluene (20 mL), and 4 Å molecular sieves (2.0 g) were used in the first reaction step. In the second step, the reduction was performed by using 96 mg of sodium borohydride (2.55 mmol, 2.8 equiv). The purification by silica gel column chromatography (ethyl acetate/*n*-hexane 1:1) afforded **28b** as a colorless solid (240 mg, 0.63 mmol, 69%): R_f = 0.42 (ethyl acetate/*n*-hexane 3:2); mp 180 °C; ^{1}H NMR (400 MHz, DMSO-d_6): δ (ppm) = 8.35 (t, J = 6.1 Hz, 1H), 7.64 (d, J = 8.4 Hz, 1H), 7.39 (m, 2H), 7.31 (m, 2H), 7.13 (m, 4H), 6.87 (t, J = 6.0 Hz, 1H), 6.24 (m, 2H), 4.43 (d, J = 6.1 Hz, 2H), 4.32 (d, J = 6.0 Hz, 2H), 3.79 (s, 3H); ^{13}C NMR (100 MHz, DMSO-d_6): δ (ppm) = 164.8, 161.1 (d, J = 240.0 Hz), 161.0 (d, J = 240.0 Hz), 158.9, 152.6, 136.5 (d, J = 2.9 Hz), 135.8 (d, J = 2.9 Hz), 132.5, 129.2 (d, J = 8.1 Hz), 129.0 (d, J = 8.1 Hz), 115.1 (d, J = 18.5 Hz), 114.8 (d, J = 18.5 Hz), 109.2, 104.5, 94.9, 55.4, 45.3, 41.7; IR (ATR): $\tilde{\nu}$ = 3401, 3324 (m, ν_{N-H}), 3022, 2922 (w, ν_{C-H}), 1591 (s, $\nu_{C=O}$), 1542 (m, δ_{N-H}); ESI-HRMS: calcd for $[C_{22}H_{20}N_2O_2F_2 + H]^+$, 383.1566; found, 383.1564; cpd purity (220 nm): 100%.

2,6-Dihydroxy-4-methylnicotinonitrile (31). 2-Cyanoacetamide (28.0 g, 400 mmol), ethyl 3-oxobutanoate (50.5 mL, 400.0 mmol, 1.0 equiv), and KOH (28.0 g, 508 mmol, 1.3 equiv) were dissolved in methanol (200 mL). The reaction

https://doi.org/10.1021/acsomega.1c07103
ACS Omega 2022, 7, 7989−8012

mixture was stirred at 65 °C. After 2 h, it was cooled to room temperature. A colorless precipitate, which was formed while cooling, was filtered off and washed with ethanol. Afterward, the filter cake was redissolved in hot water. The resulting solution was acidified with conc. aq HCl, and again a precipitate formed, which was filtered off and washed with ethanol to obtain **31** as a colorless solid (45.1 g, 300 mmol, 75%): R_f = 0.70 (*n*-butanol/AcOH/water 8:1:1); mp decomp.; ^{1}H NMR (400 MHz, DMSO-d_6): δ (ppm) = 5.25 (s, 1H), 2.09 (s, 3H); ^{13}C NMR HMBC (100 MHz, DMSO-d_6): δ (ppm) = 163.4 (5), 162.9 (1), 157.1 (3), 119.2 (7), 95.6 (2), 82.7 (4), 20.6 (6); IR (ATR): $\tilde{\nu}$ = 2221 (m, $\nu_{C\equiv N}$).

2,6-Dichloro-4-methylnicotinonitrile (32). 2,6-Dihydroxy-4-methylnicotinonitrile (1.25 g, 8.3 mmol) and benzyltrimethylammonium chloride (7.50 g, 40.4 mmol, 4.9 equiv) were dissolved in phosphorus oxychloride (8.0 mL, 87.7 mmol, 10.5 equiv). The reaction mixture was stirred at 90 °C in an apparatus equipped with a reflux condenser and a $CaCl_2$ drying tube. After 16 h, it was cooled to room temperature and carefully poured on ice water. A colorless precipitate formed, which was filtered off and washed with water. The crude product was recrystallized from methanol/water to obtain the title product as a colorless solid (857 mg, 4.58 mmol, 55%): R_f = 0.74 (ethyl acetate/*n*-hexane 1:3); mp 112 °C; ^{1}H NMR (400 MHz, DMSO-d_6): δ (ppm) = 7.82 (q, J = 0.7 Hz, 1H), 2.54 (d, J = 0.7 Hz, 3H); ^{13}C NMR (100 MHz, DMSO-d_6): δ (ppm) = 158.2, 152.2, 150.8, 124.8, 113.7, 110.1, 20.1; IR (ATR): $\tilde{\nu}$ = 3058, 2978 (w, ν_{C-H}), 2221 (m, $\nu_{C\equiv N}$).

2,6-Dichloro-4-methylnicotinic Acid (33). 2,6-Dichloro-4-methylnicotinonitrile (5.89 g, 31.5 mmol) was suspended in a mixture of conc. sulfuric acid (13.0 mL) and conc. nitric acid (4.5 mL). The mixture was stirred at 105 °C. After 2 h, it was cooled to room temperature and carefully poured on ice water (250 mL). The resulting aq suspension was extracted with ethyl acetate (3 × 250 mL). The combined organic phases were washed with brine, dried over Na_2SO_4, and concentrated under reduced pressure. The resulting residue was redissolved in a 1 M aq NaOH solution (100 mL). Afterward, the solution was filtered, and the filtrate was acidified with conc. aq HCl. A precipitate formed, which was filtered off and washed with water to obtain **33** as a colorless solid (5.01 g, 24.3 mmol, 77%): R_f = 0.59 (*n*-butanol/AcOH/water 8:1:1); mp 141 °C; ^{1}H NMR (400 MHz, DMSO-d_6): δ (ppm) = 14.22 (s, 1H), 7.61 (s, 1H), 2.35 (s, 3H); ^{13}C NMR (100 MHz, DMSO-d_6): δ (ppm) = 166.0, 150.7, 148.7, 144.6, 130.5, 124.9, 18.7; IR (ATR): $\tilde{\nu}$ = 3300−2500 (b, ν_{O-H}), 1699 (s, $\nu_{C=O}$).

6-Chloro-2-methoxy-4-methylnicotinic Acid (34). A 60% suspension of NaH in mineral oil (2.43 g, 60.7 mmol, 2.5 equiv) was suspended in dry THF (50 mL) under an atmosphere of argon. The mixture was cooled to 0 °C. Methanol (1080 μL, 26.70 mmol, 1.1 equiv) and a solution of 2,6-dichloro-4-methylnicotinic acid (5.00 g, 24.3 mmol) in dry THF (50 mL) were added successively. The reaction mixture was warmed to 70 °C and stirred for 7 h while maintaining the temperature. Subsequently, the reaction mixture was cooled to room temperature and quenched by adding water (100 mL). The resulting aq mixture was adjusted to pH 12 by the addition of a 2 M aq NaOH solution and extracted with ethyl acetate (100 mL). The organic phase was discarded, and the aq phase was adjusted to pH 2−3 with conc. aq HCl. Subsequently, it was extracted with ethyl acetate (2 × 200 mL). The combined organic phases were washed with brine, dried over Na_2SO_4, filtrated, and concentrated under reduced pressure to obtain **34** as a beige solid (4.72 g, 23.4 mmol, 96%): R_f = 0.78 (*n*-butanol/AcOH/water 8:1:1); mp 166 °C; ^{1}H NMR (400 MHz, DMSO-d_6): δ (ppm) = 13.39 (s, 1H), 7.09 (s, 1H), 3.87 (s, 3H), 2.17 (s, 3H); ^{13}C NMR (100 MHz, DMSO-d_6): δ (ppm) = 166.6, 159.4, 149.8, 147.0, 117.4, 118.0, 54.3, 18.4; IR (ATR): $\tilde{\nu}$ = 3002, 2954 (w, ν_{C-H}), 3300−2500 (b, ν_{O-H}), 1686 (s, $\nu_{C=O}$).

***N*-Butyl-6-chloro-2-methoxy-4-methylnicotinamide (35a).** 6-Chloro-2-methoxy-4-methylnicotinic acid (2.19 g, 10.9 mmol) was dissolved in dry THF (15 mL), and one drop of dry dimethylformamide (DMF) was added. The mixture was cooled to 0 °C, and a solution of oxalyl chloride (1860 μL, 21.75 mmol, 2.0 equiv) in dry THF (15 mL) was added dropwise. After complete addition, the cooling was removed, and the reaction mixture was stirred at room temperature for 2 h. Subsequently, all volatiles were removed under reduced pressure, and the residue was dissolved in 20 mL of dry THF. The resulting solution was added dropwise to a solution of *n*-butylamine (3.22 mL, 32.6 mmol, 3.0 equiv) in dry THF (20 mL) at 0 °C. Afterward, the cooling was removed, and the reaction mixture was stirred at room temperature. After 16 h, ethyl acetate (200 mL) was added. The resulting solution was extracted with water (2 × 100 mL), washed with brine, dried over Na_2SO_4, filtrated, and concentrated under reduced pressure. The crude residue was purified by silica gel column chromatography (ethyl acetate/*n*-hexane 3:7), which yielded **35a** as a colorless solid (1.71 g, 6.7 mmol, 61%): R_f = 0.81 (ethyl acetate/*n*-hexane 2:1); mp 57 °C; ^{1}H NMR (400 MHz, DMSO-d_6): δ (ppm) = 8.30 (t, J = 5.7 Hz, 1H), 7.04 (s, 1H), 3.82 (s, 3H), 3.19 (td, J = 6.9, 5.7 Hz, 2H), 2.19 (s, 3H), 1.45 (m, 2H), 1.34 (m, 2H), 0.89 (t, J = 7.3 Hz, 3H); ^{13}C NMR (100 MHz, DMSO-d_6): δ (ppm) = 164.1, 159.6, 149.7, 146.1, 120.4, 117.8, 54.0, 38.3, 31.0, 19.5, 18.0, 13.6; IR (ATR): $\tilde{\nu}$ = 3220 (m, ν_{N-H}), 3068, 2961 (w, ν_{C-H}), 1645 (s, $\nu_{C=O}$), 1624 (m, δ_{N-H}).

6-Chloro-*N*-(4-fluorobenzyl)-2-methoxy-4-methylnicotinamide (35b). 6-Chloro-2-methoxy-4-methylnicotinic acid (500 mg, 2.48 mmol) was dissolved in dry THF (15 mL), and one drop of dry DMF was added. The mixture was cooled to 0 °C, and a solution of oxalyl chloride (638 μL, 7.44 mmol, 3.0 equiv) in dry THF (15 mL) was added dropwise. After complete addition, the cooling was removed, and the reaction mixture was stirred at room temperature for 3 h. Subsequently, all volatiles were removed under reduced pressure. The residue was dissolved in 10 mL of dry DCM. The resulting solution was added dropwise to a solution of 4-fluorobenzylamine (340 μL, 2.98 mmol, 1.2 equiv) and TEA (691 μL, 4.96 mmol, 2.0 equiv) in dry DCM (10 mL) at 0 °C. Afterward, the cooling was removed, and the reaction mixture was stirred at room temperature. After 16 h, additional DCM (100 mL) was added. The resulting solution was extracted successively with a saturated aq $NaHCO_3$ solution (100 mL) and a 2 M aq HCl solution (100 mL). The organic phase was washed with brine, dried over Na_2SO_4, filtrated, and concentrated under reduced pressure. The crude residue was purified by silica gel column chromatography (ethyl acetate/*n*-hexane 3:2), which yielded **35b** as a colorless solid (402 mg, 1.30 mmol, 53%): R_f = 0.29 (ethyl acetate/*n*-hexane 1:1); mp 127 °C; ^{1}H NMR (400 MHz, DMSO-d_6): δ (ppm) = 8.89 (t, J = 6.0 Hz, 1H), 7.38 (m, 2H), 7.18 (m, 2H), 7.05 (d, J = 0.6 Hz, 1H), 4.42 (d, J = 6.0 Hz, 2H), 3.86 (s, 3H), 2.18 (d, J = 0.6 Hz, 3H); ^{13}C NMR (100 MHz, DMSO-d_6): δ (ppm) = 164.5, 161.2 (d, J = 242.1 Hz), 159.6, 149.9, 146.4, 135.3 (d, J

https://doi.org/10.1021/acsomega.1c07103
ACS Omega 2022, 7, 7989−8012

= 3.0 Hz), 129.1 (d, J = 8.1 Hz), 119.9, 117.9, 115.0 (d, J = 21.3 Hz), 54.1, 41.5, 18.0; IR (ATR): $\tilde{\nu}$ = 3310 (m, ν_{N-H}), 3067, 2954 (w, ν_{C-H}), 1635 (s, $\nu_{C=O}$), 1604 (m, δ_{N-H}).

***N*-Butyl-6-[(4-fluorobenzyl)amino]-2-methoxy-4-methylnicotinamide (36a).** In a microwave vessel, *N*-butyl-6-chloro-2-methoxy-4-methylnicotinamide (788 mg, 3.07 mmol) was dissolved in 4-fluorobenzylamine (2.50 mL, 21.77 mmol, 7.1 equiv). The mixture was stirred in a microwave reactor at 165 °C for 1 h in a closed vessel. Subsequently, the reaction mixture was cooled to room temperature, dissolved in ethyl acetate (200 mL), and extracted with water (2 × 100 mL). The organic phase was washed with brine, dried over Na_2SO_4, filtrated, and concentrated under reduced pressure. The crude residue was purified by flash chromatography (mobile phase: ethyl acetate/*n*-hexane with 0−60% ethyl acetate) and successive recrystallization (ethanol/water), which yielded **36a** as a colorless solid (73 mg, 0.21 mmol, 7%): R_f = 0.61 (ethyl acetate/*n*-hexane 2:1); mp 132 °C; ^{1}H NMR (400 MHz, DMSO-d_6): δ (ppm) = 7.84 (t, J = 5.7 Hz, 1H), 7.35 (m, 2H), 7.16 (t, J = 5.7 Hz, 1H), 5.88 (s, 1H), 7.11 (m, 2H), 4.42 (d, J = 6.1 Hz, 2H), 3.69 (s, 3H), 3.12 (td, J = 6.8, 5.7 Hz, 2H), 2.04 (s, 3H), 1.41 (m, 2H), 1.31 (m, 2H), 0.87 (t, J = 7.3 Hz, 3H); ^{13}C NMR (100 MHz, DMSO-d_6): δ (ppm) = 166.0, 161.0 (d, J = 241.65 Hz), 159.3, 156.5, 147.5, 137.1 (d, J = 3.0 Hz), 129.0 (d, J = 8.0 Hz), 114.8 (d, J = 21.1 Hz), 108.3, 100.0, 52.6, 43.5, 38.3, 31.2, 19.5, 18.9, 13.7; IR (ATR): $\tilde{\nu}$ = 3281 (m, ν_{N-H}), 2944 (w, ν_{C-H}), 1601 (s, $\nu_{C=O}$), 1544 (m, δ_{N-H}); ESI-HRMS: calcd for $[C_{19}H_{25}N_3O_2F + H]^+$, 346.1925; found, 346.1929; cpd purity (220 nm): 100%.

***N*-(4-Fluorobenzyl)-6-[(4-fluorobenzyl)amino]-2-methoxy-4-methylnicotinamide (36b).** The synthesis was carried out as described for **36a**. 6-Chloro-*N*-(4-fluorobenzyl)-2-methoxy-4-methylnicotinamide (400 mg, 1.30 mmol) and 4-fluorobenzylamine (1490 μL, 12.96 mmol, 10.0 equiv) were used. The purification by flash chromatography (mobile phase: ethyl acetate/*n*-hexane with 50−100% ethyl acetate) and successive recrystallization (ethanol/water) afforded **36b** as a colorless solid (121 mg, 0.31 mmol, 23%): R_f = 0.80 (ethyl acetate/*n*-hexane 3:2); mp 148 °C; ^{1}H NMR (400 MHz, DMSO-d_6): δ (ppm) = 8.44 (t, J = 6.2 Hz, 1H), 7.36 (m, 4H), 7.22 (t, J = 6.2 Hz, 1H), 7.14 (m, 4H), 5.90 (s, 1H), 4.43 (d, J = 6.0 Hz, 2H), 4.35 (d, J = 6.1 Hz, 2H), 3.73 (s, 3H), 2.04 (s, 3H); ^{13}C NMR (100 MHz, DMSO-d_6): δ (ppm) = 166.3, 161.0 (d, J = 240.0 Hz), 161.0 (d, J = 240.0 Hz), 159.4, 156.7, 147.8, 137.0 (d, J = 2.9 Hz), 136.0 (d, J = 2.9 Hz), 129.1 (d, J = 8.1 Hz), 128.9 (d, J = 8.1 Hz), 114.8 (d, J = 21.2 Hz), 114.8 (d, J = 21.2 Hz), 107.6, 100.2, 52.7, 43.5, 41.5, 19.0; IR (ATR): $\tilde{\nu}$ = 3325 (m, ν_{N-H}), 3040, 2920 (w, ν_{C-H}), 1605 (s, $\nu_{C=O}$), 1537 (m, δ_{N-H}). ESI-HRMS: calcd for $[C_{22}H_{22}N_3O_2F_2 + H]^+$, 398.1675; found, 398.1671; cpd purity (220 nm): 100%.

***N*-(4-Fluorobenzyl)-6-[(4-fluorobenzyl)amino]-4-methyl-2-oxo-1,2-dihydropyridine-3-carboxamide (37).** *N*-(4-Fluorobenzyl)-6-[(4-fluorobenzyl)amino]-4-methyl-2-oxo-1,2-dihydropyridine-3-carboxamide was a side product in the synthesis of *N*-(4-fluorobenzyl)-6-[(4-fluorobenzyl)-amino]-2-methoxy-4-methylnicotinamide. It was separated from the main product by flash chromatography and was further purified by recrystallization (ethanol/water). The title compound was obtained as a colorless solid (108 mg, 0.28 mmol, 22%): R_f = 0.48 (ethyl acetate); mp 196 °C; ^{1}H NMR (400 MHz, DMSO-d_6): δ (ppm) = 10.97 (s, 1H), 10.17 (s, 1H), 7.38 (m, 2H), 7.31 (m, 2H), 7.19 (m, 2H), 7.13 (m, 2H), 7.06 (t, J = 5.8 Hz, 1H), 5.45 (s, 1H), 4.40 (d, J = 6.1 Hz, 2H), 4.38 (d, J = 5.8 Hz, 2H) 2.43 (s, 3H); ^{13}C NMR (100 MHz, DMSO-d_6): δ (ppm) = 166.3, 162.8, 161.4 (d, J = 242.0 Hz), 161.0 (d, J = 241.0 Hz), 150.6, 136.5 (d, J = 3.0 Hz), 134.3 (d, J = 3.0 Hz), 129.2 (d, J = 8.2 Hz), 129.1 (d, J = 8.0 Hz), 115.3 (d, J = 21.4 Hz), 114.9 (d, J = 21.0 Hz), 103.7, 91.8, 43.9, 41.1, 23.8 (one signal is missing, perhaps due to peak overlap); IR (ATR): $\tilde{\nu}$ = 3337 (m, ν_{N-H}), 3035, 2978 (w, ν_{C-H}), 1619 (s, $\nu_{C=O}$), 1603 (m, δ_{N-H}).

Methyl 4-Amino-2-bromobenzoate (39). Methyl 2-bromo-4-nitrobenzoate (2.00 g, 7.7 mmol) was dissolved in ethyl acetate (100 mL). $SnCl_2$ (7.29 g, 38.5 mmol, 5.0 equiv) was added, and the mixture was stirred at 70 °C for 4 h. Afterward, it was cooled to room temperature, and a sat. aq $NaHCO_3$ solution (100 mL) was added. The phases were separated, and the aq phase was extracted with ethyl acetate (2 × 100 mL). The combined organic phases were washed with brine, dried over Na_2SO_4, and filtered through a pad of silica gel. The silica gel pad was rinsed with additional ethyl acetate, and the combined filtrates were concentrated under reduced pressure to obtain **39** as a colorless solid (1.61 g, 7.0 mmol, 91%): R_f = 0.34 (ethyl acetate/*n*-hexane 1:4); mp 96 °C; ^{1}H NMR (400 MHz, DMSO-d_6): δ (ppm) = 7.63 (d, J = 8.6 Hz, 1H), 6.86 (d, J = 2.2 Hz, 1H), 6.55 (dd, J = 8.6, 2.3 Hz, 1H), 6.14 (s, 2H), 3.73 (s, 3H); ^{13}C NMR (100 MHz, DMSO-d_6): δ (ppm) = 165.0, 153.4, 133.5, 123.1, 118.0, 115.5, 111.9, 51.5; IR (ATR): $\tilde{\nu}$ = 3408, 3320 (m, ν_{N-H}), 3082, 2950 (w, ν_{C-H}), 1638 (s, $\nu_{C=O}$), 1634 (m, δ_{N-H}).

Methyl 2-Bromo-4-[(4-fluorobenzyl)amino]benzoate (40). The synthesis was carried out according to general procedure A. Methyl 4-amino-2-bromobenzoate (1.63 g, 7.1 mmol), 4-fluorobenzaldehyde (758 μL, 7.06 mmol, 1.0 equiv), toluene (50 mL), and 4 Å molecular sieves (5.0 g) were used in the first reaction step. In the second step, the reduction was performed by using 1.19 g of sodium borohydride (35.3 mmol, 5.0 equiv). The purification by silica gel column chromatography (ethyl acetate/*n*-hexane 2:8) afforded **40** as a colorless solid (2.09 g, 6.17 mmol, 87%): R_f = 0.53 (ethyl acetate/*n*-hexane 2:8); mp 80 °C; ^{1}H NMR (400 MHz, DMSO-d_6): δ (ppm) = 7.65 (d, J = 8.7 Hz, 1H), 7.37 (m, 2H), 7.26 (t, J = 6.0 Hz, 1H), 7.17 (m, 2H), 6.87 (d, J = 2.4 Hz, 1H), 6.61 (dd, J = 8.8, 2.4 Hz, 1H), 4.33 (d, J = 5.9 Hz, 2H), 3.73 (s, 3H); ^{13}C NMR (100 MHz, DMSO-d_6): δ (ppm) = 165.0, 161.2 (d, J = 242.4 Hz), 152.4, 135.0 (d, J = 2.9 Hz), 133.3, 129.1 (d, J = 8.1 Hz), 123.2, 116.8, 116.1, 115.2 (d, J = 21.3 Hz), 110.6, 51.5, 44.9; IR (ATR): $\tilde{\nu}$ = 3354 (m, ν_{N-H}), 3024, 2946 (w, ν_{C-H}), 1678 (s, $\nu_{C=O}$), 1585 (m, δ_{N-H}).

Methyl 2-Bromo-4-[(*tert*-butoxycarbonyl)(4-fluorobenzyl)amino]benzoate (41). Methyl 2-bromo-4-[(4-fluorobenzyl)amino]benzoate (2.00 g, 5.9 mmol) was dissolved in DCM (50 mL). TEA (1230 μL, 8.87 mmol, 1.5 equiv), di-*tert*-butyl dicarbonate (1.94 g, 8.9 mmol, 1.5 equiv), and 4-dimethylaminopyridine (72 mg, 0.59 mmol, 0.1 equiv) were added successively. The reaction mixture was stirred at room temperature for 16 h. Afterward, it was concentrated under reduced pressure. The resulting crude residue was directly subjected to silica gel column chromatography (ethyl acetate/*n*-hexane 2:3) to afford **41** as a colorless oil (2.26 g, 5.2 mmol, 87%): R_f = 0.19 (ethyl acetate/*n*-hexane 1:9); ^{1}H NMR (400 MHz, DMSO-d_6): δ (ppm) = 7.72 (d, J = 8.5 Hz, 1H), 7.67 (d, J = 2.1 Hz, 1H), 7.36 (dd, J = 8.5, 2.2 Hz, 1H), 7.24 (m, 2H), 7.14 (m, 2H), 4.91 (s, 2H), 3.82 (s, 3H), 1.40 (s,

https://doi.org/10.1021/acsomega.1c07103
ACS Omega 2022, 7, 7989−8012

9H); ^{13}C NMR (100 MHz, DMSO-d_6): δ (ppm) = 165.5, 161.3 (d, J = 243.0 Hz), 153.2, 145.5, 133.9 (d, J = 3.0 Hz), 131.1, 130.6, 129.0 (d, J = 8.3 Hz), 128.2, 124.6, 120.1, 115.3 (d, J = 21.3 Hz), 81.22, 52.5, 51.2, 27.7; IR (ATR): $\tilde{\nu}$ = 2977 (w, ν_{C-H}), 1730, 1700 (s, $\nu_{C=O}$).

Methyl 4-[(*tert*-Butoxycarbonyl)(4-fluorobenzyl)-amino]-2-[(trimethylsilyl)ethynyl]benzoate (42). Tetrakis(triphenylphosphine)palladium(0) (290 mg, 0.25 mmol, 0.05 equiv) and CuI (96 mg, 0.50 mmol, 0.1 equiv) were set under an argon atmosphere. Methyl 2-bromo-4-[(*tert*-butoxycarbonyl)(4-fluorobenzyl)amino]benzoate (2.20 g, 5.0 mmol) and ethynyl(trimethyl)silane (1070 μL, 7.53 mmol, 1.5 equiv) were dissolved in a mixture of DMF (12 mL) and TEA (8 mL). This solution was degassed using the freeze−pump−thaw method. Afterward, it was added to the mixture of tetrakis(triphenylphosphine)palladium(0) and CuI. The resulting solution was stirred at 60 °C for 4 h. Subsequently, the reaction was quenched by the addition of water (200 mL), and the mixture was extracted with DCM (200 mL). The organic phase was dried over Na_2SO_4, filtrated, and concentrated under reduced pressure. The crude residue was purified by silica gel column chromatography (ethyl acetate/*n*-hexane 1:9), which yielded **42** as a dark-red oil (1.73 g, 3.8 mmol, 76%): R_f = 0.39 (ethyl acetate/*n*-hexane 1:9); ^{1}H NMR (400 MHz, DMSO-d_6): δ (ppm) = 7.79 (d, J = 8.6 Hz, 1H), 7.47 (d, J = 2.2 Hz, 1H), 7.36 (dd, J = 8.6, 2.3 Hz, 1H), 7.23 (m, 2H), 7.14 (m, 2H), 4.90 (s, 2H), 3.81 (s, 3H), 1.39 (s, 9H), 0.23 (s, 9H); ^{13}C NMR (100 MHz, DMSO-d_6): δ (ppm) = 165.4, 161.3 (d, J = 242.8 Hz), 153.2, 145.0, 134.0 (d, J = 3.0 Hz), 130.6, 130.6, 129.0 (d, J = 8.1 Hz), 128.7, 126.0, 122.5, 115.3 (d, J = 21.4 Hz), 102.8, 99.6, 80.9, 52.0, 51.2, 27.7, −0.27; IR (ATR): $\tilde{\nu}$ = 2958 (w, ν_{C-H}), 2157 (w, $\nu_{C\equiv C}$), 1701 (s, $\nu_{C=O}$).

Methyl 4-[(*tert*-Butoxycarbonyl)(4-fluorobenzyl)-amino]-2-ethynylbenzoate (43). Methyl 4-[(*tert*-butoxycarbonyl)(4-fluorobenzyl)amino]-2-[(trimethylsilyl)-ethynyl]benzoate (1.69 g, 3.7 mmol) and K_2CO_3 (512 mg, 3.70 mmol, 1.0 equiv) were dissolved in 20 mL of methanol. The reaction mixture was stirred at room temperature. After 1 h, 100 mL of an ice-cold 1 M aq HCl solution was added, and the resulting mixture was extracted with DCM (100 mL). The organic phase was dried over Na_2SO_4, filtrated, and concentrated under reduced pressure. The crude residue was purified by silica gel column chromatography (ethyl acetate/*n*-hexane 1:4), which yielded **43** as a dark-red oil (1.19 g, 3.1 mmol, 84%): R_f = 0.63 (ethyl acetate/*n*-hexane 1:4); ^{1}H NMR (400 MHz, DMSO-d_6): δ (ppm) = 7.77 (d, J = 8.6 Hz, 1H), 7.48 (d, J = 2.3 Hz, 1H), 7.37 (dd, J = 8.6, 2.3 Hz, 1H), 7.21 (m, 2H), 7.12 (m, 2H), 4.89 (s, 2H), 4.40 (s, 1H), 3.79 (s, 3H), 1.38 (s, 9H); ^{13}C NMR (100 MHz, DMSO-d_6): δ (ppm) = 165.2, 161.3 (d, J = 242.8 Hz), 153.2, 145.0, 134.0 (d, J = 3.0 Hz), 130.9, 130.5, 128.9 (d, J = 8.4 Hz), 128.7, 126.0, 122.2, 115.3 (d, J = 21.6 Hz), 85.7, 81.2, 81.0, 52.1, 51.2, 27.7; IR (ATR): $\tilde{\nu}$ = 2977 (w, ν_{C-H}), 1697 (s, $\nu_{C=O}$).

Methyl 4-[(*tert*-Butoxycarbonyl)(4-fluorobenzyl)-amino]-2-ethylbenzoate (44). Methyl 4-[(*tert*-butoxycarbonyl)(4-fluorobenzyl)amino]-2-ethynylbenzoate (1.10 g, 2.9 mmol) was dissolved in methanol (30 mL). Pd/C (10% Pd, 50% water wet, 300 mg) was added, and the suspension was carefully set under a hydrogen atmosphere (balloon pressure) and stirred at 40 °C. After 16 h, the reaction mixture was filtered through a pad of Celite. The filtrate was concentrated under reduced pressure to obtain **44** as a colorless oil (951 mg, 2.46 mmol, 86%): R_f = 0.42 (ethyl acetate/*n*-hexane 1:9); ^{1}H NMR (400 MHz, DMSO-d_6): δ (ppm) = 7.70 (d, J = 8.4 Hz, 1H), 7.17 (m, 6H), 4.88 (s, 2H), 3.79 (s, 3H), 2.84 (q, J = 7.5 Hz, 2H), 1.39 (s, 9H), 1.09 (t, J = 7.5 Hz, 3H); ^{13}C NMR (100 MHz, DMSO-d_6): δ (ppm) = 166.8, 161.2 (d, J = 242.5 Hz), 153.5, 145.8, 145.1, 134.3 (d, J = 3.0 Hz), 130.7, 129.0 (d, J = 8.2 Hz), 127.2, 125.6, 123.0, 115.2 (d, J = 21.3 Hz), 80.5, 51.9, 51.4, 27.8, 26.7, 15.8; IR (ATR): $\tilde{\nu}$ = 2975 (w, ν_{C-H}), 1698 (s, $\nu_{C=O}$).

4-[(*tert*-Butoxycarbonyl)(4-fluorobenzyl)amino]-2-ethylbenzoic Acid (45). KOH (512 mg, 9.29 mmol, 4.0 equiv) was dissolved in a mixture of methanol (30 mL) and water (10 mL). Subsequently, methyl 4-[(*tert*-butoxycarbonyl)(4-fluorobenzyl)amino]-2-ethylbenzoate (900 mg, 2.32 mmol) was suspended in the resulting solution. The reaction mixture was stirred at 40 °C for 24 h. After complete conversion, methanol was removed under reduced pressure. The resulting aq solution was cooled to 0 °C and acidified to pH 3−4 with a 2 M aq HCl solution. Afterward, it was extracted with DCM (3 × 100 mL). The combined organic phases were dried over Na_2SO_4, filtrated, and concentrated under reduced pressure to obtain **45** as a colorless solid (789 mg, 2.11 mmol, 91%): mp 106 °C; ^{1}H NMR (400 MHz, DMSO-d_6): δ (ppm) = 7.71 (d, J = 8.4 Hz, 1H), 7.23 (m, 2H), 7.14 (m, 4H), 4.88 (s, 2H), 2.87 (q, J = 7.5 Hz, 2H), 1.40 (s, 9H), 1.10 (t, J = 7.5 Hz, 3H); ^{13}C NMR (100 MHz, DMSO-d_6): δ (ppm) = 168.1, 161.2 (d, J = 242.7 Hz), 153.5, 145.7, 144.8, 134.4 (d, J = 3.0 Hz), 130.9, 129.0 (d, J = 8.2 Hz), 127.2, 126.8, 122.9, 115.2 (d, J = 21.4 Hz), 80.5, 51.5, 27.8, 26.8, 15.9; IR (ATR): $\tilde{\nu}$ = 2978 (w, ν_{C-H}), 3300−2500 (b, ν_{O-H}), 1684 (s, $\nu_{C=O}$).

***tert*-Butyl [3-Ethyl-4-(propylcarbamoyl)phenyl](4-fluorobenzyl)carbamate (46).** 4-[(*tert*-Butoxycarbonyl)(4-fluorobenzyl)amino]-2-ethylbenzoic acid (180 mg, 0.48 mmol), HATU (367 mg, 0.96 mmol, 2.0 equiv), *N*,*N*-diisopropylethylamine (DIPEA) (336 μL, 1.93 mmol, 4.0 equiv), and *n*-propylamine (59 μL, 0.72 mmol, 1.5 equiv) were dissolved in DMF (10 mL) successively. The resulting mixture was stirred at room temperature. After 8 h, the reaction mixture was quenched by the addition of water (100 mL). The resulting suspension was extracted with DCM (100 mL). The organic phase was washed with water (2 × 100 mL), dried over Na_2SO_4, filtrated, and concentrated under reduced pressure. The crude residue was purified by silica gel column chromatography (ethyl acetate/*n*-hexane 3:7), which yielded **46** as a colorless oil (156 mg, 0.38 mmol, 78%): R_f = 0.29 (ethyl acetate/*n*-hexane 1:4); ^{1}H NMR (400 MHz, DMSO-d_6): δ (ppm) = 8.24 (t, J = 5.7 Hz, 1H), 7.14 (m, 7H), 4.84 (s, 2H), 3.15 (td, J = 6.9, 5.7 Hz, 2H), 2.64 (q, J = 7.5 Hz, 2H), 1.48 (m, 2H), 1.40 (s, 9H), 1.08 (t, J = 7.5 Hz, 3H), 0.88 (t, J = 7.4 Hz, 3H); ^{13}C NMR (100 MHz, DMSO-d_6): δ (ppm) = 168.6, 161.2 (d, J = 242.5 Hz), 153.8, 142.5, 142.0, 134.5 (d, J = 3.0 Hz), 134.3, 129.0 (d, J = 8.3 Hz), 127.4, 126.7, 122.9, 115.2 (d, J = 21.3 Hz), 80.2, 51.8, 40.6, 27.9, 25.7, 22.3, 15.7, 11.4; IR (ATR): $\tilde{\nu}$ = 3295 (m, ν_{N-H}), 2967 (w, ν_{C-H}), 1695, 1638 (s, $\nu_{C=O}$), 1604 (m, δ_{N-H}).

2-Ethyl-4-[(4-fluorobenzyl)amino]-*N*-propylbenzamide hydrochloride (47). *tert*-Butyl [3-ethyl-4-(propylcarbamoyl)phenyl](4-fluorobenzyl)carbamate (350 mg, 0.84 mmol) was dissolved in DCM (5 mL) and treated with TFA (5.0 mL, 65.34 mmol, 77.4 equiv). The resulting solution was stirred at room temperature for 6 h. Subsequently, additional DCM (100 mL) was added, and the solution was extracted with a saturated aq $NaHCO_3$ solution (100 mL).

https://doi.org/10.1021/acsomega.1c07103
ACS Omega 2022, 7, 7989−8012

The organic phase was dried over Na_2SO_4, filtrated, and concentrated under reduced pressure. The crude residue was purified by silica gel column chromatography (ethyl acetate/*n*-hexane 3:7), which yielded the product as a colorless oil. To obtain a solid, the hydrochloride salt was formed. For this reason, the residue was dissolved in ethyl acetate. The resulting solution was cooled to 0 °C, and HCl gas was passed through the solution over a period of 30 min to precipitate a hydrochloride salt. The precipitate was filtered off to obtain **47** as a colorless solid (266 mg, 0.76 mmol, 90%): R_f = 0.65 (free base, mobile phase: ethyl acetate/*n*-hexane 3:2); mp decomp.; ^{1}H NMR (400 MHz, MeOH-d_4): δ (ppm) = 7.46 (m, 3H), 7.26 (m, 2H), 7.17 (m, 2H), 4.63 (s, 2H), 3.35 (m, 2H), 2.80 (q, J = 7.6 Hz, 2H), 1.66 (m, 2H), 1.21 (t, J = 7.6 Hz, 3H), 1.01 (t, J = 7.4 Hz, 3H); ^{13}C NMR (100 MHz, MeOH-d_4): δ (ppm) = 171.7, 165.0 (d, J = 248.0 Hz), 146.0, 138.8, 137.8, 133.9 (d, J = 8.8 Hz), 130.2, 128.6, 124.6, 121.2, 117.1 (d, J = 22.0 Hz), 55.5, 42.8, 27.3, 23.7, 16.0, 12.0; IR (ATR): $\tilde{\nu}$ = 3272 (m, ν_{N-H}), 2965 (w, ν_{C-H}), 1637 (s, $\nu_{C=O}$), 1604 (m, δ_{N-H}). ESI-HRMS: calcd for $[C_{19}H_{23}N_2OF + H]^+$, 315.1867; found, 315.1861; cpd purity (220 nm): 100%.

4-Methyl-2,6-dimorpholinonicotinonitrile (53). 2,6-Dichloro-4-methylnicotinonitrile (1.00 g, 5.4 mmol) was suspended in 2-propanol (100 mL). Morpholine (2790 μL, 14.32 mmol, 6.0 equiv) was added, and the mixture was stirred at 170 °C in a sealed vessel. After 5 h, the mixture was cooled to room temperature and concentrated under reduced pressure. The residue was dissolved in 100 mL of ethyl acetate, and the resulting solution was extracted with water (100 mL). The organic phase was washed with brine and dried over Na_2SO_4. 100 mL of *n*-hexane was added to the organic phase, and the mixture was passed through a pad of silica gel. Afterward, the silica gel pad was rinsed with additional 100 mL of an *n*-hexane/ethyl acetate mixture (1:1). The eluates were combined and concentrated under reduced pressure to obtain **53** as a beige solid (1.26 g, 4.4 mmol, 82%): R_f = 0.48 (ethyl acetate/*n*-hexane 1:1); mp 141 °C; ^{1}H NMR (400 MHz, DMSO-d_6): δ (ppm) = 6.34 (d, J = 0.9 Hz, 1H), 3.69 (m, 4H), 3.65 (m, 4H), 3.55 (m, 4H), 3.49 (m, 4H), 2.28 (d, J = 0.7 Hz, 3H); ^{13}C NMR (100 MHz, DMSO-d_6): δ (ppm) = 161.4, 157.9, 153.6, 118.5, 100.0, 82.4, 65.9, 65.8, 48.4, 44.3, 20.5; IR (ATR): $\tilde{\nu}$ = 2968 (w, ν_{C-H}), 2191 (m, $\nu_{C\equiv N}$).

(4-Methyl-2,6-dimorpholinopyridin-3-yl)-methanamine (54). The synthesis was carried out according to general procedure B. 4-Methyl-2,6-dimorpholinonicotinonitrile (250 mg, 0.87 mmol) was used as the reactant. The title compound was obtained as a beige solid (93 mg, 0.32 mmol, 37%): R_f = 0.66 (DCM/MeOH/TEA 9.5:0.5:1); mp 194 °C; ^{1}H NMR (400 MHz, DMSO-d_6): δ (ppm) = 7.86 (s, 2H), 6.45 (s, 1H), 3.94 (s, 2H), 3.70 (m, 4H), 3.68 (m, 4H), 3.43 (m, 4H), 2.93 (m, 4H), 2.30 (s, 3H); ^{13}C NMR (100 MHz, DMSO-d_6): δ (ppm) = 160.7, 157.7, 150.3, 110.4, 103.7, 66.3, 65.9, 51.3, 44.9, 35.0, 19.6; IR (ATR): $\tilde{\nu}$ = 2957 (w, ν_{C-H}), 1597 (m, δ_{N-H}).

4-Fluoro-*N*-[(4-methyl-2,6-dimorpholinopyridin-3-yl)-methyl]benzamide (55a). The synthesis was carried out as described for **66**. (4-Methyl-2,6-dimorpholinopyridin-3-yl)-methanamine (218 mg, 0.75 mmol), 4-fluorobenzoyl chloride (106 μL, 0.90 mmol, 1.2 equiv), and TEA (208 μL, 1.49 mmol, 2.0 equiv) were used. The purification by silica gel column chromatography (ethyl acetate/*n*-hexane 1:1) and successive recrystallization (methanol/water) afforded **55a** as a colorless solid (243 mg, 0.59 mmol, 79%): R_f = 0.31 (ethyl acetate/*n*-hexane 1:1); mp decomp.; ^{1}H NMR (400 MHz, DMSO-d_6): δ (ppm) = 8.40 (t, J = 4.2 Hz, 1H), 7.93 (m, 2H), 7.25 (m, 2H), 6.39 (s, 1H), 4.43 (d, J = 4.2 Hz, 2H), 3.69 (m, 8H, 15-H), 3.40 (m, 4H), 3.00 (m, 4H), 2.21 (s, 3H); ^{13}C NMR (100 MHz, DMSO-d_6): δ (ppm) = 165.3, 163.8 (d, J = 248.1 Hz), 160.3, 157.0, 150.5, 130.8 (d, J = 2.9 Hz), 130.0 (d, J = 8.9 Hz), 115.0 (d, J = 21.6 Hz), 112.0, 103.0, 66.3, 66.0, 51.3, 45.2, 37.2, 19.4; IR (ATR): $\tilde{\nu}$ = 3261 (m, ν_{N-H}), 2957 (w, ν_{C-H}), 1624 (s, $\nu_{C=O}$), 1598 (s, δ_{N-H}); ESI-HRMS: calcd for $[C_{22}H_{27}N_4O_3F + H]^+$, 415.2140; found, 415.2123; cpd purity (220 nm): 100%.

2-(3,5-Difluorophenyl)-*N*-[(4-methyl-2,6-dimorpholinopyridin-3-yl)methyl]acetamide (55b). The synthesis was carried out as described for **61**. (4-Methyl-2,6-dimorpholinopyridin-3-yl)methanamine (93 mg 0.32 mmol), 2-(3,5-difluorophenyl)acetic acid (66 mg, 0.38 mmol, 1.2 equiv), and CDI (124 mg, 0.76 mmol, 2.4 equiv) were used. The purification by silica gel column chromatography (ethyl acetate/*n*-hexane 1:1) and successive recrystallization (methanol/water) afforded **55b** as a colorless solid (119 mg, 0.27 mmol, 84%): R_f = 0.35 (ethyl acetate/*n*-hexane 1:1); mp 239 °C; ^{1}H NMR (400 MHz, DMSO-d_6): δ (ppm) = 8.08 (t, J = 4.3 Hz, 1H), 7.09 (m, 1H), 6.96 (m, 2H), 6.38 (s, 1H), 4.18 (d, J = 4.2 Hz, 2H), 3.67 (m, 4H), 3.60 (m, 4H), 3.46 (s, 2H), 3.38 (m, 4H), 2.91 (m, 4H), 2.15 (s, 3H); ^{13}C NMR (100 MHz, DMSO-d_6): δ (ppm) = 168.9, 162.1 (dd, J = 245.5, 13.5 Hz), 160.3, 157.1, 150.5, 140.9 (t, J = 9.9 Hz), 112.0 (dd, J = 18.3, 6.5 Hz), 111.8, 102.9, 101.8 (t, J = 25.7 Hz), 66.2, 65.9, 51.3, 45.2, 41.6, 36.5, 19.2; IR (ATR): $\tilde{\nu}$ = 3293 (m, ν_{N-H}), 2969 (w, ν_{C-H}), 1632 (s, $\nu_{C=O}$), 1594 (s, δ_{N-H}); ESI-HRMS: calcd for $[C_{23}H_{28}N_4O_3F_2 + H]^+$, 447.2202; found, 447.2199; cpd purity (220 nm): 99%.

4,4′-(4-Methylpyridine-2,6-diyl)dimorpholine (56). 4,4′-(4-Methylpyridine-2,6-diyl)dimorpholine was a side product in the synthesis of (4-methyl-2,6-dimorpholinopyridin-3-yl)methanamine. It was obtained as a colorless solid by concentrating the ethyl acetate filtrate under reduced pressure (88 mg, 0.33 mmol, 38%): R_f = 0.65 (ethyl acetate/*n*-hexane 1:1); mp 118 °C; ^{1}H NMR (400 MHz, DMSO-d_6): δ (ppm) = 5.96 (s, 2H), 3.66 (m, 8H), 3.34 (m, 8H), 2.14 (s, 3H); ^{13}C NMR (100 MHz, DMSO-d_6): δ (ppm) = 158.1, 149.3, 97.0, 66.0, 45.2, 21.4; IR (ATR): $\tilde{\nu}$ = 3075, 2983 (w, ν_{C-H}).

6-Amino-2-chloro-4-methylnicotinonitrile (57). 6-Amino-2-chloro-4-methylnicotinonitrile is a side product in the synthesis of 2-amino-6-chloro-4-methylnicotinonitrile. It was separated from the main product by flash chromatography. The title compound was obtained as a colorless solid (403 mg, 2.41 mmol, 14%): R_f = 0.49 (ethyl acetate/*n*-hexane 1:3); mp 240 °C; ^{1}H NMR (400 MHz, DMSO-d_6): δ (ppm) = 7.37 (s, 2H), 6.33 (s, 1H), 2.29 (s, 3H); ^{13}C NMR (100 MHz, DMSO-d_6): δ (ppm) = 160.9, 152.7, 151.9, 116.1, 106.6, 95.1, 19.9; IR (ATR): $\tilde{\nu}$ = 3388, 3319 (m, ν_{N-H}), 2218 (m, $\nu_{C\equiv N}$), 1644 (m, δ_{N-H}).

2-Amino-6-chloro-4-methylnicotinonitrile (58). 2,6-Dichloro-4-methylnicotinic acid (2.00 g, 10.7 mmol) was suspended in a saturated solution of ammonia in 2-propanol (100 mL). The mixture was stirred in a sealed vessel at 70 °C. After 9 h, the reaction mixture was cooled to room temperature and concentrated under reduced pressure. The crude residue was purified by flash chromatography (ethyl acetate/*n*-hexane, 25−50% ethyl acetate) to obtain **58** as a slightly yellow solid (811 mg, 4.84 mmol, 20%): R_f = 0.44 (ethyl acetate/*n*-hexane 1:1); mp 255 °C; ^{1}H NMR (400

https://doi.org/10.1021/acsomega.1c07103
ACS Omega 2022, 7, 7989−8012

MHz, DMSO-d_6): δ (ppm) = 7.26 (s, 2H), 6.68 (s, 1H), 2.32 (s, 3H); ^{13}C NMR (100 MHz, DMSO-d_6): δ (ppm) = 160.2, 156.0, 152.8, 115.5, 112.3, 88.9, 19.7; IR (ATR): $\tilde{\nu}$ = 3378, 3313 (m, ν_{N-H}), 2219 (m, $\nu_{C\equiv N}$), 1642 (m, δ_{N-H}).

2-Amino-4-methyl-6-morpholinonicotinonitrile (59). 2-Amino-6-chloro-4-methylnicotinonitrile (800 mg, 4.77 mmol) was suspended in 2-propanol (100 mL). Morpholine (1240 μL, 14.32 mmol, 3.0 equiv) was added, and the mixture was stirred at 170 °C in a sealed vessel. After 3 h, the mixture was cooled to room temperature and filtered through a pad of Celite. The filtrate was concentrated under reduced pressure to a final volume of about 20 mL. Water was added to form a precipitate, which was filtered off to obtain **59** as an off-white solid (925 mg, 4.26 mmol, 89%): R_f = 0.50 (ethyl acetate/*n*-hexane 1:1); mp 160 °C; ^{1}H NMR (400 MHz, DMSO-d_6): δ (ppm) = 6.30 (s, 2H), 6.06 (s, 1H), 3.62 (m, 4H), 3.51 (m, 4H), 2.19 (s, 3H); ^{13}C NMR (100 MHz, DMSO-d_6): δ (ppm) = 160.2, 159.0, 152.0, 118.1, 96.4, 77.9, 65.7, 44.3, 20.2; IR (ATR): $\tilde{\nu}$ = 3416, 3337 (m, ν_{N-H}), 2988 (w, ν_{C-H}), 2202 (m, $\nu_{C\equiv N}$), 1643 (m, δ_{N-H}).

3-(Aminomethyl)-4-methyl-6-morpholinopyridin-2-amine (60). The synthesis was carried out according to general procedure B. 2-Amino-4-methyl-6-morpholinonicotinonitrile (250 mg, 1.2 mmol) was used as the reactant. The title compound was obtained as a beige solid (86 mg, 0.39 mmol, 34%), used for the following reaction without any further purification and characterization.

***N*-[(2-Amino-4-methyl-6-morpholinopyridin-3-yl)methyl]-2-(3,5-difluorophenyl)acetamide (61).** 2-(3,5-Difluorophenyl)acetic acid (80 mg, 0.46 mmol, 1.2 equiv) was dissolved in THF (20 mL). CDI (151 mg, 0.93 mmol, 2.4 equiv) was added in one portion, and the mixture was stirred at room temperature. After 16 h, a solution of (4-methyl-2,6-dimorpholinopyridin-3-yl)methanamine (86 mg, 0.39 mmol) in THF (10 mL) was added, and the reaction mixture was continued to stir at room temperature for additional 2 h. Afterward, ethyl acetate (100 mL) was added. The resulting solution was extracted with water (3 × 100 mL), washed with brine, dried over Na_2SO_4, filtrated, and concentrated under reduced pressure. The crude residue was purified by silica gel column chromatography (ethyl acetate/*n*-hexane 4:1) and successive recrystallization (methanol/water) to obtain **61** as a colorless solid (101 mg, 0.27 mmol, 69%): R_f = 0.21 (ethyl acetate/*n*-hexane 7:3); mp 234 °C; ^{1}H NMR (400 MHz, DMSO-d_6): δ (ppm) = 8.38 (t, J = 5.7 Hz, 1H), 7.08 (m, 1H), 6.97 (m, 2H), 5.85 (s, 1H), 5.56 (s, 2H), 4.08 (d, J = 5.7 Hz, 2H), 3.63 (m, 4H), 3.48 (s, 2H), 3.29 (m, 4H), 2.17 (s, 3H); ^{13}C NMR (100 MHz, DMSO-d_6): δ (ppm) = 169.7, 162.1 (dd, J = 245.4 Hz, 13.5 Hz), 157.4, 156.8, 148.0, 140.6 (t, J = 9.9 Hz), 112.2 (dd, J = 18.2 Hz, 6.4 Hz), 104.7, 101.9 (t, J = 25.8 Hz), 97.0, 66.0, 45.3, 41.3 (t, J = 2.2 Hz), 34.9, 19.4; IR (ATR): $\tilde{\nu}$ = 3480, 3364, 3295 (m, ν_{N-H}), 3072, 2966 (w, ν_{C-H}), 1634 (s, $\nu_{C=O}$), 1620 (m, δ_{N-H}); ESI-HRMS: calcd for $[C_{19}H_{22}N_4O_2F_2 + H]^+$, 377.1784; found, 377.1775; cpd purity (220 nm): 100%.

3,4-Dimethyl-6-morpholinopyridin-2-amine (62). 2-Amino-4-methyl-6-morpholinonicotinonitrile (326 mg, 1.50 mmol) was dissolved in methanol (40 mL), and Pd/C (10% Pd, 50% water wet, 100 mg) was added. The suspension was carefully set under a hydrogen atmosphere (balloon pressure) and stirred at 40 °C. After 48 h, the reaction mixture was filtered through a pad of Celite, and the filtrate was concentrated under reduced pressure. The residue was redissolved in ethyl acetate and filtered through a pad of silica gel. The silica gel pad was rinsed with additional ethyl acetate. Afterward, the filtrate was concentrated under reduced pressure again, and the crude residue was recrystallized (methanol/water) to obtain the title product as a colorless solid (245 mg, 1.8 mmol, 79%): R_f = 0.33 (ethyl acetate/*n*-hexane 1:1); mp 125 °C; ^{1}H NMR (400 MHz, DMSO-d_6): δ (ppm) = 5.83 (s, 1H), 5.21 (s, 2H), 3.64 (m, 4H), 3.24 (m, 4H), 2.07 (s, 3H), 1.86 (s, 3H); ^{13}C NMR (100 MHz, DMSO-d_6): δ (ppm) = 156.3, 156.1, 146.3, 103.5, 97.1, 66.1, 45.6, 20.0, 11.6; IR (ATR): $\tilde{\nu}$ = 3464, 3367 (m, ν_{N-H}), 2962 (w, ν_{C-H}), 1605 (m, δ_{N-H}).

6-Amino-4-methyl-2-morpholinonicotinonitrile (63). The synthesis was carried out as described for **59**. 6-Amino-2-chloro-4-methylnicotinonitrile (400 mg, 2.39 mmol) and morpholine (618 μL, 7.16 mmol, 3.0 equiv) were used. **63** was obtained as an off-white solid (455 mg, 2.09 mmol, 87%): R_f = 0.36 (ethyl acetate/*n*-hexane 1:1); mp 135 °C; ^{1}H NMR (400 MHz, DMSO-d_6): δ (ppm) = 6.66 (s, 2H), 5.90 (s, 1H), 3.67 (m, 4H), 3.44 (m, 4H), 2.19 (s, 3H); ^{13}C NMR (100 MHz, DMSO-d_6): δ (ppm) = 162.9, 160.0, 152.5, 118.9, 100.5, 81.7, 66.0, 48.5, 20.1; IR (ATR): $\tilde{\nu}$ = 3446, 3342 (m, ν_{N-H}), 2965 (w, ν_{C-H}), 2200 (m, $\nu_{C\equiv N}$), 1640 (m, δ_{N-H}).

6-[(4-Fluorobenzyl)amino]-4-methyl-2-morpholinonicotinonitrile (64). 6-Amino-4-methyl-2-morpholinonicotinonitrile (500 mg, 2.29 mmol) and 4-fluorobenzaldehyde (266 μL, 2.52 mmol, 1.1 equiv) were dissolved in DCM (30 mL) and stirred at room temperature. After 16 h, the reaction mixture was concentrated under reduced pressure. The residue was dissolved in methanol (30 mL), $NaBH_3CN$ (1.15 g, 18.3 mmol, 8.0 equiv) was added in portions over a period of 1 h, and the reaction mixture was continued to stir at room temperature. After 24 h, the reaction mixture was quenched by the addition of 100 mL of water. The mixture was extracted with ethyl acetate (100 mL). The organic phase was washed with brine, dried over Na_2SO_4, filtrated, and concentrated under reduced pressure. The crude residue was purified by silica gel column chromatography (ethyl acetate/*n*-hexane 1:3) to obtain **64** as a colorless solid (311 mg, 0.95 mmol, 42%): R_f = 0.70 (ethyl acetate/*n*-hexane 1:1); mp 100 °C; ^{1}H NMR (400 MHz, DMSO-d_6): δ (ppm) = 7.82 (s, 1H), 7.32 (m, 2H), 7.13 (m, 2H), 5.98 (s, 1H), 4.45 (d, J = 5.9 Hz, 2H), 3.63 (m, 4H), 3.45 (m, 4H), 2.19 (s, 3H); ^{13}C NMR (100 MHz, DMSO-d_6): δ (ppm) = 162.3, 161.1 (d, J = 241.0 Hz), 158.2, 149.7, 136.2, 129.1 (d, J = 8.1 Hz), 118.9, 114.9 (d, J = 21.1 Hz), 101.0, 87.3, 65.9, 48.3, 41.8, 20.1; IR (ATR): $\tilde{\nu}$ = 3408 (m, ν_{N-H}), 2955 (w, ν_{C-H}), 2199 (m, $\nu_{C\equiv N}$), 1592 (s, δ_{N-H}).

5-(Aminomethyl)-*N*-(4-fluorobenzyl)-4-methyl-6-morpholinopyridin-2-amine (65). The synthesis was carried out according to general procedure B. 6-[(4-Fluorobenzyl)amino]-4-methyl-2-morpholinonicotinonitrile (500 mg, 1.54 mmol) was used as the reactant. The title compound was obtained as a beige solid (265 mg, 0.80 mmol, 52%), used for the following reaction without any further purification and characterization.

Isobutyl ({6-[(4-Fluorobenzyl)amino]-4-methyl-2-morpholinopyridin-3-yl}methyl)carbamate (66). 5-(Aminomethyl)-*N*-(4-fluorobenzyl)-4-methyl-6-morpholinopyridin-2-amine (265 mg, 0.80 mmol) was dissolved in DCM (20 mL), and TEA (224 μL, 1.60 mmol, 2.0 equiv) was added in one portion. The reaction mixture was cooled to 0 °C, and a solution of isobutyl chloroformate (125 μL, 0.96 mmol, 1.2 equiv) in DCM (10 mL) was added dropwise over a period of

https://doi.org/10.1021/acsomega.1c07103
ACS Omega 2022, 7, 7989−8012

30 min. Cooling was removed, and the reaction mixture was stirred at room temperature. After 16 h, additional DCM (70 mL) was added, and the solution was extracted with water (3 × 100 mL). The organic phase was dried over Na_2SO_4, filtrated, and concentrated under reduced pressure. The resulting crude residue was purified by silica gel column chromatography (ethyl acetate/*n*-hexane 1:1) and successive recrystallization (methanol/water) to obtain **66** as a colorless solid (244 mg, 0.57 mmol, 71%): R_f = 0.62 (ethyl acetate/*n*-hexane 1:1); mp 129 °C; ^{1}H NMR (400 MHz, DMSO-d_6): δ (ppm) = 7.34 (m, 2H), 7.10 (m, 2H), 7.06 (s, 1H), 6.85 (t, J = 6.2 Hz, 1H), 6.02 (s, 1H), 4.40 (d, J = 6.1 Hz, 2H), 4.12 (d, J = 4.6 Hz, 2H), 3.73 (d, J = 6.7 Hz, 2H), 3.65 (m, 4H), 2.89 (m, 4H), 2.10 (s, 3H), 1.80 (m, 1H), 0.85 (d, J = 6.7 Hz, 6H); ^{13}C NMR (100 MHz, DMSO-d_6): δ (ppm) = 160.9 (d, J = 240.0 Hz), 160.6, 156.3, 149.5, 137.4, 137.4, 129.1 (d, J = 7.9 Hz), 114.7 (d, J = 21.2 Hz), 110.7, 103.7, 69.5, 66.4, 51.4, 43.4, 37.8, 27.7, 19.0, 18.8; IR (ATR): $\tilde{\nu}$ = 3314 (m, ν_{N-H}), 2957 (w, ν_{C-H}), 1681 (s, $\nu_{C=O}$), 1607 (m, δ_{N-H}); ESI-HRMS: calcd for $[C_{23}H_{31}N_4O_3F + H]^+$, 431.2453; found, 431.2438; cpd purity (220 nm): 100%.

log $D_{7.4}$ Estimation. The log $D_{7.4}$ values were estimated using a common HPLC-based method in accordance with guideline OPPTS 830.7570 of the United States Environmental Protection Agency (EPA). The HPLC measurements were performed with a Phenomenex Luna 5 μm Phenyl-Hexyl 100 Å column (150 × 4.6 mm). A mixture of methanol (75%) and Tris/HCl buffer (25%) at pH 7.4 was used as the mobile phase at a flow rate of 1.0 mL/min. First, the capacity factors of seven reference substances recommended in the guideline referenced above (acetophenone, benzene, ethyl benzoate, benzophenone, phenyl benzoate, diphenyl ether, and bibenzyl), which cover the required log $D_{7.4}$ range of 1.7−4.8, were determined from their retention times. Uracil was used to measure the unretained peak time. To obtain a calibration function, the logarithm of the capacity factors for the reference substances was then plotted against the corresponding log P values taken from the mentioned guideline, which are equivalent to the log $D_{7.4}$ values for non-ionizable compounds like the reference substances used for calibration. With this calibration function, it was possible to estimate the log $D_{7.4}$ value from the corresponding retention time for each compound to be tested. For the measurement, 2 mg of the reference substances was each dissolved in 1 mL of methanol. A reference mixture was then obtained by combining 50 μL of each reference solution. The reference mixture was measured before and after the substances to be tested. The mean value from both measurements was used for the calibration line. The substances to be tested were injected as a solution in methanol (2 mg/mL), and the retention time was determined as the mean value from two measurements.

K_V7.2/3 Channel Opening Assay. The cell culture of the K_V7.2/3 transfected HEK293 cells (HEK293 KCNQ2/3 cells from SB Drug Discovery, Glasgow, UK) used for the assay and the processing of the obtained data were performed as described in earlier work.[27,29] Briefly, 60,000 cells/well were seeded into 96-well microtiter plates for fluorescence-based assays (4titude Vision Plate Black 96-Well microtiter plates from ThermoScientic) and incubated for 24 h. After incubation, the medium was changed to 200 μL/well loading buffer containing 5 mmol/L probenecid and incubated for 1 h at room temperature. Subsequently, the test compounds dissolved in DMSO were added to the wells to the desired concentrations and further incubated for 30 min. As a control, the loading buffer with a DMSO concentration corresponding to the substance samples (1% (V/V)) was used. Fluorescence measurements were performed on the Infinite F200 Pro plate reader (Tecan) set at extinction/emission wavelengths of 485 and 535 nm, respectively. After measuring the background fluorescence (baseline) for 20 s, a stimulus buffer (25 mmol/L K^+, 15 mmol/L Tl^+) was added just before the fluorescence of each well was measured.

The calculations to obtain dose−response curves were performed in the same manner as in previous investigations.[27,29] Briefly, the fluorescence intensity was normalized with the baseline signal (F/F_0) at each time of signal acquisition. To obtain the corrected negative control, a value of 1 was subtracted from the normalized value of the negative control. Subsequently, the value of the corrected negative control was subtracted from the maximum (corr. F/F_0) value of a compound in a defined concentration (corr. $\Delta F/F_0$) and then plotted against the logarithmic concentration. The EC_{50} value was calculated as relative values with GraphPad Prism 6 (La Jolla, CA, USA), that is, the inflection points of the sigmoidal curves. The E_{max} value, the maximum response, indicates the intrinsic activity of a compound. This value was determined relative to flupirtine (**1**), where the maximum corr. $\Delta F/F_0$ value of flupirtine (**1**) was defined as 100%. The EC_{50} and E_{max} value of a compound is the mean of at least three independent experiments ± standard deviation (SD).

Hepatic Cell Viability Assay. The culturing of the mouse liver TAMH and human liver cancer HEP-G2 cell lines and the MTT assay used to evaluate cell viability were carried out as previously described elsewhere in detail.[27,29] Briefly, 20,000 cells/well of the TAMH cell line, grown in a serum-free DMEM/F12 medium and supplemented with 5% PANEXIN NTA, 10 mM nicotinamide and 10 μg/mL gentamicin sulfate, and 15,000 cells/well of the HEP-G2 cell line, grown in RPMI 1640 (PAN Biotech), supplemented with 10% heat-inactivated fetal bovine serum and 1% penicillin/streptomycin, were seeded into 96-well microtiter plates and incubated at 37 °C in 5% CO_2 atmosphere for 24 h. Compounds, dissolved in DMSO, were serially diluted into the respective culture medium to give a 1% (v/v) DMSO solution in five to nine concentrations of the compound. The medium in the wells was then replaced with the medium containing the compounds. Control wells contained an equivalent number of cells and 1% (v/v) DMSO. Wells without cells were used to determine the background optical density (OD) and were treated as the control wells. After 24 or 48 h of incubation with the compound, the respective medium was replaced with a fresh medium supplemented with 10% (v/v) of a 2.5 mg/mL solution of MTT. The plates were incubated for 4 h. Then, the culture medium was carefully aspirated off and 50 μL of DMSO was added to each well to dissolve the formazan crystals. The ODs of each well were measured at λ = 570 nm with a SpectraMax 190 microplate reader.

For determination of cell viability, the ODs of the test compound (T) and control (C) wells were corrected by subtracting the bank value. The calculated $T/C_{corr.}$ values were plotted against the log(concentration). The LD_{50} and LD_{25} values were determined by using GraphPad Prism 6. After interpolation of a sigmoidal standard curve, the LD_{50} and LD_{25} values accounted for 50 or 75% of viability, respectively. If even the highest tested concentration of a compound did not reduce cell viability to 75%, the LD_{25} was reported as higher than the

https://doi.org/10.1021/acsomega.1c07103
ACS Omega 2022, 7, 7989−8012

highest tested concentration. The values are given as the mean with SD of at least three independent experiments.

Molecular modeling. All calculations were performed with Maestro and included applications of the Schrödinger release 2020-4 (Maestro, Schrödinger, LLC, New York, NY, 2021). Desmond v6.4 with CUDA support was used for all molecular dynamics simulations.[51]

Structure Preparation. The cryo-EM structure of the homotetrameric $K_V7.2$ potassium channel with retigabine (**2**) (RCSB PDB 7CR2)[50] was prepared by the Protein Preparation Wizard.[52] Missing side chains and loops were replaced by Prime,[53,54] followed by a restraint minimization to a heavy atom root-mean-square deviation value of 0.3 Å using OPLS3e force field parameters.[55] Both chains B and C were rebuilt to the corresponding $K_V7.3$ sequence by homology modeling (energy-based) within the Multiple Sequence Viewer application to obtain the heterotetrameric $K_V7.2/3$ structure.

Molecular Docking. The box center and size for grid generation were estimated by the bound retigabine (**2**) of the previously generated homology model. Glide[56] molecular docking calculations of **28b** and **36b** were performed using an induced fit approach with an extended sampling protocol. In total, 80 protein models with optimized side chains were generated, while an implicit membrane was placed on the transmembrane helices. No further constraints were applied, and the results were visually inspected.

T-REMD Simulation. Compounds **26b** and **36b** were solvated in a cubic box of TIP3P water[57] with a buffer of 1 nm to the solute. A temperature replica-exchange molecular dynamics simulation[58] was performed for each molecule by using eight replicas on a quadratically distributed temperature range between 310 and 350 K. Prior to the replica-exchange simulations, each system was minimized for 100 ps, and the standard relaxation protocol was performed to equilibrate them to the desired baseline temperature and pressure. Exchange attempts were performed every 1.2 ps, and snapshots were written in 5 ps intervals. In total, 10,000 structures were obtained for each compound after a 50 ns simulation time in the *NVT* ensemble. The time step was set to 2 fs, and the temperature was maintained using a Nosé−Hoover thermostat.[59] Long-range electrostatics are described by the particle mesh Ewald method, while the short-range interaction cutoffs were set to 1 nm with a 0.1 nm switching function.

■ ASSOCIATED CONTENT

Supporting Information

The Supporting Information is available free of charge at https://pubs.acs.org/doi/10.1021/acsomega.1c07103.

^{1}H and ^{13}C NMR spectra, HMBC spectra used for the discrimination of regioisomers **57** and **58**, assignment of NMR signals, and data used for log $D_{7.4}$ estimation (PDF)

■ AUTHOR INFORMATION

Corresponding Author

Andreas Link − *Institute of Pharmacy, University of Greifswald, 17489 Greifswald, Germany;* orcid.org/0000-0003-1262-6636; Email: link@uni-greifswald.de; Fax: (+49) (0)3834 4204895

Authors

Konrad W. Wurm − *Institute of Pharmacy, University of Greifswald, 17489 Greifswald, Germany*

Frieda-Marie Bartz − *Institute of Pharmacy, University of Greifswald, 17489 Greifswald, Germany*

Lukas Schulig − *Institute of Pharmacy, University of Greifswald, 17489 Greifswald, Germany;* orcid.org/0000-0002-4614-3395

Anja Bodtke − *Institute of Pharmacy, University of Greifswald, 17489 Greifswald, Germany*

Patrick J. Bednarski − *Institute of Pharmacy, University of Greifswald, 17489 Greifswald, Germany;* orcid.org/0000-0002-9589-8241

Complete contact information is available at: https://pubs.acs.org/10.1021/acsomega.1c07103

Notes

The authors declare no competing financial interest.

■ ACKNOWLEDGMENTS

K.W.W. and F.M.B. are funded by grants DFG LI 765/7-2 and DFG BE 1287/6-2 awarded to A.L. and P.J.B. by the Deutsche Forschungsgemeinschaft (DFG—German Research Foundation). We thank Anne Schüttler and Maria Hühr for excellent technical assistance.

■ REFERENCES

(1) Pähler, A. Reactive Metabolite Assessment in Drug Discovery and Development in Support of Safe Drug Design. In *Drug-Induced Liver Toxicity*; Chen, M., Will, Y., Eds.; Methods in Pharmacology and Toxicology; Springer New York, 2018; pp 263−281.

(2) Baillie, T. A. Drug-protein adducts: past, present, and future. *Med. Chem. Res.* **2020**, *29*, 1093−1104.

(3) Stepan, A. F.; Walker, D. P.; Bauman, J.; Price, D. A.; Baillie, T. A.; Kalgutkar, A. S.; Aleo, M. D. Structural alert/reactive metabolite concept as applied in medicinal chemistry to mitigate the risk of idiosyncratic drug toxicity: a perspective based on the critical examination of trends in the top 200 drugs marketed in the United States. *Chem. Res. Toxicol.* **2011**, *24*, 1345−1410.

(4) Scheuch, E.; Methling, K.; Bednarski, P. J.; Oswald, S.; Siegmund, W. Quantitative LC-MS/MS determination of flupirtine, its N-acetylated and two mercapturic acid derivatives in man. *J. Pharm. Biomed. Anal.* **2015**, *102*, 377−385.

(5) Methling, K.; Reszka, P.; Lalk, M.; Vrana, O.; Scheuch, E.; Siegmund, W.; Terhaag, B.; Bednarski, P. J. Investigation of the in vitro metabolism of the analgesic flupirtine. *Drug Metab. Dispos.* **2009**, *37*, 479−493.

(6) European Medicines Agency. Assessment report for flupirtine containing medicinal products. 2013. https://www.ema.europa.eu/en/documents/referral/flupirtine-containing-medicines-article-107i-procedure-prac-assessment-report_en.pdf (accessed Dec 15, 2019).

(7) Siegmund, W.; Modess, C.; Scheuch, E.; Methling, K.; Keiser, M.; Nassif, A.; Rosskopf, D.; Bednarski, P. J.; Borlak, J.; Terhaag, B. Metabolic activation and analgesic effect of flupirtine in healthy subjects, influence of the polymorphic NAT2, UGT1A1 and GSTP1. *Br. J. Clin. Pharmacol.* **2015**, *79*, 501−513.

(8) Cho, T.; Uetrecht, J. How Reactive Metabolites Induce an Immune Response That Sometimes Leads to an Idiosyncratic Drug Reaction. *Chem. Res. Toxicol.* **2017**, *30*, 295−314.

(9) Nicoletti, P.; Werk, A. N.; Sawle, A.; Shen, Y.; Urban, T. J.; Coulthard, S. A.; Bjornsson, E. S.; Cascorbi, I.; Floratos, A.; Stammschulte, T.; Gundert-Remy, U.; Nelson, M. R.; Aithal, G. P.; Daly, A. K. HLA-DRB1*16: 01-DQB1*05: 02 is a novel genetic risk factor for flupirtine-induced liver injury. *Pharmacogenet. Genomics* **2016**, *26*, 218−224.

https://doi.org/10.1021/acsomega.1c07103
ACS Omega 2022, 7, 7989−8012

(10) Puls, F.; Agne, C.; Klein, F.; Koch, M.; Rifai, K.; Manns, M. P.; Borlak, J.; Kreipe, H. H. Pathology of flupirtine-induced liver injury: a histological and clinical study of six cases. *Virchows Arch.* **2011**, *458*, 709−716.
(11) Hempel, R.; Schupke, H.; McNeilly, P. J.; Heinecke, K.; Kronbach, C.; Grunwald, C.; Zimmermann, G.; Griesinger, C.; Engel, J.; Kronbach, T. Metabolism of retigabine (D-23129), a novel anticonvulsant. *Drug Metab. Dispos.* **1999**, *27*, 613−622.
(12) Groseclose, M. R.; Castellino, S. An Investigation into Retigabine (Ezogabine) Associated Dyspigmentation in Rat Eyes by MALDI Imaging Mass Spectrometry. *Chem. Res. Toxicol.* **2019**, *32*, 294−303.
(13) Clark, S.; Antell, A.; Kaufman, K. New antiepileptic medication linked to blue discoloration of the skin and eyes. *Ther. Adv. Drug Saf.* **2015**, *6*, 15−19.
(14) European Medicines Agency. Withdrawal of pain medicine flupirtine endorsed: serious liver problems continued to be reported despite previous restrictions. 2018. https://www.ema.europa.eu/en/documents/press-release/withdrawal-pain-medicine-flupirtine-endorsed_en.pdf (accessed Dec 15, 2019).
(15) Brickel, N.; Hewett, K.; Rayner, K.; McDonald, S.; De'Ath, J.; Daniluk, J.; Joshi, K.; Boll, M. C.; Tiamkao, S.; Vorobyeva, O.; Cooper, J. Safety of retigabine in adults with partial-onset seizures after long-term exposure: focus on unexpected ophthalmological and dermatological events. *Epilepsy Behav.* **2020**, *102*, 106580.
(16) Cuevas, J.; Harper, A. A.; Trequattrini, C.; Adams, D. J. Passive and active membrane properties of isolated rat intracardiac neurons: regulation by H- and M-currents. *J. Neurophysiol.* **1997**, *78*, 1890−1902.
(17) Brown, D. A.; Passmore, G. M. Neural KCNQ (Kv7) channels. *Br. J. Pharmacol.* **2009**, *156*, 1185−1195.
(18) Zaika, O.; Lara, L. S.; Gamper, N.; Hilgemann, D. W.; Jaffe, D. B.; Shapiro, M. S. Angiotensin II regulates neuronal excitability via phosphatidylinositol 4,5-bisphosphate-dependent modulation of Kv7 (M-type) K^+ channels. *J. Physiol.* **2006**, *575*, 49−67.
(19) Dalby-Brown, W.; Hansen, H.; Korsgaard, M.; Mirza, N.; Olesen, S.-P. Kv7 Channels: Function, Pharmacology and Channel Modulators. *Curr. Top. Med. Chem.* **2006**, *6*, 999−1023.
(20) Pharmacology of Potassium Channels. *Handbook of Experimental Pharmacology*; Gamper, N., Wang, K., Eds.; Springer, 2021; Vol. *267*.
(21) Yadav, N. K.; Shukla, T.; Upmanyu, N.; Pandey, S. P.; Khan, M. A.; Jain, D. K. Concise review: Therapeutic potential of flupirtine maleate. *J. Drug Delivery Ther.* **2019**, *9*, 467−471.
(22) Nissenkorn, A.; Kornilov, P.; Peretz, A.; Blumkin, L.; Heimer, G.; Ben-Zeev, B.; Attali, B. Personalized treatment with retigabine for pharmacoresistant epilepsy arising from a pathogenic variant in the KCNQ2 selectivity filter. *Epileptic Disord.* **2021**, *23*, 695−705.
(23) Martyn-St James, M.; Glanville, J.; McCool, R.; Duffy, S.; Cooper, J.; Hugel, P.; Lane, P. W. The efficacy and safety of retigabine and other adjunctive treatments for refractory partial epilepsy: a systematic review and indirect comparison. *Seizure* **2012**, *21*, 665−678.
(24) Vigil, F. A.; Bozdemir, E.; Bugay, V.; Chun, S. H.; Hobbs, M.; Sanchez, I.; Hastings, S. D.; Veraza, R. J.; Holstein, D. M.; Sprague, S. M.; M Carver, C.; Cavazos, J. E.; Brenner, R.; Lechleiter, J. D.; Shapiro, M. S. Prevention of brain damage after traumatic brain injury by pharmacological enhancement of KCNQ (Kv7, "M-type") K+ currents in neurons. *J. Cereb. Blood Flow Metab.* **2019**, *40*, 1256−1273.
(25) Wainger, B. J.; Macklin, E. A.; Vucic, S.; McIlduff, C. E.; Paganoni, S.; Maragakis, N. J.; Bedlack, R.; Goyal, N. A.; Rutkove, S. B.; Lange, D. J.; Rivner, M. H.; Goutman, S. A.; Ladha, S. S.; Mauricio, E. A.; Baloh, R. H.; Simmons, Z.; Pothier, L.; Kassis, S. B.; La, T.; Hall, M.; Evora, A.; Klements, D.; Hurtado, A.; Pereira, J. D.; Koh, J.; Celnik, P. A.; Chaudhry, V.; Gable, K.; Juel, V. C.; Phielipp, N.; Marei, A.; Rosenquist, P.; Meehan, S.; Oskarsson, B.; Lewis, R. A.; Kaur, D.; Kiskinis, E.; Woolf, C. J.; Eggan, K.; Weiss, M. D.; Berry, J. D.; David, W. S.; Davila-Perez, P.; Camprodon, J. A.; Pascual-Leone, A.; Kiernan, M. C.; Shefner, J. M.; Atassi, N.; Cudkowicz, M. E. Effect of Ezogabine on Cortical and Spinal Motor Neuron Excitability in Amyotrophic Lateral Sclerosis. *JAMA Neurol.* **2021**, *78*, 186−196.
(26) Tan, A.; Costi, S.; Morris, L. S.; van Dam, N. T.; Kautz, M.; Whitton, A. E.; Friedman, A. K.; Collins, K. A.; Ahle, G.; Chadha, N.; Do, B.; Pizzagalli, D. A.; Iosifescu, D. V.; Nestler, E. J.; Han, M.-H.; Murrough, J. W. Effects of the KCNQ channel opener ezogabine on functional connectivity of the ventral striatum and clinical symptoms in patients with major depressive disorder. *Mol. Psychiatr.* **2020**, *25*, 1323−1333.
(27) Bock, C.; Surur, A. S.; Beirow, K.; Kindermann, M. K.; Schulig, L.; Bodtke, A.; Bednarski, P. J.; Link, A. Sulfide Analogues of Flupirtine and Retigabine with Nanomolar K V 7.2/K V 7.3 Channel Opening Activity. *ChemMedChem* **2019**, *14*, 952−964.
(28) Zhang, Y.-M.; Xu, H.-Y.; Hu, H.-N.; Tian, F.-Y.; Chen, F.; Liu, H.-N.; Zhan, L.; Pi, X.-P.; Liu, J.; Gao, Z.-B.; Nan, F.-J. Discovery of HN37 as a Potent and Chemically Stable Antiepileptic Drug Candidate. *J. Med. Chem.* **2021**, *64*, 5816−5837.
(29) Surur, A. S.; Bock, C.; Beirow, K.; Wurm, K.; Schulig, L.; Kindermann, M. K.; Siegmund, W.; Bednarski, P. J.; Link, A. Flupirtine and retigabine as templates for ligand-based drug design of KV7.2/3 activators. *Org. Biomol. Chem.* **2019**, *17*, 4512−4522.
(30) Hughes, T. B.; Swamidass, S. J. Deep Learning to Predict the Formation of Quinone Species in Drug Metabolism. *Chem. Res. Toxicol.* **2017**, *30*, 642−656.
(31) Zhao, H.; Fu, H.; Qiao, R. Copper-catalyzed direct amination of ortho-functionalized haloarenes with sodium azide as the amino source. *J. Org. Chem.* **2010**, *75*, 3311−3316.
(32) Grupe, M.; Bentzen, B. H.; Benned-Jensen, T.; Nielsen, V.; Frederiksen, K.; Jensen, H. S.; Jacobsen, A.-M.; Skibsbye, L.; Sams, A. G.; Grunnet, M.; Rottländer, M.; Bastlund, J. F. In vitro and in vivo characterization of Lu AA41178: A novel, brain penetrant, pan-selective Kv7 potassium channel opener with efficacy in preclinical models of epileptic seizures and psychiatric disorders. *Eur. J. Pharmacol.* **2020**, *887*, 173440.
(33) Yap, J. L.; Hom, K.; Fletcher, S. Ortho-selectivity in the nucleophilic aromatic substitution (SNAr) reactions of 3-substituted, 2,6-dichloropyridines with alkali metal alkoxides. *Tetrahedron Lett.* **2011**, *52*, 4172−4176.
(34) Orton, T. C.; Lowery, C. Practolol metabolism. III. Irreversible binding of [14C]practolol metabolite(s) to mammalian liver microsomes. *J. Pharmacol. Exp. Ther.* **1981**, *219*, 207−212.
(35) Limban, C.; Nuţă, D. C.; Chiriţă, C.; Negreş, S.; Arsene, A. L.; Goumenou, M.; Karakitsios, S. P.; Tsatsakis, A. M.; Sarigiannis, D. A. The use of structural alerts to avoid the toxicity of pharmaceuticals. *Toxicol. Reptiles* **2018**, *5*, 943−953.
(36) Stumpfe, D.; Hu, H.; Bajorath, J. Evolving Concept of Activity Cliffs. *ACS Omega* **2019**, *4*, 14360−14368.
(37) Schönherr, H.; Cernak, T. Profound Methyl Effects in Drug Discovery and a Call for New C-H Methylation Reactions. *Angew. Chem., Int. Ed.* **2013**, *52*, 12256−12267.
(38) Aynetdinova, D.; Callens, M. C.; Hicks, H. B.; Poh, C. Y. X.; Shennan, B. D. A.; Boyd, A. M.; Lim, Z. H.; Leitch, J. A.; Dixon, D. J. Installing the "magic methyl" −C-H methylation in synthesis. *Chem. Soc. Rev.* **2021**, *50*, 5517−5563.
(39) Steverlynck, J.; Sitdikov, R.; Rueping, M. The Deuterated "Magic Methyl" Group: A Guide to Site-Selective Trideuteromethyl Incorporation and Labeling by Using CD_3 ReagentsThe Deuterated "Magic Methyl". *Chem.—Eur. J.* **2021**, *27*, 11751−11772.
(40) Angell, R.; Aston, N. M.; Bamborough, P.; Buckton, J. B.; Cockerill, S.; deBoeck, S. J.; Edwards, C. D.; Holmes, D. S.; Jones, K. L.; Laine, D. I.; Patel, S.; Smee, P. A.; Smith, K. J.; Somers, D. O.; Walker, A. L. Biphenyl amide p38 kinase inhibitors 3: Improvement of cellular and in vivo activity. *Bioorg. Med. Chem. Lett.* **2008**, *18*, 4428−4432.
(41) Quancard, J.; Bollbuck, B.; Janser, P.; Angst, D.; Berst, F.; Buehlmayer, P.; Streiff, M.; Beerli, C.; Brinkmann, V.; Guerini, D.; Smith, P. A.; Seabrook, T. J.; Traebert, M.; Seuwen, K.; Hersperger, R.; Bruns, C.; Bassilana, F.; Bigaud, M. A Potent and Selective S1P1

https://doi.org/10.1021/acsomega.1c07103
ACS Omega 2022, 7, 7989−8012

Antagonist with Efficacy in Experimental Autoimmune Encephalomyelitis. *Chem. Biol.* **2012**, *19*, 1142−1151.
(42) Davis, M.; Stamper, B. D. TAMH: A Useful In Vitro Model for Assessing Hepatotoxic Mechanisms. *BioMed Res. Int.* **2016**, *2016*, 4780872.
(43) Ramirez, T.; Strigun, A.; Verlohner, A.; Huener, H.-A.; Peter, E.; Herold, M.; Bordag, N.; Mellert, W.; Walk, T.; Spitzer, M.; Jiang, X.; Sperber, S.; Hofmann, T.; Hartung, T.; Kamp, H.; van Ravenzwaay, B. Prediction of liver toxicity and mode of action using metabolomics in vitro in HepG2 cells. *Arch. Toxicol.* **2018**, *92*, 893−906.
(44) Mosedale, M.; Watkins, P. B. Understanding Idiosyncratic Toxicity: Lessons Learned from Drug-Induced Liver Injury. *J. Med. Chem.* **2020**, *63*, 6436−6461.
(45) Chen, M.; Borlak, J.; Tong, W. High lipophilicity and high daily dose of oral medications are associated with significant risk for drug-induced liver injury. *Hepatology* **2013**, *58*, 388−396.
(46) McEuen, K.; Borlak, J.; Tong, W.; Chen, M. Associations of Drug Lipophilicity and Extent of Metabolism with Drug-Induced Liver Injury. *Int. J. Mol. Sci.* **2017**, *18*, 1335.
(47) Bellettato, C. M.; Scarpa, M. Possible strategies to cross the blood-brain barrier. *Ital. J. Pediatr.* **2018**, *44*, 131.
(48) Daina, A.; Michielin, O.; Zoete, V. SwissADME: a free web tool to evaluate pharmacokinetics, drug-likeness and medicinal chemistry friendliness of small molecules. *Sci. Rep.* **2017**, *7*, 42717.
(49) Ryu, J. Y.; Lee, J. H.; Lee, B. H.; Song, J. S.; Ahn, S.; Oh, K.-S. PredMS: a random Forest model for predicting metabolic stability of drug candidates in human liver microsomes. *Bioinformatics* **2021**, *38*, 364−368.
(50) Li, X.; Zhang, Q.; Guo, P.; Fu, J.; Mei, L.; Lv, D.; Wang, J.; Lai, D.; Ye, S.; Yang, H.; Guo, J. Molecular basis for ligand activation of the human KCNQ2 channel. *Cell Res.* **2021**, *31*, 52−61.
(51) Bowers, K. J.; Chow, E.; Xu, H.; Dror, R. O.; Eastwood, M. P.; Gregersen, B. A.; Klepeis, J. L.; Kolossvary, I.; Moraes, M. A.; Sacerdoti, F. D.; Salmon, J. K.; Shan, Y.; Shaw, D. E. Scalable algorithms for molecular dynamics simulations on commodity clusters. In *SC 06: Proceedings of the 2006 ACM/IEEE Conference on Supercomputing, Tampa, Florida, November 11−17, 2006*; Horner-Miller, B., Ed.; ACM Press: New York, USA, 2006; 84−es.
(52) Madhavi Sastry, G.; Adzhigirey, M.; Day, T.; Annabhimoju, R.; Sherman, W. Protein and ligand preparation: parameters, protocols, and influence on virtual screening enrichments. *J. Comput. Aided Mol. Des.* **2013**, *27*, 221−234.
(53) Jacobson, M. P.; Pincus, D. L.; Rapp, C. S.; Day, T. J. F.; Honig, B.; Shaw, D. E.; Friesner, R. A. A hierarchical approach to all-atom protein loop prediction. *Proteins* **2004**, *55*, 351−367.
(54) Jacobson, M. P.; Friesner, R. A.; Xiang, Z.; Honig, B. On the Role of the Crystal Environment in Determining Protein Side-chain Conformations. *J. Mol. Biol.* **2002**, *320*, 597−608.
(55) Harder, E.; Damm, W.; Maple, J.; Wu, C.; Reboul, M.; Xiang, J. Y.; Wang, L.; Lupyan, D.; Dahlgren, M. K.; Knight, J. L.; Kaus, J. W.; Cerutti, D. S.; Krilov, G.; Jorgensen, W. L.; Abel, R.; Friesner, R. A. OPLS3: A Force Field Providing Broad Coverage of Drug-like Small Molecules and Proteins. *J. Chem. Theory Comput.* **2016**, *12*, 281−296.
(56) Friesner, R. A.; Murphy, R. B.; Repasky, M. P.; Frye, L. L.; Greenwood, J. R.; Halgren, T. A.; Sanschagrin, P. C.; Mainz, D. T. Extra Precision Glide: Docking and Scoring Incorporating a Model of Hydrophobic Enclosure for Protein−Ligand Complexes. *J. Med. Chem.* **2006**, *49*, 6177−6196.
(57) Mark, P.; Nilsson, L. Structure and Dynamics of the TIP3P, SPC, and SPC/E Water Models at 298 K. *J. Phys. Chem. A* **2001**, *105*, 9954−9960.
(58) Qi, R.; Wei, G.; Ma, B.; Nussinov, R. Replica Exchange Molecular Dynamics: A Practical Application Protocol with Solutions to Common Problems and a Peptide Aggregation and Self-Assembly Example. *Methods Mol. Biol.* **2018**, *1777*, 101−119.
(59) Evans, D. J.; Holian, B. L. The Nose-Hoover thermostat. *J. Chem. Phys.* **1985**, *83*, 4069−4074.

https://doi.org/10.1021/acsomega.1c07103
ACS Omega 2022, 7, 7989−8012

7.3 Publikation III

Replacing the oxidation-sensitive triaminoaryl chemotype of problematic K_V7 channel openers: exploration of a nicotinamide scaffold

Konrad W. Wurm, Frieda-Marie Bartz, Lukas Schulig, Anja Bodtke, Patrick J. Bednarski, Andreas Link

Archiv der Pharmazie **2022**, zur Begutachtung eingereicht.

Beiträge der Autoren

Konrad W. Wurm	Planung und Durchführung der Synthesen Analytische Charakterisierung Erstellen des Manuskripts
Frieda-Marie Bartz	Biologische Testung
Lukas Schulig	Durchführung von Modelling und Moleküldynamiksimulationen
Anja Bodtke	Durchführung der HRMS- und NMR-Messungen
Patrick J. Bednarski	Korrektur des Manuskripts
Andreas Link	Anleitung bei der Bearbeitung des Projekts Erstellen des Manuskripts

_____ _____

Konrad Wurm Andreas Link

WILEY-VCH

Archiv der Pharmazie

Replacing the oxidation-sensitive triaminoaryl chemotype of problematic K_V7 channel openers: exploration of a nicotinamide scaffold

Konrad W. Wurm,[1] Frieda-Marie Bartz,[1] Lukas Schulig,[1] Anja Bodtke,[1] Patrick J. Bednarski,[1] and Andreas Link[1],*

1 Institute of Pharmacy, University of Greifswald, Greifswald, Germany

*Correspondence:
Prof. Dr. A. Link
Institute of Pharmacy
University of Greifswald
Friedrich-Ludwig-Jahn-Str. 17, 17489 Greifswald, Germany
Fax: (+49) (0)3834 4204895
E-mail: link@uni-greifswald.de

WILEY-VCH

Archiv der Pharmazie

Abstract

Kv7 channel openers have proven their therapeutic value in the treatment of pain as well as epilepsy, and moreover, they hold the potential to expand into additional indications with unmet medical needs. However, the clinically validated but meanwhile discontinued Kv7 channel openers flupirtine and retigabine bear an oxidation-sensitive triaminoraryl scaffold, which is suspected of causing adverse drug reactions via the formation of quinoid oxidation products. Here, we report the design and synthesis of nicotinamide analogs and related compounds that remediate the liability in the chemical structure of flupirtine and retigabine. Optimization of a nicotinamide lead structure yielded analogs with excellent Kv7.2/3 opening activity, as evidenced by EC_{50} values approaching the single-digit nanomolar range. On the other hand, weighted Kv7.2/3 opening activity data including inactive compounds, allowed for the establishment of structure-activity relationships and a plausible binding mode hypothesis verified by docking and molecular dynamics simulations.

KEYWORDS flupirtine, KCNQ, K_v7, nicotinamide, retigabine

WILEY-VCH

Archiv der Pharmazie

1 INTRODUCTION

K_V7 (KCNQ) channels are homo or heterotetrameric, voltage-gated potassium channels expressed in various tissues,[1] whereby especially heterotetrameric neuronal K_V7 channels predominantly composed of $K_V7.2$ and $K_V7.3$ subunits are validated pharmacological targets.[2] In general, K_V7 activation induces hyperpolarization of cell membranes, through which the ion channels contribute to controlling neuronal excitability. By increasing the action potential threshold[3] and medium afterhyperpolarization while reducing spike frequency,[4] K_V7 channels act as a "brake" for hyperexcitability.[5] Moreover, their opening probability can be influenced by small-molecule ligands,[6] making them attractive therapeutic targets, particularly for a range of neurological diseases.[5]

For example, the administration of K_V7 channel openers was recently discussed for the therapy of various forms of brain damage, including chronic stress-induced brain injury (CSBI) as well as traumatic brain injury (TBI), for which currently no pharmacotherapeutic treatment options exist. In both cases, animal models suggest that reducing the underlying neuronal hyperexcitability by enhancing K_V7-mediated potassium currents might offer a protective effect. Thus, K_V7 channel activation may be a novel therapeutic intervention strategy against post-TBI and CSBI brain damage.[7] Furthermore, a recent review by Costi et al. examined the promising potential of K_V7 channel openers as novel antidepressants and concluded that existing preclinical and clinical studies provide initial evidence of a significant antidepressant effect.[8] Consequently, their conclusions support the conduct of larger randomized controlled clinical trials to validate the potential of K_V7 channel openers as a treatment option for depressive disorders. These overall encouraging results are somewhat clouded by the fact that following the withdrawal of flupirtine (**1**, Figure 1) and retigabine (**2**, USAN: ezogabine) due to adverse drug reactions, no specific and safe K_V7 channel opener is currently available for therapeutic use in humans, which may hamper further development of this class of drugs as potential TBI/CSBI therapeutics or antidepressants.

Moreover, the failure of the two established drugs with their unique mechanism of action also leaves the desire for a replacement in the clinically validated indications of pain[9] and epilepsy.[10] For example, in the case of $K_V7.2$-related epilepsy due to loss-of-function variants, the use of K_V7 channel openers proved indispensable. As a result, there are currently calls for the reintroduction of retigabine for personalized treatment, despite its side effects that led to a withdrawal decision.[11] A therapeutic gap with worrying consequences also remained in the field of pain therapy since metamizole, despite its known association with blood dyscrasias, is increasingly used in Germany as a substitute for flupirtine, which has led to a growing number of metamizole-induced neutropenia cases.[12] Against this background, there is an urgent need for a safe replacement for flupirtine and retigabine to close the existing therapeutic gaps and enable the expansion of the therapeutic potential of K_V7 channel openers.

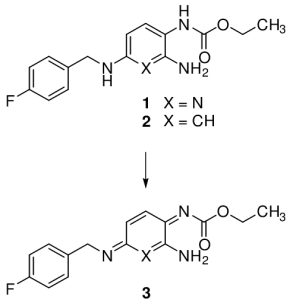

FIGURE 1 Structures of flupirtine (**1**), retigabine (**2**), and their elusive *para* quinone diimine or azaquinone diimine oxidation products (**3**). *Ortho* quinone diimines or azaquinone diimines are also conceivable but not shown.

The reasons for the failure of flupirtine and retigabine have been analyzed in detail in our previous work.[13,14] In essence, the adverse drug reactions responsible for withdrawal, particularly hepatotoxicity with flupirtine[15] and discoloration of the skin and ocular tissues with retigabine,[16] seem not related to the activation of K_V7 channels. Rather, they are most likely attributed to the oxidation-sensitive triaminoraryl scaffold both drugs have in common. As depicted in Figure 1, clear evidence points to the oxidative formation of reactive quinone diimine or azaquinone diimine metabolites such as **3** as the underlying cause of the adverse reactions in both cases.[17,18] Consequently, a possible approach to obtain safer replacements of flupirtine and retigabine is to screen for entirely new chemotypes, as done in the case of the very recently published compound ZK-21 (**8**, Figure 2), which has a 4-aminotetrahydroquinoline scaffold.[19] Moreover, the novel dual-mechanism K_V7 channel opener GRT-X (**7**) that activates both K_V7 potassium channels and the mitochondrial translocator protein (TSPO) likewise has no noteworthy structural similarities with the triaminoaryl type K_V7 channel openers.[20] Hence, new chemotypes such as **7** or **8** could represent a conceivable way to prevent the adverse effects that are presumably closely linked to the metabolically and chemically labile structure of flupirtine and retigabine. However, radical structural changes also increase the risk of unexpected new toxicities, as in the case of PF-04895162, a structural distinct K_V7 channel opener that was found to disrupt bile acid homeostasis and thus failed in phase I clinical trials.[21]

A more conservative but straightforward approach to obtain safer K_V7 channel openers is to conduct minor structural changes in a ligand-based design. Such strategies have led to analogs with potent K_V7 opening activity like HN37 (**4**) or the retigabine analog **5**. Although both compounds demonstrated improved chemical stability compared to retigabine, their design does not entirely exclude the

WILEY-VCH

Archiv der Pharmazie

formation of quinone diimine oxidation products as it still includes a *para* diaminobenzene and a triaminobenzene structural motif, respectively.[22]

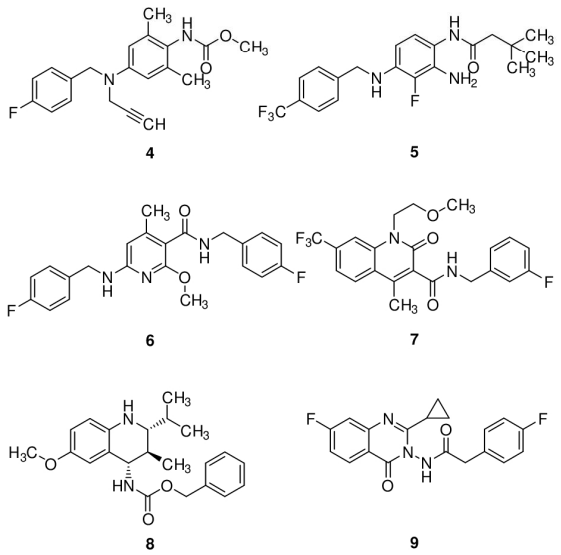

FIGURE 2 Selection of recently published K_V7 channel openers with scaffolds related to flupirtine and retigabine (**4**-**6**) and structurally distinct compounds with new chemotypes (**7**-**9**).

Recently, our group also reported a ligand-based strategy, which in contrast to the approaches mentioned above, focused on completely avoiding structural motifs liable to quinoid metabolite formation. For this purpose, the substitution pattern of the central aromatic core of flupirtine and retigabine was redesigned.[23] In short, the oxidation-sensitive triaminoaryl structure was transformed into a nicotinamide scaffold without ortho/para-positioned nitrogen or oxygen atoms. However, further structural changes were necessary to maintain an acceptable $K_V7.2/3$ opening activity, such as the introduction of an additional methyl group together with a benzylic amide side chain. The resulting compound **6** demonstrated good $K_V7.2/3$ opening activity with an EC_{50} value of 0.310 µM, hence ranging between flupirtine and retigabine in terms of potency. Unfortunately, due to its lipophilic character ($\log D_{7.4}$ = 4.1) and low fraction of sp^3 hybridized carbon atoms, the compound proved to be poorly soluble in water, which limited the toxicity testing and, thus, requires additional structural optimization. To overcome this shortcoming of analog **6** and further improve the $K_V7.2/3$ opening activity, a hybridization approach was intended, using the water-soluble and highly potent analog **10** (EC_{50} = 0.011 µM) as a hybridization partner, which, however, is not devoid of the risk of azaquinone diimine formation (Figure 3).[24] To anticipate a selected result of the biological testing, the hybridization product **18a** showed promising $K_V7.2/3$ channel opening activity and thus served as a starting point for further structural modifications. For this purpose, the structure of **18a** was divided into five zones (Figure 3, A-E), each of which was subjected to substitution with selected structural elements to investigate structure-activity relationships, shed light on a possible binding mode, and further improve the $K_V7.2/3$ opening activity. Particular 6-morpholinonicotinamides such as **18a** have been previously described in a patent by Grünenthal.[25] Still, a comprehensive description of the underlying SARs and a basic toxicological characterization were lacking and could be provided by this study. In addition, we expanded the existing work to include new substituents not previously considered, some of which may not be covered by the referenced patent.

WILEY-VCH

Archiv der Pharmazie

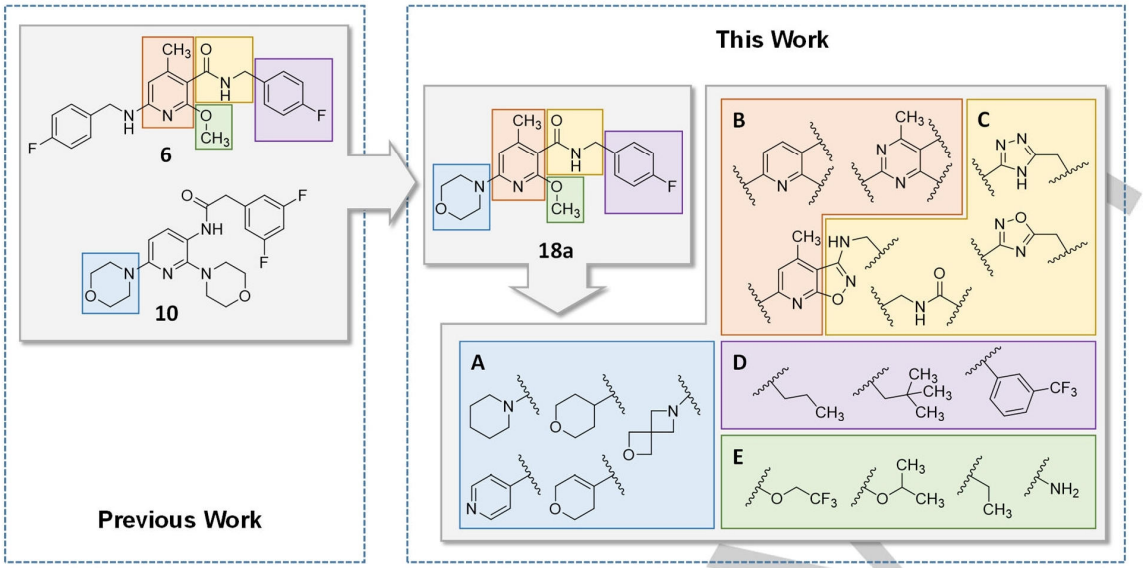

FIGURE 3 Recently published $K_V7.2/3$ openers **6** and **10**, the hybridization approach conducted in this work, yielding analog **18a**, and further structural modifications.

2 RESULTS AND DISCUSSION

2.1 Chemistry

In the first step, the above-mentioned hybridization product **18a** and analogous compounds derived from it with modifications predominantly located in zones A and E were synthesized. The conducted structural changes in zone A were primarily aimed at elucidating the role of the morpholine ring in molecular recognition by the $K_V7.2/3$ binding site. For this reason, the morpholine ring was replaced by carba analogs to help elucidate the possible role of the morpholine nitrogen atom. In particular, a tetrahydro-2*H*-pyran ring, a 3,6-dihydro-2*H*-pyran substituent, and a pyridin-4-yl residue were considered as morpholine replacements by synthesizing analogs **17**, **20**, and **21** (Scheme 1). In general, while the morpholine ring is deemed a privileged structure with advantageous physicochemical, biological, and metabolic properties,[26] in rare cases, it can be oxidized to reactive and potentially toxic iminium metabolites, as described for the multiple receptor tyrosine kinase inhibitor foretinib (not shown).[27] Consequently, the carba analogs **17**, **20**, and **21** also represent alternatives that do not possess this potential metabolic lability. In addition, the strategy of substituting a heteroatom for a methine or methylene group was also applied by synthesizing the piperidine derivative **18e**. Moreover, an attempt was made to further improve the water solubility of the analogs by reducing the compound lipophilicity. For this reason, a 2-oxa-6-azaspiro[3.3]heptane moiety was investigated in the case of analog **18f**. This bioisosteric replacement for a terminal morpholine ring had been shown to lower the lipophilicity of a corresponding molecule effectively.[28]

Regarding zone E, different strategies were followed. First, an additional effort was made to improve the aqueous solubility of the analogs by reintroducing the primary amino group from flupirtine and retigabine in analog **14**. Although the amino group, as a single ortho substituent of the amide function, led to inactive nicotinamide or benzamide analogs in our previous work, it has not yet been evaluated in combination with the advantageous ortho methyl group, which was also able to reconstitute the lost activity in the case of methoxy-substituted compounds such as **6**.[23] Second, a different approach was aimed at improving the $K_V7.2/3$ opening activity by varying the alkoxy residues. As described in our recent publication, the docking of **6** in combination with conformational analysis indicated that the methoxy group, together with the ortho methyl substituent, causes a favorable dihedral angle of the amide function.[23] By synthesizing analogs **18b** and **18c**, it was investigated whether bulkier alkoxy substituents may further enhance the beneficial effect on $K_V7.2/3$ opening by increasing steric interactions and rotational energy barriers.

The initial series of nicotinamide derivatives was synthesized starting from 2,6-dichloro-4-methylnicotinic acid (**11**), whereby various substituents were introduced in position 2 of the pyridine ring in the first reaction step (Scheme 1). In particular, an amino group was attached via a copper-catalyzed Ullmann-type reaction by using sodium azide as a nitrogen source to obtain aminopyridine **12**. According to Zhao et al., the reaction is supposed to proceed via an intermediate azidopyridine (not shown), which is reduced directly in situ to the corresponding primary amine **12**.[29] In contrast, the introduction of alkoxy substituents, yielding **15a-c**, was performed via simple nucleophilic substitution reactions. The alcoholate, which served as the nucleophile, was generated in situ by reacting the corresponding alcohol with sodium hydride. Both reactions to introduce substituents at position 2 of the pyridine ring proceeded regioselectively at this specific position. The reason for the regioselectivity is probably a directing effect of the carboxyl function of **11**, which in both cases forms cyclic, five- or six-membered transition states, respectively, involving either a sodium alcoholate or a copper azide complex.[29,30]

WILEY-VCH

Archiv der Pharmazie

After introducing substituents at position 2 of the pyridine ring, the amide coupling allowed for the synthesis of all analogs. The activation of the nicotinic acid derivatives was performed either, as in the case of amino nicotinic acid derivative **12**, via the formation of an acyl imidazole after reaction with CDI or via generation of acyl chlorides in a DMF-catalyzed reaction with oxalyl chloride carried out in the case of **15a**-**c**. Both activated carboxylic acid species (not shown) were reacted directly, without prior isolation, with the corresponding amines to give the desired amides **13** and **16a**-**d**.

In order to introduce a substituent at position 6 of the pyridine ring, two different methods were principally applied. C-C bonds were formed via Suzuki coupling reactions by using the corresponding boronic acid or boronic acid pinacol ester to yield compounds **17** and **20**. The tetrahydropyran substituent in the case of analog **21** was obtained by catalytic hydrogenation of the dihydropyran precursor **20**. In contrast, the introduction of amino substituents at position 6 in the case of compounds **18a**-**f** was not carried out with a palladium catalyst but by nucleophilic substitution reactions, which were performed by microwave-assisted heating. In the case of all methoxy-substituted compounds (**18a**, **d**, **e**), a by-product was formed, causing low yields of the desired products. In the synthesis of compound **18a**, it was isolated and identified as the demethylated analog **19a**. Contrary to a methoxy residue, a 1-methyl-ethoxy and a 2,2,2-trifluoroethoxy substituent incorporated in compounds **18b**/**c** were stable under identical reaction conditions. 2-Oxa-6-azaspiro[3.3]heptane oxalate required for synthesizing the spiro analog **18f** was prepared in a two-step synthesis according to a protocol described in the literature (not shown).[31] Briefly, 4-methylbenzenesulfonamide was reacted with pentaerythritol tribromide to generate the spiro partial structure in a double ring closure reaction. In the second step, the tosyl protective group was cleaved reductively with magnesium, and the resulting amine was precipitated as an oxalate salt. In the synthesis of compound **18f**, the free amine was released from its salt in situ by adding the stronger base DBU to the reaction mixture.

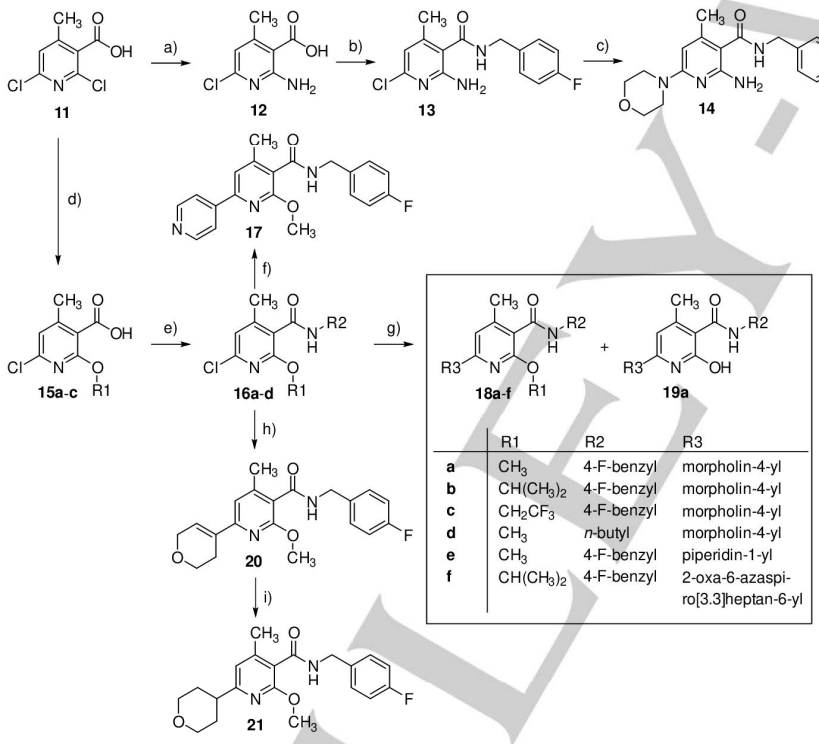

	R1	R2	R3
a	CH_3	4-F-benzyl	morpholin-4-yl
b	$CH(CH_3)_2$	4-F-benzyl	morpholin-4-yl
c	CH_2CF_3	4-F-benzyl	morpholin-4-yl
d	CH_3	*n*-butyl	morpholin-4-yl
e	CH_3	4-F-benzyl	piperidin-1-yl
f	$CH(CH_3)_2$	4-F-benzyl	2-oxa-6-azaspiro[3.3]heptan-6-yl

SCHEME 1 Synthesis of nicotinamide analogs **14**-**21** with modifications in zones A, D, and E. a) NaN_3, K_2CO_3, CuI, ethane-1,2-diamine, EtOH, Ar, reflux, 28 h, 54%; b) 1. CDI, THF, 50 °C, 1 h, 2. 4-fluorobenzylamine, THF, rt, 12 h, 35%; c) morpholine, NMP, 165 °C, μW irradiation, 1 h, 73%; d) appropriate alcohol, NaH, THF, 0 °C–70 °C, 7–23 h, 96–99%; e) 1. $(COCl)_2$, DMF, DCM, 0 °C–rt, 3 h, 2. amine, TEA, DCM, 0 °C–rt, 16 h, 49–61%; f) pyridin-4-ylboronic acid, $Pd(PPh_3)_4$, Na_2CO_3, 1,4-dioxane, H_2O, Ar, 140 °C, μW irradiation, 0.5 h, 59%; g) amine, NMP, 165 °C, 0.5–1 h, 28–53%; h) 1-cyclohexeneboronic acid pinacol ester, $Pd(PPh_3)_4$, Na_2CO_3, 1,4-dioxane, H_2O, Ar, 140 °C, μW irradiation, 15 min, 86%; i) H_2, Pd/C, MeOH, rt, 5 h, 74%.

Since the pronounced structural change from a 4-fluorobenzylamino residue in **6** to a morpholino substituent in **18a** was possible without significantly affecting the activity, the question of the pharmacophore arises. Analogue **29** (Scheme 2) was synthesized to clarify whether the morpholine ring is part of the core pharmacophore or, on the contrary, molecular recognition might even be possible without a morpholine ring. Analogously, derivatives **25** and **28a**/**b** were synthesized in which the methyl group or the alkoxy group were missing to clarify the role of the specific substituents, thus testing our hypothesis that ortho disubstitution of the amide group might be essential for $K_V7.2/3$ opening activity of nicotinamide analogs.

In general, nicotinamide derivatives with missing substituents in positions 2, 4, or 6 of the pyridine ring were prepared by synthetic routes similar to those of the nicotinamide analogs **18a**-**f** mentioned above. The synthesis of the nor-analog **25** was performed

WILEY-VCH

Archiv der Pharmazie

analogously to the synthesis of **18a** with the difference that 2,6-dichloronicotinic acid (**22**) was used as starting material instead of 2,6-dichloro-4-methylnicotinic acid (**11**). The amide coupling in the second reaction step to obtain **24** was done by using the coupling reagents DIC and HOBt (Scheme 2). In the case of the analogs **28a**/**b**, in which the substituents in position 2 or positions 2 and 4 are absent, the introduction of the methoxy group in the first step was skipped. After the amide coupling, yielding **26a**/**b**, the substitution reaction to introduce the morpholino substituent was carried out, which in this case required less drastic reaction conditions compared to the synthesis of analogs **18a**-**f**. Conventional heating to 80 °C instead of microwave-assisted heating to 165 °C proved sufficient. Since two chloro substituents were accessible for the reaction, a mixture of two regioisomers was formed and subsequently separated by silica gel column chromatography to obtain the desired morpholino nicotinamides **27a**/**b** and their corresponding regioisomers (not shown). Analytical discrimination of the regioisomers by NMR was not possible at this stage. However, after reductive cleavage of the chloro substituent in the following reaction step, confirmation of the identity of the desired analogs **28a**/**b** based on ^{1}H-NMR spectroscopy was possible by analyzing the pyridine proton signals. In the case of **28a**, two singlets were observed, unequivocally confirming the morpholino substituent in position 6 of the pyridine ring. The same applies to **28b**, where a doublet with ^{3}J coupling (9.0 Hz), a doublet with ^{4}J coupling (2.5 Hz), and a doublet of doublets (J = 9.0, 2.5 Hz) verify the desired 6-morpholino nicotinamide structure while excluding morpholino substitution at position 2. Analogously, the chloro substituent of compound **17b** was cleaved following the same catalytic hydrogenation procedure in order to obtain analog **29**, which lacks a substituent in zone A.

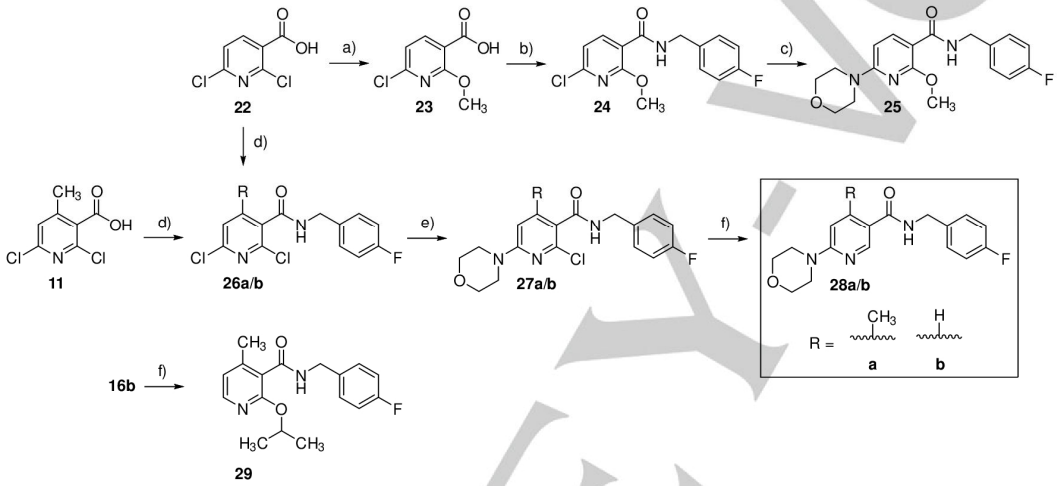

SCHEME 2 Synthesis of nicotinamide analogs **25**, **28a**/**b**, and **29** lacking selected substituents of the central pyridine ring. a) MeOH, NaH, THF, 0–70 °C, 7 h, 79%; b) 4-fluorobenzylamine, DIC, HOBt, DMF, rt, 16 h, 65%; c) morpholine, NMP, 165 °C, µW irradiation, 30 min, 36%; d) 4-fluorobenzylamine, DIC, HOBt, DMF, rt, 16 h, 46–86%; e) morpholine, MeOH or 2-propanol, reflux, 1–3 d, 23–26%; f) H_2, Pd/C, TEA, MeOH, rt, 2–5 h, 64–66%.

Regarding zone B, a replacement of the central pyridine ring of the nicotinamide scaffold with a pyrimidine ring could be an interesting structural change since various examples exist where this bioisosteric exchange led to improved biological activity on different targets.[32] In analogy to these literature cases, a pyrimidine ring with its altered electronic properties and reduced basicity may also influence the ligand binding to K_V7.2/3 channels. The envisioned pyrimidine analogs were accessible via the Biginelli multicomponent reaction, which in its original form, however, does not provide access to alkoxy substituted compounds. For this reason, the resulting analogs **40a**-**c** contain an ethyl group instead of a methoxy substituent in zone E.

The initial Biginelli reaction, which involved an acid-catalyzed cyclocondensation of ethyl acetoacetate (**32**), propionaldehyde (**31**), and urea (**30**), yielded the 3,4-dihydropyrimidin-2(1*H*)-one **33**, which was converted into the corresponding pyrimidin-2(1*H*)-one **34** in a subsequent oxidation step with nitric acid (Scheme 3). The following chlorination was carried out according to a modified procedure of Zhao et al. by heating **34** in excess phosphoryl chloride.[33] In the course of the reaction, the 3,4-dihydropyrimidin-2(1*H*)-one **34** probably forms an intermediate dichlorophosphate (not shown), as it was suggested for the chlorination of related quinazolin-4(3*H*)-ones.[34] Subsequently, the dichlorophosphate was attacked by a chloride ion in an S_NAr reaction, yielding the chloropyrimidine **35**. The additional use of a base such as triethylamine, sometimes described in the literature for similar reactions,[35] has been evaluated but did not result in an improved yield. After the chlorination, two different synthetic routes were investigated. For the synthesis of analog **40a**, the ethyl ester function of **35** was hydrolyzed under alkaline conditions, which gave the corresponding carboxylic acid **36**. This was followed by a coupling reaction with HATU yielding amide **37**. In the final step, the morpholino substituent was introduced by applying the same microwave-assisted method used for the nicotinamides to obtain the final analog **40a**. For the entire six-step synthesis of **40a**, a poor cumulative yield of only 2.8% was calculated. In retrospect, the ester hydrolysis in the first reaction step has proven particularly unfavorable because the yield was reduced by an undesired by-product. The side product was not isolated, but the chloropyrimidine structure of **35** was suspected to be affected by the alkaline hydrolysis leading to a pyrimidinone by-product. For this reason, the reaction sequence was rearranged, resulting in an alternative synthetic route for analogs **40b**/**c**. In particular, compared to the synthesis of **40a**, the morpholino substituent was introduced first to give compound **38**, while the hydrolysis of the ethyl ester to obtain carboxylic

WILEY-VCH

Archiv der Pharmazie

acid **39** took place in the following step since hydrolysis of the chloropyrimidine structure is thus not a concern. Overall, the modified reaction sequence and the use of DIC and HOBt instead of HATU as amide coupling reagents in the last step to obtain the final amides **40b**/**c** enabled an improved cumulative yield of 7.7%.

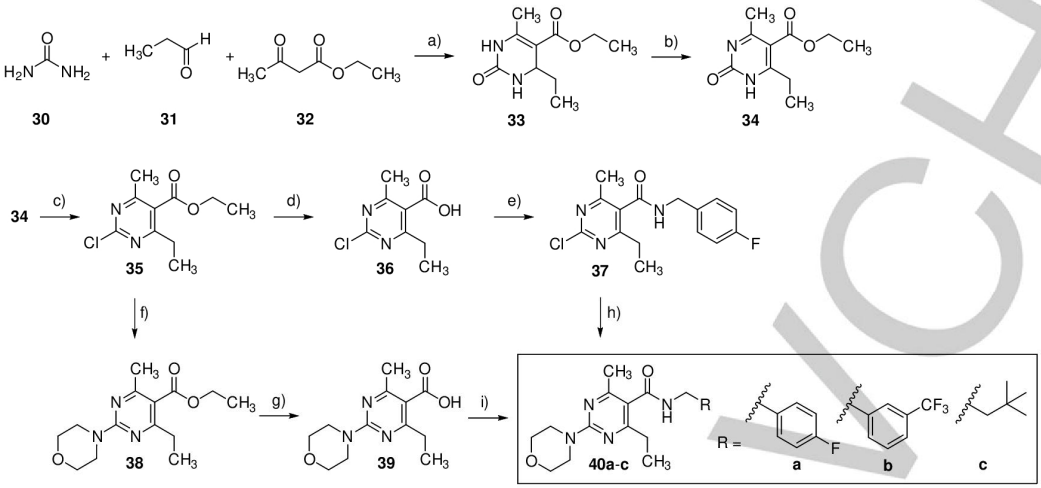

SCHEME 3 Synthesis of pyrimidine analogs **40a**-**c**. a) AcOH, EtOH, 90 °C, 20 h, 32%; b) HNO_3, H_2O, -10 °C, 15 min, 87%; c) $POCl_3$, 110 °C, 1 h, 45%; d) KOH, H_2O, THF, rt, 12 h, 72%; e) 4-fluorobenzylamine, HATU, DIPEA, DMF, rt, 16 h, 42%; f) morpholine, EtOH, 80 °C, 2 h, 90%; g) KOH, EtOH, H_2O, 80 °C, 4 h, 84%; h) morpholine, NMP, 165 °C, µW irradiation, 20 min, 73%; i) amine, DIC, HOBt, DMF, rt, 16 h, 79–81%.

The carbamate partial structure of retigabine is supposedly involved in the formation of hydrogen bonds to the $K_V7.2$ binding site, which are also conserved in the case of nicotinamide derivative **6** as predicted by molecular docking.[23,36] Apart from that, mainly hydrophobic interactions contribute to the binding of compound **6**. Accordingly, the particular importance of the amide group can be anticipated, which was further explored by variation of the amide partial structure following three different approaches. The first structural change attempted in this direction was to replace the amide function with bioisosteric cyclic amide mimetics such as a 1,2,4-oxadiazole or a 1,2,4-triazole ring, resulting in analogs **47** and **54**. A similar approach was recently used successfully in the optimization of a GPR88 agonist (not shown), where an amide bioisosteric replacement with a variety of azoles, followed by lead optimization, provided a potent and efficacious triazole-based GPR88 agonist.[37] The second strategy was the incorporation of an amide-like structure into a fused ring system. Here, the isoxazolo[5,4-*b*]pyridin-3-amine **44** was synthesized, representing a conformationally restricted analog. A comparable approach yielded, for example, highly potent benzo[*d*]isoxazol-3-amine based sEH inhibitors with single-digit nanomolar IC_{50} values from a benzamide lead structure.[38] The third structural change carried out in this context was a shift of the amide group realized by transforming the *N*-benzylnicotinamide **18a** to the *N*-(pyridin-3-ylmethyl)benzamide analog **49**; thus altering the hydrogen-bonding ability as well as the flexibility and conformation in this part of the scaffold.

The synthesis of the isoxazolo[5,4-*b*]pyridin-3-amine analog **44** as a cyclic and conformationally restricted nicotinamide replacement could be realized in three steps (Scheme 4). The starting point was 2,6-dichloro-4-methylnicotinonitrile (**41**), whose chloro substituent in position 6 was replaced by a morpholino residue through nucleophilic substitution. The reaction proceeded regioselectively with a preference for position 6, as reported by Antczak et al.[39] Nevertheless, a small amount of the regioisomer substituted at position 2 was formed. The mixture of the two resulting regioisomers was separated by chromatography, and the desired regioisomer **42** was cyclized to afford the corresponding isoxazolo[5,4-*b*]pyridin-3-amine **43** by reaction with acetohydroxamic acid. This method involved a convenient one-pot procedure where the *ortho* chloro nicotinonitrile forms an *N*-[(3-cyanopyridin-2-yl)oxy]acetamide intermediate after nucleophilic substitution of the chloro substituent with a hydroxamate anion, followed by in situ base-catalyzed intramolecular cyclization and subsequent elimination of the acetyl residue.[40] By reacting the amino group of compound **43** with 4-fluorobenzaldehyde, an imine (not shown) was formed in the last reaction step, which was reduced to the corresponding secondary amine without prior isolation by hydrosilylation with triethylsilane and trifluoroacetic acid to obtain the final analog **44**.

The synthesis of the oxadiazole derivative **47** began with the above-mentioned compound **42** (Scheme 4). In the first step, a methoxy group was introduced by substituting the remaining chloro substituent with sodium methoxide. The nitrile function of the resulting compound **45** was then converted to the corresponding amidoxime **46** by treatment with an aqueous solution of hydroxylamine. This reaction required an unusually long time (4 days) for complete conversion, which is presumably attributed to the ortho-disubstitution of the nitrile function and the resulting restricted steric accessibility. The electron-donating properties of the morpholino and methoxy substituents may also have reduced the reactivity of the nitrile function for nucleophilic attack by hydroxylamine. While most syntheses of oxadiazoles reported in the literature proceed via amidoxime precursors such as **46**, the methods differ in the use of diverse activated carboxylic acid derivatives as acylating agents and in the reaction conditions applied for ring closure.[41] In this particular case, the amidoxime **46** was acylated with phenylacetyl chloride. The corresponding acylation product (not shown) was not isolated, but a ring closure was induced directly by the addition of tetrabutylammonium fluoride (TBAF) as a catalyst. Mechanistically, the ring closure

WILEY-VCH

Archiv der Pharmazie

reaction of the *O*-acyl amidoxime intermediate to the final oxadiazole analog **47** is supposed to proceed via an intramolecular attack of the amidoxime nitrogen atom on the carbonyl carbon atom of the acyl group, followed by dehydration of the resulting dihydro-oxadiazolol. Both steps are facilitated by TBAF, whose fluoride ion acts as a strong base in polar aprotic solvents such as THF.[42]

The *N*-(pyridin-3-ylmethyl)benzamide analog **49** with a shifted carbonyl group compared to the initial nicotinamide scaffold was synthesized from the nicotinonitrile **45** in two steps. First, the nitrile group of **45** was reduced by catalytic hydrogenation with Raney nickel as a catalyst to obtain the primary amine **48**. Then, in the second step, **48** was acylated by reaction with 4-fluorobenzoyl chloride, yielding the final analog **49**.

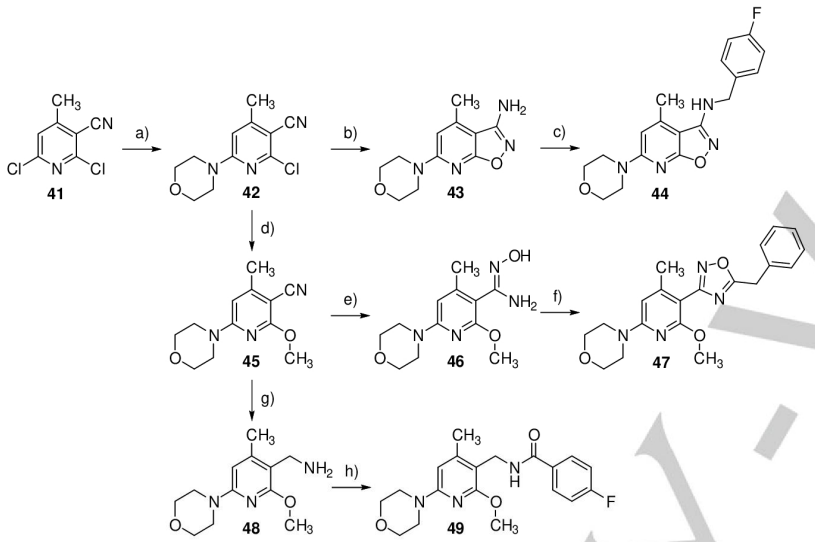

SCHEME 4 Synthesis of analogs **44**, **47**, and **49** with modifications in zone C. a) morpholine, MeOH, 0 °C–rt, 16 h, 70%; b) acetohydroxamic acid, *t*-BuOK, Ar, DMF, RT–50 °C, 5.5 h, 43%; c) 4-fluorobenzaldehyde, $(C_2H_5)_3SiH$, TFA, DCM, RT–60 °C, 25 h, 80%; d) NaOMe, MeOH, reflux, 24 h, 90%; e) hydroxylamine (aq.), EtOH, reflux, 4 d, 99%; f) 1. 2-phenylacetyl chloride, TEA, DCM, 0 °C, 1 h, 2. TBAF, THF, rt, 2 h, 36%; g) Ni, H_2, NH_3, MeOH, 50 °C, 5 h, 71%; h) 4-fluorobenzoyl chloride, TEA, DCM, rt, 16 h, 64%.

The above-mentioned nicotinic acid derivative **15a** was also used as a starting point for synthesizing the triazole derivative **54** (Scheme 5). In the first step, the corresponding methyl ester **50** was obtained by alkylation of **15a** with iodomethane. This was followed by substituting the chlorine atom of **50** to afford the morpholino derivative **51**, whose methyl ester function was subjected to hydrazinolysis yielding the hydrazide **52**. The following triazole formation proved problematic since two attempts to achieve a ring closure reaction were initially unsuccessful. The first approach was based on the reaction of hydrazide **52** with the Pinner salt **56** to give the *N*-(1-iminoalkyl)-hydrazide **53**. According to the literature, ring closure to obtain the triazole structure should occur by heating compounds like **53** to the melting point under reduced pressure without solvent.[43] However, in this particular case, the procedure provided a complex mixture of products with little, if any, yield of the desired product according to TLC reaction control. A second unsuccessful attempt was based on a copper-catalyzed tandem addition–oxidative cyclization reaction described by Ueda and Nagasawa.[44] Unfortunately, in this specific case, the reaction between nitrile **45** and amidinium salt **57**, previously prepared by ammonolysis of the Pinner salt **56**, did not lead to any product formation. Finally, the triazole synthesis succeeded by applying the method of Yeung et al., which includes a one-step, base-catalyzed condensation of the hydrazide **52** with 4-fluorobenzonitrile (**55**).[45]

WILEY-VCH

Archiv der Pharmazie

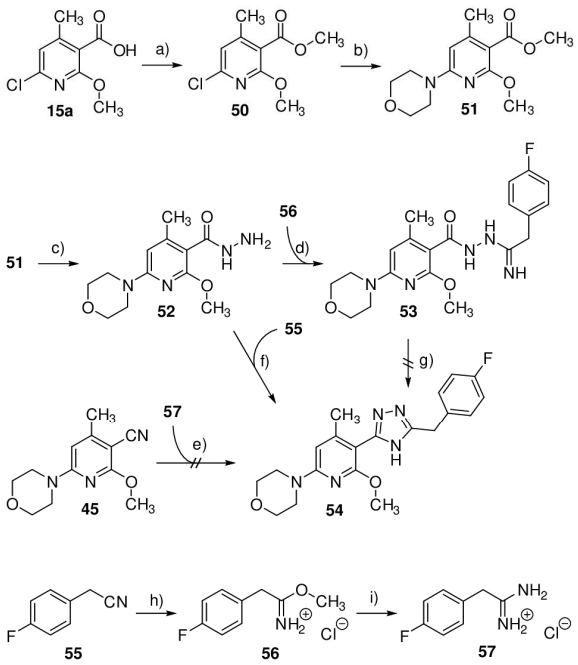

SCHEME 5 Synthesis of the 1,2,4-triazole analog **54**. a) CH_3I, K_2CO_3, DMF, rt, 8 h, 98%; b) morpholine, TEA, NMP, 90 °C, 2 d, 39%; c) N_2H_4*H_2O, MeOH, reflux, 24 h, 67%; d) NaOMe, MeOH, 0 °C–rt, 24 h, 47%; e) CuBr, Cs_2CO_3, DMSO, 120 °C, 24 h; f) K_2CO_3, *n*-BuOH, 150 °C, µW irradiation, 4 h, 47%; g) 220 °C, 0.1 mbar, 10 min; h) HCl, MeOH, 0 °C, 3 h, 58%; i) NH_3, MeOH, rt, 24 h, 61%.

2.2 Pharmacology/Biology/Modeling

2.2.1 Evaluation of K_V7.2/3 opening activity

The K_V7.2/3 opening activity was determined by applying a commercially available assay on HEK293 cells that overexpress the heterotetrameric K_V7.2/3 channel. The assay exploits the permeability of potassium channels for thallium ions and is based on a thallium-sensitive fluorescent dye, which is trapped inside the cell after esterase cleavage. Thallium influx through K_V7.2/3 channels generates a fluorescence signal whose intensity correlates with the extent of channel opening. Based on the data generated this way, EC_{50} values were calculated, indicating the concentration at which the half-maximum fluorescence signal and, thus, the half-maximum K_V7.2/3 opening activity was achieved. In addition to EC_{50} values, the efficacy, i.e., the maximum response, of the analogs relative to flupirtine was calculated. Both values can be found in Table 1 for all analogs. Based on these results, structure-activity relationships were derived, which are systematically discussed below.

WILEY-VCH

Archiv der Pharmazie

Table 1. K_V7.2/3 channel opening activity, in vitro toxicity, and log$D_{7.4}$ values of the synthesized compounds **14**-**54** in comparison to flupirtine and retigabine.[a]

		HEK-293		TAMH		HEP-G2		
Entry	**Log$D_{7.4}$**	**EC_{50} [b] [µM]**	**Efficacy [%]**	**LD_{50} [c] [µM]**	**LD_{25} [d] [µM]**	**LD_{50} [c] [µM]**	**LD_{25} [d] [µM]**	**LD_{25}/ EC_{50} [f]**
Flu [g]	2.0	1.837 ± 0.844	100	487 ± 51	103 ± 47	547 ± 111	74 ± 40	40
Ret [g]	2.1	0.249 ± 0.052	134 ± 16	>400	>400	>400	269 ± 166	1080
6 [g]	4.1	0.310 ± 0,119	105 ± 12	>63	>63	>16	>16	52
10 [g]	3.6	0.011 ± 0.004	111 ± 7	>500	212 ± 140	>500	231 ± 141	19273
14	2.2	6.858 ± 1.319	113 ± 28	>500	349 ± 36	>500	123 ± 73	18
17	2.7	0.500 ± 0.105	112 ± 11	>63	>63	>63	26 ± 20	52
18a	3.0	0.117 ± 0.029	144 ± 11	>63	>63	>63	>63	539
18b	3.8	0.017 ± 0.009	132 ± 16	>31	>31	>31	15 ± 1	882
18c	3.3	0.012 ± 0.004	117 ± 19	>15	>15	>15	>15	1250
18d	2.6	3.799 ± 1.730	170 ± 4	>250	>250	>250	>250	66
18e	4.7	0.040 ± 0.007	127 ± 1	>31	>31	>31	32 ± 11	775
18f	3.8	- [e]	- [e]	>63	>63	>63	>63	-
19a	2.4	- [e]	- [e]	>63	30 ± 17	>63	28 ± 16	-
20	3.1	0.143 ± 0.003	111 ± 11	>125	>125	>63	>63	440
21	3.1	2.402 ± 0.759	129 ± 16	>125	>125	>125	>125	52
25	3.8	- [e]	- [e]	>125	77 ± 35	>125	75 ± 24	-
28a	2.4	8.632 ± 1.876	76 ± 19	>250	169 ± 29	>250	126 ± 36	15
28b	2.3	- [e]	- [e]	>125	>125	>125	>125	-
29	2.6	- [e]	- [e]	>125	13 ± 3	>125	>125	-
40a	3.0	0.126 ± 0.035	114 ± 10	>31	>31	>31	20 ± 12	159
40b	3.5	0.035 ± 0.028	104 ± 12	>31	>31	>31	>31	886
40c	3.4	2.134 ± 0.591	52 ± 11	>63	>63	>63	>63	30
44	3.2	- [e]	- [e]	>125	>125	>125	>125	-
47	4.7	1.179 ± 0.193	45 ± 4	>30	>30	>30	>30	25
49	3.6	- [e]	- [e]	>31	>31	>63	29 ± 5	-
54	3.3	2.245 ± 0.338	149 ± 25	>30	>30	>30	>30	13

[a] Log$D_{7.4}$ values were estimated by employing an HPLC-based method. HEK293 cells overexpressing the K_V7.2/3 channel were used to obtain the EC_{50} values by applying a fluorimetric assay. LD values were determined by an MTT assay in TAMH and HEP-G2 cell lines after 24 h of exposure. EC_{50} and LD values are means of ≥ 3 independent determinations ± standard deviations. [b] Necessary concentration to reach half-maximal K_V7.2/3 channel opening activity. [c] Concentration required to reduce cell viability to 50% compared to untreated controls. [d] Concentration required to reduce cell viability to 75% compared to untreated controls. [e] No K_V7.2/3 channel opening activity up to a concentration of 20 µM. [f] The lower of both LD_{25} values was used to calculate the LD_{25}/EC_{50} ratio. If no LD_{25} value could be determined, the maximum tested concentration was used for calculation. [g] Previously published values.[14,23,24]

Regarding zone A, the replacement of the 4-fluorobenzylamino residue of **6** with a morpholine ring in **18a** led to a significant boost in activity as intended by the hybridization approach. In particular, the EC_{50} value of **18a** decreased compared to **6** from 0.310 µM to 0.117 µM, and at the same time, the efficacy increased from 105% to 144%, although the reported outstanding K_V7.2/3 opening activity of the second hybridization partner **10** was not quite reached. In contrast, the complete deletion of a substituent in zone A resulted in a total loss of activity in the case of analog **29**, which clearly confirmed the morpholine ring as part of the core pharmacophore.
Both heteroatoms of the morpholino substituent, on the other hand, do not appear to be of essential importance for K_V7.2/3 opening. This was evident in the case of the morpholine oxygen atom, where a replacement with a methylene group even led to improved K_V7.2/3 opening. The corresponding piperidine derivative **18e** exhibited a 2.9-fold reduced EC_{50} value compared to the direct morpholino counterpart **18a**. This observation correlates with molecular docking results (Figure 4B/C), which predicted the morpholine ring to occupy a hydrophobic cavity with no involvement of the oxygen atom in any hydrogen bond interactions.

WILEY-VCH

Archiv der Pharmazie

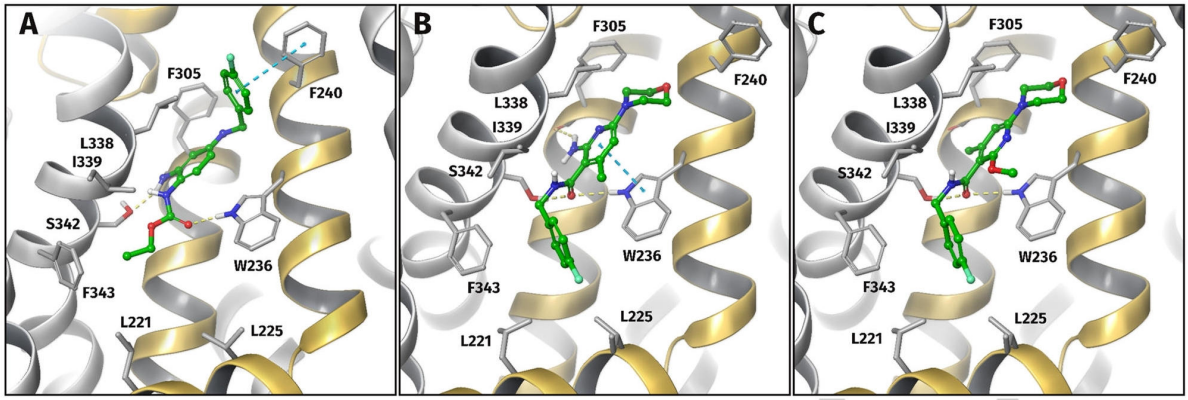

FIGURE 4 Predicted binding poses of retigabine (A), **14** (B), and **18a** (C). The hydrogen bonds to W236 and S342 are maintained for all compounds, although the central pyridine ring is slightly displaced compared to retigabine. Therefore, the primary amino group of **14** does not participate in hydrogen bond formation with S342 as predicted for retigabine. Instead, it is shifted into a more hydrophobic cavity, which is also occupied by the methyl substituent of **18a**. The 4-fluorobenzyl group binds to a larger hydrophobic pocket formed by L221, L225, and F343 as previously reported for other derivatives.[23] The π-π interactions to W236 (represented as blue dashed lines) can be observed for all three ligands during molecular dynamics simulations, depending on the distinct orientation of the aromatic rings. The color of the secondary structure elements represents the respective chains of K_V7.2 (gold) and K_V7.3 (silver) in the K_V7.2/3-heterotetramer.

In contrast, when considering only the activity data, it was initially presumed that the morpholine nitrogen atom might contribute substantially to binding since the corresponding methine analog **21**, bearing a tetrahydropyran ring, showed a considerably 20-fold decrease in potency compared to the direct morpholino congener **18a**. However, the dihydropyran derivative **20**, which also has a carbon atom in place of the morpholine nitrogen atom, was approximately as potent as **18a**. This observation, combined with molecular docking results displayed in Figure 4, in turn, rather implies that the tertiary amino group of the morpholine ring does not participate in direct interactions with the K_V7.2/3 binding site but instead might favor an advantageous molecular geometry. Specifically, the morpholine nitrogen nonbonding pair of electrons interacts with the electron-deficient pyridine π-system and thus probably favors a coplanar conformation, which is also assumed to be probable for the dihydropyran moiety of **20** since the double bond is in conjugation with the adjacent pyridine ring. These conformational considerations were confirmed by quantum mechanical calculations using density functional theory (DFT), which revealed energetic minima at a dihedral angle of approximately 0/180° and high rotational energy barriers for a morpholino as well as a dihydropyran substituent (Figure 5A/D). In contrast, a twisted conformation is probably energetically preferred by the 2-(tetrahydro-2*H*-pyran-4-yl)pyridine moiety of **21** owing to the sp^3 hybridized methine carbon atom, as verified by the dihedral scanning plot, which shows a global minimum at 60° and low rotational energy barriers (Figure 5C). Viewed in correlation with the corresponding docking poses, which also indicate a coplanar orientation of the pyridine ring with the adjacent heterocyclic substituent, the different molecular geometries suggest that the inferior K_V7.2/3 opening activity of **21** compared to **18a** and **20** is mainly due to a conformational preorganization of **18a** and **20**, which may reduce the entropic costs of ligand binding.

Regarding the other zone A substituents, an aromatic residue, such as a pyridine ring in analog **17**, was also found to be tolerated since the incorporated biaryl structure is expected to favor a coplanar conformation, too (Figure 5E). However, despite the beneficial coplanarity, compound **17** was still 4.3-fold less potent than the direct morpholino analog **18a**, but this may be attributed to other reasons, such as the flat and rigid geometry of the 4-pyridyl moiety, which deviates considerably from the chair conformation expected for a morpholine ring.[46] Consequently, this specific conformation of the morpholino substituent, which a pyridine substituent cannot adopt, might be required for good K_V7.2/3 channel opening since it is also observed in molecular dynamics simulations of corresponding analogs (Figure 4B/C).

Despite the presence of a tertiary amino partial structure as with a morpholino substituent, the spiro analog **18f** showed no K_V7.2/3 opening activity up to 20 μM. Presumably, the 2-oxa-6-azaspiro[3.3]heptane substituent is slightly too long for an adequate fit into the K_V7.2/3 binding pocket since the distance between the nitrogen and the oxygen atom is 4.3 Å compared to 2.8 Å for morpholine.[28] Moreover, the substituent has a rather linear geometry and differs significantly from the chair conformation of morpholine, which is presumed to be favorable for K_V7.2/3 opening. Regarding physicochemical properties, contrary to cases reported in the literature, the introduction of the 2-oxa-6-azaspiro[3.3]heptane substituent did not result in a decreased lipophilicity, as originally intended by this structural change. Indeed, as with the corresponding morpholino substituted compound **18b**, the log$D_{7.4}$ value of the spiro analog **18f** was determined to be 3.8.

WILEY-VCH

Archiv der Pharmazie

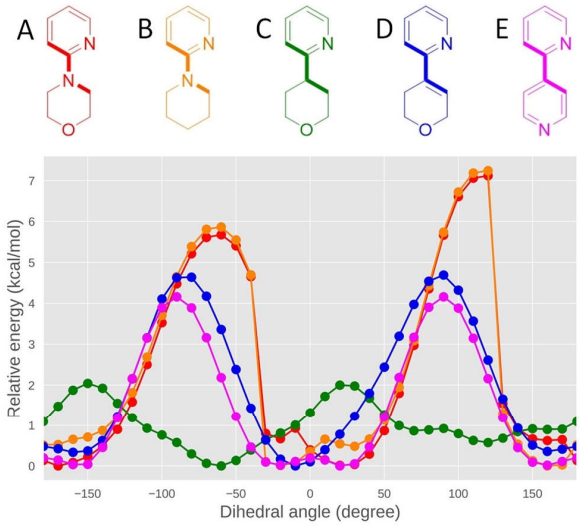

FIGURE 5 Dihedral angle scanning for various pyridine scaffolds using B3LYP-D3/6-31G(d,p). The calculations were performed with Jaguar version 11.5 (Schrödinger, LLC, New York, NY, 2022).[47]

Concerning zone B, very potent pyrimidine analogs with nanomolar $K_V7.2/3$ opening activity were obtained (**40a**/**b**), indicating that a central pyrimidine ring is well tolerated. However, since the corresponding analogs also bear an alkyl residue in zone E instead of an alkoxy substituent due to the chosen synthesis route via the Biginelli reaction, no final, conclusive statement can be made with certainty about the influence of the pyrimidine ring. Nevertheless, the almost identical EC_{50} values of the closely related analogs **18a** and **40a** suggest that the pyrimidine ring did not significantly affect the $K_V7.2/3$ opening activity compared to a pyridine core, which is also supported by very similar docking poses of the corresponding analogs with no specific interaction of the additional pyrimidine nitrogen atom.

Contrary to the possible role of the pyrimidine ring, however, a valid judgment can be made on the importance of the methyl substituent in zone B, which must be considered in conjunction with the second ortho substituent of the amide group in zone E. In particular, compound **25**, which differs from the submicromolar active analog **18a** only in the absence of the methyl group, as well as compound **28b**, which lacks both ortho substituents of the amide group, were inactive up to a concentration of 20 µM. In contrast, compound **28a**, which has a methyl substituent attached to the pyridine core but lacks the second ortho substituent in zone E, was still active, albeit weakly potent, with a 70-fold reduced EC_{50} value compared to **18a**. Based on these observations, two conclusions can be drawn concerning the possible role of the methyl group in zone B. Firstly, viewed in isolation, the methyl group seems to be slightly more important for $K_V7.2/3$ opening than the second ortho substituent of the amide group since the methylated analog **28a** was still weakly active while **25** and **28b**, both lacking the methyl group, were completely inactive. Secondly, however, only the presence of both amide ortho substituents, as in the case of **18a**, allows sufficient $K_V7.2/3$ opening activity with submicromolar potency. Essentially, these results complete the evidence supporting our earlier hypothesis that the ortho disubstitution of the amide function is necessary to favor a molecular geometry that matches the bound-state conformation of the nicotinamide analogs in which the amide group is rotated out of the aromatic plane.[23] In contrast, a methoxy residue as the only amide ortho substituent, as in **25**, probably stabilizes an unfavorable coplanar orientation of the amide group through intramolecular hydrogen bonding. This negative effect is impossible with a methyl group as the sole ortho substituent, which is why the methylated analog **28a**, in contrast to compound **25** bearing a methoxy residue, was at least weakly active.

By modifying zone C, the possible role of the N-substituted amide group was investigated, which is presumed to be a crucial structural element of the initial nicotinamide scaffold. A first structural change based on the incorporation of an amide-analogous partial structure into an isoxazolo[5,4-*b*]pyridin-3-amine scaffold proved clearly detrimental to $K_V7.2/3$ opening since the corresponding analog **44** was inactive up to a concentration of 20 µM. This observation essentially confirms the hypothesis formulated above that the amide group in the bound state conformation is probably rotated out of the pyridine plane, which of course, is not possible in the case of the conformationally restricted isoxazolo[5,4-*b*]pyridine analog **44**.

A different attempt to replace the amide function of **18a** with heterocyclic amide bioisosteres was slightly more successful, yielding the weakly to moderately active compounds **47** and **54**, which provided valuable SAR insights despite their overall inferior $K_V7.2/3$ opening activity. As suggested by docking and molecular dynamics simulations, the amide group of nicotinamide analogs could be involved in direct interactions with the $K_V7.2/3$ binding site as both a hydrogen bond donor and acceptor. In particular, the role of the amide function as a hydrogen bond donor was partially elucidated by the cyclic amide bioisosteres since the triazole ring of analog **54** provides a hydrogen atom similar to an amide group. In contrast, the oxadiazole structure of **47** is not able to act as a hydrogen bond donor. Consistent with this assumption, docking predicted the triazole ring of **54** to mimic the original amide group by forming both hydrogen

WILEY-VCH

Archiv der Pharmazie

bond interactions, and moreover, it may even be involved in a third hydrogen bond to S342 (Figure 6B). Contrary, the docking pose of the oxadiazole analog **47** shows a different orientation due to the lack of hydrogen bonding with I339 and S342 (Figure 6A). Albeit the hydrogen bond donor ability seems not essential for K_V7.2/3 opening, it may still play an important role, as the triazole analog **54** had a superior efficacy of 149%, whereas the oxadiazole analog **47** was on the verge of inactivity with an efficacy of only 45%. Presumably, the putative hydrogen bond interactions of the triazole derivative **54** result in a slight shift of the S6' alpha helix, which is part of the pore-forming domain, thereby enhancing the K_V7.2/3 opening of **54** compared to the oxadiazole analog **47**.

In addition to these findings regarding the possible role of a hydrogen bond donor ability, analog **54** also provided a novel substance class of K_V7.2/3 openers since, to our knowledge, **54** is the first 1,2,4-triazole derivative described to address this target. Indeed, there is still room for improvement in terms of potency, but considering the superior efficacy of **54**, it was even slightly more active than flupirtine, indicated by an overall left-shifted concentration-activity curve.

The third structural modification affecting the amide region again resulted in an inactive compound. The *N*-(pyridin-3-ylmethyl)benzamide analog **49** with a displaced amide carbonyl group compared to the original nicotinamide scaffold demonstrated no K_V7.2/3 opening activity up to 20 µM, thus underlining the crucial importance of the amide group for K_V7.2/3 opening and confirming the postulated binding mode. By shifting the carbonyl group of the original amide partial structure while maintaining the position of the amide NH moiety, two important mechanisms contributing to ligand binding are disrupted at once. In detail, steric interactions of the amide group with ortho substituents on the pyridine core are vastly reduced, and one of the two presumed hydrogen bonds of the amide function is also prevented.

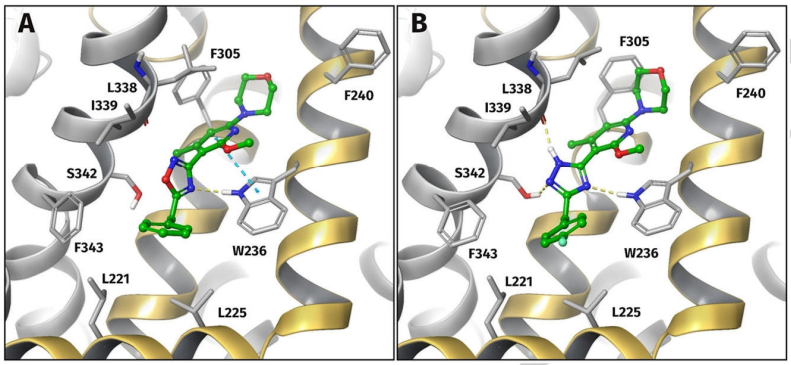

FIGURE 6 Predicted binding poses of **47** (A) and **54** (B). The triazole ring forms hydrogen bonds to the S342 sidechain and the I339 backbone carbonyl oxygen atom, probably affecting the S6' alpha helix, which is part of the pore-forming domains. The color of the secondary structure elements represents the respective chains of K_V7.2 (gold) and K_V7.3 (silver) in the K_V7.2/3-heterotetramer.

According to molecular docking, the amide side chain in zone D is likely to occupy a hydrophobic cavity formed essentially by L221, L225, and F343, which has so far been mainly addressed with benzyl moieties. However, from a physicochemical point of view, this type of amide side chain, inherited from lead **6**, remains a certain hindrance to the desired increased aqueous solubility. Therefore, while incorporating polar structural elements in this region of the scaffold did not seem expedient, attempts were made to replace the benzyl moiety with aliphatic side chains to increase the overall sp^3 fraction and thus possibly improve the water solubility. The corresponding compounds **18d** and **40c** were both found to be moderately active with EC_{50} values slightly inferior to flupirtine but showed a remarkable difference in efficacy. Whereas analog **40c** bearing a bulky 3,3-dimethylbutyl sidechain achieved only 52% efficacy, an *n*-butyl side chain in **18d** resulted in an impressive 170% efficacy, which was the best of all compounds tested in this study (Figure 7). Consequently, despite the clear negative impact on the EC_{50} value, an *n*-butyl sidechain may still represent an attractive structural element for future designs since analog **18d** not only showed the best efficacy but was also one of the most soluble substances in the toxicity tests carried out where it could be tested up to 250 µM. The detrimental effect of the *n*-butyl amide side chain on the EC_{50} value might be partially compensated when combined with successful substituents in zones A and E of the scaffold. However, considering only the K_V7.2/3 opening activity while leaving aside physicochemical properties, a benzylic amide side chain was still clearly superior. The beneficial effect could even be enhanced by replacing the initially used 4-fluorobenzyl moiety with a 3-(trifluoromethyl)benzyl residue, as revealed by a **40a** and **40b** comparison, where this structural change led to a 3.6-fold increase in potency. The observed boost in K_V7.2/3 opening activity might be attributed to a π-π-interaction between the benzyl side chain and F343 being strengthened upon trifluoromethylation. This is consistent with computational studies by Mottishaw and Sun, which demonstrated that trifluoromethylation of an aromatic core results in improved π-π-interactions compared to direct monofluorination, as indicated by increased intermolecular interaction energies and reduced π–π distances.[48]

WILEY-VCH

Archiv der Pharmazie

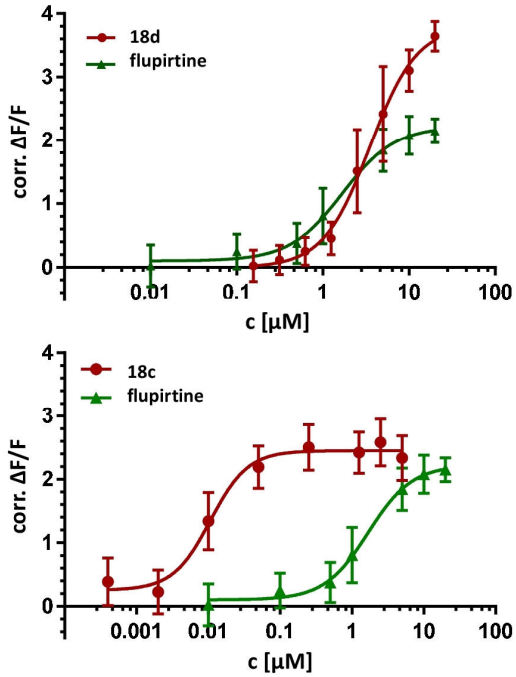

FIGURE 7 The concentration-activity curves for $K_V7.2/3$ opening of analogs **18c** and **18d** in comparison to flupirtine demonstrate the excellent potency of **18c** (EC_{50} = 0.012 µM) as well as the superior efficacy of **18d** (E_{max} = 170%).

Regarding the investigated substituents in zone E, the impression emerged that sterically more demanding substituents with increased lipophilicity favor $K_V7.2/3$ opening. A replacement of the methoxy group of **18a** with a 2,2,2-trifluoroethoxy or a 1-methyl-ethoxy substituent increased the potency of the corresponding analogs **18b** and **18c** significantly by a factor of 6.9 and 9.8, respectively, leading to an excellent EC_{50} value of 0.012 µM in the case of **18c** (Figure 7). This is noteworthy since the predicted binding poses of the nicotinamide analogs indicate that the alkoxy substituents do not interact directly with the binding pocket but rather point in the opposite direction towards the vicinity of the $K_V7.2/3$ channel (Figure 4C). Consistent with the assumption about the orientation of the alkoxy substituents, an exchange of the methoxy group for an isosteric ethyl residue in analog **40a** was also tolerated well, as there are no specific interactions of the alkoxy oxygen atom with the $K_V7.2/3$ binding site predicted.

However, without direct contact with the binding site, the question arises of how the bulky and lipophilic alkoxy substituents were able to improve $K_V7.2/3$ opening. Remarkably, the position of the $K_V7.2/3$ binding site may be relevant in this case since it is situated in the transmembrane region of the channel on the protein-phospholipid interface (Figure 8). Hence, the bulky and lipophilic alkoxy substituents in zone E, which are presumed to face in the direction of the cell membrane, may improve possible interactions with adjacent lipid tails. Such ligand-lipid interactions have so far been underestimated as influencing factors of drug activity. However, they are becoming increasingly important in drug design as a growing number of intramembrane binding sites are revealed by X-ray crystallography and cryogenic electron microscopy.[49] Consequently, for various small molecules and targets, it is assumed that ligand-lipid interactions are significantly involved in ligand binding. A prominent and impressive example of ligand-lipid interactions is ivacaftor (not shown), a potentiator of the cystic fibrosis transmembrane conductance regulator (CFTR) that binds to a site within the transmembrane region of the CFTR chloride channel. The molecule bears two *tert*-butyl groups that interact with lipids of the adjacent membrane and shield the polar part of the ligand, which is responsible for molecular recognition via hydrogen bonds, against the phospholipid interface.[49] Conceivably, the lipophilic alkoxy substituents of **18b** and **18c** function in a similar way as the *tert*-butyl groups of ivacaftor. To confirm the postulated ligand-lipid interactions, a molecular dynamics simulation was performed with **18c** and a $K_V7.2/3$ channel, which was inserted in a phosphatidylcholine bilayer simulating the cell membrane. The result presented in Figure 8 clearly shows that the trifluoroethoxy group, together with the 4-fluorophenyl ring, is able to shield the polar part of the molecule, i.e. the amide group and the pyridine nitrogen atom, from the adjacent lipid layer, thus improving hydrophobic interactions with lipid tails.

In contrast to the alkoxy substituents, the considerably more hydrophilic primary amino function of **14** resulted in a reduced $\log D_{7.4}$ value and, as intended, in an improved solubility in toxicity testing, but at the same time caused an unexpected drastic loss of $K_V7.2/3$ opening activity. Consequently, the question arises why the primary amino function is well tolerated in flupirtine and retigabine, whereas it appears to be clearly disadvantageous in nicotinamide analogs. In this case, there are probably several reasons to consider. First, molecular dynamics simulations indicate that the amino function of **14** is slightly shifted in the binding pocket compared to the amino group of retigabine. As a result, the hydrogen bond to S342, which is assumed to be advantageous, is not predicted as with retigabine (Figure 4B). Second, in the case of **14**, the methyl group is located on the lipid-facing side of the molecule. Therefore, the shielding

WILEY-VCH

Archiv der Pharmazie

against the cell membrane is likely reduced compared to bulky lipophilic alkoxy residues of analogs **18b**/**c**. Finally, with a log$D_{7.4}$ value of 2.2, compound **14** is also the most hydrophilic of the nicotinamide analogs, which may inhibit diffusion through the lipid layer and thus impede the compound from reaching the intramembrane binding site.

The same may also apply to analog **19a**, which has a hydroxy group in place of the primary amino substituent of **14**. Remarkably, in contrast to the still weakly active compound **14**, analog **19a** turned out to be completely inactive up to a concentration of 20 µM. The even worse performance of a hydroxy group compared to the amino substituent of **14** might be attributed to a tautomeric relationship of **19a**, whose 2-hydroxypyridine form is likely in equilibrium with the 2-pyridone form. This is particularly relevant as docking suggests that the central pyridine ring of nicotinamide analogs is involved in π-π-interactions with the W236 indole side chain, similar to the phenyl ring of retigabine (Figure 4). This specific interaction is presumed to be highly relevant for ligand binding since it could be shown that a mutation of W236 completely abolishes the effect of retigabine.[50] Consequently, this crucial interaction might be weakened in the case of the nonaromatic 2-pyridone tautomer of **19a**, hence leading to the observed inactivity.

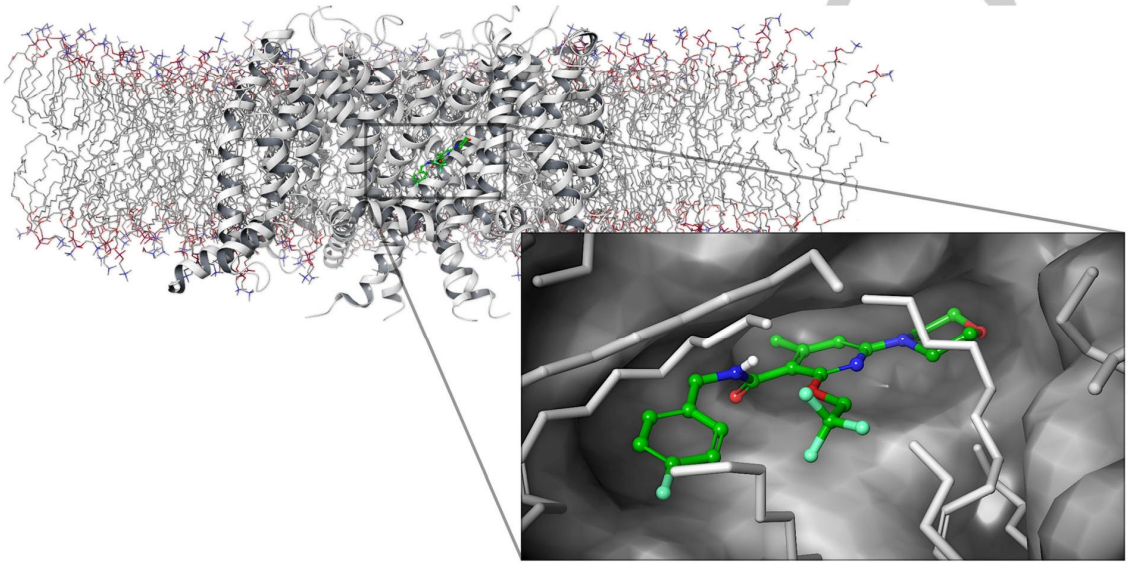

FIGURE 8 Predicted binding mode of **18c** from combined ligand docking and all-atom molecular dynamics simulations. The trifluoroethoxy group points towards the membrane and shields it from the hydrophilic parts of the ligand.

2.2.2 Evaluation of in vitro toxicity

Flupirtine-induced severe hepatotoxicity is a very rare phenomenon with a reporting rate of 1.68 cases per 100,000 patient-years.[51] For this reason, it was not reported in any in vitro or in vivo toxicity studies during preclinical and clinical development, and thus flupirtine has long been considered a well-tolerated analgesic.[9,52] In accordance, in vitro LD_{50} values of flupirtine were determined in the range of 500 µM, hence significantly exceeding therapeutically relevant concentrations, which are in the low single-digit micromolar range.[53] In general, idiosyncratic toxicity, as suspected for flupirtine, is very difficult to reproduce in an in vitro toxicity model due to the multifactorial causes,[54] which in the case of flupirtine probably include both the formation of potentially toxic metabolites and involvement of the adaptive immune system.[18,55] Despite all efforts, currently, no in vitro or in vivo model exists that reliably predicts idiosyncratic drug-induced liver injury (DILI),[56] which is reflected in the fact that idiosyncratic hepatotoxicity is still one of the two most common reasons for drug withdrawals, restrictions and project terminations.[57] For these reasons, since flupirtine usually behaves uncritically in standard toxicity tests and no adequate assay for idiosyncratic hepatotoxicity exists, the toxicological evaluation carried out in this work should not be understood as a proof of concept to verify the design hypothesis but rather as a general examination of the new scaffolds for potential intrinsic toxicity. This standard toxicological characterization was carried out on two hepatic cell lines with an MTT assay, which essentially measures metabolic activity as an indicator of cell viability. The method is based on the mitochondrial reduction of 3-(4,5-dimethylthiazol-2-yl)-2,5-diphenyltetrazolium bromide (MTT) to the corresponding formazan, which can be quantified colorimetrically.[58] The human HEP-G2 and mouse TAMH cell lines used for this assay are well established for in vitro hepatotoxicity testing.[59]

A limitation in toxicity testing that inherently demands that much higher concentrations are applied than in activity testing continued to be the relatively poor water solubility of most analogs, which was already problematic for compound **6**.[23] Remarkably, the introduction of a morpholino substituent in **18a** did not result in significantly improved solubility. Like analog **6**, the morpholino derivative **18a** could only be tested up to a concentration of 63 µM, which was surprising since the log$D_{7.4}$ value was reduced from 4.1 to 3.0, and at the same time, the fraction of sp^3 hybridized carbon atoms was increased from 0.18 to 0.37. However, the three-dimensional structure of

WILEY-VCH

Archiv der Pharmazie

18a and the other morpholino-substituted analogs is probably still rather flat due to the coplanar conformation of the morpholino substituent and the central aromatic ring, which might favor aggregation and thus prevent noticeably improved water solubility. This hypothesis is supported by the increased aqueous solubility of analog **21**, which could be tested up to a concentration of 125 µM and was thus about twice as soluble as **18a**. The reason for this difference is probably the tetrahydropyran ring of **21**, which does not prefer a coplanar conformation like the morpholine ring of **18a**, as discussed above. Since no LD_{50} value could be determined for any analog due to the limited water solubility, LD_{25} values were calculated, which indicate the concentration that was necessary to reduce the cell viability to 75% in order to enable a comparison of the analogs regarding their hepatotoxic potential. Nevertheless, for 12 of the 22 analogs, no LD_{25} value could be determined for either cell line because the required concentrations could not be reached. However, apart from the poor water solubility, the lack of LD values principally indicates that most of the analogs do not possess a pronounced level of in vitro hepatotoxicity at concentrations required for $K_V7.2/3$ opening.

While it was possible to derive structure-activity relationships for $K_V7.2/3$ opening, an analysis of the toxicity data displayed in Table 1 does not allow a clear correlation with certain structural elements to set up any valid structure-toxicity relationships. However, the nicotinamide scaffold per se does not appear to be of toxicological concern. This becomes apparent when the analogs with low water solubility are initially left aside, and instead, the focus is placed on the more soluble substances such as **14**, **18d**, **21**, or **28a**/**b**. These analogs displayed rather uncritical levels of in vitro hepatotoxicity with higher LD_{25} values compared to flupirtine. Nevertheless, focusing on the remaining analogs, there are some compounds that appear to perform worse than flupirtine and retigabine. This applies, for example, to the nanomolar active analogs **18b** and **18e**, for which LD_{25} values of 15 µM and 32 µM, respectively, were determined for the HEP-G2 cell line. However, the structural similarity of the compounds to the significantly less toxic analogs **14** and **18d** suggests that the specific chemical structure may not be responsible for the reduced LD_{25} values. Instead, the reason could be the overall increased lipophilicity of **18b** and **18e**, which was among the highest of the current analogs as indicated by $\log D_{7.4}$ values of 3.8 and 4.7, respectively. This would be consistent with an analysis of 1036 FDA-approved drugs suggesting that compound lipophilicity is statistically significantly associated with DILI risk.[60]

However, it must be emphasized that it is not possible to define a general LD limit at which a substance is to be classified as hepatotoxic. Tham et al. reported LD_{50} values of ten proven hepatotoxic drugs determined by the MTT assay on HEP-G2 cells, which extend over a wide concentration range from 25 µM to 20 mM.[61] Therefore, LD values on their own are not very meaningful and must always be considered in relation to the biological activity, which among other factors, ultimately determines the necessary therapeutic concentration. For this reason, LD_{25}/EC_{50} ratios were calculated for all active analogs, thus enabling a preliminary estimation of the therapeutic range. Considering these LD_{25}/EC_{50} ratios, the highly potent analogs **18b** and **18e** appear to have significantly improved therapeutic safety windows compared to flupirtine despite lower absolute LD_{25} values. The same applies to compound **18c** with an LD_{25}/EC_{50} ratio of 1,250 that even surpasses retigabine, for which no hepatotoxic effect is known. Overall, only the weakly to moderately active analogs **14**, **28a**, **40c**, **47**, and **54** have a poorer preliminary therapeutic range than flupirtine, whereby the exact LD_{25}/EC_{50} ratios of **40c**, **47**, and **54** are actually unknown since the maximum soluble concentrations were used for the calculation due to the lack of LD_{25} values; therefore the calculated LD_{25}/EC_{50} ratios represent worst-case scenarios. In summary, the potential to cause intrinsic hepatotoxicity appears to be low for most analogs based on preliminary in vitro toxicity data. However, as mentioned above, the results of the MTT assay may not be predictive of idiosyncratic hepatotoxicity.

3 CONCLUSION

The $K_V7.2/3$ opening activity of nicotinamide lead compound **6** could be successfully improved by introducing a morpholino substituent and a 2,2,2-trifluoroethoxy group. The resulting compound **18c** was 150 times more potent than flupirtine and 20 times more potent than retigabine while also demonstrating a superior toxicity/activity ratio. The water solubility of **18c** and related compounds was still low, but considering the nanomolar activity, it might be sufficient for further development, which in perspective also includes in vivo assays. Moreover, the $K_V7.2/3$ activity data of the structurally distinct analogs provided profound structure-activity relationships, which could be correlated with docking and molecular dynamics simulations to hypothesize a plausible binding mechanism for the nicotinamide derivatives. As a result, the ortho disubstitution of the amide function was confirmed as an essential structural feature. In addition, the role of a cyclic substituent in position 6 of the pyridine ring was clarified, which must be aligned coplanar to the central pyridine ring but still has to allow for a flexible conformation to fit into the binding pocket adequately. Finally, a bulky alkoxy group is presumed to better shield the analogs in their intramembrane binding site from the adjacent lipid layer by improving ligand-lipid interactions. Taken together, the SAR findings obtained in this work provide a strong basis for future drug design.

4 EXPERIMENTAL

4.1 Chemistry

4.1.1 General remarks

WILEY-VCH

Archiv der Pharmazie

The starting materials, reagents, and solvents were commercially available and purchased from Sigma Aldrich, VWR, TCI, or ABCR. All chemicals were used as received unless specified otherwise. Anhydrous solvents were obtained from Acros Organics, except THF, which was dried by refluxing over sodium. Microwave-supported syntheses were conducted using an Anton Paar Monowave 300 reactor in closed vessel mode with an integrated IR sensor for temperature control. NMR spectra were recorded on a Bruker Avance III device at 400 MHz (^{1}H) and 100 MHz (^{13}C), respectively, using $CDCl_3$, DMSO-d_6, or MeOH-d_4 as solvents. The chemical shifts were referenced to the internal standard tetramethylsilane (TMS) and reported in parts per million (ppm). The coupling constants (*J*) are in Hz, and the following abbreviations were used to designate the multiplicities: br = broad, s = singlet, d = doublet, t = triplet, q = quartet, m = multiplet, and combinations thereof. MIR spectroscopy was performed with an ALPHA FT-IR instrument from Bruker Optics equipped with a diamond ATR accessory unit. A Bruker Elute UHPLC with Bruker compact QTOF-MS, a Bruker maXis LC-QTOF-MS, or a Shimadzu LCMS-IT-TOF system, each operated with ESI ionization, were used to measure the HRAM-MS data. HPLC analysis with UV detection at 220 nm using the 100% method determined the purity of all final compounds to be >95%. The melting points were measured with an automated Büchi Melting Point M-565 device. Analytical thin-layer chromatography was carried out on silica gel 60 F_{254} aluminium plates obtained from Merck, and visualization was accomplished with UV light. Column chromatography on silica gel was performed using silica gel 60 from Carl Roth with a particle size of 20–45 µm. Flash chromatographic separations were conducted using the Sepacore system from Büchi with 25 g or 50 g Biotage SNAP KP-SIL columns, or alternatively, an Interchim puriFlash XS 520Plus system in combination with 80 g puriFlash 30SI-HP or 25 g puriFlash 15SI-HP columns. The InChI codes of the investigated analogs are provided as Supporting Information. The Supporting Information also contains ^{1}H-NMR and ^{13}C-NMR spectra of all synthesized compounds as well as HPLC traces of the final compounds. All new compounds were fully characterized, including purity by HPLC and HRAM-MS data within 4 ppm accuracy.

4.1.2 Synthesis and Characterization

General procedure A: introduction of alkoxy substituents

A 60% suspension of NaH in mineral oil (2.5 equiv., 1.21 mmol/mL) was suspended in dry THF under an argon atmosphere, and the resulting suspension was cooled to 0 °C. A solution of the chosen alcohol (1.2 equiv., 0.58 mmol/mL) in dry THF and a solution of the required chloropyridine (5.2–24.3 mmol, 0.49 mmol/mL) in dry THF were added successively. Afterward, the reaction mixture was heated to 70 °C and stirred at 70 °C until the TLC control indicated complete conversion (7–23 h). The reaction was quenched by the addition of water (100 mL). The resulting aq. mixture was adjusted to pH 12 by the addition of a 2 M aq. NaOH solution and extracted with ethyl acetate (100 mL). The organic phase was discarded, and the aq. phase was adjusted to pH 2–3 with conc. HCl. Subsequently, it was extracted with ethyl acetate again (2 × 50–235 mL). Finally, the combined organic phases were washed with brine, dried over Na_2SO_4, filtrated, and concentrated under reduced pressure.

General procedure B: amide coupling with oxalyl chloride

Under an argon atmosphere, the required nicotinic acid derivative (2.5–12.1 mmol, 0.2 mmol/mL) was dissolved in dry DCM, and a catalytic amount of dry DMF was added. The mixture was cooled to 0 °C, and a solution of oxalyl chloride (3.0 equiv., 2.0 mmol/mL) in dry DCM was added dropwise. After complete addition, the cooling was discontinued, and the reaction mixture was stirred at room temperature for 3 h. Subsequently, all volatiles were removed under reduced pressure, and the residue was redissolved in dry DCM (10–48 mL). The resulting solution was added dropwise to a solution of amine reactant (1.2 equiv., 0.3 mmol/mL) and triethylamine (2.0 equiv., 0.5 mmol/mL) in dry DCM at 0 °C under stirring. Afterward, the cooling was discontinued, and the reaction mixture was stirred at room temperature. After 16 h, additional DCM (50–240 mL) was added. The resulting solution was extracted successively with an equal volume of a saturated aq. $NaHCO_3$ solution and a 2 M aq. HCl solution. Finally, the organic phase was washed with brine, dried over Na_2SO_4, filtrated, and concentrated under reduced pressure to obtain the crude product.

General procedure C: microwave-assisted nucleophilic substitution

The required chloropyridine (0.9–3.0 mmol, 0.33 mmol/mL) was dissolved in NMP. Subsequently, the corresponding amine (5.0 equiv.) was added, and the mixture was heated in a microwave reactor at 165 °C in a closed vessel under stirring. After complete conversion (30–60 min), the reaction mixture was cooled to room temperature, dissolved in ethyl acetate (100 mL), and extracted with water (2 × 100 mL). Finally, the organic phase was washed with brine, dried over Na_2SO_4, filtrated, and concentrated under reduced pressure to obtain the crude product.

General procedure D: amide coupling with DIC and HOBt

The required carboxylic acid (1.0–5.8 mmol, 0.15 mmol/mL) was dissolved in DMF. HOBt (2.0 equiv.), DIC (2.0 equiv.) and the corresponding amine (1.5 equiv.) were added successively, and the reaction mixture was stirred at room temperature. After 16 h, the solution was partitioned between ethyl acetate (50–290 mL) and an equal volume of water. The organic phase was extracted with the same volume of water again (2 ×), washed with brine, dried over Na_2SO_4, filtrated, and concentrated under reduced pressure to obtain the crude product.

General procedure E: dechlorination by catalytic hydrogenation

The required chloropyridine (0.3–3.0 mmol, 0.02 mmol/mL) was dissolved in methanol. Pd/C (10% Pd, 50% water wet, 0.1 equiv.) and triethylamine (1.5 equiv.) were added. Subsequently, the suspension was carefully set under a hydrogen atmosphere (balloon pressure) and stirred at room

WILEY-VCH

Archiv der Pharmazie

temperature. After complete conversion (2–5 h), the reaction mixture was filtered through a pad of celite, and the filtrate was concentrated under reduced pressure to obtain the crude product.

2-Amino-6-chloro-4-methylnicotinic acid (12)

2,6-Dichloro-4-methylnicotinic acid (950 mg, 4.61 mmol), K_2CO_3 (1275 mg, 9.22 mmol, 2.0 equiv.), CuI (176 mg, 0.92 mmol, 0.2 equiv.), NaN_3 (1199 mg, 18.44 mmol, 4.0 equiv.), and ethane-1,2-diamine (62 µL, 0.92 mmol, 0.2 equiv.) were successively dissolved/suspended in ethanol (90 mL). The reaction mixture was set under an atmosphere of argon and stirred under reflux. After 23 h, additional amounts of K_2CO_3 (382 mg, 2.77 mmol, 0.6 equiv.), CuI (53 mg, 0.28 mmol, 0,06 equiv.), NaN_3 (360 mg, 5.5 mmol, 1.2 equiv.) and ethane-1,2-diamine (19 µL, 0.28 mmol, 0.06 equiv.) were added, and the reaction was continued for 5 h under the same conditions. Afterward, the reaction mixture was filtered through a pad of silica gel. Subsequently, the silica gel pad was rinsed with ethanol, and the combined eluates were concentrated under reduced pressure. The residue was dissolved in a 1 M aq. KOH solution and the product was precipitated by the addition of conc. HCl. Finally, the precipitate was filtered off to obtain **12** as a brown solid (467 mg, 2.50 mmol, 54%).

R_f = 0.63 (toluene/ethanol/AcOH 5:4:1); mp = 178 °C; ^{1}H-NMR (400 MHz, DMSO-d_6): δ(ppm) = 13.36 (s, 1H), 7.20 (s, 2H), 6.54 (s, 1H), 2.38 (s, 3H); ^{13}C-NMR (100 MHz, DMSO-d_6): δ(ppm) = 168.8, 159.7, 154.0, 151.1, 113.86, 106.23, 22.21; IR (ATR): $\tilde{\nu}$ = 3406, 3282 (m, ν_{N-H}), 3300–2500 (b, ν_{O-H}), 1681 (s, $\nu_{C=O}$), 1619 (s, δ_{N-H}).

2-Amino-6-chloro-*N*-(4-fluorobenzyl)-4-methylnicotinamide (13)

Compound **12** (424 mg, 2.27 mmol) was dissolved in THF (22 mL). CDI (737 mg, 4.56 mmol, 2.0 equiv.) was added in one portion, and the mixture was stirred at 50 °C. After 1 h, the solution was cooled to room temperature, 4-fluorobenzylamine (1040 µL, 9.09 mmol) was added, and the mixture was continued to stir at room temperature. After 12 h, ethyl acetate (100 mL) was added. The resulting solution was extracted with a saturated aq. $NaHCO_3$ solution (100 mL), washed with brine, dried over Na_2SO_4, filtrated, and concentrated under reduced pressure. Finally, the crude residue was purified by silica gel column chromatography (ethyl acetate/*n*-hexane 2:3) to obtain **13** as a slightly yellow solid (236 mg, 0.80 mmol, 35%).

R_f = 0.70 (ethyl acetate/*n*-hexane 7:3); mp = 169 °C; ^{1}H-NMR (400 MHz, DMSO-d_6): δ(ppm) = 8.87 (t, *J* = 6.0 Hz, 1H), 7.43 – 7.33 (m, 2H), 7.22 – 7.11 (m, 2H), 6.49 (s, 1H), 6.14 (s, 2H), 4.41 (d, *J* = 5.9 Hz, 2H), 2.10 (s, 3H); ^{13}C-NMR (100 MHz, DMSO-d_6): δ(ppm) = 166.3, 161.2 (d, *J* = 242.4 Hz), 156.6, 148.0, 147.9, 135.4 (d, *J* = 3.1 Hz), 129.6 (d, *J* = 8.2 Hz), 115.2, 115.0 (d, *J* = 21.3 Hz), 112.4, 41.9, 18.8; IR (ATR): $\tilde{\nu}$ = 3441, 3278 (m, ν_{N-H}), 1613 (s, $\nu_{C=O}$).

2-Amino-*N*-(4-fluorobenzyl)-4-methyl-6-morpholinonicotinamide (14)

The synthesis was conducted from **13** (350 mg, 1.19 mmol) and morpholine in accordance with general procedure C. The crude residue was purified by silica gel column chromatography (ethyl acetate/n-hexane 7:3) and successive recrystallization (methanol/water) to obtain **14** as a slightly yellow solid (300 mg, 0.87 mmol, 73%).

R_f = 0.34 (ethyl acetate/n-hexane 7:3); mp = 177 °C; ^{1}H-NMR (400 MHz, DMSO-d_6): δ(ppm) = 8.41 (t, *J* = 6.0 Hz, 1H), 7.41 – 7.31 (m, 2H), 7.20 – 7.10 (m, 2H), 5.86 (s, 1H), 5.63 (s, 2H), 4.39 (d, *J* = 6.0 Hz, 2H), 3.67 – 3.60 (m, 4H), 3.41 – 3.34 (m, 4H), 2.14 (s, 3H); ^{13}C-NMR (100 MHz, DMSO-d_6): δ(ppm) = 168.1, 161.1 (d, *J* = 242.0 Hz), 157.9, 156.2, 146.5, 135.9 (d, *J* = 2.9 Hz), 129.4 (d, *J* = 8.1 Hz), 115.0 (d, *J* = 21.3 Hz), 105.6, 96.7, 66.0, 44.9, 41.8, 20.5; IR (ATR): $\tilde{\nu}$ = 3458, 3346, 3254 (m, ν_{N-H}), 3049, 2974 (w, ν_{C-H}), 1583 (s, $\nu_{C=O}$), 1531 (m, δ_{N-H}); ESI-HRAM-MS (*m/z*): calcd. for $[C_{18}H_{21}N_4O_2F+H]^+$ 345.1721, found 345.1708; cpd purity (220 nm): 99.6%.

6-Chloro-2-methoxy-4-methylnicotinic acid (15a)

The synthesis was conducted from 2,6-dichloro-4-methylnicotinic acid (5.00 g, 24.3 mmol) and methanol in accordance with general procedure A to obtain **15a** as a beige-colored solid (4.72 g, 23.4 mmol, 96%).

R_f = 0.78 (*n*-butanol/AcOH/water 8:1:1); mp: 166 °C; ^{1}H-NMR (400 MHz, DMSO-d_6): δ(ppm) = 13.39 (s, 1H), 7.09 (s, 1H), 3.87 (s, 3H), 2.17 (s, 3H); ^{13}C-NMR (100 MHz, DMSO-d_6): δ(ppm) = 166.6, 159.4, 149.8, 147.0, 118.0, 117.4, 54.3, 18.4; IR (ATR): $\tilde{\nu}$ = 3002, 2954 (w, ν_{C-H}), 3300–2500 (b, ν_{O-H}), 1686 (s, $\nu_{C=O}$).

WILEY-VCH

Archiv der Pharmazie

6-Chloro-2-isopropoxy-4-methylnicotinic acid (15b)

The synthesis was carried out from 2,6-dichloro-4-methylnicotinic acid (2.50 g, 12.1 mmol) and 2-propanol following general procedure A to obtain **15b** as a beige-colored solid (2.75 g, 12.0 mmol, 99%), which was used for the following reaction without any further characterization and purification.

6-Chloro-4-methyl-2-(2,2,2-trifluoroethoxy)nicotinic acid (15c)

The synthesis was conducted from 2,6-dichloro-4-methylnicotinic acid (1.25 g, 6.1 mmol) and 2,2,2-trifluoroethanol in accordance with general procedure A to obtain **15c** as a beige-colored solid (1.62 g, 6.0 mmol, 99%), which was used for the following reaction without any further characterization and purification.

6-Chloro-*N*-(4-fluorobenzyl)-2-methoxy-4-methylnicotinamide (16a)

The synthesis was carried out from **15a** (500 mg, 2.48 mmol) and 4-fluorobenzylamine according to general procedure B. The crude residue was purified by silica gel column chromatography (ethyl acetate/*n*-hexane 3:2), which yielded **16a** as a colorless solid (402 mg, 1.30 mmol, 53%).

R_f = 0.29 (ethyl acetate/*n*-hexane 1:1); mp: 127 °C; ^{1}H-NMR (400 MHz, DMSO-d_6): δ(ppm) = 8.89 (t, *J* = 6.0 Hz, 1H), 7.43 – 7.33 (m, 2H), 7.24 – 7.08 (m, 2H), 7.05 (d, *J* = 0.6 Hz, 1H), 4.42 (d, *J* = 6.0 Hz, 2H), 3.86 (s, 3H), 2.18 (d, *J* = 0.6 Hz, 3H); ^{13}C-NMR (100 MHz, DMSO-d_6): δ(ppm) = 164.5, 161.2 (d, *J* = 242.1 Hz), 159.6, 149.9, 146.4, 135.3 (d, *J* = 3.0 Hz), 129.1 (d, *J* = 8.1 Hz), 119.9, 117.9, 115.0 (d, *J* = 21.3 Hz), 54.1, 41.5, 18.0; IR (ATR): $\tilde{\nu}$ = 3310 (m, ν_{N-H}), 3067, 2954 (w, ν_{C-H}), 1635 (s, $\nu_{C=O}$), 1604 (m, δ_{N-H}).

6-Chloro-*N*-(4-fluorobenzyl)-2-(propan-2-yloxy)-4-methylnicotinamide (16b)

The synthesis was carried out from **15b** (2.78 g, 12.1 mmol) and 4-fluorobenzylamine according to general procedure B. The crude residue was purified by flash chromatography (mobile phase: ethyl acetate/*n*-hexane with 0–30% ethyl acetate), which yielded **16b** as a colorless solid (2.10 g, 6.2 mmol, 51%).

R_f = 0.83 (ethyl acetate/*n*-hexane 2:1); mp: 122 °C; ^{1}H-NMR (400 MHz, DMSO-d_6): δ(ppm) = 8.82 (t, *J* = 6.1 Hz, 1H), 7.45 – 7.35 (m, 2H), 7.21 – 7.11 (m, 2H), 7.00 (s, 1H), 5.16 (sept, *J* = 6.2 Hz, 1H), 4.42 (d, *J* = 6.1 Hz, 2H), 2.19 (s, 3H), 1.26 (d, *J* = 6.1 Hz, 6H); ^{13}C-NMR (100 MHz, DMSO-d_6): δ(ppm) = 164.6, 161.2 (d, *J* = 242.0 Hz), 158.9, 149.9, 146.3, 135.4 (d, *J* = 3.0 Hz), 129.0 (d, *J* = 8.1 Hz), 120.4, 117.4, 114.8 (d, *J* = 21.0 Hz), 69.4, 41.3, 21.7, 18.0; (ATR): $\tilde{\nu}$ = 3267 (m, ν_{N-H}), 3078, 2982 (w, ν_{C-H}), 1632 (s, $\nu_{C=O}$).

6-Chloro-*N*-(4-fluorobenzyl)-4-methyl-2-(2,2,2-trifluoroethoxy)nicotinamide (16c)

The synthesis was conducted from **15c** (1.25 g, 4.64 mmol) and 4-fluorobenzylamine following general procedure B. The crude residue was purified by silica gel column chromatography (ethyl acetate/*n*-hexane 2:3), which yielded **16c** as a beige-colored solid (855 mg, 2.27 mmol, 49%).

R_f = 0.67 (ethyl acetate/*n*-hexane 1:1); mp: 127 °C; ^{1}H-NMR (400 MHz, DMSO-d_6): δ(ppm) = 8.98 (t, *J* = 6.0 Hz, 1H), 7.43 – 7.32 (m, 2H), 7.21 (d, *J* = 0.6 Hz, 1H), 7.18 – 7.07 (m, 2H), 4.96 (q, *J* = 9.0 Hz, 2H), 4.44 (d, *J* = 6.0 Hz, 2H), 2.24 (d, *J* = 0.6 Hz, 3H); ^{13}C-NMR (100 MHz, DMSO-d_6): δ(ppm) = 163.7, 161.2 (d, *J* = 242.1 Hz), 157.1, 151.1, 146.1, 135.1 (d, *J* = 3.0 Hz), 129.0 (d, *J* = 8.1 Hz), 123.7 (q, *J* = 277.7 Hz), 120.0, 119.6, 114.9 (d, *J* = 21.3 Hz), 62.3 (q, *J* = 35 Hz), 41.5, 18.1; (ATR): $\tilde{\nu}$ = 3404 (m, ν_{N-H}), 3013, 2924 (w, ν_{C-H}), 1613 (s, $\nu_{C=O}$).

N-Butyl-6-chloro-2-methoxy-4-methylnicotinamide (16d)

The synthesis was carried out from **15a** (2.19 g, 10.87 mmol) and *n*-butylamine according to general procedure B. The crude residue was purified by silica gel column chromatography (ethyl acetate/*n*-hexane 3:7), which yielded **16d** as a colorless solid (1.71 g, 6.7 mmol, 61%).

R_f = 0.81 (ethyl acetate/*n*-hexane 2:1); mp: 57 °C; ^{1}H-NMR (400 MHz, DMSO-d_6): δ(ppm) = 8.30 (t, *J* = 5.7 Hz, 1H), 7.04 (s, 1H), 3.82 (s, 3H), 3.19 (td, *J* = 6.9, 5.7 Hz, 2H), 2.19 (s, 3H), 1.51 – 1.40 (m, 2H), 1.43 – 1.27 (m, 2H), 0.89 (t, *J* = 7.3 Hz, 3H); ^{13}C-NMR (100 MHz, DMSO-d_6): δ(ppm) = 164.1, 159.6, 149.7, 146.1, 120.4, 117.8, 54.0, 38.3, 31.0, 19.5, 18.0, 13.6; IR (ATR): $\tilde{\nu}$ = 3220 (m, ν_{N-H}), 3068, 2961 (w, ν_{C-H}), 1645 (s, $\nu_{C=O}$), 1624 (m, δ_{N-H}).

WILEY-VCH

Archiv der Pharmazie

N-(4-Fluorobenzyl)-6-methoxy-4-methyl-(2,4'-bipyridine)-5-carboxamide (17)

In a microwave vessel, compound **16a** (210 mg, 0.68 mmol) was dissolved in 1,4-dioxane (2 mL). 880 µl of a 2 M aq. solution of Na_2CO_3 (1.76 mmol, 2.6 equiv.), tetrakis(triphenylphosphine)palladium(0) (79 mg, 0.07 mmol, 0.1 equiv.) and pyridin-4-ylboronic acid (100 mg, 0.82 mmol, 1.2 equiv.) were added. Argon was passed through the reaction mixture for 30 min. Afterward, the mixture was heated in a microwave reactor at 140 °C under stirring. After 30 min, the reaction mixture was cooled to room temperature, water (100 mL) was added, and the aq. suspension was extracted with ethyl acetate (100 mL). The organic phase was washed with brine, dried over Na_2SO_4, filtrated, and concentrated under reduced pressure. The crude residue was purified by flash chromatography (ethyl acetate/*n*-hexane, 70–90% ethyl acetate) and subsequent recrystallization (methanol/water), which yielded **17** as a beige-colored solid (140 mg, 0.40 mmol, 59%).

R_f = 0.29 (ethyl acetate/*n*-hexane 3:1); mp: 139 °C; ^{1}H-NMR (400 MHz, DMSO-d_6): δ(ppm) = 8.93 (t, *J* = 6.1 Hz, 1H), 8.74 – 8.68 (m, 2H), 8.10 – 8.04 (m, 2H), 7.69 (d, *J* = 0.7 Hz, 1H), 7.47 – 7.38 (m, 2H), 7.26 – 7.15 (m, 2H), 4.46 (d, *J* = 6.0 Hz, 2H), 4.01 (s, 3H), 2.29 (s, 3H); ^{13}C-NMR (100 MHz, DMSO-d_6): δ(ppm) = 165.2, 161.2 (d, *J* = 242.1 Hz), 159.8, 150.3, 150.0, 147.7, 144.8, 135.5 (d, *J* = 3.1 Hz), 129.1 (d, *J* = 8.2 Hz), 121.5, 120.6, 116.0, 115.0 (d, *J* = 21.3 Hz), 53.4, 41.5, 18.4; (ATR): $\tilde{\nu}$ = 3330 (m, ν_{N-H}), 3023, 2951 (w, ν_{C-H}), 1633 (s, $\nu_{C=O}$), 1594 (m, δ_{N-H}); ESI-HRAM-MS (*m/z*): calcd. for $[C_{20}H_{19}N_3O_2F+H]^+$ 352.1456, found 352.1463; cpd purity (220 nm): 99.5%.

N-(4-Fluorobenzyl)-2-methoxy-4-methyl-6-morpholinonicotinamide (18a)

The synthesis was conducted from **16a** (300 mg, 0.97 mmol) and morpholine in accordance with general procedure C. The crude residue was purified by flash chromatography (mobile phase: ethyl acetate/*n*-hexane with 50–100% ethyl acetate) and successive recrystallization (methanol/water), which yielded **18a** as a colorless solid (126 mg, 0.35 mmol, 36%).

R_f = 0.60 (ethyl acetate/*n*-hexane 3:2); mp: 192 °C; ^{1}H-NMR (400 MHz, DMSO-d_6): δ(ppm) = 8.52 (t, *J* = 6.2 Hz, 1H), 7.43 – 7.33 (m, 2H), 7.21 – 7.10 (m, 2H), 6.22 (s, 1H), 4.38 (d, *J* = 6.1 Hz, 2H), 3.80 (s, 3H), 3.73 – 3.65 (m, 4H), 3.47 – 3.40 (m, 4H), 2.13 (s, 3H); ^{13}C-NMR (100 MHz, DMSO-d_6): δ(ppm) = 166.1, 161.1 (d, *J* = 241.7 Hz), 158.8, 157.0, 148.6, 135.9 (d, *J* = 2.9 Hz), 128.9 (d, *J* = 8.1 Hz), 114.9 (d, *J* = 21.0 Hz), 109.6, 99.5, 65.9, 52.7, 45.0, 41.5, 19.2; IR (ATR): $\tilde{\nu}$ = 3330 (m, ν_{N-H}), 3049, 2997 (w, ν_{C-H}), 1627 (s, $\nu_{C=O}$); ESI-HRAM-MS (*m/z*): calcd. for $[C_{19}H_{23}N_3O_3F+H]^+$ 360.1718, found 360.1717; cpd purity (220 nm): 100.0%.

N-(4-Fluorobenzyl)-2-(propyl-2-oxy)-4-methyl-6-morpholinonicotinamide (18b)

The synthesis was conducted from **16b** (596 mg, 1.77 mmol) and morpholine in accordance with general procedure C. The crude residue was purified by silica gel column chromatography (ethyl acetate/*n*-hexane 1:1) and successive recrystallization (ethanol/water), which yielded **18b** as a colorless solid (356 mg, 0.92 mmol, 52%).

R_f = 0.54 (ethyl acetate/*n*-hexane 2:1); mp: 134 °C; ^{1}H-NMR (400 MHz, DMSO-d_6): δ(ppm) = 8.41 (t, *J* = 6.2 Hz, 1H), 7.45 – 7.36 (m, 2H), 7.19 – 7.09 (m, 2H), 6.20 (s, 1H), 5.16 (sept, *J* = 6.2 Hz, 1H), 4.39 (d, *J* = 6.1 Hz, 2H), 3.73 – 3.63 (m, 4H), 3.47 – 3.36 (m, 4H), 2.14 (s, 3H), 1.24 (d, *J* = 6.2 Hz, 6H); ^{13}C-NMR (100 MHz, DMSO-d_6): δ(ppm) = 166.2, 161.0 (d, *J* = 241.7 Hz), 158.1, 157.0, 148.6, 135.9 (d, *J* = 3.0 Hz), 128.9 (d, *J* = 8.0 Hz), 114.7 (d, *J* = 21.2 Hz), 110.0, 99.4, 67.6, 65.8, 45.0, 41.4, 22.0, 19.2; (ATR): $\tilde{\nu}$ = 3277 (m, ν_{N-H}), 2967 (w, ν_{C-H}), 1619 (s, $\nu_{C=O}$), 1591 (m, δ_{N-H}); ESI-HRAM-MS (*m/z*): calcd. for $[C_{21}H_{27}N_3O_3F+H]^+$ 388.2031, found 388.2030; cpd purity (220 nm): 99.8%.

N-(4-Fluorobenzyl)-4-methyl-6-morpholino-2-(2,2,2-trifluoroethoxy)nicotinamide (18c)

The synthesis was conducted from **16c** (500 mg, 1.33 mmol) and morpholine in accordance with general procedure C. The crude residue was purified by silica gel column chromatography (ethyl acetate/*n*-hexane 1:1) and successive recrystallization (methanol/water), which yielded **18c** as a colorless solid (212 mg, 0.50 mmol, 37%).

R_f = 0.56 (ethyl acetate/*n*-hexane 3:2); mp: 164 °C; ^{1}H-NMR (400 MHz, DMSO-d_6): δ(ppm) = 8.61 (t, *J* = 6.1 Hz), 7.42 – 7.32 (m, 2H), 7.17 – 7.05 (m, 2H), 6.35 (s, 1H), 4.89 (q, *J* = 9.2 Hz, 2H), 4.39 (d, *J* = 6.0 Hz, 2H), 3.72 – 3.65 (m, 4H), 3.49 – 3.42 (m, 4H), 2.16 (s, 3H); ^{13}C-NMR (100 MHz, DMSO-d_6): δ(ppm) = 165.38, 161.1 (d, *J* = 241.8 Hz), 156.7, 156.3, 149.4, 135.6 (d, *J* = 2.9 Hz), 128.8 (d, *J* = 8.0 Hz), 124.1 (q, *J* = 278.1 Hz), 114.7 (d, *J* = 21.2 Hz), 109.4, 101.0, 65.8, 61.2 (q, *J* = 34.5 Hz), 44.9, 41.5, 19.1; (ATR): $\tilde{\nu}$ = 3291 (m, ν_{N-H}), 2978 (w, ν_{C-H}), 1617 (s, $\nu_{C=O}$), 1602 (s, δ_{N-H}); ESI-HRAM-MS (*m/z*): calcd. for $[C_{20}H_{22}N_3O_3F_4+H]^+$ 428.1592, found 428.1591; cpd purity (220 nm): 98.2%.

WILEY-VCH

Archiv der Pharmazie

N-Butyl-2-methoxy-4-methyl-6-morpholinonicotinamide (18d)

The synthesis was conducted from **16d** (770 mg, 3.0 mmol) and morpholine in accordance with general procedure C. The crude residue was purified by flash chromatography (mobile phase: ethyl acetate/*n*-hexane with 0–100% ethyl acetate) and successive recrystallization (ethanol/water), which yielded **18d** as a colorless solid (250 mg, 0.85 mmol, 28%).

R_f = 0.43 (ethyl acetate/*n*-hexane 2:1); mp: 135 °C; ^{1}H-NMR (400 MHz, DMSO-d_6): δ(ppm) = 7.93 (t, *J* = 5.7 Hz, 1H), 6.20 (s, 1H), 3.76 (s, 3H), 3.71 – 3.65 (m, 4H), 3.46 – 3.39 (m, 4H), 3.15 (td, *J* = 6.9, 5.7 Hz, 2H), 2.13 (s, 3H), 1.50 – 1.38 (m, 2H), 1.42 – 1.26 (m, 2H), 0.89 (t, *J* = 7.3 Hz, 3H); ^{13}C-NMR (100 MHz, DMSO-d_6): δ(ppm) = 165.7, 158.7, 156.9, 148.3, 110.3, 99.4, 65.9, 52.6, 45.1, 38.4, 31.1, 19.5, 19.1, 13.7; (ATR): $\tilde{\nu}$ = 3303 (m, ν_{N-H}), 3067, 2967 (w, ν_{C-H}), 1625 (s, $\nu_{C=O}$), 1594 (m, δ_{N-H}); ESI-HRAM-MS (*m/z*): calcd. for $[C_{16}H_{26}N_3O_3+H]^+$ 308.1969, found 308.1968; cpd purity (220 nm): 99.7%.

N-(4-Fluorobenzyl)-2-methoxy-4-methyl-6-(piperidin-1-yl)nicotinamide (18e)

The synthesis was conducted from **16a** (400 mg, 1.30 mmol) and piperidine in accordance with general procedure C. The crude residue was purified by flash chromatography (mobile phase: ethyl acetate/*n*-hexane with 30–70% ethyl acetate) and successive recrystallization (methanol/water), which yielded **18e** as a colorless solid (161 mg, 0.45 mmol, 35%).

R_f = 0.76 (ethyl acetate/*n*-hexane 1:1); mp: 147 °C; ^{1}H-NMR (400 MHz, DMSO-d_6): δ(ppm) = 8.49 (t, *J* = 6.2 Hz, 1H), 7.48 – 7.30 (m, 2H), 7.26 – 7.05 (m, 2H), 6.19 (s, 1H), 4.38 (d, *J* = 6.1 Hz, 2H), 3.79 (s, 3H), 3.65 – 3.40 (m, 4H), 2.13 (s, 3H), 1.67 – 1.57 (m, 2H), 1.57 – 1.48 (m, 4H); ^{13}C-NMR (100 MHz, DMSO-d_6): δ(ppm) = 166.2, 161.0 (d, *J* = 241.8 Hz), 158.9, 156.7, 148.6, 136.0 (d, *J* = 2.9 Hz), 128.9 (d, *J* = 8.2 Hz), 114.8 (d, *J* = 21.1 Hz), 108.1, 99.4, 52.6, 45.5, 41.5, 24.9, 24.3, 19.3; (ATR): $\tilde{\nu}$ = 3335 (m, ν_{N-H}), 2948 (w, ν_{C-H}), 1626 (s, ν_{C-O}), 1593 (s, δ_{N-H}); ESI-HRAM-MS (*m/z*): calcd. for $[C_{20}H_{25}N_3O_2F+H]^+$ 358.1925, found 358.1954; cpd purity (220 nm): 99.7%.

N-(4-Fluorobenzyl)-2-isopropoxy-4-methyl-6-(2-oxa-6-azaspiro[3.3]heptan-6-yl)nicotinamide (18f)

The synthesis was conducted from **16b** (500 mg, 1.49 mmol) and 2-oxa-6-azaspiro[3.3]heptane oxalate (856 mg, 2.97 mmol, 2.0 equiv.) following general procedure C. Deviating from general procedure C, DBU (665 µL, 4.45 mmol, 3.0 equiv.) was added to the reaction mixture. The crude residue was purified by flash chromatography (mobile phase: ethyl acetate/*n*-hexane with 60–100% ethyl acetate), which yielded **18f** as a slightly yellow solid (314 mg, 0.79 mmol, 53%).

R_f = 0.32 (ethyl acetate/*n*-hexane 1:1); mp: 146 °C; ^{1}H-NMR (400 MHz, DMSO-d_6): δ(ppm) = 8.39 (t, *J* = 6.2 Hz, 1H), 7.45 – 7.36 (m, 2H), 7.19 – 7.09 (m, 2H), 5.77 (s, 1H), 5.17 (sept, *J* = 6.2 Hz, 1H), 4.71 (s, 4H), 4.38 (d, *J* = 6.1 Hz, 2H), 4.06 (s, 4H), 2.11 (s, 3H), 1.25 (d, *J* = 6.2 Hz, 6H); ^{13}C-NMR (100 MHz, DMSO-d_6): δ(ppm) = 166.3, 161.0 (d, *J* = 241.6 Hz), 158.7, 158.5, 148.0, 135.9 (d, *J* = 2.9 Hz), 128.9 (d, *J* = 8.0 Hz), 114.7 (d, *J* = 21.1 Hz), 109.7, 98.3, 79.9, 67.5, 59.6, 41.4, 38.3, 22.0, 18.9; (ATR): $\tilde{\nu}$ = 3329 (m, ν_{N-H}), 2932 (m, ν_{C-H}), 1628 (s, $\nu_{C=O}$), 1591 (s, δ_{N-H}); ESI-HRAM-MS (*m/z*): calcd. for $[C_{22}H_{27}N_3O_3F+H]^+$ 400.2031, found 400.2033; cpd purity (220 nm): 98.4%.

N-(4-Fluorobenzyl)-4-methyl-6-morpholino-2-oxo-1,2-dihydropyridine-3-carboxamide (19a)

Compound **19a** was a side product in the synthesis of **18a**. It was separated from the main product by flash chromatography and further purified by recrystallization (methanol/water). The title compound was obtained as a colorless solid (132 mg, 0.38 mmol, 39%).

R_f = 0.42 (ethyl acetate); mp: 225 °C (decomp.); ^{1}H-NMR (400 MHz, DMSO-d_6): δ(ppm) = 11.12 (s, 1H), 9.73 (s, 1H), 7.39 – 7.29 (m, 2H), 7.18 – 7.08 (m, 2H), 5.76 (s, 1H), 4.40 (d, *J* = 5.9 Hz, 2H), 3.70 – 3.63 (m, 4H), 3.42 – 3.35 (m, 4H), 2.41 (s, 3H); ^{13}C-NMR (100 MHz, DMSO-d_6): δ(ppm) = 166.3, 162.4, 161.0 (d, *J* = 241.8 Hz), 155.8, 152.8, 136.3 (d, *J* = 3.0 Hz), 129.0 (d, *J* = 8.0 Hz), 114.9 (d, *J* = 21.2 Hz), 106.3, 95.2, 65.5, 46.0, 41.2, 22.7; IR (ATR): $\tilde{\nu}$ = 3303 (m, ν_{N-H}), 3060, 2924 (w, ν_{C-H}), 1656 (s, $\nu_{C=O}$); ESI-HRAM-MS (*m/z*): calcd. for $[C_{16}H_{20}N_3O_3F+H]^+$ 346.1561, found 346.1564; cpd purity (220 nm): 100.0%.

6-(3,6-Dihydro-2*H*-pyran-4-yl)-*N*-(4-fluorobenzyl)-2-methoxy-4-methylnicotinamide (20)

In a microwave vessel, **16a** (600 mg, 1.94 mmol) was dissolved in 1,4-dioxane (4 mL). 1.76 mL of a 2 M aq. solution of Na_2CO_3 (3.5 mmol, 1.8 equiv.), tetrakis(triphenylphosphine)palladium(0) (112 mg, 0.10 mmol, 0.05 equiv.) and 2-(cyclohex-1-en-1-yl)-4,4,5,5-tetramethyl-1,3,2-dioxaborolane (490 mg, 2.33 mmol, 1.2 equiv.) were added. Argon was passed through the reaction mixture for 30 min. Afterward, the mixture was heated in a microwave reactor

WILEY-VCH

Archiv der Pharmazie

at 140 °C. After 15 min, the reaction mixture was cooled to room temperature, water (100 mL) was added, and the aq. suspension was extracted with ethyl acetate (100 mL). The organic phase was washed with brine, dried over Na_2SO_4, filtrated, and concentrated under reduced pressure. The crude residue was purified by flash chromatography (ethyl acetate/*n*-hexane, 10–30% ethyl acetate) and successive recrystallization (methanol/water), which yielded **20** as a colorless solid (595 mg, 1.67 mmol, 86%).

R_f = 0.50 (ethyl acetate/*n*-hexane 1:1); mp: 167 °C; ^{1}H-NMR (400 MHz, $CDCl_3$): δ(ppm) = 7.48 – 7.30 (m, 2H), 7.14 – 6.96 (m, 2H), 6.89 – 6.78 (m, 2H), 6.58 (s, 1H), 4.64 (d, *J* = 5.8 Hz, 2H), 4.49 – 4.32 (m, 2H), 3.98 (s, 3H), 3.94 (t, *J* = 5.5 Hz, 2H), 2.65 – 2.54 (m, 2H), 2.45 (s, 3H); ^{13}C-NMR (100 MHz, $CDCl_3$): δ(ppm) = 166.5, 162.4 (d, *J* = 245.4 Hz), 159.8, 154.3, 150.1, 134.3 (d, *J* = 3.3 Hz), 133.4, 129.5 (d, *J* = 8.1 Hz), 127.1, 117.2, 115.7 (d, *J* = 21.4 Hz), 114.7, 66.0, 64.5, 53.7, 43.2, 25.8, 20.4; (ATR): $\tilde{\nu}$ = 3325 (m, ν_{N-H}), 1631 (s, $\nu_{C=O}$), 1590 (m, δ_{N-H}); ESI-HRAM-MS (*m/z*): calcd. for $[C_{20}H_{22}N_2O_3F+H]^+$ 357.1609, found 357.1607; cpd purity (220 nm): 99.5%.

N-(4-Fluorobenzyl)-2-methoxy-4-methyl-6-(oxan-4-yl)nicotinamide (21)

Compound **20** (250 mg, 0.70 mmol) was dissolved in methanol (20 mL). Pd/C (10% Pd, 50% water wet, 150 mg) was added, the suspension was carefully set under a hydrogen atmosphere (balloon pressure), and the reaction mixture was stirred at room temperature. After 5 h, the resulting mixture was filtered through a pad of celite, and the filtrate was concentrated under reduced pressure. The crude residue was purified by silica gel column chromatography (ethyl acetate/*n*-hexane 2:3) and successive recrystallization (methanol/water) to obtain **21** as a colorless solid (186 mg, 0.52 mmol, 74%).

R_f = 0.46 (ethyl acetate/*n*-hexane 1:1); mp: 124 °C; ^{1}H-NMR (400 MHz, DMSO-d_6): δ(ppm) = 8.81 (t, *J* = 6.1 Hz, 1H), 7.50 – 7.31 (m, 2H), 7.28 – 7.06 (m, 2H), 6.77 (s, 1H), 4.41 (d, *J* = 6.1 Hz, 2H), 4.02 – 3.90 (m, 2H), 3.86 (s, 3H), 3.50 – 3.36 (m, 2H), 2.91 – 2.73 (m, 1H), 2.16 (s, 3H), 1.83 – 1.70 (m, 4H); ^{13}C-NMR (100 MHz, DMSO-d_6): δ(ppm) = 165.6, 161.3, 160.8 (d, *J* = 241.0 Hz), 159.2, 146.7, 135.6 (d, *J* = 3.0 Hz), 129.0 (d, *J* = 8.1 Hz), 118.8, 115.5, 114.9 (d, *J* = 21.2 Hz), 67.0, 53.0, 41.8, 41.4, 31.7, 18.2; (ATR): $\tilde{\nu}$ = 3351 (m, ν_{N-H}), 3051, 2949 (w, ν_{C-H}), 1634 (s, $\nu_{C=O}$), 1596 (m, δ_{N-H}); ESI-HRAM-MS (*m/z*): calcd. for $[C_{20}H_{24}N_2O_3F+H]^+$ 359.1765, found 359.1759; cpd purity (220 nm): 100.0%.

6-Chloro-2-methoxynicotinic acid (23)

The synthesis was conducted from 2,6-dichloronicotinic acid (1.00 g, 5.2 mmol) and methanol in accordance with general procedure A. The crude residue was purified by recrystallization (toluene/*n*-hexane) to obtain **23** as a slightly pink-colored solid (768 mg, 4.09 mmol, 79%).

R_f = 0.68 (ethyl acetate/toluene/acetic acid 5:5:1); mp: 176 °C; ^{1}H-NMR (400 MHz, DMSO-d_6): δ(ppm) = 13.14 (s, 1H), 8.16 (d, *J* = 7.8 Hz, 1H), 7.18 (d, *J* = 7.9 Hz, 1H), 3.92 (s, 3H); ^{13}C-NMR (100 MHz, DMSO-d_6): δ(ppm) = 165.1, 161.4, 150.2, 143.9, 116.5, 113.8, 54.4; (ATR): $\tilde{\nu}$ = 2958 (w, ν_{C-H}), 3200–2500 (b, ν_{O-H}), 1687 (s, $\nu_{C=O}$).

6-Chloro-*N*-(4-fluorobenzyl)-2-methoxynicotinamide (24)

The synthesis was conducted from **23** (300 mg, 1.60 mmol) and 4-fluorobenzylamine in accordance with general procedure D. The crude residue was purified by flash chromatography (mobile phase: ethyl acetate/*n*-hexane with 10–70% ethyl acetate) and successive recrystallization (methanol/water), which yielded **24** as a beige-colored solid (308 mg, 1.05 mmol, 65%).

R_f = 0.52 (ethyl acetate/*n*-hexane 1:3); mp: 101 °C; ^{1}H-NMR (400 MHz, DMSO-d_6): δ(ppm) = 8.80 (t, *J* = 6.0 Hz, 1H), 8.15 (d, *J* = 7.9 Hz, 1H), 7.42 – 7.32 (m, 2H), 7.22 (d, *J* = 7.9 Hz, 1H), 7.21 – 7.11 (m, 2H), 4.48 (d, *J* = 6.1 Hz, 2H), 3.98 (s, 3H); ^{13}C-NMR (100 MHz, DMSO-d_6): δ(ppm) = 162.9, 161.1 (d, *J* = 241.6 Hz), 159.9, 148.8, 142.9, 135.5 (d, *J* = 3.0 Hz), 129.1 (d, *J* = 8.1 Hz), 117.0, 116.6, 115.0 (d, *J* = 21.4 Hz), 54.6, 42.0; (ATR): $\tilde{\nu}$ = 3416 (m, ν_{N-H}), 3091, 2953 (w, ν_{C-H}), 1652 (s, $\nu_{C=O}$), 1582 (m, δ_{N-H}).

N-(4-Fluorobenzyl)-2-methoxy-6-morpholinonicotinamide (25)

The synthesis was conducted from **24** (250 mg, 0.85 mmol) and morpholine in accordance with general procedure C. The crude residue was purified by flash chromatography (mobile phase: ethyl acetate/*n*-hexane with 70–100% ethyl acetate) and successive recrystallization (methanol/water), which yielded **25** as a colorless solid (105 mg, 0.30 mmol, 36%).

R_f = 0.46 (ethyl acetate/*n*-hexane 1:1); mp: 129 °C; ^{1}H-NMR (400 MHz, DMSO-d_6): δ(ppm) = 8.41 (t, *J* = 6.1 Hz, 1H), 8.05 (d, *J* = 8.5 Hz, 1H), 7.42 – 7.26 (m, 2H), 7.20 – 7.08 (m, 2H), 6.46 (d, *J* = 8.7 Hz, 1H), 4.46 (d, *J* = 6.1 Hz, 2H), 3.94 (s, 3H), 3.76 – 3.63 (m, 4H), 3.62 – 3.49 (m, 4H); ^{13}C-NMR

WILEY-VCH

Archiv der Pharmazie

(100 MHz, DMSO-d_6): δ(ppm) = 163.7, 161.0 (d, *J* = 242.0 Hz), 159.7, 158.5, 142.3, 136.3 (d, *J* = 3.0 Hz), 129.0 (d, *J* = 8.1 Hz), 114.9 (d, *J* = 21.2 Hz), 103.4, 98.8, 65.8, 53.2, 44.6, 41.8; (ATR): $\tilde{\nu}$ = 3403 (m, ν_{N-H}), 2987 (w, ν_{C-H}), 1642 (s, $\nu_{C=O}$), 1596 (s, δ_{N-H}); ESI-HRAM-MS (*m/z*): calcd. for $[C_{18}H_{21}N_3O_3F+H]^+$ 346.1561, found 346.1558; cpd purity (220 nm): 98.7%.

2,6-Dichloro-*N*-(4-fluorobenzyl)-4-methylnicotinamide (26a)

The synthesis was conducted from 2,6-dichloro-4-methylnicotinic acid (1.19 g, 5.8 mmol) and 4-fluorobenzylamine in accordance with general procedure D. The crude residue was purified by flash chromatography (mobile phase: ethyl acetate/*n*-hexane with 10–50% ethyl acetate) and successive recrystallization (acetone/water), which yielded **26a** as a pale yellow solid (835 mg, 2.66 mmol, 46%).

R_f = 0.77 (ethyl acetate/*n*-hexane 1:1); mp: 161 °C; ^{1}H-NMR (400 MHz, DMSO-d_6): δ(ppm) = 9.17 (t, *J* = 5.9 Hz, 1H), 7.57 (d, *J* = 0.8 Hz, 1H), 7.46 – 7.36 (m, 2H), 7.25 – 7.14 (m, 2H), 4.46 (d, *J* = 5.9 Hz, 2H), 2.26 (d, *J* = 0.7 Hz, 3H); ^{13}C-NMR (100 MHz, DMSO-d_6): δ(ppm) = 163.9, 161.3 (d, *J* = 242.5 Hz), 151.2, 148.2, 145.4, 134.8 (d, *J* = 3.0 Hz), 132.6, 129.6 (d, *J* = 8.2 Hz), 124.6, 115.1 (d, *J* = 21.3 Hz), 41.8; (ATR): $\tilde{\nu}$ = 3249 (m, ν_{N-H}), 3078 (w, ν_{C-H}), 1638 (s, $\nu_{C=O}$).

2,6-Dichloro-*N*-(4-fluorobenzyl)nicotinamide (26b)

The synthesis was conducted from 2,6-dichloronicotinic acid (500 mg, 2.60 mmol) and 4-fluorobenzylamine in accordance with general procedure D. The crude residue was purified by silica gel column chromatography (ethyl acetate/*n*-hexane 1:1) and successive recrystallization (methanol/water), which yielded **26b** as a colorless solid (673 mg, 2.25 mmol, 86%).

R_f = 0.63 (ethyl acetate/*n*-hexane 1:1); mp: 168 °C; ^{1}H-NMR (400 MHz, DMSO-d_6): δ(ppm) = 9.16 (t, *J* = 5.9 Hz, 1H), 8.03 (d, *J* = 8.0 Hz, 1H), 7.67 (d, *J* = 8.0 Hz, 1H), 7.50 – 7.32 (m, 2H), 7.26 – 7.11 (m, 2H), 4.46 (d, *J* = 5.9 Hz, 2H); ^{13}C-NMR (100 MHz, DMSO-d_6): δ(ppm) = 164.2, 161.3 (d, *J* = 242.5 Hz), 149.2,145.8, 141.2, 134.8 (d, *J* = 3.0 Hz), 132.1, 129.3 (d, *J* = 8.1 Hz), 123.6, 115.1 (d, *J* = 21.3 Hz), 41.9; (ATR): $\tilde{\nu}$ = 3253 (m, ν_{N-H}), 3052 (w, ν_{C-H}), 1638 (s, $\nu_{C=O}$), 1574 (m, δ_{N-H}).

2-Chloro-*N*-(4-fluorobenzyl)-4-methyl-6-morpholinonicotinamide (27a)

Compound **26a** (600 mg, 1.92 mmol) was dissolved in 2-propanol (50 mL). Morpholine (835 µL, 9.58 mmol, 5.0 equiv.) was added, and the reaction mixture was stirred under reflux. After 3 d, it was cooled to room temperature, and all volatiles were removed under reduced pressure. The crude residue was purified by flash chromatography (mobile phase: ethyl acetate/*n*-hexane with 50–100% ethyl acetate), which yielded **27a** as a pale yellow solid (160 mg, 0.44 mmol, 23%).

R_f = 0.26 (ethyl acetate/*n*-hexane 1:1); mp: 186 °C; ^{1}H-NMR (400 MHz, DMSO-d_6): δ(ppm) = 8.88 (t, *J* = 6.0 Hz, 1H), 7.45 – 7.33 (m, 2H), 7.22 – 7.12 (m, 2H), 6.70 (s, 1H), 4.40 (d, *J* = 6.0 Hz, 2H), 3.73 – 3.60 (m, 4H), 3.51 – 3.38 (m, 4H), 2.14 (s, 3H); ^{13}C-NMR (100 MHz, DMSO-d_6): δ(ppm) = 165.5, 161.2 (d, *J* = 242.1 Hz), 157.9, 148.5, 144.4, 135.4 (d, *J* = 3.0 Hz), 129.4 (d, *J* = 8.1 Hz), 122.5, 115.0 (d, *J* = 21.3 Hz), 106.1, 65.8, 44.9, 41.7, 19.1.

2-Chloro-*N*-(4-fluorobenzyl)-6-morpholinonicotinamide (27b)

Compound **26b** (600 mg, 2.01 mmol) was dissolved in methanol (30 mL). Morpholine (437 µL, 5.02 mmol, 2.5 equiv.) was added, and the reaction mixture was stirred under reflux. After 24 h, it was cooled to room temperature, and all volatiles were removed under reduced pressure. The crude residue was purified by flash chromatography (mobile phase: ethyl acetate/*n*-hexane with 50–100% ethyl acetate), which yielded **27b** as a pale yellow solid (180 mg, 0.51 mmol, 26%).

R_f = 0.33 (ethyl acetate/*n*-hexane 1:1); mp: 153 °C; ^{1}H-NMR (400 MHz, DMSO-d_6): δ(ppm) = 8.77 (t, *J* = 6.1 Hz, 1H), 7.67 (d, *J* = 8.6 Hz, 1H), 7.40 – 7.31 (m, 2H), 7.20 – 7.10 (m, 2H), 6.81 (d, *J* = 8.6 Hz, 1H), 4.39 (d, *J* = 6.0 Hz, 2H), 3.70 – 3.63 (m, 4H), 3.53 – 3.44 (m, 4H); ^{13}C-NMR (100 MHz, DMSO-d_6): δ(ppm) = 165.4, 161.2 (d, *J* = 242.1 Hz), 158.4, 145.1, 139.9, 135.4 (d, *J* = 3.0 Hz), 129.2 (d, *J* = 8.3 Hz), 120.2, 115.0 (d, *J* = 21.3 Hz), 104.8, 65.7, 44.7, 41.9; (ATR): $\tilde{\nu}$ = 3261 (m, ν_{N-H}), 2970 (w, ν_{C-H}), 1623 (s, $\nu_{C=O}$), 1556 (m, δ_{N-H}).

N-(4-Fluorobenzyl)-4-methyl-6-morpholinonicotinamide (28a)

The synthesis was conducted from **27a** (130 mg, 0.36 mmol) following general procedure E. The crude residue was purified by silica gel column chromatography (ethyl acetate) and successive recrystallization (methanol/water) to obtain **28a** as a colorless solid (75 mg, 0.23 mmol, 64%).

WILEY-VCH

Archiv der Pharmazie

R_f = 0.34 (ethyl acetate/*n*-hexane 3:1); mp: 192 °C; ^{1}H-NMR (400 MHz, DMSO-d_6): δ(ppm) = 8.71 (t, *J* = 6.0 Hz, 1H), 8.23 (s, 1H), 7.41 – 7.31 (m, 2H), 7.21 – 7.11 (m, 2H), 6.70 (s, 1H), 4.40 (d, *J* = 6.0 Hz, 2H), 3.72 – 3.65 (m, 4H), 3.53 – 3.46 (m, 4H), 2.34 (s, 3H); ^{13}C-NMR (100 MHz, DMSO-d_6): δ(ppm) = 167.1, 161.1 (d, *J* = 242.1 Hz), 159.4, 147.3, 146.9, 135.9 (d, *J* = 3.2 Hz), 129.0 (d, *J* = 8.1 Hz), 121.9, 115.0 (d, *J* = 21.3 Hz), 107.8, 65.9, 44.8, 41.7, 20.0; (ATR): $\tilde{\nu}$ = 3285 (m, ν_{N-H}), 2930 (w, ν_{C-H}), 1621 (s, $\nu_{C=O}$), 1604 (m, δ_{N-H}); ESI-HRAM-MS (*m/z*): calcd. for $[C_{18}H_{21}N_3O_2F+H]^+$ 330.1612, found 330.1616; cpd purity (220 nm): 99.6%.

N-(4-Fluorobenzyl)-6-morpholinonicotinamide (28b)

The synthesis was conducted from **27b** (110 mg, 0.32 mmol) following general procedure E. The crude residue was purified by silica gel column chromatography (ethyl acetate) and successive recrystallization (methanol/water) to obtain **28b** as a colorless solid (64 mg, 0.20 mmol, 65%).

R_f = 0.43 (ethyl acetate/*n*-hexane 3:1); mp: 212 °C; ^{1}H-NMR (400 MHz, DMSO-d_6): δ(ppm) = 8.83 (t, *J* = 6.0 Hz, 1H), 8.66 (d, *J* = 2.5 Hz, 1H), 8.01 (dd, *J* = 9.0, 2.5 Hz, 1H), 7.39 – 7.29 (m, 2H), 7.19 – 7.09 (m, 2H), 6.86 (d, *J* = 9.0 Hz, 1H), 4.43 (d, *J* = 5.9 Hz, 2H), 3.72 – 3.65 (m, 4H), 3.59 – 3.52 (m, 4H); ^{13}C-NMR (100 MHz, DMSO-d_6): δ(ppm) = 164.9, 161.1 (d, *J* = 241.0 Hz), 160.0, 147.9, 136.5, 136.0 (d, *J* = 3.0 Hz), 129.2 (d, *J* = 8.1 Hz), 118.8, 114.9 (d, *J* = 21.2 Hz), 105.6, 65.9, 44.7, 41.7; (ATR): $\tilde{\nu}$ = 3298 (m, ν_{N-H}), 2966 (w, ν_{C-H}), 1627 (s, $\nu_{C=O}$), 1597 (s, δ_{N-H}); ESI-HRAM-MS (*m/z*): calcd. for $[C_{17}H_{19}N_3O_2F+H]^+$ 316.1456, found 316.1463; cpd purity (220 nm): 97.9%.

N-(4-Fluorobenzyl)-2-isopropoxy-4-methylnicotinamide (29)

The synthesis was conducted from **16b** (1.00 g, 3.0 mmol) following general procedure E. The crude residue was purified by silica gel column chromatography (ethyl acetate/*n*-hexane 2:3) and successive recrystallization (methanol/water) to obtain **29** as a colorless solid (591 mg, 1.96 mmol, 66%).

R_f = 0.57 (ethyl acetate/*n*-hexane 1:1); mp: 107 °C; ^{1}H-NMR (400 MHz, DMSO-d_6): δ(ppm) = 8.78 (t, *J* = 6.2 Hz, 1H), 8.02 (d, *J* = 5.2 Hz, 1H), 7.48 – 7.38 (m, 2H), 7.21 – 7.10 (m, 2H), 6.84 (d, *J* = 5.3 Hz, 1H), 5.24 (sept, *J* = 6.2 Hz, 1H), 4.43 (d, *J* = 6.1 Hz, 2H), 2.18 (s, 3H), 1.26 (d, *J* = 6.2 Hz, 6H); ^{13}C-NMR (100 MHz, DMSO-d_6): δ(ppm) = 165.5, 161.1 (d, *J* = 241.8 Hz), 159.2, 146.2, 146.0, 135.6 (d, *J* = 3.0 Hz), 128.9 (d, *J* = 8.1 Hz), 121.5, 118.3, 114.8 (d, *J* = 21.2 Hz), 67.9, 41.3, 21.9, 18.1; (ATR): $\tilde{\nu}$ = 3283 (m, ν_{N-H}), 3066, 2992 (w, ν_{C-H}), 1629 (s, $\nu_{C=O}$), 1588 (m, δ_{N-H}); ESI-HRAM-MS (*m/z*): calcd. for $[C_{17}H_{20}N_2O_3F+H]^+$ 303.1503, found 303.1498; cpd purity (220 nm): 99.4%.

Ethyl 4-ethyl-6-methyl-2-oxo-1,2,3,4-tetrahydropyrimidine-5-carboxylate (33)

Urea (16.5 g, 275 mmol, 1.1 equiv.) was suspended in ethanol (60 mL). Afterward, ethyl 3-oxobutanoate (31.6 mL, 250 mmol), propanal (19.7 mL, 275 mmol, 1.1 equiv.), and a catalytic amount of acetic acid were added. The mixture was stirred in a closed vessel at 90 °C. After 20 h, the reaction mixture was poured into water. The resulting precipitate was filtered off and recrystallized from ethanol. Finally the recrystallized product was washed with a small amount of a mixture of ethanol and water (1:1) to obtain **33** as a colorless solid (17.0 g, 80 mmol 32%).

R_f = 0.41 (ethyl acetate); mp: 183 °C (lit mp: 179 – 181 °C);[62] ^{1}H-NMR (400 MHz, DMSO-d_6): δ(ppm) = 8.91 (s, 1H), 7.28 (s, 1H), 4.15 – 3.99 (m, 3H), 2.17 (s, 3H), 1.42 (qd, *J* = 7.4, 5.3 Hz, 2H), 1.19 (t, *J* = 7.1 Hz, 3H), 0.79 (t, *J* = 7.4 Hz, 3H); ^{13}C-NMR (100 MHz, DMSO-d_6): δ(ppm) = 165.5, 152.8, 148.4, 98.8, 59.0, 51.3, 29.6, 17.7, 14.2, 8.5; IR (ATR): $\tilde{\nu}$ = 3241, 3117 (m, ν_{N-H}), 2960 (w, ν_{C-H}), 1720, 1701 (s, $\nu_{C=O}$).

Ethyl 6-ethyl-4-methyl-2-oxo-1,2-dihydropyrimidine-5-carboxylate (34)

Nitric acid (50%, 25 mL) was cooled to -10 °C. Subsequently, compound **33** (8.50 g, 40.1 mmol) was added in portions over a period of 5 min while maintaining the temperature at -10 °C. After complete addition, the mixture was stirred additional 10 min at -10 °C. Afterward, K_2CO_3 was added to adjust the pH to 7. The resulting aq. solution was extracted with ethyl acetate (10 × 100 mL). The combined organic phases were washed with brine, dried over Na_2SO_4, filtrated, and concentrated under reduced pressure to obtain **34** as an orange solid (7.30 g, 34.7 mmol, 87%).

R_f = 0,45 (DCM/methanol 9:1); mp: 99 °C; ^{1}H-NMR (400 MHz, DMSO-d_6): δ(ppm) = 12.14 (s, 1H), 4.27 (q, *J* = 7.1 Hz, 2H), 2.64 (q, *J* = 7.5 Hz, 2H), 2.33 (s, 3H), 1.29 (t, *J* = 7.1 Hz, 3H), 1.14 (t, *J* = 7.5 Hz, 3H); ^{13}C-NMR (100 MHz, DMSO-d_6): δ(ppm) = 165.4, 155.2, 108.5, 61.0, 27.9, 20.8, 13.9, 12.5 (two ^{13}C signals are apparently missing, possibly due to overlapping since the number of ^{13}C signals of the predecessor compound **33** and the successor compound **35** is correct); IR (ATR): $\tilde{\nu}$ = 2978 (w, ν_{C-H}), 1709, 1645 (s, $\nu_{C=O}$), 1556 (m, δ_{N-H}).

WILEY-VCH

Archiv der Pharmazie

Ethyl 2-chloro-6-ethyl-4-methyl-1,2-dihydropyrimidine-5-carboxylate (35)

Compound **34** (1.10 g, 5.2 mmol) was dissolved in phosphorus oxychloride (3.20 mL, 18.4 mmol, 10.6 equiv.) and stirred for 1 h at 110 °C. Subsequently, all volatiles were removed under reduced pressure. The residue was suspended in ice water (100 mL), and the resulting suspension was extracted with ethyl acetate (3 × 100 mL). The combined organic phases were washed with brine, dried over Na_2SO_4, filtrated, and concentrated under reduced pressure. The crude residue was purified by silica gel column chromatography (ethyl acetate/*n*-hexane 1:3), which yielded **35** as an orange liquid (540 mg, 2.36 mmol, 45%).

R_f = 0.74 (ethyl acetate/*n*-hexane 1:3); ^{1}H-NMR (400 MHz, DMSO-d_6): δ(ppm) = 4.41 (q, *J* = 7.1 Hz, 2H), 2.75 (q, *J* = 7.5 Hz, 2H), 2.48 (s, 3H), 1.33 (t, *J* = 7.1 Hz, 3H), 1.20 (t, *J* = 7.5 Hz, 3H); ^{13}C-NMR (100 MHz, DMSO-d_6): δ(ppm) = 171.7, 167.7, 165.8, 159.5, 124.8, 62.1, 28.3, 22.2, 13.8, 12.4; IR (ATR): $\tilde{\nu}$ = 2981 (w, $\nu_{C\text{-}H}$), 1726 (s, $\nu_{C=O}$).

2-Chloro-4-ethyl-6-methylpyrimidine-5-carboxylic acid (36)

Compound **35** (2.74 g, 12.0 mmol) was dissolved in THF (20 mL). The resulting solution was added to a solution of KOH (1.87 g, 47.9 mmol, 4.0 equiv.) in water (80 mL). The resulting mixture was stirred at room temperature for 12 h. Afterward, it was extracted with ethyl acetate (100 mL). The organic phase was discarded, and the aq. phase was acidified to pH 2–3 with conc. aq. HCl. Subsequently, it was extracted with ethyl acetate again (5 × 100 mL). The combined organic phases were washed with brine, dried over Na_2SO_4, filtrated, and concentrated under reduced pressure. The resulting dark brown solid (1.74 g, 8.7 mmol, 72%) was used for the following reaction without characterization or any further purification.

2-Chloro-4-ethyl-*N*-(4-fluorobenzyl)-6-methylpyrimidine-5-carboxamide (37)

Compound **36** (650 mg, 3.24 mmol), HATU (1.48 g, 3.9 mmol, 1.2 equiv.), DIPEA (1130 µL, 6.48 mmol, 2.0 equiv.) and 4-fluorobenzylamine (555 µL, 4.86 mmol, 1.5 equiv.) were successively dissolved in DMF (10 mL). The mixture was stirred at room temperature. After 8 h, the reaction was quenched by the addition of water (100 mL). The resulting suspension was extracted with ethyl acetate (100 mL). The organic phase was washed with water (2 × 100 mL) and brine, dried over Na_2SO_4, filtrated, and concentrated under reduced pressure. Finally, the crude residue was purified by silica gel column chromatography (ethyl acetate/*n*-hexane 1:1), which yielded **37** as a colorless oil (420 mg, 1.37 mmol, 42%).

R_f = 0.51 (ethyl acetate/*n*-hexane 1:1); mp: 172 °C; ^{1}H-NMR (400 MHz, DMSO-d_6): δ(ppm) = 9.14 (t, *J* = 5.9 Hz, 1H), 7.44 – 7.35 (m, 2H), 7.25 – 7.14 (m, 2H), 4.46 (d, *J* = 5.9 Hz, 2H), 2.63 (q, *J* = 7.5 Hz, 2H), 2.35 (s, 3H), 1.15 (t, *J* = 7.5 Hz, 3H); ^{13}C-NMR (100 MHz, DMSO-d_6): δ(ppm) = 170.7, 166.6, 165.0, 161.3 (d, *J* = 242.8 Hz), 158.5, 134.8 (d, *J* = 3.0 Hz), 129.7 (d, *J* = 8.2 Hz), 128.9, 115.2 (d, *J* = 21.3 Hz), 41.9, 27.7, 21.5, 12.5; IR (ATR): $\tilde{\nu}$ = 3259 (m, $\nu_{N\text{-}H}$), 3080, 2977 (w, $\nu_{C\text{-}H}$), 1637 (s, $\nu_{C=O}$), 1608 (m, $\delta_{N\text{-}H}$).

Ethyl 4-ethyl-6-methyl-2-morpholinopyrimidine-5-carboxylate (38)

Compound **35** (4.72 g, 20.7 mmol) was dissolved in ethanol (100 mL). Morpholine (5.35 mL, 62.0 mmol, 3.0 equiv.) was added, and the reaction mixture was stirred at 80 °C. After 2 h, volatiles were removed under reduced pressure. The resulting crude residue was purified by silica gel column chromatography (ethyl acetate/*n*-hexane 2:8) to obtain **38** as a yellow oil (5.20 g, 18.6 mmol, 90%).

R_f = 0.79 (ethyl acetate/*n*-hexane 1:3); ^{1}H-NMR (400 MHz, DMSO-d_6): δ(ppm) = 4.29 (q, *J* = 7.1 Hz, 2H), 3.83 – 3.73 (m, 4H), 3.70 – 3.61 (m, 4H), 2.65 (q, *J* = 7.5 Hz, 2H), 2.34 (s, 3H), 1.30 (t, *J* = 7.1 Hz, 3H), 1.15 (t, *J* = 7.5 Hz, 3H); ^{13}C-NMR (100 MHz, DMSO-d_6): δ(ppm) = 170.1, 167.4, 165.8, 159.7, 114.0, 65.9, 60.7, 43.7, 28.8, 23.3, 13.9, 12.6; (ATR): $\tilde{\nu}$ = 2972 (w, $\nu_{C\text{-}H}$), 1711 (s, $\nu_{C=O}$).

4-Ethyl-6-methyl-2-morpholinopyrimidine-5-carboxylic acid (39)

Compound **38** (5.00 g, 17.9 mmol) was dissolved in ethanol (10 mL). A solution of KOH (4.93 g, 89.5 mmol) in water (20 mL) was added, and the reaction mixture was stirred at 80 °C. After 4 h, all volatiles were removed under reduced pressure. The residue was dissolved in water (10 mL), and the resulting solution was acidified to pH 2–3 with conc. aq. HCl. Afterward, it was extracted with ethyl acetate (3 × 100 mL). The combined organic phases were dried over Na_2SO_4, filtrated, and concentrated under reduced pressure. The crude residue was purified by silica gel column chromatography (ethyl acetate/acetic acid 9:1) and successive recrystallization (toluene/*n*-hexane) to obtain **39** as a beige-colored solid (3.79 g, 15.1 mmol, 84%).

R_f = 0,68 (ethyl acetate/toluene/acetic acid 5:5:1); mp: 130 °C; ^{1}H-NMR (400 MHz, DMSO-d_6): δ(ppm) = 13.02 (s, 1H), 3.86 – 3.70 (m, 4H), 3.70 – 3.58 (m, 4H), 2.69 (q, *J* = 7.5 Hz, 2H), 2.36 (s, 3H), 1.15 (t, *J* = 7.5 Hz, 3H); ^{13}C-NMR (100 MHz, DMSO-d_6): δ(ppm) = 169.8, 169.1, 165.5, 159.7, 115.2, 66.0, 43.7, 28.8, 23.5, 12.6; (ATR): $\tilde{\nu}$ = 2967 (w, $\nu_{C\text{-}H}$), 3300–2500 (b, $\nu_{O\text{-}H}$), 1675 (s, $\nu_{C=O}$).

WILEY-VCH

Archiv der Pharmazie

4-Ethyl-*N*-(4-fluorobenzyl)-6-methyl-2-morpholinopyrimidine-5-carboxamide (40a)

The synthesis was conducted from **37** (380 mg, 1.24 mmol) and morpholine in accordance with general procedure C. The crude residue was purified by silica gel column chromatography (ethyl acetate/*n*-hexane 1:1) and successive recrystallization (methanol/water), which yielded **40a** as a colorless solid (324 mg, 0.90 mmol, 73%).

R_f = 0.66 (ethyl acetate/*n*-hexane 3:2); mp: 187 °C; ^{1}H-NMR (400 MHz, DMSO-d_6): δ(ppm) = 8.82 (t, *J* = 6.0 Hz, 1H), 7.42 – 7.32 (m, 2H), 7.23 – 7.12 (m, 2H), 4.40 (d, *J* = 5.9 Hz, 2H), 3.72 – 3.69 (m, 4H), 3.65 – 3.62 (m, 4H), 2.46 (q, *J* = 7.5 Hz, 2H, partially overlapped by DMSO signal), 2.19 (s, 3H), 1.11 (t, *J* = 7.5 Hz, 3H); ^{13}C-NMR (100 MHz, DMSO-d_6): δ(ppm) = 167.7, 167.4, 163.3, 161.2 (d, *J* = 243.5 Hz), 160.0, 135.5 (d, *J* = 3.2 Hz), 129.5 (d, *J* = 8.1 Hz), 119.7, 115.0 (d, *J* = 21.3 Hz), 66.0, 43.8, 41.9, 27.8, 22.0, 12.5; IR (ATR): $\tilde{\nu}$ = 3241 (m, ν_{N-H}), 2975 (w, ν_{C-H}), 1628 (s, $\nu_{C=O}$); ESI-HRAM-MS (*m/z*): calcd. for $[C_{19}H_{24}N_4O_2F+H]^+$ 359.1878, found 359.1878; cpd purity (220 nm): 99.7%.

4-Ethyl-6-methyl-2-morpholino-*N*-[3-(trifluoromethyl)benzyl]pyrimidine-5-carboxamide (40b)

The synthesis was conducted from **39** (250 mg, 1.00 mmol) and (3-(Trifluoromethyl)phenyl)methanamine (214 µL, 1.49 mmol, 1.5 equiv.) following general procedure D. The crude residue was purified by silica gel column chromatography (ethyl acetate/*n*-hexane 2:3) and successive recrystallization (methanol/water), which yielded **40b** as a colorless solid (320 mg, 0.78 mmol, 79%).

R_f = 0.50 (ethyl acetate/*n*-hexane 1:1); mp: 162 °C; ^{1}H-NMR (400 MHz, DMSO-d_6): δ(ppm) = 8.94 (t, *J* = 6.1 Hz, 1H), 7.72 – 7.68 (m, 1H), 7.68 – 7.56 (m, 3H), 4.52 (d, *J* = 6.0 Hz, 2H), 3.77 – 3.68 (m, 4H), 3.68 – 3.56 (m, 4H), 2.48 (m, 2H, overlapped by DMSO signal), 2.21 (s, 3H), 1.12 (t, *J* = 7.5 Hz, 3H); ^{13}C-NMR (100 MHz, DMSO-d_6): δ(ppm) = 167.7, 167.6, 163.3, 160.0, 140.8, 131.6, 129.4, 129.1 (q, *J* = 31.3 Hz), 124.3 (q, *J* = 270.7 Hz), 123.8 (q, *J* = 3.9 Hz), 123.6 (q, *J* = 4.0 Hz), 119.5, 66.0, 43.8, 42.1, 27.8, 21.9, 12.4; (ATR): $\tilde{\nu}$ = 3251 (m, ν_{N-H}), 2978 (w, ν_{C-H}), 1634 (s, $\nu_{C=O}$), 1571 (m, δ_{N-H}); ESI-HRAM-MS (*m/z*): calcd. for $[C_{20}H_{24}N_4O_2F_3+H]^+$ 409.1846, found 409.1845; cpd purity (220 nm): 99.7%.

N-(3,3-Dimethylbutyl)-4-ethyl-6-methyl-2-morpholinopyrimidine-5-carboxamide (40c)

The synthesis was conducted from **39** (250 mg, 1.00 mmol) and 3,3-dimethylbutan-1-amine hydrochloride (274 mg, 1.99 mmol, 2.0 equiv.) following general procedure D. Deviating from general procedure D, triethylamine (416 µL, 2.99 mmol, 3.0 equiv.) was added and to the reaction mixture. The crude residue was purified by silica gel column chromatography (ethyl acetate/*n*-hexane 2:3) and successive recrystallization (methanol/water), which yielded **40c** as a colorless solid (269 mg, 0.80 mmol, 81%).

R_f = 0.59 (ethyl acetate/*n*-hexane 1:1); mp: 159 °C; ^{1}H-NMR (400 MHz, DMSO-d_6): δ(ppm) = 8.22 (t, *J* = 5.6 Hz, 1H), 3.74 – 3.67 (m, 4H), 3.67 – 3.60 (m, 4H), 3.22 (m, 2H), 2.50 (m, 2H, overlapped by DMSO signal), 2.21 (s, 3H), 1.45 – 1.37 (m, 2H), 1.14 (t, *J* = 7.5 Hz, 3H), 0.92 (s, 9H); ^{13}C-NMR (100 MHz, DMSO-d_6): δ(ppm) = 167.5, 167.0, 163.2, 159.9, 120.2, 66.0, 43.8, 42.5, 35.5, 29.6, 29.2, 27.8, 22.0, 12.5; (ATR): $\tilde{\nu}$ = 3226 (w, ν_{N-H}), 3067, 2952 (m, ν_{C-H}), 1620 (m, $\nu_{C=O}$); ESI-HRAM-MS (*m/z*): calcd. for $[C_{18}H_{30}N_4O_2+H]^+$ 335.2442, found 335.2444; cpd purity (220 nm): 100.0%.

2-Chloro-4-methyl-6-morpholinonicotinonitrile (42)

2,6-Dichloro-4-methylnicotinonitrile (1.50 g, 8.0 mmol) was dissolved in methanol (15 mL). The solution was cooled to 0 °C, and a solution of morpholine (1.75 mL, 20.1 mmol, 2.5 equiv.) in methanol (5 mL) was added dropwise under stirring. After complete addition, the cooling was removed, and the reaction mixture was stirred for 16 h at room temperature. Subsequently, all volatiles were removed under reduced pressure, and the residue was dissolved in ethyl acetate (100 mL). The resulting solution was extracted with water (2 × 100 mL), washed with brine, dried over Na_2SO_4, filtrated, and concentrated under reduced pressure. The crude residue was purified by flash chromatography (mobile phase: ethyl acetate/*n*-hexane with 30–70% ethyl acetate), which yielded **42** as a colorless solid (1.33 g, 5.6 mmol, 70%).

R_f = 0.45 (ethyl acetate/*n*-hexane 1:1); mp: 156 °C (lit mp: 158 – 160 °C);[63] ^{1}H-NMR (400 MHz, DMSO-d_6): δ(ppm) = 6.88 (d, *J* = 0.8 Hz, 1H), 3.78 – 3.64 (m, 4H), 3.64 – 3.49 (m, 4H), 2.36 (d, *J* = 0.8 Hz, 3H); ^{13}C-NMR (100 MHz, DMSO-d_6): δ(ppm) = 158.3, 153.5, 151.1, 115.9, 105.5, 95.9, 65.6, 44.5, 20.3; (ATR): $\tilde{\nu}$ = 2982 (w, ν_{C-H}), 2211 (m, $\nu_{C\equiv N}$).

4-Methyl-6-morpholinoisoxazolo[5,4-*b*]pyridin-3-amine (43)

Acetohydroxamic acid (556 mg, 7.40 mmol, 2.2 equiv.) and potassium *tert*-butoxide (755 mg, 6.73 mmol, 2.0 equiv.) were set under an atmosphere of argon and dissolved in dry DMF (10 mL). The resulting mixture was stirred at room temperature for 30 min. Subsequently, a solution of **42** (800 mg, 3.37 mmol) in dry DMF (10 mL) was added. The reaction mixture was stirred at 50 °C for 5 h. Afterward, it was concentrated under reduced pressure.

WILEY-VCH

Archiv der Pharmazie

The resulting residue was purified by flash chromatography (mobile phase: ethyl acetate/*n*-hexane with 50–90% ethyl acetate), which yielded **43** as a colorless solid (343 mg, 1.45 mmol, 43%).

R_f = 0.43 (ethyl acetate/*n*-hexane 3:1); mp: 223 °C (decomp.); ^{1}H-NMR (400 MHz, DMSO-d_6): δ(ppm) = 6.56 (d, *J* = 1.1 Hz, 1H), 5.80 (s, 2H), 3.72 – 3.65 (m, 4H), 3.59 – 3.52 (m, 4H), 2.49 (d, *J* = 0.8 Hz, 3H); ^{13}C-NMR (100 MHz, DMSO-d_6): δ(ppm) = 169.5, 159.7, 158.8, 145.5, 103.4, 97.3, 65.8, 45.0, 18.4; (ATR): $\tilde{\nu}$ = 3473, 3293 (m, ν_{N-H}), 2961 (w, ν_{C-H}).

N-(4-Fluorobenzyl)-4-methyl-6-morpholinoisoxazolo[5,4-*b*]pyridin-3-amine (44)

Compound **43** (333 mg, 1.41 mmol) was suspended in dry DCM (30 mL). The suspension was set under an atmosphere of argon. 4-Fluorobenzaldehyde (181 µL, 1.69 mmol, 1.2 equiv.) was added, and the mixture was stirred at room temperature. After 1 h, triethylsilane (675 µL, 4.23 mmol, 3.0 equiv.) and TFA (324 µL, 4.23 mmol, 3.0 equiv.) were added, the temperature was raised to 60 °C, and stirring was continued for 24 h. Afterward, 70 mL of DCM were added, and the resulting solution was extracted with a sat. aq. $NaHCO_3$ solution (100 mL). The organic phase was dried over Na_2SO_4, filtrated, and concentrated under reduced pressure. The resulting residue was purified by flash chromatography (mobile phase: ethyl acetate/*n*-hexane with 40–70% ethyl acetate) and successive recrystallization (methanol/water), which yielded **44** as a colorless solid (386 mg, 1.12 mmol, 80%).

R_f = 0.39 (ethyl acetate/*n*-hexane 1:1); mp: 150 °C; ^{1}H-NMR (400 MHz, DMSO-d_6): δ(ppm) = 7.49 – 7.39 (m, 2H), 7.19 – 7.09 (m, 2H), 6.65 (t, *J* = 6.1 Hz, 1H), 6.57 (d, *J* = 1.0 Hz, 1H), 4.36 (d, *J* = 6.0 Hz, 2H), 3.71 – 3.64 (m, 4H), 3.58 – 3.51 (m, 4H), 2.53 (d, *J* = 0.8 Hz, 3H); ^{13}C-NMR (100 MHz, DMSO-d_6): δ(ppm) = 169.5, 161.1 (d, *J* = 241.9 Hz), 159.6, 158.3, 145.3, 135.8 (d, *J* = 3.0 Hz), 129.4 (d, *J* = 8.2 Hz), 114.8 (d, *J* = 21.3 Hz), 103.4, 96.9, 65.8, 45.3, 45.0, 18.8; (ATR): $\tilde{\nu}$ = 3470 (m, ν_{N-H}), 2965 (w, ν_{C-H}); ESI-HRAM-MS (*m/z*): calcd. for $[C_{18}H_{20}N_4O_2F+H]^+$ 343.1565, found 343.1561; cpd purity (220 nm): 100.0%.

2-Methoxy-4-methyl-6-morpholinonicotinonitrile (45)

Compound **42** (768 mg, 3.23 mmol) was dissolved in dry methanol (30 mL). A 25% solution of sodium methoxide in methanol (2.96 mL, 12.92 mmol, 4.0 equiv.) was added, and the reaction mixture was stirred under reflux in an apparatus equipped with a $CaCl_2$ drying tube. After 24 h, it was cooled to room temperature and concentrated under reduced pressure. The residue was dissolved in ethyl acetate (100 mL), and the resulting solution was extracted with water (2 × 100 mL). The organic phase was washed with brine, dried over Na_2SO_4, filtrated, and concentrated under reduced pressure. Finally, the crude residue was purified by silica gel column chromatography (ethyl acetate/*n*-hexane 1:1), which yielded **45** as a colorless solid (678 mg, 2.91 mmol, 90%).

R_f = 0.56 (ethyl acetate/*n*-hexane 1:1); mp: 150 °C; ^{1}H-NMR (400 MHz, DMSO-d_6): δ(ppm) = 6.42 (d, *J* = 0.9 Hz, 1H), 3.88 (s, 3H), 3.71 – 3.64 (m, 4H), 3.64 – 3.57 (m, 4H), 2.29 (d, *J* = 0.8 Hz, 3H); ^{13}C-NMR (100 MHz, DMSO-d_6): δ(ppm) = 164.1, 158.2, 153.8, 116.3, 99.5, 81.6, 65.7, 53.5, 44.4, 19.9; (ATR): $\tilde{\nu}$ = 2972 (w, ν_{C-H}), 2206 (m, $\nu_{C\equiv N}$).

N'-Hydroxy-2-methoxy-4-methyl-6-morpholinonicotinimidamide (46)

Compound **45** (644 mg, 2.76 mmol) was suspended in ethanol (50 mL). A 50% aq. solution of hydroxylamine (1.63 mL, 27.6 mmol, 10.0 equiv.) was added, and the reaction mixture was stirred in a closed vessel at 90 °C for 4 d. After 24, 48, and 62 h, additional hydroxylamine solution (each time 1.63 mL, 27.6 mmol, 10.0 equiv.) was added. To terminate the reaction, it was cooled to room temperature, and all volatiles were removed under reduced pressure. The crude residue was purified by flash chromatography (mobile phase: DCM/methanol with 0–10% methanol), which yielded **46** as a colorless solid (730 mg, 2.74 mmol, 99%).

R_f = 0.69 (DCM/methanol 9:1); mp: 211 °C; ^{1}H-NMR (400 MHz, DMSO-d_6): δ(ppm) = 9.04 (s, 1H), 6.20 (s, 1H), 5.45 (s, 2H), 3.75 (s, 3H), 3.72 – 3.65 (m, 4H), 3.45 – 3.38 (m, 4H), 2.14 (s, 3H); ^{13}C-NMR (100 MHz, DMSO-d_6): δ(ppm) = 160.3, 157.1, 150.2, 148.3, 106.3, 99.2, 65.9, 52.5, 45.1, 19.0; (ATR): $\tilde{\nu}$ = 3470, 3323, 3229 (m, ν_{N-H}/ν_{O-H}), 2949 (w, ν_{C-H}), 1713 (m, $\nu_{C=N}$).

4-[5-(5-Benzyl-1,2,4-oxadiazol-3-yl)-6-methoxy-4-methylpyridin-2-yl]morpholine (47)

Compound **46** (250 mg, 0.94 mmol) was dissolved in 20 mL of DCM, and triethylamine (196 µL, 1.41 mmol, 1.5 equiv.) was added in one portion. The reaction mixture was cooled to 0 °C, and a solution of 2-phenylacetyl chloride (188 µL, 1.41 mmol, 1.5 equiv.) in DCM (5 mL) was added dropwise. After complete addition, stirring at 0 °C was continued for 1 h. Subsequently, all volatiles were removed under reduced pressure. The residue was dissolved in THF (10 mL) and treated with a 1 M solution of tetra-*n*-butylammonium fluoride in THF (939 µL, 0.94 mmol, 1.0 equiv.). The reaction mixture was stirred at room temperature for 2 h. Afterward, it was dissolved in ethyl acetate (100 mL) and extracted with water (100 mL). The organic phase was

WILEY-VCH

Archiv der Pharmazie

washed with brine, dried over Na_2SO_4, filtrated, and concentrated under reduced pressure. The crude residue was purified by flash chromatography (mobile phase: ethyl acetate/*n*-hexane with 10–50% ethyl acetate), which yielded **47** as a colorless solid (125 mg, 0.34 mmol, 36%).

R_f = 0.64 (ethyl acetate/*n*-hexane 1:1); mp: 115 °C; ^{1}H-NMR (400 MHz, DMSO-d_6): δ(ppm) = 7.40 – 7.35 (m, 4H), 7.31 (m, 1H), 6.36 (s, 1H), 4.40 (s, 2H), 3.75 (s, 3H), 3.77 – 3.66 (m, 4H), 3.55 – 3.48 (m, 4H), 2.09 (s, 3H); ^{13}C-NMR (100 MHz, DMSO-d_6): δ(ppm) = 177.6, 165.1, 160.5, 158.0, 150.8, 134.3, 129.0, 128.7, 127.3, 99.7, 97.3, 65.8, 52.9, 44.7, 31.9, 19.7; (ATR): $\tilde{\nu}$ = 2954 (w, ν_{C-H}); ESI-HRAM-MS (*m/z*): calcd. for $[C_{20}H_{23}N_4O_3+H]^+$ 367.1765, found 367.1763; cpd purity (220 nm): 99.4%.

(2-Methoxy-4-methyl-6-morpholinopyridin-3-yl)methanamine (48)

Compound **45** (600 mg, 2.57 mmol) was dissolved in a saturated solution of ammonia in methanol (50 mL). 1.00 g of a Raney nickel suspension in water (50%) was washed with methanol several times and added to the reaction mixture. The suspension was carefully set under a hydrogen atmosphere (balloon pressure) and stirred at 50 °C. After 5 h, the catalyst was removed by filtration, and the filtrate was concentrated under reduced pressure. The resulting residue was dissolved in ethyl acetate and filtrated through a pad of silica gel, which was subsequently rinsed with an additional 250 mL of ethyl acetate. The obtained filtrate was discarded. Afterward, the silica gel pad was rinsed with 100 mL of a mixture of methanol and conc. aq. ammonia solution (9:1) to elute the desired product. The filtrate was concentrated under reduced pressure to obtain **48** as a colorless oil (434 mg, 1.83 mmol, 71%), used for the following reaction without any further purification and characterization.

4-Fluoro-*N*-[(2-methoxy-4-methyl-6-morpholinopyridin-3-yl)methyl]benzamide (49)

Compound **48** (434 mg, 1.83 mmol) was dissolved in DCM (20 mL). Triethylamine (507 µL, 3.66 mmol, 2.0 equiv.) was added in one portion. The reaction mixture was cooled to 0 °C, and a solution of 4-fluorobenzoyl chloride (325 µL, 2.75 mmol, 1.5 equiv.) in DCM (20 mL) was added dropwise over a period of 30 min. Cooling was removed, and the reaction mixture was stirred at room temperature. After 16 h, the reaction mixture was concentrated under reduced pressure. The crude residue was purified by flash chromatography (mobile phase: ethyl acetate/*n*-hexane with 30–50% ethyl acetate) and successive recrystallization (methanol/water), which yielded **49** as a colorless solid (422 mg, 1.17 mmol, 64%).

R_f = 0.63 (ethyl acetate/*n*-hexane 1:1); mp: 180 °C; ^{1}H-NMR (400 MHz, DMSO-d_6): δ(ppm) = 8.31 (t, *J* = 4.7 Hz, 1H), 7.96 – 7.86 (m, 2H), 7.30 – 7.19 (m, 2H), 6.21 (s, 1H), 4.35 (d, *J* = 4.7 Hz, 2H), 3.81 (s, 3H), 3.73 – 3.66 (m, 4H), 3.44 – 3.37 (m, 4H), 2.25 (s, 3H); ^{13}C-NMR (100 MHz, DMSO-d_6): δ(ppm) = 165.0, 163.7 (d, *J* = 249.0 Hz), 160.7, 156.6, 150.2, 130.9 (d, *J* = 3.0 Hz), 130.0 (d, *J* = 8.8 Hz), 114.9 (d, *J* = 21.6 Hz), 106.7, 100.1, 65.9, 52.7, 45.2, 34.6, 19.0; (ATR): $\tilde{\nu}$ = 3309 (m, ν_{N-H}), 2972 (w, ν_{C-H}), 1623 (s, $\nu_{C=O}$), 1599 (s, δ_{N-H}); ESI-HRAM-MS (*m/z*): calcd. for $[C_{19}H_{23}N_3O_4F+H]^+$ 360.1718, found 360.1713; cpd purity (220 nm): 99.6%.

Methyl 6-chloro-2-methoxy-4-methylnicotinate (50)

Compound **15a** (2.25 g, 11.2 mmol) was dissolved in dry DMF (30 mL). K_2CO_3 (2.31 g, 16.7 mmol, 1.5 equiv.) was added, and the mixture was stirred for 30 min. Afterward, methyl iodide (1.04 mL, 16.7 mmol, 1.5 equiv.) was added dropwise, and the reaction mixture was stirred at room temperature for 8 h. Subsequently, the reaction was quenched by the addition of 150 mL of water. The resulting suspension was extracted with ethyl acetate (150 mL). The organic phase was successively washed with a sat. aq. solution of $NaHCO_3$ (2 × 100 mL) and brine, dried over Na_2SO_4, filtrated, and concentrated under reduced pressure to obtain **50** as a pale yellow solid (2.36 g, 10.9 mmol, 98%).

R_f = 0.50 (ethyl acetate/*n*-hexane 1:9); mp: 70 °C; ^{1}H-NMR (400 MHz, DMSO-d_6): δ(ppm) = 7.11 (d, *J* = 0.7 Hz, 1H), 3.85 (s, 3H), 3.82 (s, 3H), 2.24 (d, *J* = 0.6 Hz, 3H); ^{13}C-NMR (100 MHz, DMSO-d_6): δ(ppm) = 165.7, 159.7, 150.8, 147.9, 118.1, 115.6, 54.4, 52.5, 18.4; (ATR): $\tilde{\nu}$ = 3034, 2954 (w, ν_{C-H}), 1717 (s, $\nu_{C=O}$).

Methyl 2-methoxy-4-methyl-6-morpholinonicotinate (51)

Compound **50** (800 mg, 3.71 mmol) was dissolved in NMP (10 mL). Triethylamine (1030 µL, 7.42 mmol, 2.0 equiv.) and morpholine (388 µL, 4.45 mmol, 1.2 equiv.) were added successively, and the resulting solution was stirred at 90 °C for 2 d. Afterward, the reaction mixture was dissolved in ethyl acetate (100 mL) and extracted with water (3 × 100 mL). The organic phase was washed with brine, dried over Na_2SO_4, filtrated, and concentrated under reduced pressure. The crude residue was purified by flash chromatography (mobile phase: ethyl acetate/*n*-hexane with 30–40% ethyl acetate), which yielded **51** as a colorless solid (386 mg, 1.45 mmol, 39%).

R_f = 0.64 (ethyl acetate/*n*-hexane 1:1); mp: 123 °C; ^{1}H-NMR (400 MHz, DMSO-d_6): δ(ppm) = 6.26 (d, *J* = 0.8 Hz, 1H), 3.79 (s, 3H), 3.73 (s, 3H), 3.71 – 3.64 (m, 4H), 3.56 – 3.45 (m, 4H), 2.20 (d, *J* = 0.6 Hz, 3H); ^{13}C-NMR (100 MHz, DMSO-d_6): δ(ppm) = 166.9, 160.1, 157.5, 150.0, 103.9, 99.6, 65.8, 52.9, 51.5, 44.6, 19.9; (ATR): $\tilde{\nu}$ = 2918 (w, ν_{C-H}), 1747 (s, $\nu_{C=O}$).

WILEY-VCH

Archiv der Pharmazie

2-Methoxy-4-methyl-6-morpholinonicotinohydrazide (52)

Compound **51** (250 mg, 0.94 mmol) was suspended in an 80% aq. solution of hydrazine hydrate (20.0 mL, 303 mmol, 323 equiv.). The suspension was heated to reflux, and methanol was added until complete dissolution of methyl 2-methoxy-4-methyl-6-morpholinonicotinate. Subsequently, stirring under reflux was continued. After 24 h, all volatiles were removed under reduced pressure. The crude residue was purified by flash chromatography (mobile phase: DCM/methanol with 0–10% methanol), which yielded **52** as a beige-colored solid (168 mg, 0.63 mmol, 67%).

R_f = 0.73 (DCM/methanol 9:1); mp: 158 °C; ^{1}H-NMR (400 MHz, DMSO-d_6): δ(ppm) = 9.08 (s, 1H), 6.20 (s, 1H), 4.55 (s, 2H), 3.75 (s, 3H), 3.72 – 3.65 (m, 4H), 3.48 – 3.40 (m, 4H), 2.13 (s, 3H); ^{13}C-NMR (100 MHz, DMSO-d_6): δ(ppm) = 165.4, 159.0, 157.1, 148.9, 108.3, 99.4, 65.9, 52.6, 45.0, 19.1; (ATR): $\tilde{\nu}$ = 3308 (m, ν_{N-H}), 2977 (w, ν_{C-H}), 1593 (s, $\nu_{C=O}$).

2-(4-Fluorophenyl)-*N'*-(2-methoxy-4-methyl-6-morpholinonicotinoyl)acetohydrazonamide (53)

Compound **56** (169 mg, 0.83 mmol, 1.4 equiv.) was added in portions to a solution of sodium methoxide (45 mg, 0.83 mmol, 1.4 equiv.) in dry methanol (20 mL) at 0 °C. After complete addition, the cooling was removed, and the reaction mixture was stirred at room temperature. Subsequently, compound **52** (158 mg, 0.59 mmol) was added, and stirring at room temperature was continued for 24 h. Afterward, volatiles were removed under reduced pressure, and the residue was purified by silica gel column chromatography (DCM/methanol 9:1), which yielded **53** as a colorless solid (111 mg, 0.28 mmol, 47%).

R_f = 0.57 (DCM/methanol 9:1); mp: 219 °C; ^{1}H-NMR (400 MHz, DMSO-d_6): δ(ppm) = 9.45 (s, 1H), 7.47 – 7.34 (m, 2H), 7.28 – 7.09 (m, 2H), 6.23 (s, 1H), 6.08 (s, 2H), 3.76 (s, 3H), 3.73 – 3.59 (m, 4H), 3.54 – 3.41 (m, 4H), 3.37 (s, 2H), 2.15 (s, 3H); ^{13}C-NMR (100 MHz, DMSO-d_6): δ(ppm) = 161.1, 161.0 (d, J = 240.0 Hz), 159.1, 157.0, 152.3, 149.0, 134.0, 130.6 (d, J = 8.0 Hz), 114.9 (d, J = 21.1 Hz), 99.5, 65.9, 52.7, 45.1, 39.1, 19.1; (ATR): $\tilde{\nu}$ = 3389, 3220 (m, ν_{N-H}), 3047, 2986 (w, ν_{C-H}), 1653 (m, $\nu_{C=O}$).

4-{5-[5-(4-fluorobenzyl)-1*H*-1,2,4-triazol-3-yl]-6-methoxy-4-methylpyridin-2-yl}morpholine (54)

Compound **52** (133 mg, 0.50 mmol), K_2CO_3 (35 mg, 0.25 mmol, 0.5 equiv.), and 2-(4-fluorophenyl)acetonitrile (180 µL, 1.50 mmol, 3.0 equiv.) were dissolved in *n*-butanol (2 mL) and stirred in a closed vessel at 150 °C in a microwave reactor. After 4 h, the reaction was cooled to room temperature, and all volatiles were removed under reduced pressure. The residue was dissolved in ethyl acetate (100 mL) and extracted with water (100 mL). The organic phase was washed with brine, dried over Na_2SO_4, filtrated, and concentrated under reduced pressure. The crude residue was purified by silica gel column chromatography (ethyl acetate/*n*-hexane 1:1), which yielded **54** as a colorless solid (90 mg, 0.23 mmol, 47%).

R_f = 0.41 (ethyl acetate/*n*-hexane 1:1); mp: 164 °C; ^{1}H-NMR (400 MHz, DMSO-d_6): δ(ppm) = 11.35 (s, 1H), 7.43 – 7.32 (m, 2H), 7.06 – 6.95 (m, 2H), 6.16 (s, 1H), 4.13 (s, 2H), 4.01 (s, 3H), 3.87 – 3.80 (m, 4H), 3.62 – 3.55 (m, 4H), 2.70 (s, 3H); ^{13}C-NMR (100 MHz, DMSO-d_6): δ(ppm) = 162.3, 161.8 (d, J = 242.0 Hz), 160.6, 157.1, 152.7, 152.5, 134.4, 130.6 (d, J = 7.9 Hz), 115.3 (d, J = 21.2 Hz), 101.9, 98.7, 66.8, 53.9, 45.3, 34.2, 23.4; (ATR): $\tilde{\nu}$ = 3220 (m, ν_{N-H}), 2977 (w, ν_{C-H}), ESI-HRAM-MS (*m/z*): calcd. for $[C_{20}H_{23}N_5O_2F+H]^+$ 384.1830, found 384.1833; cpd purity (220 nm): 98.6%.

Methyl 2-(4-fluorophenyl)acetimidate hydrochloride (56)

2-(4-Fluorophenyl)acetonitrile (3.00 mL, 25.0 mmol) was dissolved in dry methanol (20.0 mL, 49 mmol, 2.0 equiv.). The reaction mixture was set under an atmosphere of argon and cooled to 0 °C. HCl gas was passed through the solution for 3 h under stirring. Afterward, all volatiles were removed under reduced pressure. The residue was suspended in dry THF, filtered off, and rinsed with additional dry THF to obtain **56** as a colorless solid (2.94 g, 14.5 mmol, 58%).

Mp: 157 °C; ^{1}H-NMR (400 MHz, $CDCl_3$): δ(ppm) = 12.91 (s, 1H), 11.83 (s, 1H), 7.48 – 7.38 (m, 2H), 7.10 – 6.99 (m, 2H), 4.28 (s, 3H), 4.06 (s, 2H); ^{13}C-NMR (100 MHz, $CDCl_3$): δ(ppm) = 178.2, 162.9 (d, J = 247.9 Hz), 131.6 (d, J = 8.2 Hz), 126.9 (d, J = 3.3 Hz), 116.4 (d, J = 21.8 Hz), 61.3, 38.4; (ATR): $\tilde{\nu}$ = 3100–2600 (b, ν_{N-H}), 1652 (m, ν_{C-N}).

1-Amino-2-(4-fluorophenyl)ethan-1-iminium chloride (57)

Compound **56** (2.20 g, 10.8 mmol) was dissolved in dry methanol (25 mL). Ammonia gas was passed through the solution for 30 min. Subsequently, the reaction vessel was closed, and the mixture was stirred at room temperature. After 24 h, all volatiles were removed under reduced pressure. The resulting mucilaginous substance was treated with ethyl acetate to obtain **57** as a colorless solid, which was filtered off (1.25 g, 6.6 mmol, 61%).

WILEY-VCH

Archiv der Pharmazie

Mp: 134 °C; ^{1}H-NMR (400 MHz, MeOH-d_4): δ(ppm) = 7.75 – 7.29 (m, 2H), 7.29 – 6.99 (m, 2H), 3.82 (s, 2H); ^{13}C-NMR (100 MHz, MeOH-d_4): δ(ppm) = 171.6, 164.1 (d, *J* = 245.5 Hz), 132.2 (d, *J* = 8.2 Hz), 130.5 (d, *J* = 3.3 Hz), 117.1 (d, *J* = 22.0 Hz), 38.6; (ATR): $\tilde{\nu}$ = 3300–2600 (b, ν_{N-H}), 1669 (s, $\nu_{C=N}$).

4.1.3 Log$D_{7.4}$ estimation

The log$D_{7.4}$ estimation was carried out as previously reported by employing a standard HPLC-based method.[23] Briefly, the capacity factors of seven reference substances with known log$D_{7.4}$ values were determined from their retention times (acetophenone, benzene, ethyl benzoate, benzophenone, phenyl benzoate, diphenyl ether, bibenzyl) with uracil used as a dead-time marker. The logarithm of the capacity factors was then plotted against the corresponding log$D_{7.4}$ values to obtain a calibration function, which was used to calculate the log$D_{7.4}$ values for each compound of interest. For HPLC analysis, a Phenomenex Luna 5 µm Phenyl-Hexyl 100 Å column (150×4.6 mm) was used with a mixture of methanol (75%) and 10 mM Tris/HCl buffer (25%) at pH 7.4 as mobile phase at a flow rate of 1.0 mL/min. The compounds of interest were dissolved in methanol (2 mg/mL), and the retention time was determined as the mean value from two measurements. The reference substances were injected as a mixture, which was prepared by dissolving 2 mg of a reference substance in 1 mL of methanol and subsequently combining 50 µL aliquots of each reference solution. The reference mixture was measured before and after the compounds of interest. Then, the mean retention time from both measurements was used to calculate the calibration function.

4.2 Biology

4.2.1 K_V7.2/3 channel opening activity

The FLIPR Potassium Assay Kit (Molecular Devices, CA, USA) was used to determine the K_V7.2/3 channel opening activity of the synthesized analogs according to the protocol of the assay kit. HEK-293 cells transfected with KCNQ2/3 were obtained from SB Drug Discovery (Glasgow, UK). The cell culture and the data analysis were carried out as previously described elsewhere.[24,64] Briefly, the cells were grown in minimum essential medium with non-essential amino acids (Thermo Fisher Scientific), supplemented with 10% heat-inactivated fetal bovine serum, 2 mM L-glutamine, 4 µg/mL blasticidin S-HCl, 1% penicillin/streptomycin and 0.78 mg/mL G418 sulfate. The cells had been seeded at densities of 60,000 cells/well in 100 µL of cell culture media using black-walled 96-well plates with a clear bottom (4titude Vision Plates from Azenta Life Sciences) suitable for fluorimetric measurements. After incubation for 24 h, 100 µL of loading buffer containing the fluorescent dye and probenecid as an inhibitor for the anion-exchange protein were added. Afterward, the plates were incubated for 1 h at room temperature under the exclusion of light. The test compounds were serially diluted in DMSO and added to the wells to obtain a final DMSO concentration of 1% (V/V). Equally treated wells containing loading buffer and 1% DMSO without test compound were deemed as the vehicle control. After an additional 30 min of incubation, fluorimetric measurements were performed at extinction/emission wavelengths of 485 nm and 535 nm with an Infinite F200 Pro plate reader (Tecan). The baseline fluorescence signal was recorded for 20 s. Subsequently, a stimulus buffer (25 mM K^+, 15 mM Tl^+) was added to each well, and measuring the fluorescence intensity was continued for 2.5 min. The resulting data were processed by normalizing the measured fluorescence intensity with the average baseline signal (F/F_0). A correction was then performed by calculating the difference between the normalized vehicle control signal and the normalized baseline signal and subtracting the result from the F/F_0 value. To obtain a concentration-activity curve, the maximal corr. $\Delta F/F_0$ values were plotted against the logarithmic compound concentration. Relative EC_{50} values were calculated with GraphPad Prism 6 (La Jolla, CA, USA) by determining the inflection point of the resulting sigmoidal curves. The corresponding E_{max} values as a measure for the intrinsic activity were determined by relating the maximum corr. $\Delta F/F_0$ value of a specific compound to the maximum corr. $\Delta F/F_0$ value of flupirtine, which was defined as 100%. All results are means of at least three independent experiments ± standard deviation (SD).

4.2.2 Hepatic cell viability

The culturing of the TAMH and HEP-G2 cells and the MTT cell viability assay were carried out as previously described.[24,64] Briefly, TAMH mouse liver cells (School of Pharmacy, University of Washington, Seattle, WA, USA) were grown in serum-free DMEM/F12 medium supplemented with 5% PANEXIN NTA, 10 mM nicotinamide, and 10 µg/mL gentamicin. HEP-G2 human liver cancer cells (DSMZ, Braunschweig, Germany) were cultured in RPMI 1640 (PAN Biotech), supplemented with 10% heat-inactivated fetal bovine serum and 1% penicillin/streptomycin. Both cell lines were seeded into 96-well plates with 20,000 cells per well for TAMH and 15,000 cells per well for HEP-G2 and incubated at 37 °C in a 5% CO_2 atmosphere. After 24 h, the medium was replaced with fresh culture medium containing the test compounds at defined concentrations. For this purpose, the compounds were dissolved in DMSO and serially diluted in the corresponding culture medium to achieve a final concentration of 1% DMSO (V/V). Equally treated wells containing 1% DMSO without test compound were deemed as the vehicle control. Additional wells without cells were treated analogously to the control wells to determine the background optical density (OD). After 24 h of incubation with the test compounds, the medium was replaced with fresh medium containing 10% (V/V) of a 2.5 mg/mL solution of 3-(4,5-dimethylthiazol-2-yl)-2,5-diphenyltetrazolium bromide (MTT). After an additional 4 h of incubation, the culture medium in each well was removed, and DMSO (50 µL) was added to dissolve the formazan crystals. Afterward, ODs were determined at 570 nm by using a SpectraMax 190 microplate reader. A correction of the OD values of the test compound (T) and control (C) wells by subtracting the bank value followed. Subsequently, the $T/C_{corr.}$-ratios were calculated and plotted against the logarithmic compound concentration to obtain a dose-response curve. After interpolation of the sigmoidal standard curve with GraphPad Prism 6, the LD_{50} and LD_{25} values were determined as the concentrations that reduced cell viability to 50 and 75%, respectively. If no reduction in cell viability to 75% was observed at the maximum concentration possible without precipitating the compounds, the LD_{25} value was reported as higher than the highest concentration tested. All results are the means of at least three independent experiments ± standard deviation (SD).

WILEY-VCH

Archiv der Pharmazie

4.3 Molecular modeling

If not stated otherwise, all calculations were performed using the Schrodinger software suite release 2022-1 (Schrödinger, LLC, New York, NY, 2022).

4.3.1 Structure preparation

The heterotetrameric protein structure of the KCNQ2/3 potassium channel was taken from previous studies[23] and is based on the cryo-EM structure of KCNQ2 with bound retigabine (PDB 7CR2),[36] while two opposing chains were used as a template for homology modeling within the Multiple Sequence Viewer in Maestro. Finally, the obtained model was prepared by the Protein Preparation Wizard[65] to optimize the protonation states and the hydrogen bond network, followed by a restraint minimization with OPLS4 force field parameters.[66]

4.3.2 Molecular docking

All ligands were prepared using the Ligand Preparation application in Maestro and then docked into the heterotetrameric KCNQ2/3 model using an induced fit approach[67] in Glide (version 94137)[68] with standard sampling protocol of protein sidechains and an implicit membrane representation. The resulting 20 docking poses per compound were visually analyzed and selected. The compounds **14** and **18a** were re-docked into the same KCNQ2/3 retigabine binding site after molecular dynamics simulations using the Glide XP scoring function[69] for direct comparison.

4.3.3 Molecular dynamics simulations

The previously generated protein structure was prepared for molecular dynamics simulation using Desmond System Builder. The POPC bilayer membrane[70] position was placed on the transmembrane helices, and the system was solvated in an orthorhombic box with a 1 nm buffer around the protein with explicit TIP3P[71] water molecules and 0.15 M NaCl salt concentration. OPLS4 force field parameters[66] were applied in all simulations. Since the binding pockets are highly conserved, four different ligands (retigabine, **18a**, **18c**, **49**) were used in a single molecular dynamics run after molecular docking. The molecular system was minimized for 500 ps and equilibrated using the standard protocol (distributed with Desmond v6.9[72]) for membrane systems at 300 K and NpγT ensemble.[73] The production run was performed for 50 ns with a timestep of 2 fs. The temperature and pressure were maintained by a Langevin thermostat and a Langevin barostat, respectively. The snapshots were saved to the trajectory every 20 ps and analyzed using the Simulation Interaction Diagram in Maestro.

ACKNOWLEDGEMENTS

KWW and FMB are funded by grants DFG LI 765/7-2 and DFG BE 1287/6-2 awarded to AL and PJB by the Deutsche Forschungsgemeinschaft (DFG – German Research Foundation). We thank Ms. Anne Schüttler and Ms. Maria Hühr for excellent technical assistance.

CONFLICT OF INTEREST

The authors declare no conflicts of interest.

REFERENCES

[1] V. Barrese, J. B. Stott, I. A. Greenwood, *Annu. Rev. Pharmacol. Toxicol.* **2018**, *58*, 625. DOI: 10.1146/annurev-pharmtox-010617-052912

[2] D. A. Brown, G. M. Passmore, *Br. J. Pharmacol.* **2009**, *156*, 1185. DOI: 10.1111/j.1476-5381.2009.00111.x

[3] M. M. Shah, M. Migliore, I. Valencia, E. C. Cooper, D. A. Brown, *Proc. Natl. Acad. Sci. U.S.A.* **2008**, *105*, 7869. DOI: 10.1073/pnas.0802805105

[4] H. C. Peters, H. Hu, O. Pongs, J. F. Storm, D. Isbrandt, *Nat. Neurosci.* **2005**, *8*, 51. DOI: 10.1038/nn1375

[5] F. A. Vigil, C. M. Carver, M. S. Shapiro, *Front. Physiol.* **2020**, *11*, 688. DOI: 10.3389/fphys.2020.00688

[6] M. Borgini, P. Mondal, R. Liu, P. Wipf, *RSC Med. Chem.* **2021**, *12*, 483. DOI: 10.1039/D0MD00328J

[7] a) F. A. Vigil, E. Bozdemir, V. Bugay, S. H. Chun, M. Hobbs, I. Sanchez, S. D. Hastings, R. J. Veraza, D. M. Holstein, S. M. Sprague, C. M Carver, J. E. Cavazos, R. Brenner, J. D. Lechleiter, M. S. Shapiro, *J. Cereb. Blood Flow Metab.* **2019**, *40*, 1256-1273. DOI: 10.1177/0271678X19857818; b) J. Ren, J. Guo, S. Zhu, Q. Wang, R. Gao, C. Zhao, C. Feng, C. Qin, Z. He, C. Qin, Z. Wang, L. Zang, *Biol. Pharm. Bull.* **2021**, *44*, 169. DOI: 10.1248/bpb.b20-00504

[8] S. Costi, M.-H. Han, J. W. Murrough, *CNS Drugs* **2022**, *36*, 207. DOI: 10.1007/s40263-021-00885-y

WILEY-VCH

Archiv der Pharmazie

[9] M. A. Uberall, G. H. H. Mueller-Schwefe, B. Terhaag, *Curr. Med. Res. Opin.* **2012**, *28*, 1617. DOI: 10.1185/03007995.2012.726216

[10] J. A. French, B. W. Abou-Khalil, R. F. Leroy, E. M. T. Yacubian, P. Shin, S. Hall, H. Mansbach, V. Nohria, *Neurology* **2011**, *76*, 1555. DOI: 10.1212/WNL.0b013e3182194bd3

[11] A. Nissenkorn, P. Kornilov, A. Peretz, L. Blumkin, G. Heimer, B. Ben-Zeev, B. Attali, *Epileptic Disord.* **2021**, *23*, 695. DOI: 10.1684/epd.2021.1315

[12] D. Rudin, J. Spoendlin, A. L. Cismaru, E. Liakoni, N. Bonadies, U. Amstutz, C. R. Meier, S. Krähenbühl, M. Haschke, *Eur. J. Intern. Med.* **2019**, *68*, 36. DOI: 10.1016/j.ejim.2019.07.029

[13] C. Bock, A. Link, *Future Med. Chem.* **2019**, *11*, 337. DOI: 10.4155/fmc-2018-0350

[14] K. W. Wurm, F.-M. Bartz, L. Schulig, A. Bodtke, P. J. Bednarski, A. Link, *ChemMedChem* **2022**, in press. DOI: 10.1002/cmdc.202200262

[15] M. C. Michel, P. Radziszewski, C. Falconer, D. Marschall-Kehrel, K. Blot, *Br. J. Clin. Pharmacol.* **2012**, *73*, 821. DOI: 10.1111/j.1365-2125.2011.04138.x

[16] S. Clark, A. Antell, K. Kaufman, *Ther. Adv. Drug Saf.* **2015**, *6*, 15. DOI: 10.1177/2042098614560736

[17] M. R. Groseclose, S. Castellino, *Chem. Res. Toxicol.* **2019**, *32*, 294. DOI: 10.1021/acs.chemrestox.8b00313

[18] K. Methling, P. Reszka, M. Lalk, O. Vrana, E. Scheuch, W. Siegmund, B. Terhaag, P. J. Bednarski, *Drug Metab. Dispos.* **2009**, *37*, 479. DOI: 10.1124/dmd.108.024364

[19] C. C. Hernandez, R. A. Tarfa, J. Miguel I Limcaoco, R. Liu, P. Mondal, C. Hill, R. Keith Duncan, T. Tzounopoulos, C. R. J. Stephenson, M. J. O'Meara, P. Wipf, *Bioorg. Med. Chem. Lett.* **2022**, *71*, 128841. DOI: 10.1016/j.bmcl.2022.128841

[20] P. Bloms-Funke, M. Bankstahl, J. Bankstahl, C. Kneip, W. Schröder, W. Löscher, *Neuropharmacology* **2022**, *203*, 108884. DOI: 10.1016/j.neuropharm.2021.108884

[21] M. D. Aleo, J. Aubrecht, P. D Bonin, D. A. Burt, J. Colangelo, L. Luo, S. Schomaker, R. Swiss, S. Kirby, G. C Rigdon, P. Dua, *Pharmacol. Res. Perspect.* **2019**, *7*, e00467. DOI: 10.1002/prp2.467

[22] a) Y.-M. Zhang, H.-Y. Xu, H.-N. Hu, F.-Y. Tian, F. Chen, H.-N. Liu, L. Zhan, X.-P. Pi, J. Liu, Z.-B. Gao, F.-J. Nan, *J. Med. Chem.* **2021**, *64*, 5816. DOI: 10.1021/acs.jmedchem.0c02252; b) S. Musella, L. Carotenuto, N. Iraci, G. Baroli, T. Ciaglia, P. Nappi, M. G. Basilicata, E. Salviati, V. Barrese, V. Vestuto, G. Pignataro, G. Pepe, E. Sommella, V. Di Sarno, M. Manfra, P. Campiglia, I. Gomez-Monterrey, A. Bertamino, M. Taglialatela, C. Ostacolo, F. Miceli, *J. Med. Chem.* **2022**, *65*, 11340. DOI: 10.1021/acs.jmedchem.2c00911

[23] K. W. Wurm, F.-M. Bartz, L. Schulig, A. Bodtke, P. J. Bednarski, A. Link, *ACS Omega* **2022**, *7*, 7989. DOI: 10.1021/acsomega.1c07103

[24] A. S. Surur, C. Bock, K. Beirow, K. Wurm, L. Schulig, M. K. Kindermann, W. Siegmund, P. J. Bednarski, A. Link, *Org. Biomol. Chem.* **2019**, *17*, 4512. DOI: 10.1039/C9OB00511K

[25] S. Kühnert, G. Bahrenberg, A. Kless, W. Schroder, S. Lucas (Grünenthal GmbH), US 2012/0258947 Al, **2012**

[26] A. P. Kourounakis, D. Xanthopoulos, A. Tzara, *Med. Res. Rev.* **2020**, *40*, 709. DOI: 10.1002/med.21634

[27] A. A. Kadi, S. M. Amer, H. W. Darwish, M. W. Attwa, *RSC Adv.* **2017**, *7*, 36279. DOI: 10.1039/c7ra06341e

[28] S. L. Degorce, M. S. Bodnarchuk, J. S. Scott, *ACS Med. Chem. Lett.* **2019**, *10*, 1198. DOI: 10.1021/acsmedchemlett.9b00248

[29] H. Zhao, H. Fu, R. Qiao, *J. Org. Chem.* **2010**, *75*, 3311. DOI: 10.1021/jo100345t

[30] J. L. Yap, K. Hom, S. Fletcher, *Tetrahedron Lett.* **2011**, *52*, 4172. DOI: 10.1016/j.tetlet.2011.06.007

[31] P. K. Gadekar, A. Roychowdhury, P. S. Kharkar, V. M. Khedkar, M. Arkile, H. Manek, D. Sarkar, R. Sharma, V. Vijayakumar, S. Sarveswari, *Eur. J. Med. Chem.* **2016**, *122*, 475. DOI: 10.1016/j.ejmech.2016.07.001

[32] a) W. Jespers, A. Oliveira, R. Prieto-Díaz, M. Majellaro, J. Åqvist, E. Sotelo, H. Gutiérrez-de-Terán, *Molecules* **2017**, *22*, 1945. DOI: 10.3390/molecules22111945; b) J. Cai, X. Fradera, M. van Zeeland, M. Dempster, K. S. Cameron, D. J. Bennett, J. Robinson, L. Popplestone, M. Baugh, P. Westwood, J. Bruin, W. Hamilton, E. Kinghorn, C. Long, J. C. M. Uitdehaag, *Bioorg. Med. Chem. Lett.* **2010**, *20*, 4507. DOI: 10.1016/j.bmcl.2010.06.043; c) H. W. Lee, B. Y. Kim, J. B. Ahn, S. K. Kang, J. H. Lee, J. S. Shin, S. K. Ahn, S. J. Lee, S. S. Yoon, *Eur. J. Med. Chem.* **2005**, *40*, 862. DOI: 10.1016/j.ejmech.2005.03.019

[33] C. Zhao, Y. H. Choi, D. B. Khadka, Y. Jin, K.-Y. Lee, W.-J. Cho, *Bioorg. Med. Chem.* **2016**, *24*, 789. DOI: 10.1016/j.bmc.2015.12.047

WILEY-VCH

Archiv der Pharmazie

[34] E. A. Arnott, L. C. Chan, B. G. Cox, B. Meyrick, A. Phillips, *J. Org. Chem.* **2011**, *76*, 1653. DOI: 10.1021/jo102262k

[35] H.-P. Gong, Z.-J. Quan, X.-C. Wang, *Chem. Pap.* **2022**, *76*, 2529. DOI: 10.1007/s11696-021-02044-5

[36] X. Li, Q. Zhang, P. Guo, J. Fu, L. Mei, D. Lv, J. Wang, D. Lai, S. Ye, H. Yang, J. Guo, *Cell Res.* **2021**, *31*, 52. DOI: 10.1038/s41422-020-00410-8

[37] M. T. Rahman, A. M. Decker, L. Laudermilk, R. Maitra, W. Ma, S. Ben Hamida, E. Darcq, B. L. Kieffer, C. Jin, *J. Med. Chem.* **2021**, *64*, 12397. DOI: 10.1021/acs.jmedchem.1c01075

[38] H. C. Shen, F.-X. Ding, Q. Deng, S. Xu, X. Tong, X. Zhang, Y. Chen, G. Zhou, L.-Y. Pai, M. Alonso-Galicia, S. Roy, B. Zhang, J. R. Tata, J. P. Berger, S. L. Colletti, *Bioorg. Med. Chem. Lett.* **2009**, *19*, 5716. DOI: 10.1016/j.bmcl.2009.08.006

[39] M. I. Antczak, Y. Zhang, C. Wang, J. Doran, J. Naidoo, S. Voruganti, N. S. Williams, S. D. Markowitz, J. M. Ready, *J. Med. Chem.* **2017**, *60*, 3979. DOI: 10.1021/acs.jmedchem.7b00271

[40] M. G. Palermo, *Tetrahedron Lett.* **1996**, *37*, 2885. DOI: 10.1016/0040-4039(96)00425-X

[41] K. Biernacki, M. Daśko, O. Ciupak, K. Kubiński, J. Rachon, S. Demkowicz, *Pharmaceuticals* **2020**, *13*, 111. DOI: 10.3390/ph13060111

[42] A. R. Gangloff, J. Litvak, E. J. Shelton, D. Sperandio, V. R. Wang, K. D. Rice, *Tetrahedron Lett.* **2001**, *42*, 1441. DOI: 10.1016/S0040-4039(00)02288-7

[43] N. Y. Khromova, M. M. Fedorov, S. I. Malekin, A. V. Kutkin, *Russ. J. Org. Chem.* **2016**, *52*, 1490. DOI: 10.1134/S1070428016100195

[44] S. Ueda, H. Nagasawa, *J. Am. Chem. Soc.* **2009**, *131*, 15080. DOI: 10.1021/ja905056z

[45] K.-S. Yeung, M. E. Farkas, J. F. Kadow, N. A. Meanwell, *Tetrahedron Lett.* **2005**, *46*, 3429. DOI: 10.1016/j.tetlet.2005.02.167

[46] M. Xie, G. Zhu, Y. Hu, H. Gu, *J. Phys. Chem. C* **2011**, *115*, 20596. DOI: 10.1021/jp206544a

[47] A. D. Bochevarov, E. Harder, T. F. Hughes, J. R. Greenwood, D. A. Braden, D. M. Philipp, D. Rinaldo, M. D. Halls, J. Zhang, R. A. Friesner, *Int. J. Quantum Chem.* **2013**, *113*, 2110. DOI: 10.1002/qua.24481

[48] J. D. Mottishaw, H. Sun, *J. Phys. Chem. A* **2013**, *117*, 7970. DOI: 10.1021/jp403679x

[49] J. Payandeh, M. Volgraf, *Nat. Rev. Drug Discov.* **2021**, *20*, 710. DOI: 10.1038/s41573-021-00240-2

[50] A. Schenzer, T. Friedrich, M. Pusch, P. Saftig, T. J. Jentsch, J. Grötzinger, M. Schwake, *J. Neurosci.* **2005**, *25*, 5051. DOI: 10.1523/JNEUROSCI.0128-05.2005

[51] "Assessment report for flupirtine containing medicinal products", can be found under https://www.ema.europa.eu/en/documents/referral/flupirtine-containing-medicines-article-107i-procedure-prac-assessment-report_en.pdf, **2013**

[52] V. K. Naguri, R. B. Komaram, T. V. Sagar, *Asian J. Pharm. Clin. Res.* **2019**, 84. DOI: 10.22159/ajpcr.2019.v12i4.31699

[53] W. Siegmund, C. Modess, E. Scheuch, K. Methling, M. Keiser, A. Nassif, D. Rosskopf, P. J. Bednarski, J. Borlak, B. Terhaag, *Br. J. Clin. Pharmacol.* **2015**, *79*, 501. DOI: 10.1111/bcp.12522

[54] J. G. Kenna, J. Uetrecht, *Drug. Metab. Dispos.* **2018**, *46*, 1658. DOI: 10.1124/dmd.118.082719

[55] a) P. Nicoletti, A. N. Werk, A. Sawle, Y. Shen, T. J. Urban, S. A. Coulthard, E. S. Bjornsson, I. Cascorbi, A. Floratos, T. Stammschulte, U. Gundert-Remy, M. R. Nelson, G. P. Aithal, A. K. Daly, *Pharmacogenet. Genomics* **2016**, *26*, 218. DOI: 10.1097/FPC.0000000000000209; b) F. Puls, C. Agne, F. Klein, M. Koch, K. Rifai, M. P. Manns, J. Borlak, H. H. Kreipe, *Virchows Arch.* **2011**, *458*, 709. DOI: 10.1007/s00428-011-1087-9

[56] A. Segovia-Zafra, D. E. Di Zeo-Sánchez, C. López-Gómez, Z. Pérez-Valdés, E. García-Fuentes, R. J. Andrade, M. I. Lucena, M. Villanueva-Paz, *Acta Pharm. Sin. B* **2021**, *11*, 3685. DOI: 10.1016/j.apsb.2021.11.013

[57] G. A. Kullak-Ublick, R. J. Andrade, M. Merz, P. End, A. Benesic, A. L. Gerbes, G. P. Aithal, *Gut* **2017**, *66*, 1154. DOI: 10.1136/gutjnl-2016-313369

[58] T. Mosmann, *J. Immunol. Methods* **1983**, *65*, 55. DOI: 10.1016/0022-1759(83)90303-4

[59] a) T. Ramirez, A. Strigun, A. Verlohner, H.-A. Huener, E. Peter, M. Herold, N. Bordag, W. Mellert, T. Walk, M. Spitzer, X. Jiang, S. Sperber, T. Hofmann, T. Hartung, H. Kamp, B. van Ravenzwaay, *Arch. Toxicol.* **2018**, *92*, 893. DOI: 10.1007/s00204-017-2079-6; b) M. Davis, B. D. Stamper, *Biomed. Res. Int.* **2016**, *2016*, 4780872. DOI: 10.1155/2016/4780872

WILEY-VCH

Archiv der Pharmazie

[60] K. McEuen, J. Borlak, W. Tong, M. Chen, *Int. J. Mol. Sci.* **2017**, *18*, 1335. DOI: 10.3390/ijms18071335

[61] N. T. T. Tham, S.-R. Hwang, J.-H. Bang, H. Yi, Y.-I. Park, S.-J. Kang, H.-G. Kang, Y.-S. Kim, H.-O. Ku, *J. Vet. Sci.* **2019**, *20*, 34. DOI: 10.4142/jvs.2019.20.1.34

[62] A. Mobinikhaledi, N. Forughifar, J. A. Alipour Safari, E. Amini, *J. Heterocycl. Chem.* **2007**, *44*, 697. DOI: 10.1002/jhet.5570440329

[63] U. Galli, E. Ciraolo, A. Massarotti, J. P. Margaria, G. Sorba, E. Hirsch, G. C. Tron, *Molecules* **2015**, *20*, 17275. DOI: 10.3390/molecules200917275

[64] C. Bock, A. S. Surur, K. Beirow, M. K. Kindermann, L. Schulig, A. Bodtke, P. J. Bednarski, A. Link, *ChemMedChem* **2019**, *14*, 952. DOI: 10.1002/cmdc.201900112

[65] G. M. Sastry, M. Adzhigirey, T. Day, R. Annabhimoju, W. Sherman, *J. Comput. Aided Mol. Des.* **2013**, *27*, 221. DOI: 10.1007/s10822-013-9644-8

[66] C. Lu, C. Wu, D. Ghoreishi, W. Chen, L. Wang, W. Damm, G. A. Ross, M. K. Dahlgren, E. Russell, C. D. von Bargen, R. Abel, R. A. Friesner, E. D. Harder, *J. Chem. Theory Comput.* **2021**, *17*, 4291. DOI: 10.1021/acs.jctc.1c00302

[67] W. Sherman, T. Day, M. P. Jacobson, R. A. Friesner, R. Farid, *J. Med. Chem.* **2006**, *49*, 534. DOI: 10.1021/jm050540c

[68] a) R. A. Friesner, J. L. Banks, R. B. Murphy, T. A. Halgren, J. J. Klicic, D. T. Mainz, M. P. Repasky, E. H. Knoll, M. Shelley, J. K. Perry, D. E. Shaw, P. Francis, P. S. Shenkin, *J. Med. Chem.* **2004**, *47*, 1739. DOI: 10.1021/jm0306430; b) T. A. Halgren, R. B. Murphy, R. A. Friesner, H. S. Beard, L. L. Frye, W. T. Pollard, J. L. Banks, *J. Med. Chem.* **2004**, *47*, 1750. DOI: 10.1021/jm030644s

[69] R. A. Friesner, R. B. Murphy, M. P. Repasky, L. L. Frye, J. R. Greenwood, T. A. Halgren, P. C. Sanschagrin, D. T. Mainz, *J. Med. Chem.* **2006**, *49*, 6177. DOI: 10.1021/jm051256o

[70] M. Kurki, A. Poso, P. Bartos, M. S. Miettinen, *J. Chem. Inf. Model.* **2022.** DOI: 10.1021/acs.jcim.2c00395

[71] P. Mark, L. Nilsson, *J. Phys. Chem. A* **2001**, *105*, 9954. DOI: 10.1021/jp003020w

[72] K. J. Bowers, E. Chow, H. Xu, R. O. Dror, M. P. Eastwood, B. A. Gregersen, Klepeis J. L., I. Kolossvary, M. A. Moraes, F. D. Sacerdoti, Salmon J. K., Y. Shan, D. E. Shaw in *SC '06: Proceedings of the 2006 ACM/IEEE conference on Supercomputing* (Ed.: B. Horner-Miller), ACM Press, New York, USA, **2006**, 84–es. DOI: 10.1145/1188455

[73] M. Ikeguchi, *J. Comput. Chem.* **2004**, *25*, 529. DOI: 10.1002/jcc.10402

Verzeichnis der Veröffentlichungen

Peer-Review-Artikel

Konrad W. Wurm, Frieda-Marie Bartz, Lukas Schulig, Anja Bodtke, Patrick J. Bednarski, Andreas Link: Carba Analogues of Flupirtine and Retigabine with Improved Oxidation Resistance and Reduced Risk of Quinoid Metabolite Formation, *ChemMedChem* **2022**, e202200262.

Konrad W. Wurm, Frieda-Marie Bartz, Lukas Schulig, Anja Bodtke, Patrick J. Bednarski, Andreas Link: Modifications of the triaminoaryl metabophore of flupirtine and retigabine aimed at avoiding quinone diimine formation, *ACS Omega* **2022**, *7*, 7989–8012.

Abdrrahman S. Surur, Christian Bock, Kristin Beirow, Konrad Wurm, Lukas Schulig, Werner Siegmund, Patrick J. Bednarski and Andreas Link: Flupirtine and retigabine as templates for ligand-based drug design of K_V7.2/3 activators*, Org. Biomol. Chem.* **2019**, *17*, 4512–4522.

Poster

Konrad W. Wurm, Frieda-Marie Bartz, Lukas Schulig, Anja Bodtke, Patrick J. Bednarski, Andreas Link: Application of a Retro-Metabolic Drug Design Approach to Flupirtine and Retigabine Aimed at Avoiding Quinone Diimine Formation, Frontiers in Medicinal Chemistry, Freiburg, 14.–16.03.2022 online.

Eigenständigkeitserklärung

Hiermit erkläre ich, dass diese Arbeit bisher von mir weder an der Mathematisch-Naturwissenschaftlichen Fakultät der Universität Greifswald noch einer anderen wissenschaftlichen Einrichtung zum Zwecke der Promotion eingereicht wurde.

Ferner erkläre ich, dass ich diese Arbeit selbstständig verfasst und keine anderen als die darin angegebenen Hilfsmittel und Hilfen benutzt und keine Textabschnitte eines Dritten ohne Kennzeichnung übernommen habe.

_____ _____

Ort, Datum Unterschrift

Danksagung

Zuerst möchte ich mich ausdrücklich bei Prof. Dr. Andreas Link bedanken, der mich herzlich in seinen Arbeitskreis aufnahm und mir die Möglichkeit gab, diese Dissertation im Rahmen eines durch die DFG geförderten Projekts anzufertigen. Ich danke konkret auch für die konstruktive Anleitung bei der Bearbeitung des Themas, die sehr hilfreiche Einführung in das wissenschaftliche Schreiben und die Unterstützung beim Publikationsprozess, die es insgesamt ermöglichten, dass aus dieser Arbeit drei Veröffentlichungen hervorgingen. In diesem Zusammenhang danke ich auch der DFG für die Bereitstellung der Förderung des Projekts (Projektnummer 277978407).

Des Weiteren gilt mein Dank Prof. Dr. Patrick J. Bednarski für die Durchführung der biologischen Testungen in seinem Arbeitskreis und die Unterstützung beim Erstellen der dieser Arbeit zu Grunde liegenden Manuskripte. Für die Durchführung der Assays möchte ich mich an dieser Stelle auch ausdrücklich bei Frieda-Marie Bartz und Anne Schüttler bedanken.

Besonders danken möchte ich ebenfalls Dr. Lukas Schulig, dem es mit seinen Computermethoden gelang, bei den gemeinsamen Publikationen stets für ein abgerundetes Gesamtbild zu sorgen. Außerdem sei an dieser Stelle Dr. Anja Bodtke und Dr. Robert Hofstetter für die Aufnahme von Massenspektren sowie Maria Hühr für die Messung der unzähligen NMR-Spektren gedankt. Auch Tobias Oergel und Michael Tietz gilt mein Dank für die Durchführung von Nachsynthesen, die teilweise vielleicht ein wenig „schmutzig“ waren.

Des Weiteren möchte ich mich auch bei meinen Labornachbarn aus 20.15 bedanken. Sowohl Dr. Christoph Grathwol mit seinem außergewöhnlichen Musikgeschmack, der so manches Mal Erheiterung brachte, als auch Felix Potlitz mit seiner ruhigen Art sorgten jeder auf seine Weise für eine angenehme Arbeitsatmosphäre. Das Gleiche gilt für meine zeitweise „Labormitbewohnerin“ in 20.14 und Nachfolgerin am K_V7-Thema Jana Lemke, der ich außerdem viel Erfolg bei der Fortführung des Projekts wünsche.

Generell möchte ich mich bei allen ehemaligen und aktuellen Mitarbeitern des AK Link bedanken, die mich während der Promotion begleitet haben. Allen voran ist hier Dr. Christian Bock zu nennen, der mir bereits während der Diplomzeit das notwendige Rüstzeug für die organische Synthese vermittelt hat. Auch die täglichen Zusammenkünfte an der Kaffeemaschine werden mir immer in guter Erinnerung bleiben. Für diese schönen Momente des Arbeitsalltags danke ich neben den

bisher erwähnten Personen außerdem: Michael Eccius, Dr. Georg Fassauer, Tobias Keydel, Van Nguyen, Louis Schmidt und Dr. Abdrrahman Shemsu Surur. Bedanken möchte ich mich weiterhin bei Dr. Gregor Radau für die angenehme Zusammenarbeit im Rahmen des OC Praktikums sowie bei Dr. Olaf Morgenstern und bei Dr. Markus Kindermann für die kompetente Unterstützung in nomenklatorischen bzw. analytischen Fragestellungen.

Auch den Kollegen aus den anderen PMC-Arbeitskreisen möchte ich für das angenehme Miteinander danken, das mich immer gerne an meine Promotionszeit zurückdenken lassen wird: Dr. Daniel Bäcker, Dr. Steven Behnisch-Cornwell, Kristin Beirow, Malte Eichelbaum, Sylvia Ewert, Prof. Dr. Ulrike Garscha, Petra Hammerschmidt, Dr. Stefanie König, Hoai-Nhi Lam, Katharina Landenfeld, Dr. Carsten Lange, Martin Napierkowski, Anika Voigt, Patrick Werth und Dr. Lisa Wolff. Vielen Dank für die schöne Zeit.

Nicht zuletzt danke ich auch meiner Freundin Juliane für den notwendigen Ausgleich zur Arbeit, den mir unsere gemeinsame Zeit stets gibt. Mein größter Dank gilt jedoch meinen Eltern, die mir dieses Vorhaben durch ihre bedingungslose Unterstützung während der gesamten Promotionszeit und darüber hinaus erst ermöglicht haben.